NAS CR-72400
AVSSD-0090-69-RR

FINAL REPORT

THE POST-TEST ANALYSIS OF ABLATIVE MATERIALS

by

B. W. Burrell, D. P. Crowley, M. A. DeSesa,
and M. E. Ihnat

Prepared For

NATIONAL AERONAUTICS AND SPACE ADMINISTRATION

10 February 1969

CONTRACT NAS 3-10300

AVCO GOVERNMENT PRODUCTS GROUP
SPACE SYSTEMS DIVISION
201 Lowell Street
Wilmington, Massachusetts 01887

FINAL REPORT

THE POST-TEST ANALYSIS OF ABLATIVE MATERIALS

by

B. W. Burrell, D. P. Crowley, M. A. DeSesa,
and M. E. Ihnat

Prepared For

NATIONAL AERONAUTICS AND SPACE ADMINISTRATION

10 February 1969

CONTRACT NAS 3-10300

Technical Management
NASA Lewis Research Center
Cleveland, Ohio
Liquid Rocket Technology Branch
Erwin A. Edelman

AVCO GOVERNMENT PRODUCTS GROUP
SPACE SYSTEMS DIVISION
201 Lowell Street
Wilmington, Massachusetts 01887

## FOREWORD

This report describes the work performed by Avco Government Products Group, Space Systems Division under NASA LeRC Contract No. NAS 3-10300 dated 11 July 1967. Period of performance was 11 July 1967 to 15 May 1968.

The program was initially managed by Dr. M. A. DeSesa; Mr. M. E. Ihnat was assigned as interim manager; and Mr. D. M. Patterson was program manager at the completion of the program. The principal investigators during the entire program were Messrs. Bruce W. Burrell and Donald P. Crowley.

The Technical Monitor for the National Aeronautics and Space Administration, Lewis Research Center, Cleveland, Ohio, was Mr. Erwin A. Edelman of the Liquid Rocket Technology Branch.

# ABSTRACT

Silica and graphite-phenolic abaltive materials were examined before and after test firing in a rocket engine nozzle. Chemical, thermal, and physical characterizations of the post-fired nozzle chars were performed in depth at selected nozzle locations. Similar characterizations were also performed on raw billets and laboratory oven-prepared chars.

The fired nozzle char property determinations were performed on various layers removed from the char zones and included carbon, hydrogen, oxygen, and ash analysis, trace metal analyses, density, porosity, X-ray diffraction analysis, optical reflectance, photomicrographic analysis, specific heat, and thermal conductivity. Data are presented in tabular and graphical property profile format.

EDITED BY:
Editorial Services Section
P. S. FALCEY

# CONTENTS

# CONTENTS (Concl'd)

## ILLUSTRATIONS

## ILLUSTRATIONS (Cont'd)

## ILLUSTRATIONS (Cont'd)

# ILLUSTRATIONS (Cont'd)

# ILLUSTRATIONS (Cont'd)

# ILLUSTRATIONS (Cont'd)

# THE POST-TEST ANALYSIS OF ABLATIVE MATERIALS

by B. W. Burrell, D. P. Crowley, M. A. DeSesa, and M. E. Ihna.
Avco Corporation
Space Systems Division

## I. SUMMARY

Two types of ablative materials, silica phenolic MXS-89 and graphite phenolic MX4500, were examined before and after test firing in a rocket engine nozzle to determine the physical and chemical changes that occur. The findings were used to gain insight into the degradation processes for analytical ablation prediction and material improvements. The pre- and post-firing studies included a complete series of chemical, physical, and thermal property measurements of the materials in the virgin, laboratory precharred, and post-fired charred states. Interpretation of the nozzle char findings were based on the findings of laboratory char measurements. Recommendations related to further nozzle analyses and material improvements are presented.

## II. INTRODUCTION

A significant factor in the successful development of composite ablative materials has been the availability of analytical techniques for predicting performance. While these techniuqes have become ever more sophisticated, they still contain many simplifying conservative assumptions. The investigation reported herein was conducted in order to provide ablation analysts with additional insight into the effects of rocket firings on two types of ablation composites, silica phenolic and graphite phenolic, and apply the findings toward analytical ablation model program refinements and ablation material improvements in general.

The study program was designed and organized to obtain a maximum amount of material behavior characteristics by the analysis of selected regions of the rocket nozzle chars and comparing the findings with those obtained from analyses of laboratory prepared chars. Using unique testing techniques which have been successfully employed in similar studies (Ref. 1) allowed chemical, physical, and thermal properties measurements to be conducted on nozzle char powders which were machined from the fired nozzles at discrete intervals within the char layer. This provided an interrelationship of measured properties based on common in-depth char locations. Corings removed from the fired nozzles were measured to provide thermal conductivity profiles throughout the nozzle char layers. The data obtained from the various tests on the nozzle chars were compared and interpretations were made from the chemical, physical, and thermal property test data obtained from measurements of the virgin and laboratory pre-charred nozzle billets which were performed concurrent with the fired nozzle tests.

Consistent with the scope of effort of the program, preliminary conclusions based on data interpretations are advanced as well as recommendations for undertaking more comprehensive coverage of experimental nozzle char analyses. Additional recommendations are made with respect to improving rocket nozzle ablation material performance.

# III. TECHNICAL DISCUSSION

## A. TEST PROGRAM

In keeping with the objectives of this study program, that is, to gain insight into the degradation phenomena occurring in ablative materials and use this knowledge to aid in describing the chemical and physical changes which occur in the material during rocket firing, the study effort was organized and carried out in a three-phase test program. The three phases were conducted concurrently where possible and included 1) studies of the raw billet materials, 2) studies of the billet materials in a laboratory charred condition, and 3) studies of the fired nozzle chars. A detailed breakdown of the overall study program is shown in Figure 1 which illustrates the experimental test coverage within each phase: Virgin Analysis, Char Analysis, and Nozzle Char Studies. The various data interpretations arrived at during the course of the program permitted tentative conclusions since only the throat sections were studied intensively. Recommendations are made for further analyses and alternative materials considerations.

## B. TEST MATERIALS DESCRIPTION

Two general categories of materials were evaluated during the course of the reported study program: silica-phenolic and graphite-phenolic laminates. Both material types were provided by NASA LeRC to Avco/SSD in the form of virgin billets and post-fired rocket nozzles. The billets tested were designated by Fiberite Corporation as:

1. Silica Fabric/Phenolic: SN 1429-1, MXS-89, Lot D-594, Roll 1-A

2. Graphite Fabric/Phenolic: SN 1428-1, MX4501, Lot D-749, Roll 1

The following specifications were also certified by Fiberite:

1. Silica Fabric/Phenolic: Resin solids - 33.0 percent

   Volatile content - 3.5 percent

2. Graphite Fabric/Phenolic: Resin solids - 34.8 percent

   Volatile content - 5.2 percent

These materials were received from the Fiberite Corporation on 13 September 1967 in the form of 5-inch-diameter x 5-inch-long cylinders. Four fired nozzles were also received from NASA LeRC identified as:

1. Glass Cloth -- MXS-89-1

2. Glass Cloth -- MXS-89-2

3. Carbon Cloth -- MX4500-1

4. Carbon Cloth -- MX4500-2
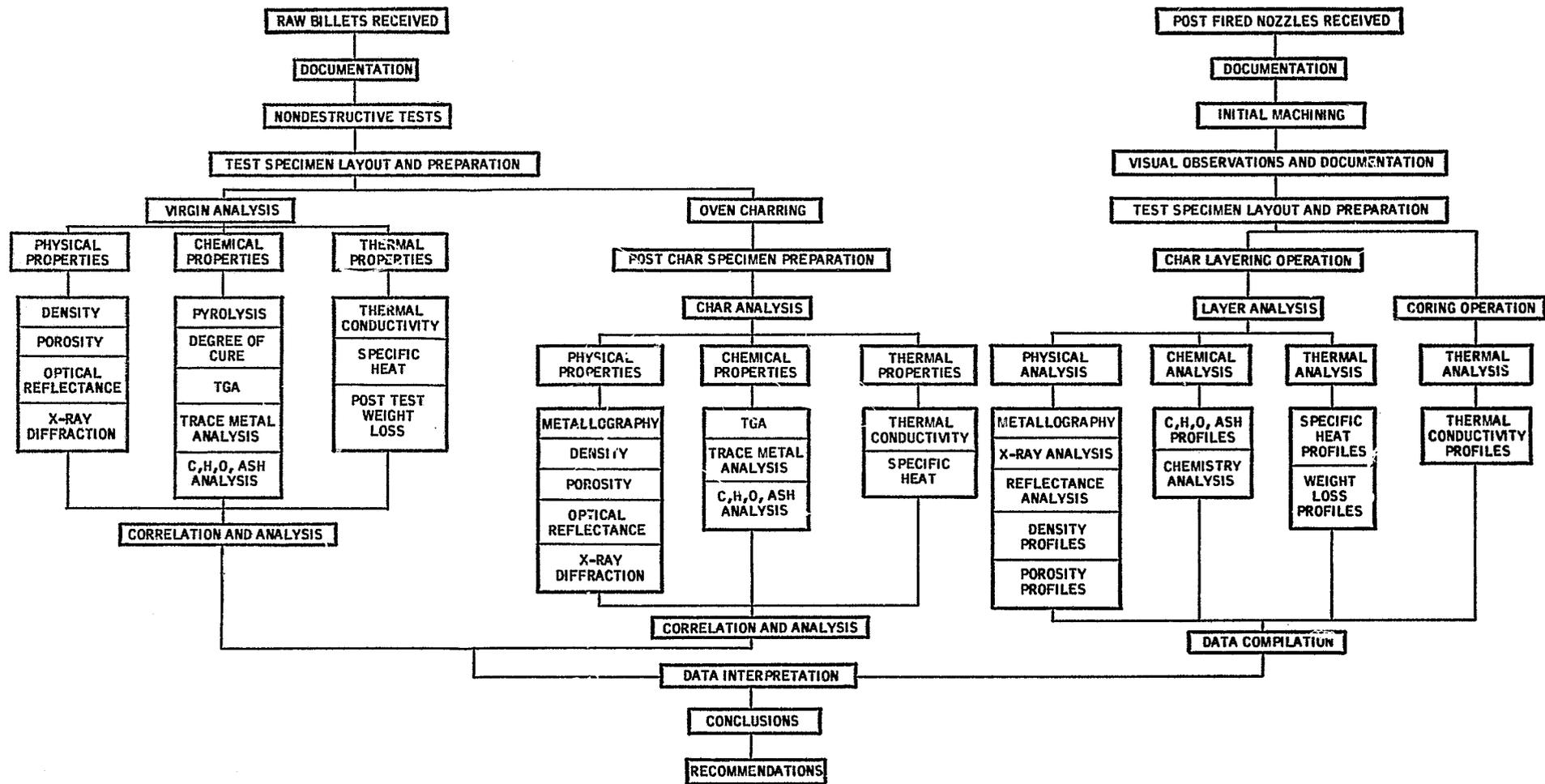
Figure 1  POST-TEST ANALYSIS OF ABLATIVE MATERIALS -- DETAIL TEST
PROGRAM SCHEDULE

78-1478

-4-

Table I, which was supplied by NASA LeRC, lists the rocket firing test parameters pertinent to the study program. The original dimensions of the fired nozzles are shown in Figure 2.

## TABLE I

### TEST DATA FOR NOZZLES SENT TO AVCO

Test Date:  1 November 1967

| Nozzle No. | Run No. | Time (sec) | Pc (psia) | O/F | *ΔRt Meas. (in.) | + Calc. (in.) | Original Throat Radius (in.) |
|---|---|---|---|---|---|---|---|
| 1. MXC4500 | 814 | 38.4 | 99.4 | 1.52 | 0.133 | 0.139 | 0.601 |
| 2. MXC4500 | 815 | 40.4 | 98.5 | 1.55 | 0.128 | 0.130 | 0.600 |
| 1. MXS89 | 816 | 51.3 | 98.2 | 1.59 | 0.120 | 0.134 | 0.600 |
| 2. MXS89 | 817 | 51.0 | 99.6 | 1.54 | 0.119 | 0.133 | 0.601 |

Propellants:  $N_2O_4$ - 50% $N_2H_4$/ 50% UDMH

NC*:  92.2 percent

*Change in throat radius

+Calculated from flow data

The virgin billets of silica-phenolic and graphite-phenolic were received in September 1967 per schedule.  A complete nondestructive test (NDT) survey of the two billets was made to characterize the billets in the as-received condition.

The detailed results of this survey are included in Appendix A in the form of a letter report (J. R. Zurbrick to M. A. DeSesa, W270-10-67-96, 4 October 1967). In brief, the silica-phenolic billet was found to be remarkably uniform in density, both axially and radially.  An area of between-ply macroporosity was detected in the center of the billet.  This is probably due to trapped volatiles since the poor thermal conductivity of this material caused the billet to cure from its end and circumference inward.  The microporosity of the silica-phenolic billet was found to be low overall but increasing from circumference to axis.

For the graphite-phenolic billet in contrast, density was greatest along the axis and decreased towards the circumference indicating that the billet cured from the inside out.  Since the graphite reinforcement has a high thermal conductivity, heat may have been conducted into the center of the billet more rapidly than the outside could cure.  Macroporosity and density differed between the upper and lower halves of the billet, perhaps caused by a difference in heat transfer to and from the billet in the curing oven if the block was lying on a metal surface.

FLOW

4.25 DIA.
±.01

2.85 DIA.
±.01

0.39
0.41

4.5
±1/32

3.5 R
BLEND

1.20
±.01
DIA.

1.23
1.24

15°

5.0 DIA.
±.01
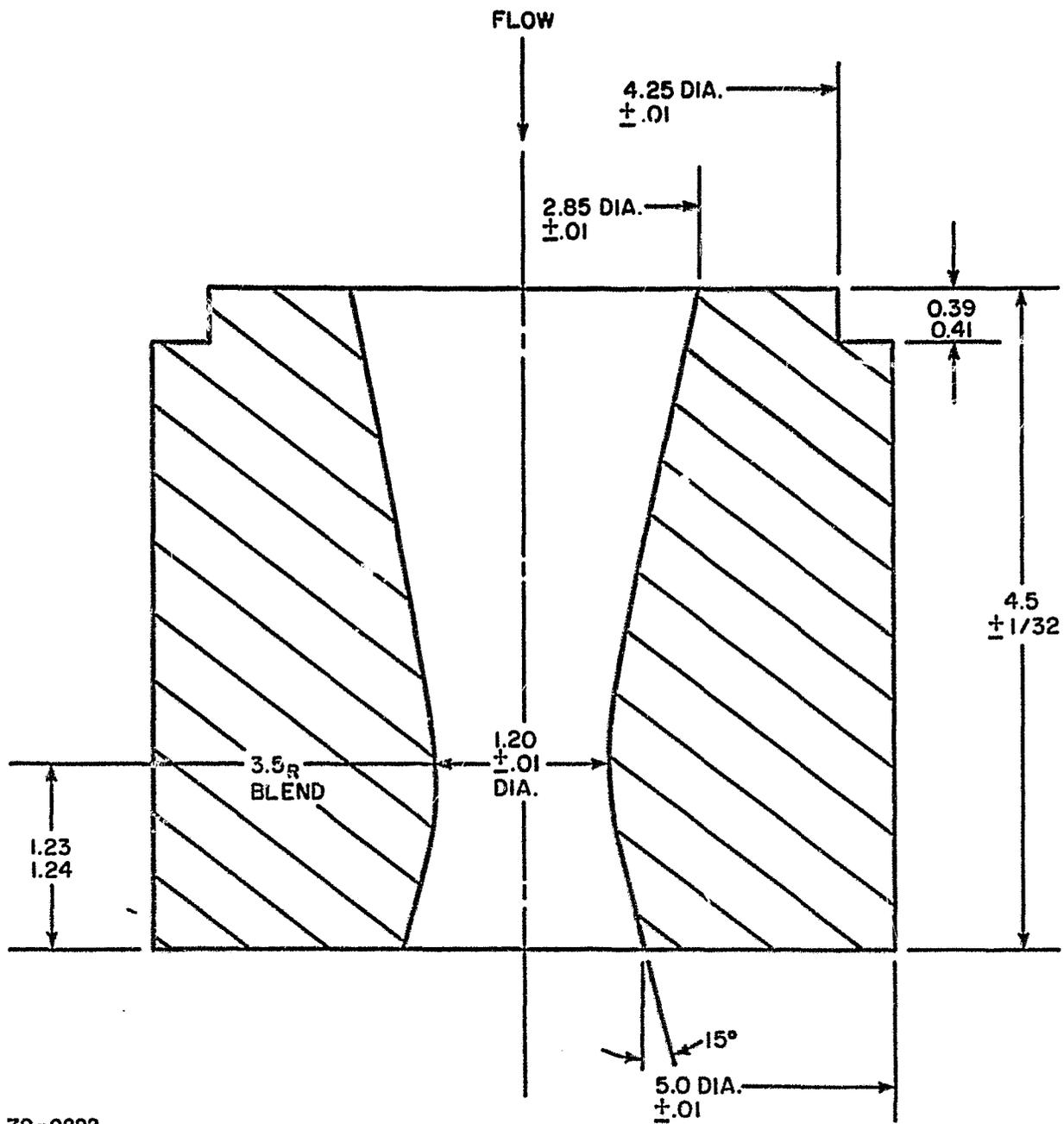
79-0292

Figure 2  ORIGINAL GEOMETRY OF UNFIRED NOZZLES

Once the nondestructive survey was completed, the billets were submitted to the Test Specimen Preparation Group. Each billet was cut in half along the center-line axis and test specimens for the characterization of the virgin material were prepared from one half while the other half was saved for possible future reference. Upon sectioning, a shrinkage crack, almost 0.5-inch long, was visible in the center of the silica-phenolic billet so that the NDT survey result was confirmed.

The four fired test nozzles were machined into half-sections allowing a view of the axial char pattern, for examination purposes and to aid in the location of the various samples to be taken for testing (see Figures 3 and 4).

The initial visual examination of the nozzles showed a distinct difference between the silica- and graphite-phenolic chars both from an in-depth and surface condition point of view. The most notable difference was the depth of chars being greater in the graphite-phenolic (about 0.5 inch) than in the silica-phenolic (about 0.3 inch), presumably due to the higher thermal diffusivity of the graphite composite. In both types of nozzles, the char depth appeared to be fairly constant throughout the length of the nozzle but abruptly diminished in depth at the nozzle entrance. The following observations summarized the initial cross section visual examination:

| GRAPHITE-PHENOLIC NOZZLES | SILICA-PHENOLIC NOZZLES |
|---|---|
| In-Depth Char Zone | In-Depth Char Zone |

GRAPHITE-PHENOLIC NOZZLES — In-Depth Char Zone

1. Apparent Char Depth -- 0.5 inch.

2. No signs of fabric layer separation in the char zone.

3. Resin degradation not apparent. Virgin to char texture grades from hard friable solid to soft granular coke.

4. No apparent percolation or redeposition of resins.

SILICA-PHENOLIC NOZZLES — In-Depth Char Zone

1. Apparent Char Depth -- 0.3 inch.

2. Extensive fabric layer separation in the char zone.

3. Resin degradation obvious. Virgin to char texture grades from hard resin, through charred resin to empty voids.

4. Resin percolation apparent - redeposition of charred resins onto fabric and molten silica apparent.

GRAPHITE-PHENOLIC NOZZLES — Interior Nozzle Surface

1. Interior nozzle surface contains no signs of a molten product.

2. Relatively smooth surface appears to have been formed by mechanical erosion; surface texture influenced by the presence of fabric weave forming what looks like minute eddies.

SILICA-PHENOLIC NOZZLES — Interior Nozzle Surface

1. Interior nozzle surface contains much molten material.

2. Somewhat coarse surface appears to be composed chiefly of molten silica which has been dragged downstream in the form of tenaceous globules. The glassy silica is apparently coated with the percolating resins which have been charred to form a black glassy coating. A layer of soot overlaid the glassy globules.
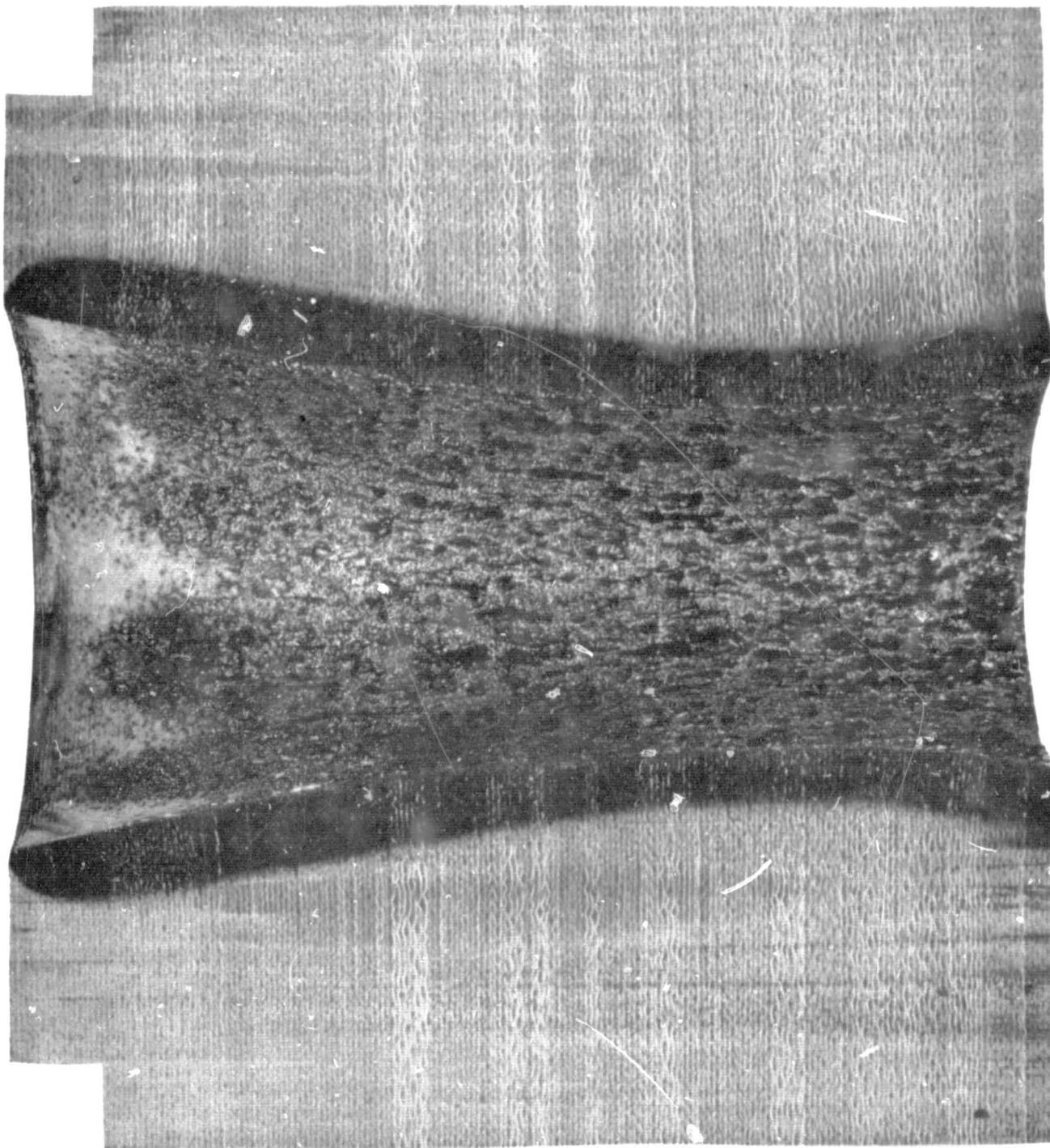
Figure 3 CUT-AWAY VIEW OF POST-FIRED SILICA-PHENOLIC MXS-89 NOZZLE
(1X MAGNIFICATION)
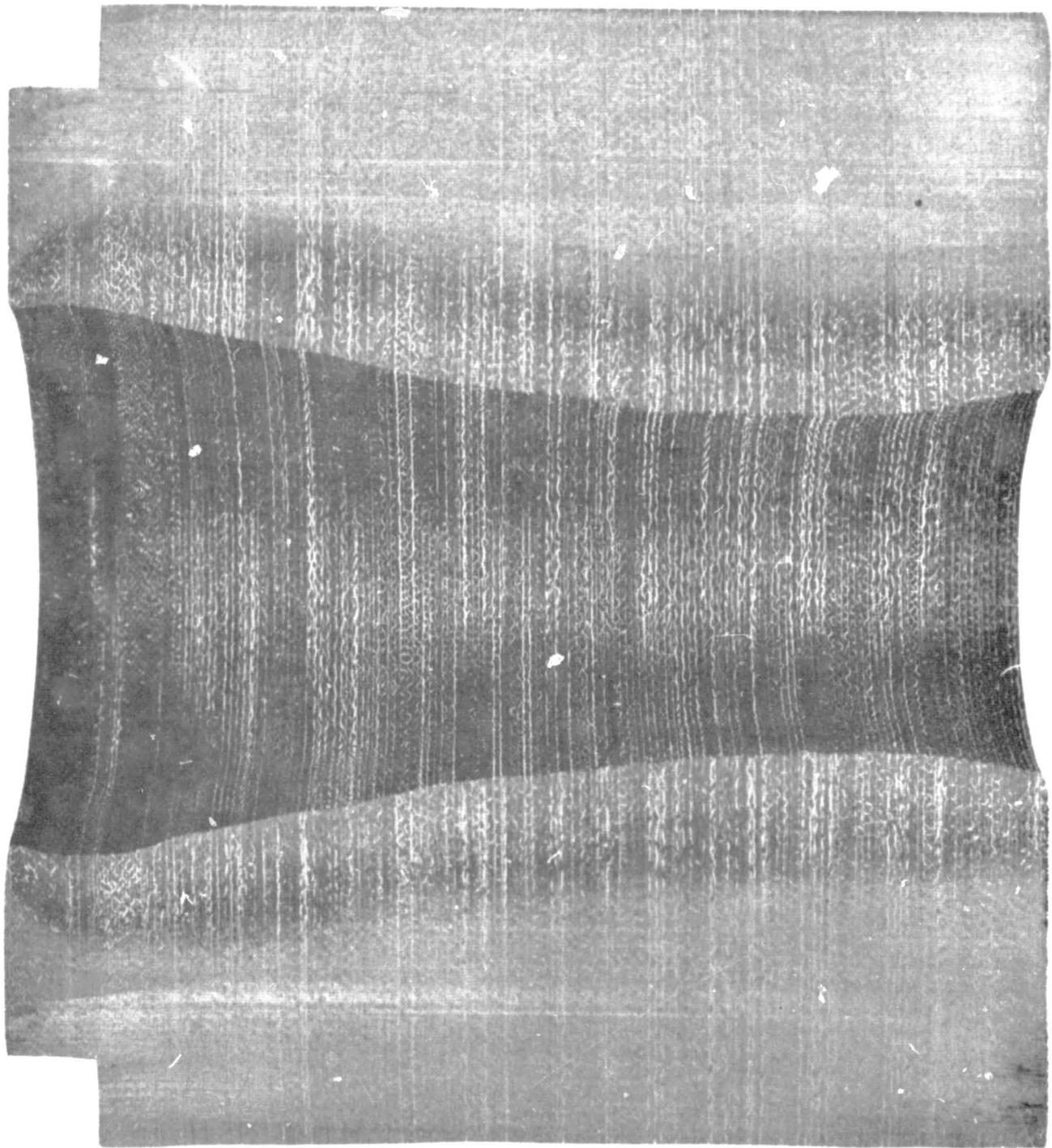
Figure 4  CUT-AWAY VIEW OF POST-FIRED GRAPHITE-PHENOLIC MX4500 NOZZLE
(1X MAGNIFICATION)

| 3. Apparent erosion of the surface at the nozzle entrance altering the nozzle divergency. | 3. Clear glassy silica present at nozzle entrance -- grades into darker color downstream -- no apparent erosion of the nozzle entrance. |

After having been cut in half, the virgin billets were machined to provide the various test specimens. The layout of the half-sections are shown in Figure 5 and illustrate the directions from which the test samples were removed from the billet. As noted in the figure, the five 1-1/4-inch-diameter corings provided the material for all oven char study measurements. The one-inch-diameter coring and its corresponding concentric ring supplied the configuration for thermal conductivity testing of the virgin material. Virgin material chemical and density evaluations were performed on the rectangular sections shown in the figure. These sections also provided material for specific heat determinations using the Differential Scan Calorimeter testing scheme, the results of which were compared to those obtained from the Method of Mixtures apparatus which utilized the six 3/8-inch-diameter corings illustrated.

After examining the eight nozzle half-sections, nozzles MX4500-2 and MXS-89-2 were selected for property analysis. One of the half-sections of each nozzle was submitted for photomicrographic analysis. The remaining halves were machined into four radial sections as shown in Figure 6. Each radial section was subsequently machined to provide specimens for the various tests. This operation was performed in anticipation of possible evidence of interest in different nozzle sections as a result of test findings in the principal radial section under investigation. Specimens for thermal conductivity measurements were taken from the various radial sections as shown in Figure 7. The figure also indicates the regions from which the specimens required for all other tests were machined. The figure illustrated that the specimens were machined to conform with the char angle at each section. Typically, a specimen was prepared and mounted in the milling machine in a manner that resulted in each layer being removed in the milling operation parallel to the plane of the virgin-char region. This precaution was taken so that the "profile" property measurements would be representative of each layer of the char analyzed.

The same criterion was maintained for thermal conductivity measurements so that the direction of heat flow was maintained, insofar as was possible, normal to the virgin-char plane. Failure to meet the above requirements results in an "averaging" phenomenon with a corresponding loss in the material evaluation precision.

C. RESULTS AND DISCUSSION

1. Characterization of Virgin Materials and Oven Reference Chars

a. Preparation of Oven Reference Chars

The five corings removed from each virgin half-section were pre-charred in dry inert atmospheres in preparation for analyses for comparison with corresponding analyses of the rocket nozzles. The charring was performed in two separate laboratory ovens. Material charring to 1000° F was performed in a controlled dry nitrogen atmosphere nickel enclosure to ensure a uniform temperature distribution. In preparation, the degradation
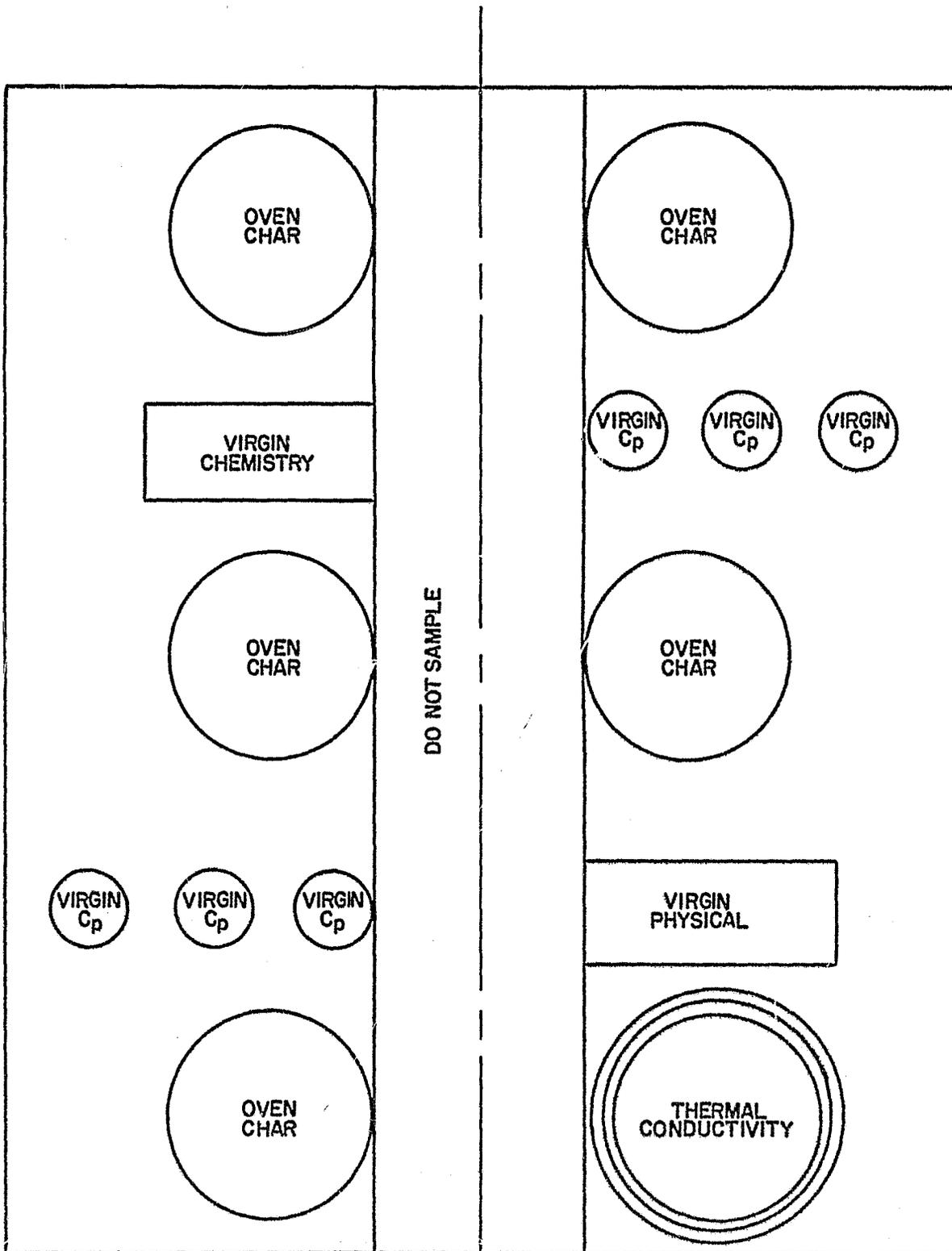
73-1479

Figure 5  BILLET MATERIAL TEST SPECIMEN LAYOUT

-11-
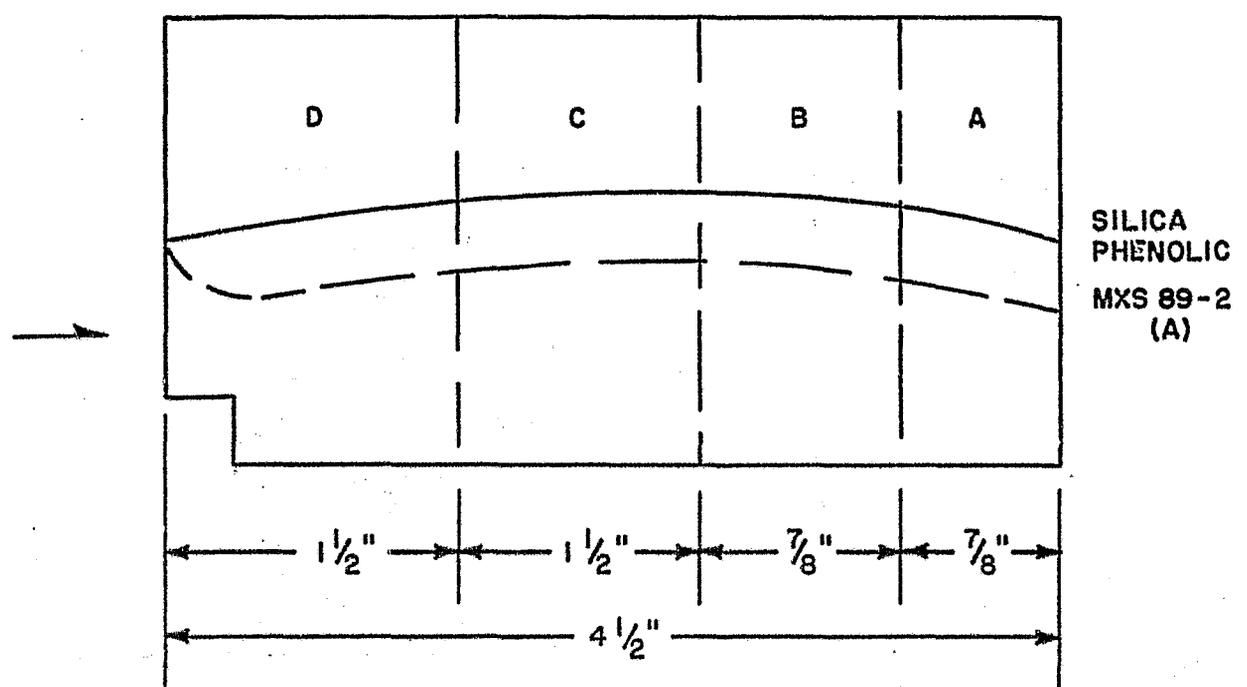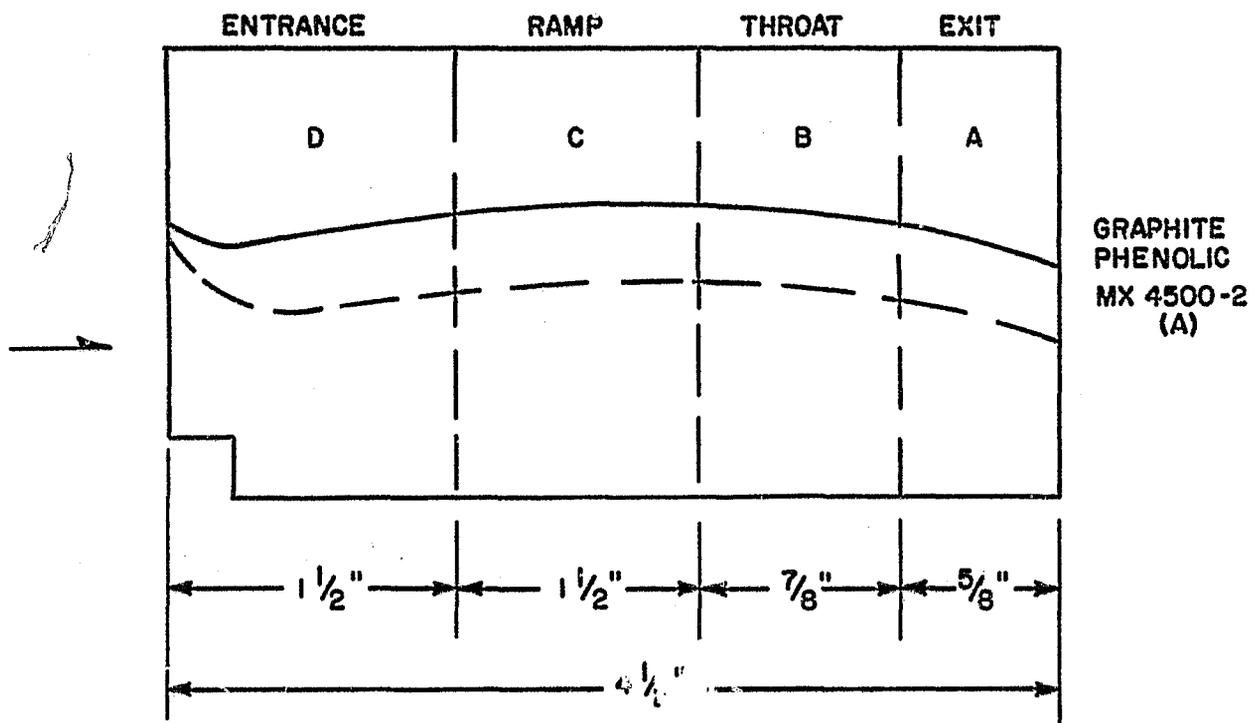
Figure 6 NOZZLE SECTION IDENTIFICATION

78-1480

THERMAL ($C_p$),
PHYSICAL & CHEMICAL
TEST SPECIMENS

THERMAL CONDUCTIVITY
SPECIMENS

CHAR ZONE

| SECTION D | SECTION C | SECTION B | SECTION A |
|-----------|-----------|-----------|-----------|
| ENTRANCE  | RAMP      | THROAT    | EXIT      |
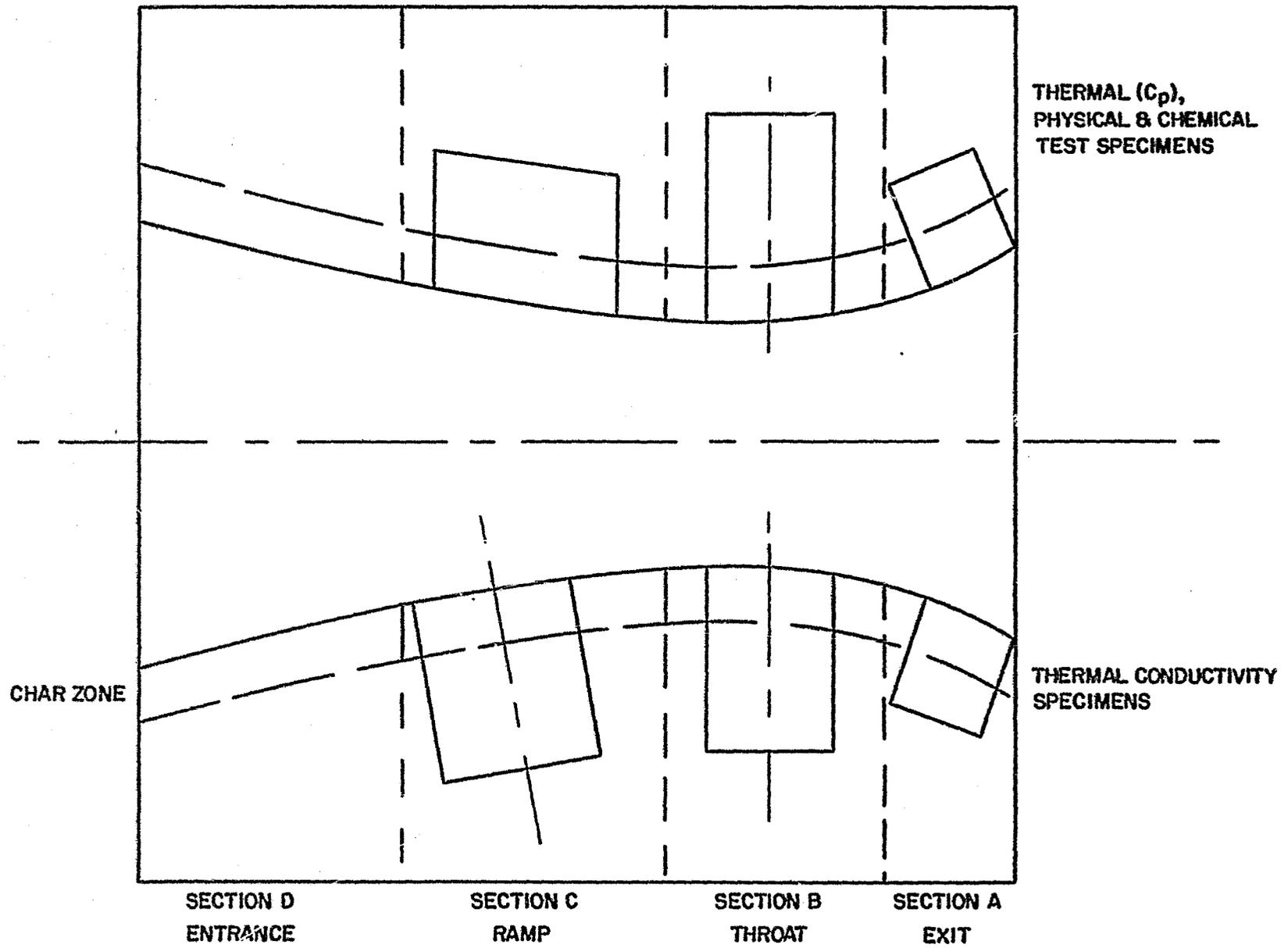
78-1481

Figure 7 FIRED NOZZLE TEST SPECIMEN LOCATION LAYOUT

container was loaded with all the test corings of each material sealed
except for the gas inlet and exit and placed in the oven. A regulated
amount of nitrogen was allowed to diffuse into the container to produce
the desired ambient atmosphere.

The heating rate was preset to approximately 200° F per hour and the con-
tainer was allowed to reach 790° F and soak there for 3 hours. The tem-
perature was then raised to 1000° F over 2.5 hours and the cores allowed
to soak for an additional 3 hours. In this controlled manner the phenolic
resin was slowly decomposed, thus avoiding internal thermal stresses and
preventing material delamination. The cool-down rate was also controlled
to avoid material splitting resulting from thermal stresses.

All specimens were then wrapped in carbon felt for support and heated at
a rate of 1000° F per hour in a Curtiss-Wright high-temperature graphite
furnace containing a nitrogen atmosphere. Each specimen was kept at the
desired final temperature for a period of 2 hours. Cores of the graphite-
phenolic material were heated to 2000°, 3000°, 3650°, and 4000°F. Cores
of the silica-phenolic material were heated to 2000° F with no difficulty,
but two attempts to reach 3000° F failed at 2700° and 2800° F when, in each
case, the core collapsed and was no longer in focus to the optical pyrom-
eter. When these cores were unwrapped from the protective carbon felt,
the degradation was so extensive that it was decided not to attempt fur-
ther high-temperature degradations until the current cores had been fully
examined.

Figures 8 and 9 show the post-charred condition of the corings prior to
being prepared for the various test measurements. The char temperatures
are noted on each figure. The extent of the delamination and decomposi-
tion of the silica-phenolic 2700° and 2800° F chars is clearly seen in
Figure 7 as is the uniformity and similarity of appearance of the graphite-
phenolic oven chars regardless of the charring temperature.

b. Pre- and Post-Char Physical Dimensions

Physical dimensions and weight measurements were performed on all the
specimen corings before charring in the various ovens and after cooling
down (except the 2700° and 2800° F MXS-89 material). Table II lists all
measurements taken and the percentage changes in dimensions and weight
determined.

It was concluded that the information in the above table cannot be
practically used for the determination of densities because of the ir-
regular geometry of the specimen corings. Density determinations are
treated elsewhere in this report. The 2700° and 2800° F physical dimen-
sions for the MSX-89 material were unattainable due to its extreme
fragility. It can be noted from the table that there was a significant
(and expected) difference in material shrinkage relative to the fabric
laminate planes. There also appeared to be a similarity in weight loss
percentages for both material types at 1000° and 2000° F char levels in-
dicating a basic similarity of the phenolic matrix constituents. The
major weight loss occurred at the 1000° F char region with only small
additional losses occurring at higher temperatures, suggesting that the

-14-

1000°F          2000°F          2700°F          2800°F
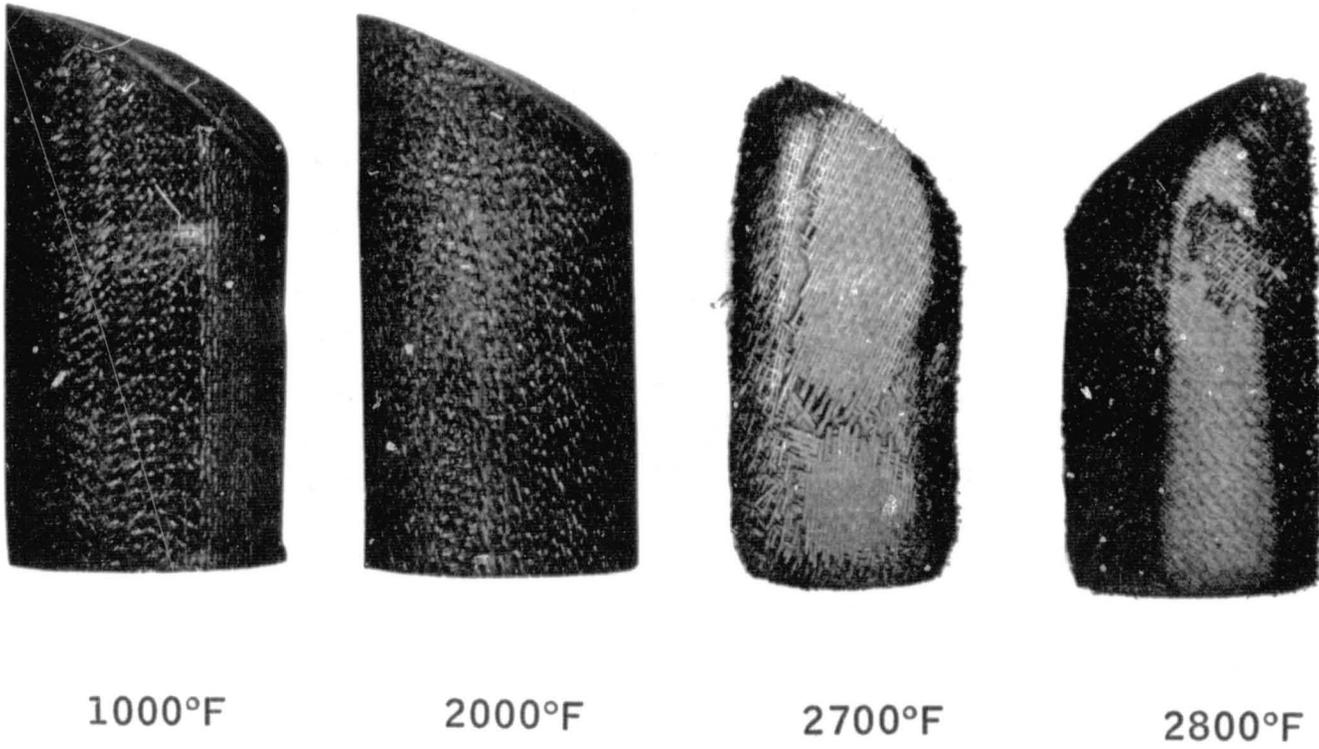
Figure 8  OVEN-CHARRED SILICA-PHENOLIC MXS-89 CORINGS
(1X MAGNIFICATION)
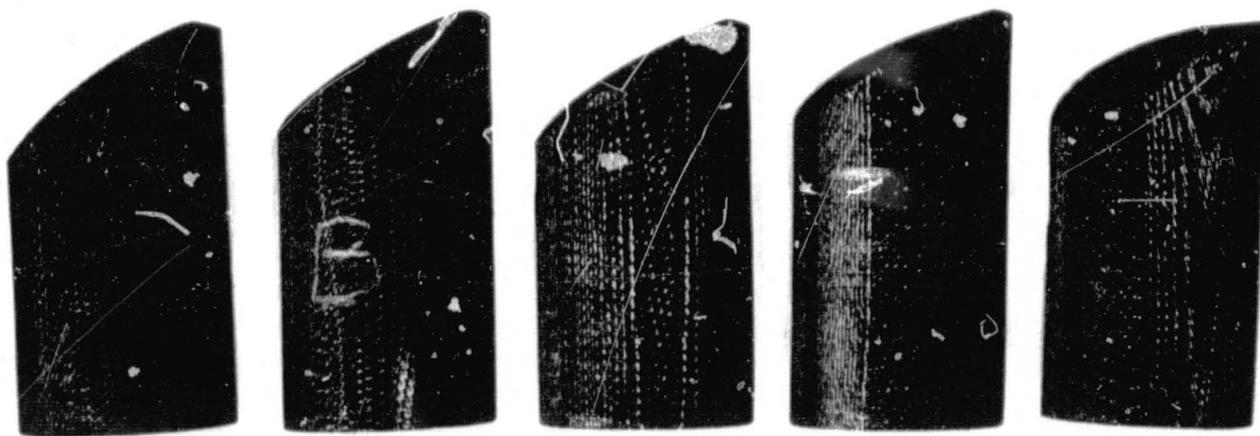
| 1000°F | 2000°F | 3000°F | 3650°F | 4000°F |

Figure 9 OVEN–CHARRED GRAPHITE–PHENOLIC MX4501 CORINGS
(1X MAGNIFICATION)

## TABLE II

### PRE- AND POST-CHAR DIMENSIONS

#### SILICA-PHENOLIC MXS-89

|  | Virgin* | Char Temperature[+] | | | |
|---|---|---|---|---|---|
|  | | 1000°F | 2000°F | 2700°F | 2800°F |
| Diameter Across Fabric Plane, in. | 1.245 | 1.211 | 1.159 | N/A | N/A |
| Diameter Along Fabric Plane, in. | 1.245 | 1.239 | 1.212 | N/A | N/A |
| Height, Nom. in. | 2.473 | 2.458 | 2.421 | N/A | N/A |
| Weight, gm | 71.5 | 61.5 | 60.0 | N/A | N/A |
| Percent Change in: | | | | | |
|    Diameter Across Fabric Plane | | -2.7 | -6.9 | | |
|    Diameter Along Fabric Plane | | -0.5 | -2.7 | | |
|    Height | | -0.6 | -2.1 | | |
|    Weight | | -14 | -16 | | |

#### GRAPHITE-PHENOLIC MX4501

|  | Virgin | 1000°F | 2000°F | 3000°F | 3650°F | 4000°F |
|---|---|---|---|---|---|---|
| Diameter Across Fabric Plane, in. | 1.247 | 1.191 | 1.178 | 1.172 | 1.147 | 1.149 |
| Diameter Along Fabric Plane, in. | 1.247 | 1.246 | 1.245 | 1.246 | 1.246 | 1.239 |
| Height, Nom. in. | 2.277 | 2.277 | 2.321 | 2.283 | 2.333 | 2.293 |
| Weight, gm | 54.9 | 45.6 | 46.0 | 44.0 | 47.8 | 46.3 |
| Percent Change in: | | | | | | |
|    Diameter Across Fabric Plane | | -4.5 | -5.5 | -5.8 | -7.8 | -7.5 |
|    Diameter Along Fabric Plane | | 0 | 0 | -0.2 | 0 | -0.3 |
|    Height | | 0 | +0.1 | +0.7 | -0.3 | -0.2 |
|    Weight | | -16.9 | -16.2 | -19.7 | -20.0 | -20.0 |

*Average values

[+]Values quoted are based on actual measurements

principal decomposition by vaporization occurs at the 1000°F level while the higher temperature reactions were in the form of chemical rearrangements unattended by any significant additional weight losses.

c. Photomicrographic Observations of Oven Chars

After the virgin material corings had been charred, the specimens were machined to provide material for metallographic analysis. The remaining portions of the precharred corings were machined for thermal, chemical, and X-ray test measurement specimens. The metallographic study series were conducted on a 1X, 5X, and 500X metallograph and included photomicrographs supporting the more critical observations. The 1X photographs were shown in the previous section (Figures 8 and 9). Figures 10 through 13 and 5X magnification photographs of the silica-phenolic MXS-89 oven chars. Char temperatures are shown on each figure. The crack density was noted to be most predominant in the 1000°F char. This phenomenon was most likely associated with the thermal stresses set up in the material as a result of being exposed to temperatures near the principal phenolic degradation phase. The 2000°F char indicated the apparent depletion of the black charred resins while the 2700° and 2800°F chars show strong evidence of compositional and structural decay. The gradation in decomposition in the 2300°F char is most likely attributed to the shorter charring time for that specimen. Of particular note in the 2700° and 2800°F char was an apparent absence of cracking.

The 500X photomicrographic series for the silica-phenolic oven chars are discussed in the following section. The 1000°F char material (Figure 14) gives evidence of the onset of resin-phenolic degradation and stress cracking. At this char temperature the silica fibers were found to be relatively undisturbed and unreacted. At 2000°F (Figure 15) the phenolic cracking and degradation continued to develop. It was also noted that a reaction between the silica fibers and the matrix may have started as indicated by the "eyebrowing" around the fibers. It was noted that fracture lines existed both in the phenolic and fiber bundle regions. At 2700°F (Figure 16) gross voids were developed (darkened area), and a breakdown of the silica fibers had occurred with corresponding melting and fusion. A notable heavy buildup of silicon carbide onto the charred matrix had also occurred at that temperature. This heavy buildup continued at 2800°F (Figure 17), the silicon being furnished by the partially depleted fibers as shown. To test for the existence of pyrolytic graphite, microscopic observations were conducted under polarized lighting. One such observation, as illustrated in Figure 18 which is the same view of the previous figure, shows the absence of pyrolytic graphite and gives a clearer description of the silicon carbide build-up. There was no evidence of a pyrolytic graphite deposition occurring in any of the silica-phenolic oven chars. This observation is attributed to the slow oven charring procedure which does not permit cracking to occur but provides the most advantageous conditions for a silicon-carbon reaction. The silicon carbide presence was confirmed by X-ray diffraction analyses discussed elsewhere in this report.

In summary, the photomicrographic series noted that:
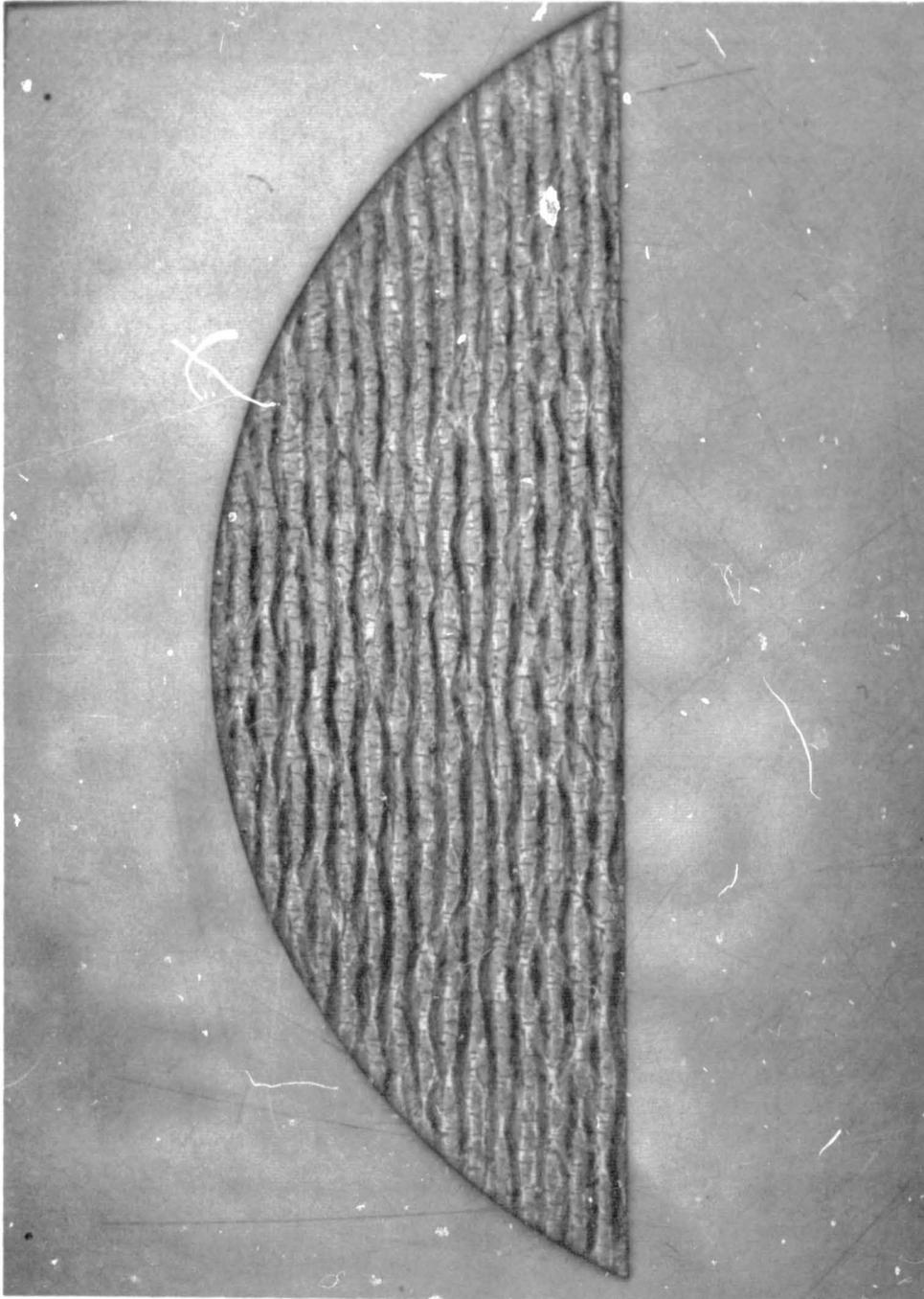
Figure 10  1000°F OVEN-CHARRED SILICA-PHENOLIC MXS-89 CORING
(5X MAGNIFICATION)
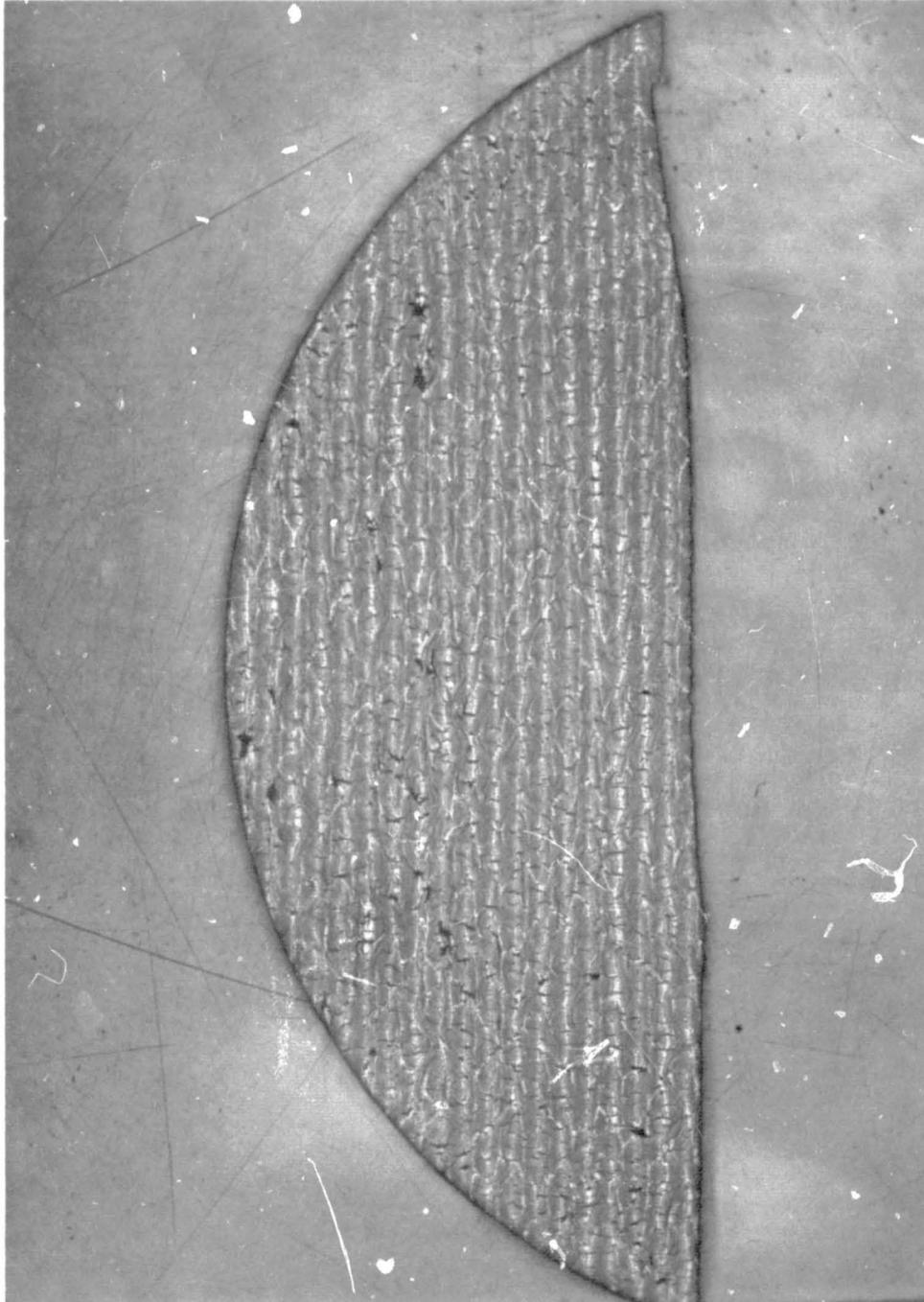
Figure 11  2000°F OVEN-CHARRED SILICA-PHENOLIC MXS-89 CORING
(5X MAGNIFICATION)
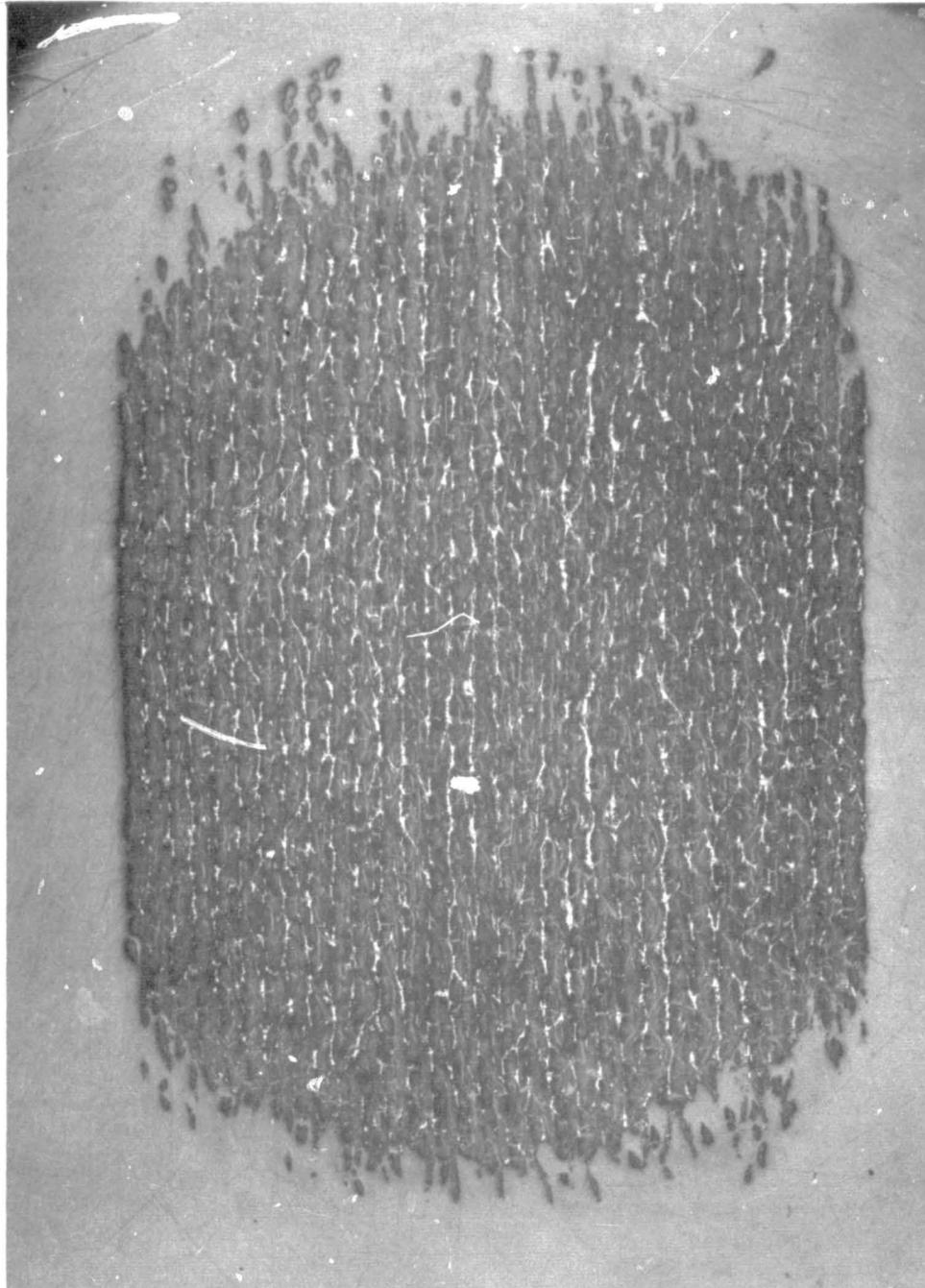
Figure 12  2700°F OVEN-CHARRED SILICA-PHENOLIC MXS-89 CORING
(5X MAGNIFICATION)
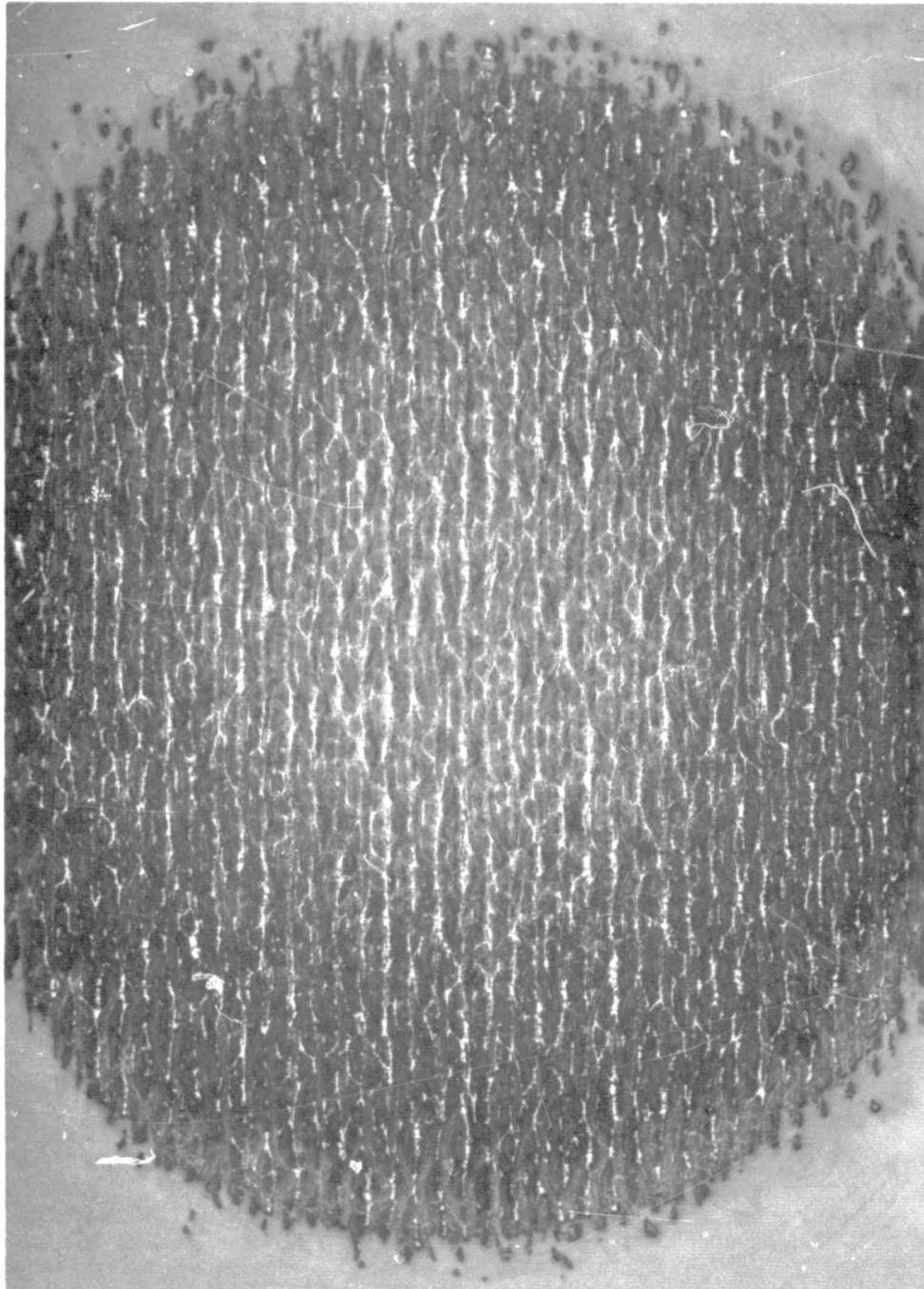
Figure 13   2800°F OVEN-CHARRED SILICA-PHENOLIC MXS-89 CORING
(5X MAGNIFICATION)

Figure 14  1000°F OVEN-CHARRED SILICA-PHENOLIC MXS-89 CORING
(500X MAGNIFICATION)

Figure 15  2000°F OVEN-CHARRED SILICA-PHENOLIC MXS-89 CORING
(500X MAGNIFICATION)
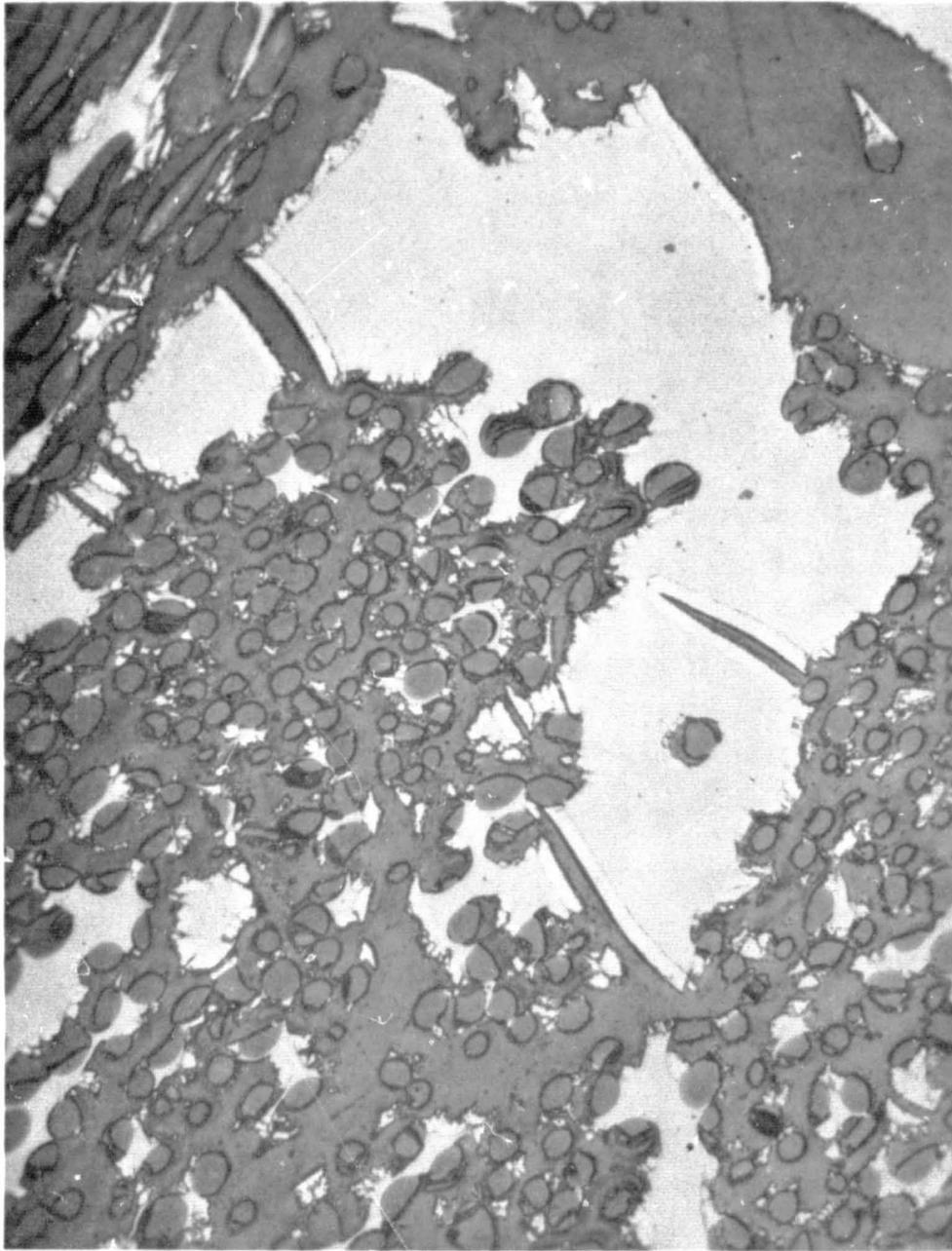
Figure 16  2700°F OVEN-CHARRED SILICA-PHENOLIC MXS-89 CORING
(500X MAGNIFICATION)

Figure 17 2800°F OVEN-CHARRED SILICA-PHENOLIC MXS-89 CORING
(500X MAGNIFICATION)

Figure 18  2800°F OVEN-CHARRED SILICA-PHENOLIC MXS-89 CORING
(500X MAGNIFICATION -- POLARIZED LIGHTING)

1) the principal silica-phenolic degradation occurred at approximately 1000°F and was attended by thermal stress cracking of the phenolic matrix;

2) the matrix degradation continued to 2000°F and was probably time-dependent;

3) at 2000°F no significant reaction occurred between the charred matrix and the silica fibers;

4) increasing the material temperature by an additional 700°F yielded a significant silica-carbon reaction and was attended by depletion of the silica fibers;

5) at 2700° and 2800°F a large production of silicon carbide occurred; and

6) no pyrolytic graphite was produced by oven charring this material.

The graphite-phenolic MX4501 oven chars were also subjected to the same metallographic analysis. Figures 19 through 23 are the 5X photomicrographics of the corings shown collectively in Figure 9. The most pronounced observation was in the variation of the apparent crack density of the oven chars. The density appeared to increase from 1000° to 3000°F and then decreased toward the 4000°F temperature. Unlike the silica-phenolic chars the 5X photographic tonal variation was insignificant. This suggested a similarity in the graphite-phenolic composition at all char temperatures to 4000°F. From the 500X observations it can be seen that when the material was charred to 1000°F (Figure 24) the phenolic matrix, which was generally grainy and nonuniform, yielded the typical thermal cracking. The graphite fibers indicated no evidence of a reaction between the fibers and the phenolic. The herringbone patterns which occur in the various photos of this series are attributable to optical interference patterns from the photographic lighting. At 2000°F (Figure 25) the phenolic continued to decompose with no apparent alteration of the graphite fibers occurring. At this temperature the matrix graininess decreased and became more uniform. The decrease in graininess continued to 3000°F (Figure 26) where it reached its apparent finest texture. Still the graphite fiber remained unchanged; however, some local nonuniformity of the charred phenolic was evident. From 3650°F (Figure 27) to 4000°F (Figure 28) the phenolic matrix texture increased in coarseness to a point where it was significantly similar to that of the 1000°F char. There was also evidence in Figures 26 and 27 that the carbon or graphite in the charred phenolic grew in size (or crystallinity).

In summary the following notations were made for the MX4501 material:

1) The graphite-phenolic matrix apparently contained graphite powder as a result of coming in contact with the graphite fabric during the billet fabrication stage.

2) The phenolic matrix degradation occurred at 1000°F and continued up to 3000°F.
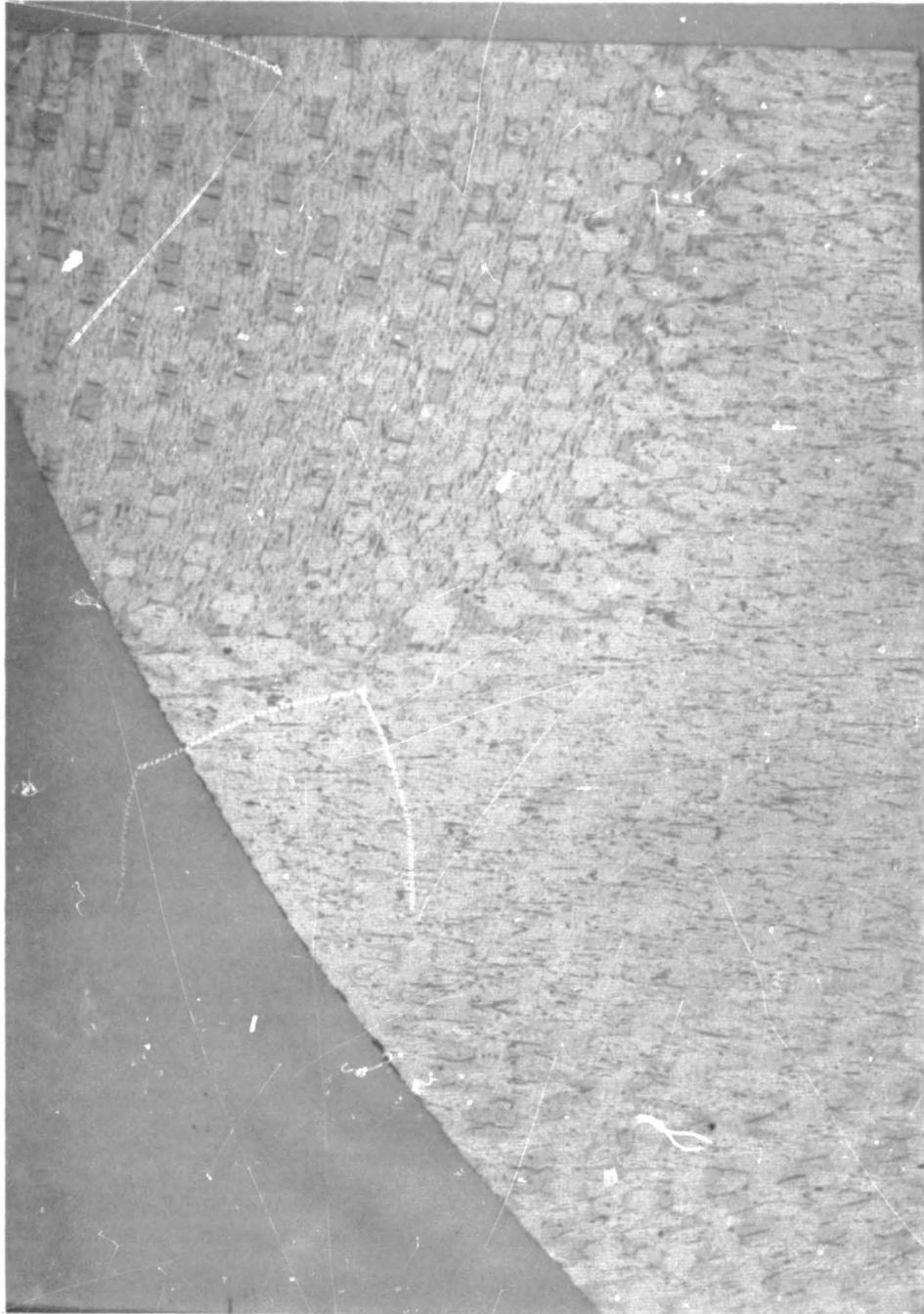
Figure 19  1000°F OVEN-CHARRED GRAPHITE-PHENOLIC MX4501 CORING
(5X MAGNIFICATION)
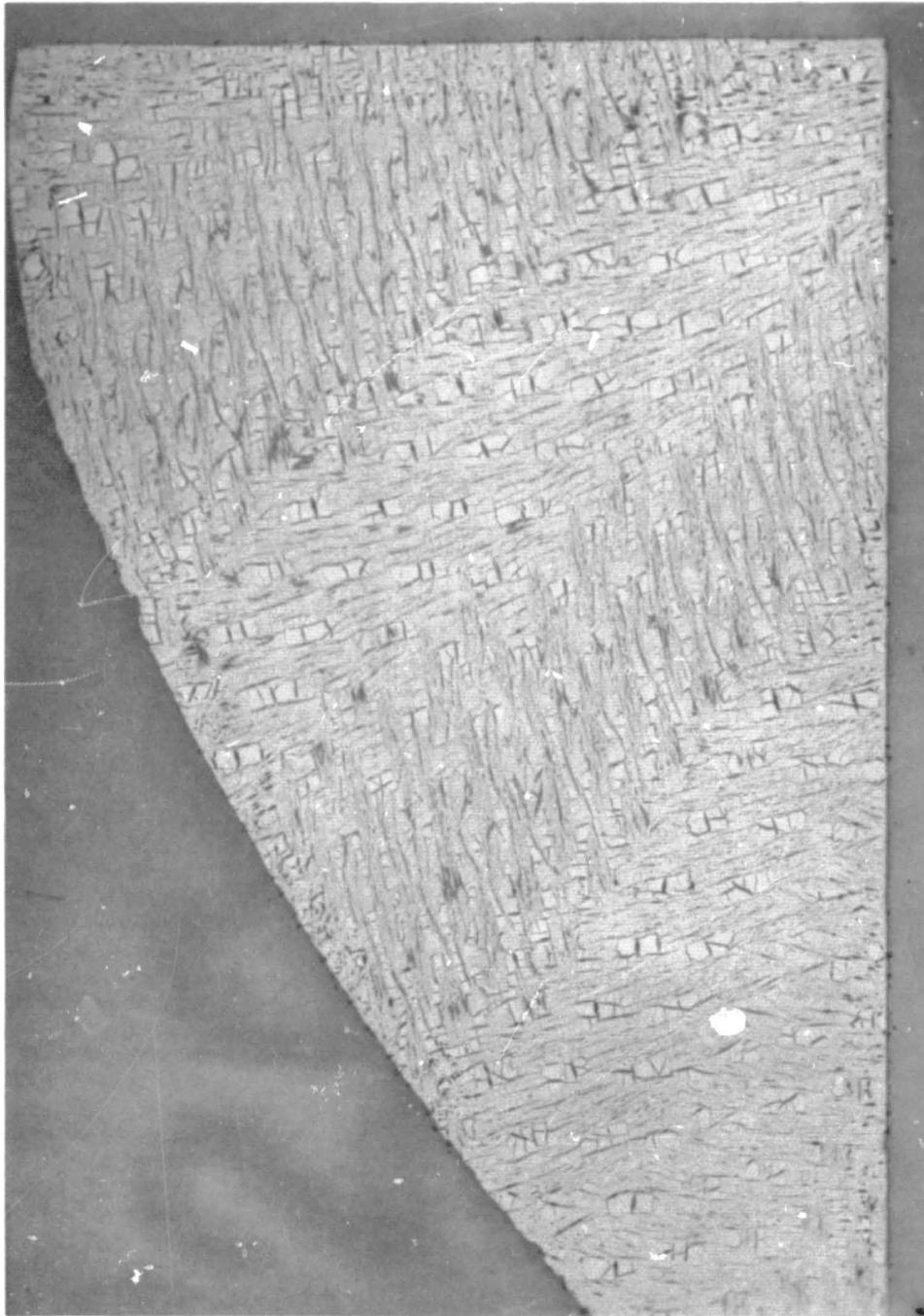
Figure 20  2000°F OVEN-CHARRED GRAPHITE-PHENOLIC MX4501 CORING
(5X MAGNIFICATION)
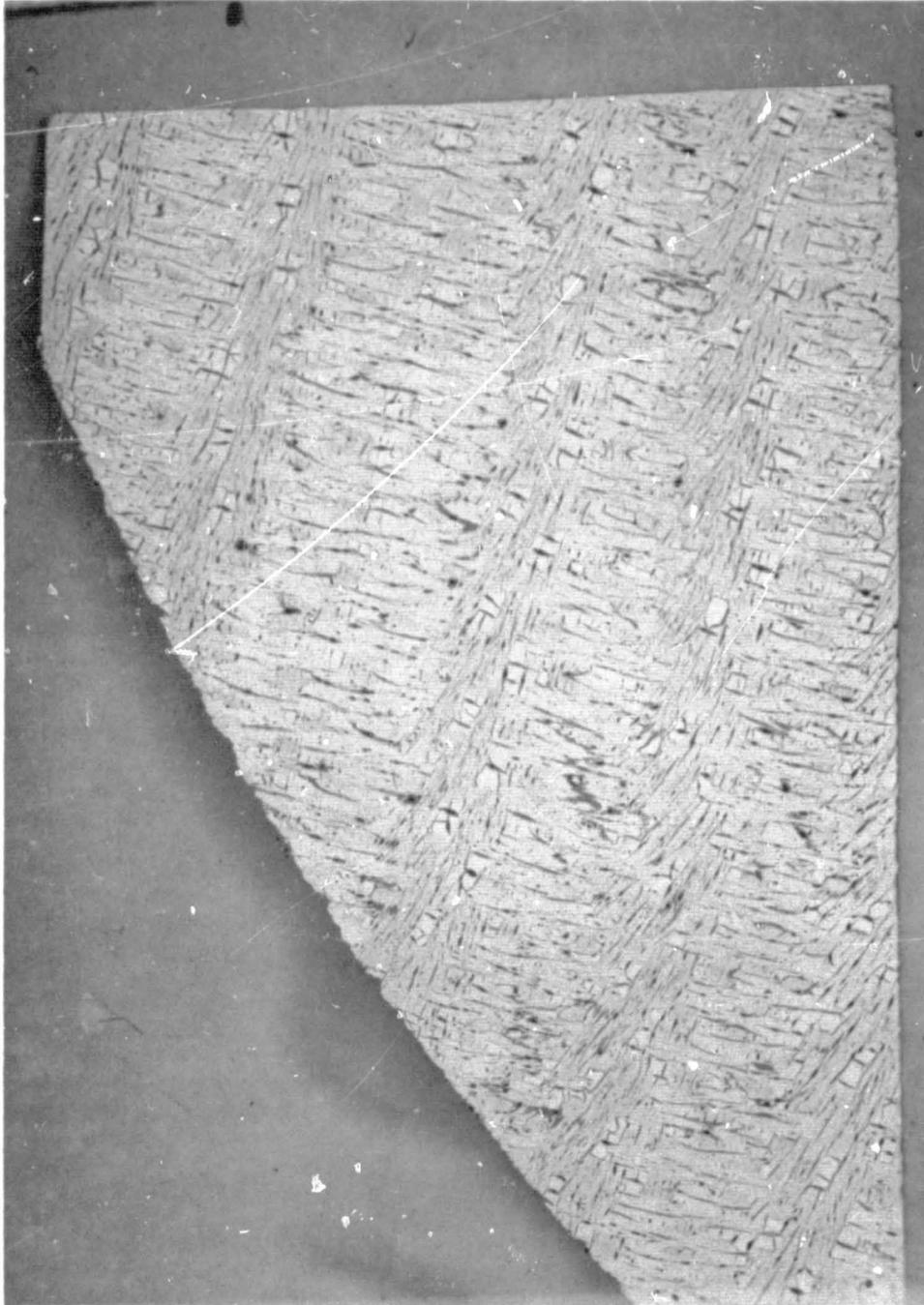
Figure 21   3000°F OVEN-CHARRED GRAPHITE-PHENOLIC MX4501 CORING
(5X MAGNIFICATION)
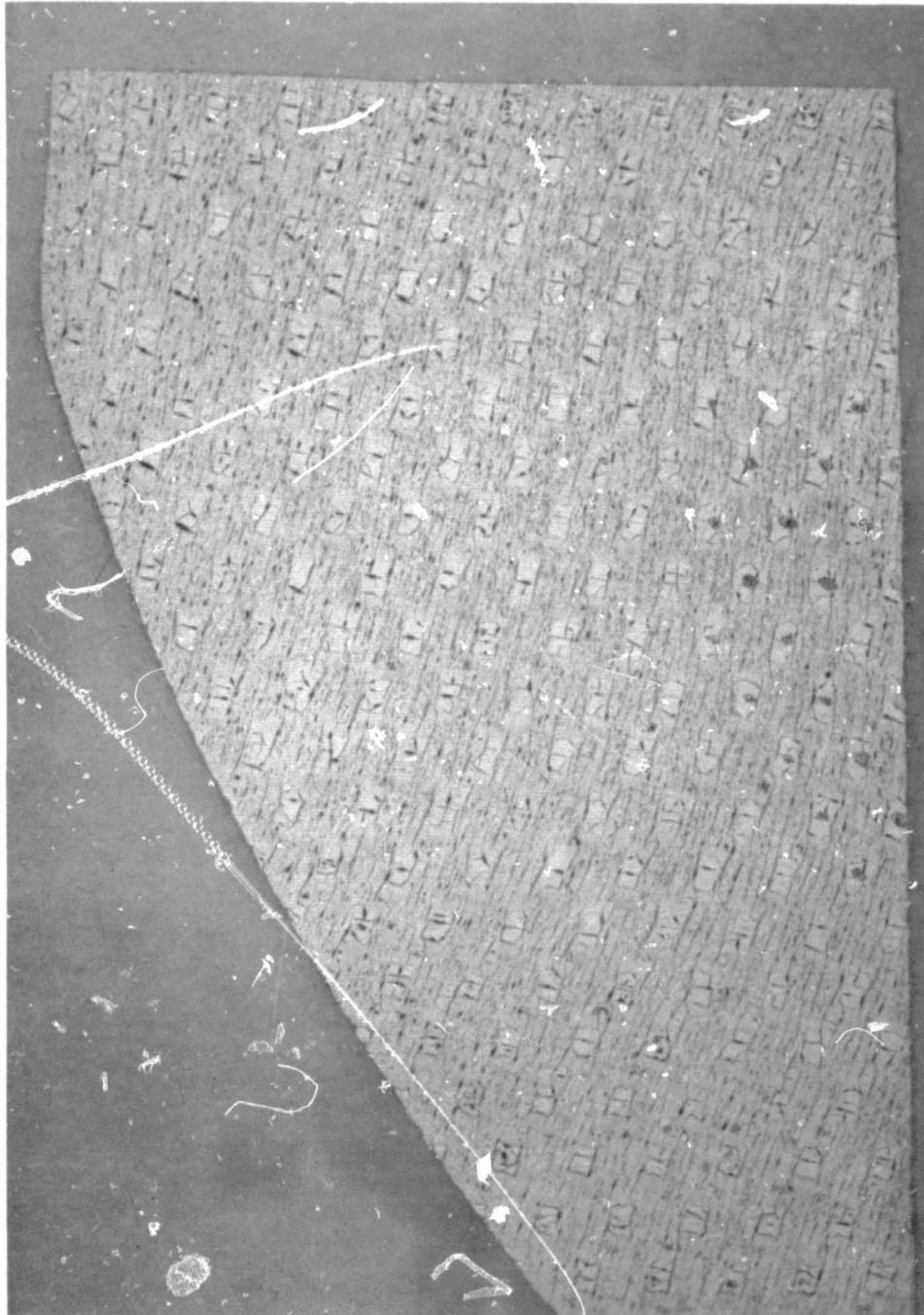
Figure 22  3650°F OVEN-CHARRED GRAPHITE-PHENOLIC MX4501 CORING
(5X MAGNIFICATION)

Figure 23 4000°F OVEN-CHARRED GRAPHITE-PHENOLIC MX4501 CORING
(5X MAGNIFICATION)

Figure 24  1000°F OVEN-CHARRED GRAPHITE-PHENOLIC MX4501 CORING
(500X MAGNIFICATION)
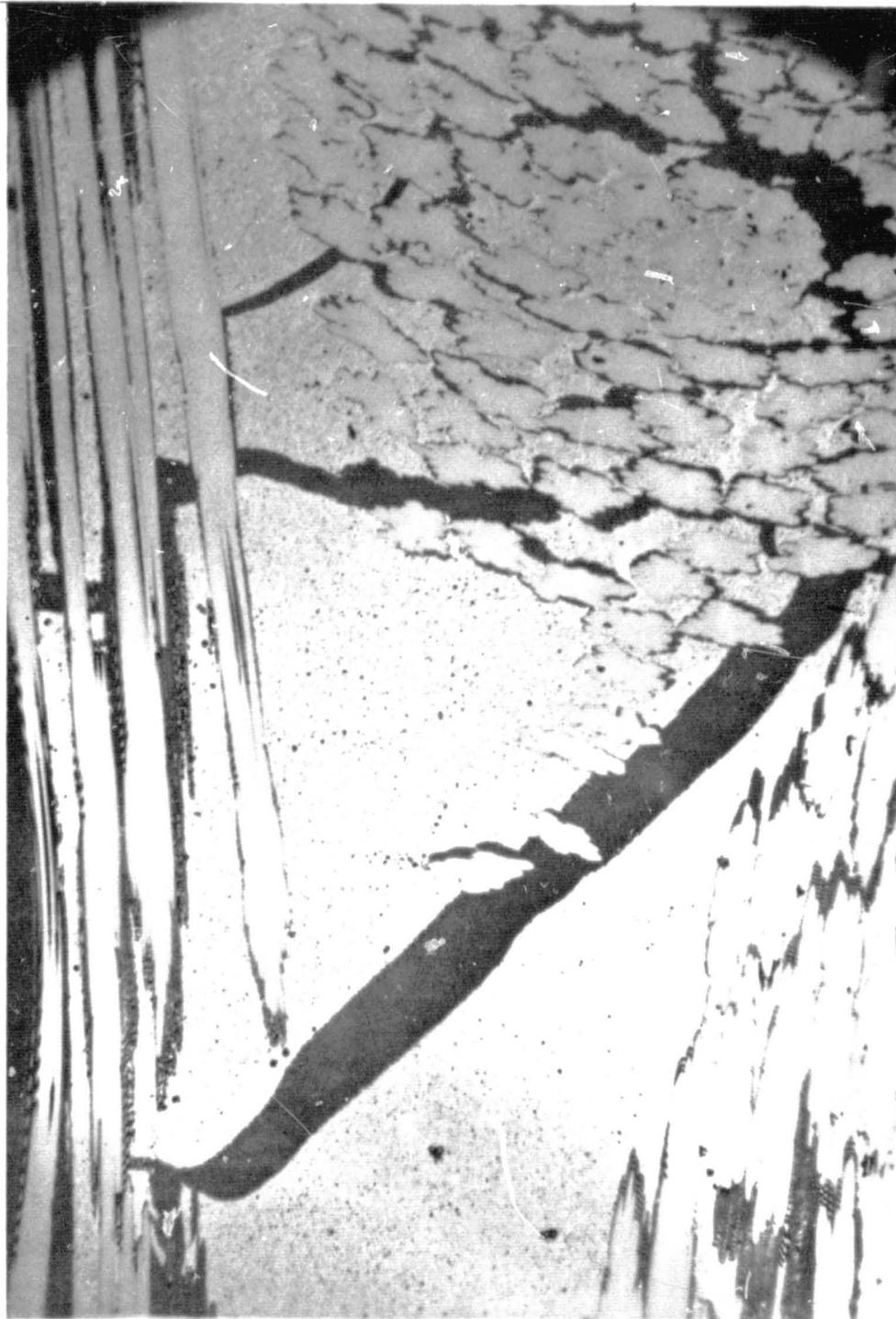
Figure 25  2000°F OVEN-CHARRED GRAPHITE-PHENOLIC MX4501 CORING
(500X MAGNIFICATION)

Figure 26  3000°F OVEN-CHARRED GRAPHITE-PHENOLIC MX4501 CORING
(500X MAGNIFICATION)
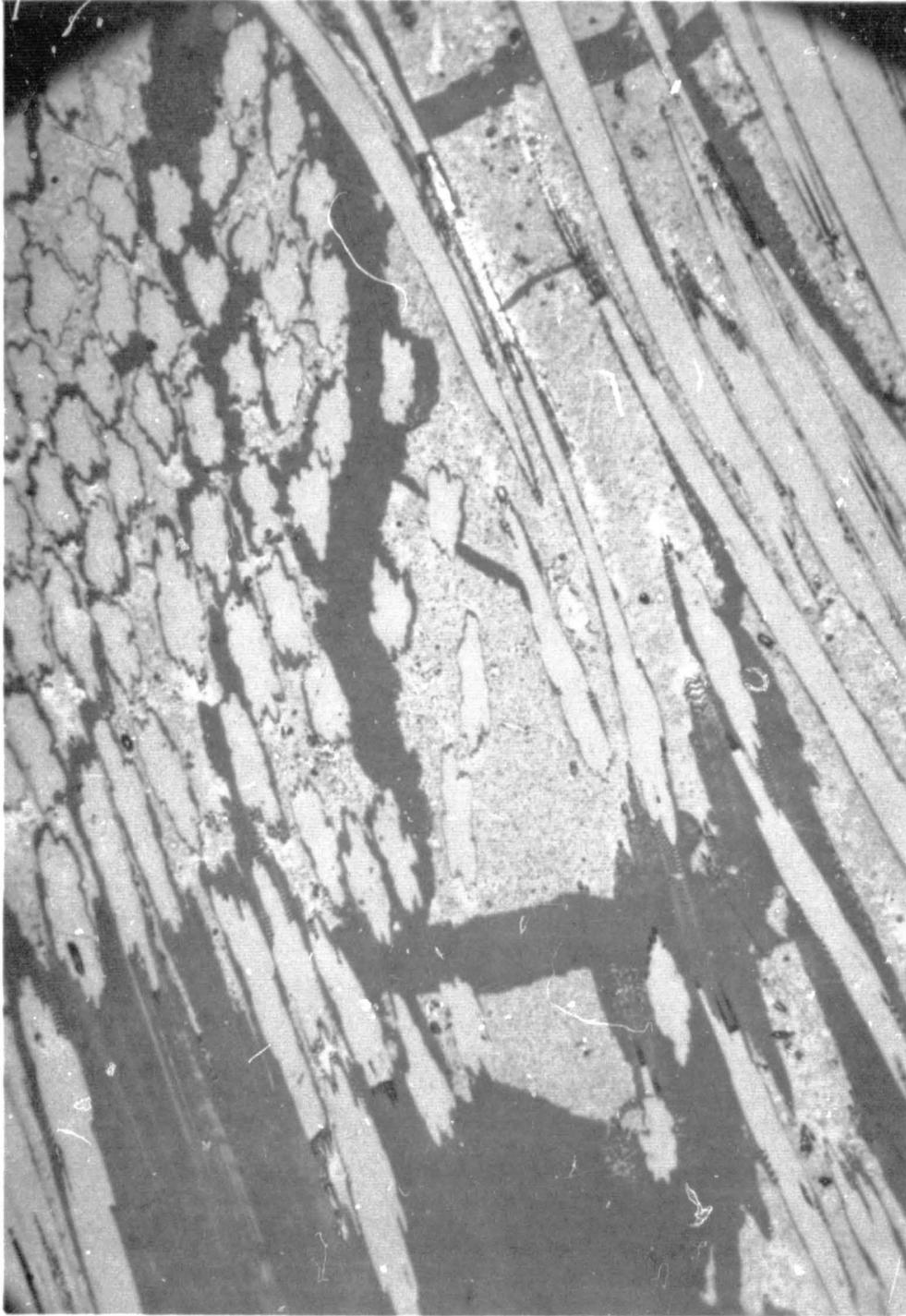
Figure 27  3650°F OVEN-CHARRED GRAPHITE-PHENOLIC MX4501 CORING
(500X MAGNIFICATION)

Figure 28  4000°F OVEN-CHARRED GRAPHITE-PHENOLIC MX4501 CORING
(500X MAGNIFICATION)

3)  Thermal stress cracks occurred in the matrix at all char temperatures.

4)  The graphite fabric material was physically stable at all char temperatures.

5)  No pyrolytic graphite was produced by oven charring of MX4501 material to 4000°F.

6)  A coarse-fine-coarse transition in the phenolic matrix texture occurred over the 1000° to 4000°F char temperatures with the finest texture occurring at 3000°F.

7)  The increase in matrix coarseness was most likely attributable to carbon crystal growth.

d.  Physical and Chemical Property Determinations

1)  Physical and Chemical Properties of Virgin Materials and Oven Reference Chars -- The degree of cure, density, porosity, and chemical composition including trace metals was obtained for the virgin silica-phenolic and the virgin graphite-phenolic materials.  These are given in Table III.  The carbon content of the resin alone could not be determined directly for the graphite-phenolic composite and was calculated under the assumption that the ratio of carbon and hydrogen is the same in both materials.

Table III contains density, porosity, and chemical composition including trace metals for all but one of the oven reference chars prepared from the virgin silica-phenolic material.  A 2400°F char was prepared later in the program for X-ray diffraction analysis to determine whether silicon carbide formation would occur between the charring temperatures of 2000° and 2700°F.  Included in Table IV are the following data for oven reference chars prepared from virgin graphite-phenolic material:  density, porosity, percent graphite filler, and hydrogen content.

The results in Table IV, in particular the resin content, density, and porosity, reflect for the most part the changes one would anticipate when filled phenolic resins were exposed to high temperatures in an inert atmosphere, and illustrate the density-char temperature relationships for the silica-phenolic and graphite-phenolic materials.  Porosity-char temperature functions are shown in Figures 29 through 32.

The apparent increase in concentration of sodium, potassium, and titanium found in the silica-phenolic oven chars was not expected.  It was felt that metal concentrations might decrease with increasing charring temperature and possibly provide a useful temperature indicator with which to establish char temperature profiles.  The apparent increased concentrations of these metals over the virgin sample may simply reflect a variation throughout the billet, from which the samples were taken, because the sample used as virgin was taken from a different location than were the reference chars.  For this reason, the results are inconclusive.  Another exception was noted, namely, the density, porosity, residues and carbon

-39-

## TABLE III

## COMPOSITION DATA OF VIRGIN MATERIALS

|  | Silica-Phenolic | Graphite-Phenolic |
|---|---|---|
| Degree of Cure | 99.1 | 99.2 |
| Density, $lb/ft^3$ | 101.8 | 83.8 |
| Porosity, percent | 1.1 | 4.8 |
| Resin Content, Wt. percent | 37.4 | 44 |
| Reinforcement, Wt. percent | 62.6 | 56 |
| Resin Composition |  |  |
|     Carbon, Wt. percent | 26.6 | [a]31.4 |
|     Hydrogen, Wt. percent | 2.2 | 2.6 |
|     Nitrogen, Wt. percent | 0.0 | 0.0 |
|     Oxygen, Wt. percent | [b]8.6 | [b]10.0 |
| Reinforcement Composition |  |  |
|     $SiO_2$, Wt. percent | 99.1 | — |
|     Al ppm | 2400 | — |
|     Ca ppm | 2 | 48 |
|     Fe ppm | — | 5 |
|     K ppm | 5 | <1 |
|     Li ppm | 3 | — |
|     Mg ppm | 1 | 9 |
|     Na ppm | 14 | 26 |
|     Ti ppm | 2300 | 7 |

[a]Because of the graphite reinforcement, it is impossible to determine directly the carbon content of the resin alone. The value given is calculated under the assumption that the ratio of carbon and hydrogen is the same in both materials.

[b]By difference.

TABLE IV

COMPOSITION DATA ON OVEN REFERENCE CHARS

| | Silica-Phenolic | | | | Graphite-Phenolic | | | | |
|---|---|---|---|---|---|---|---|---|---|
| | 1000°F | 2000°F | 2700°F | 2800°F | 1000°F | 2000°F | 3000°F | 3650°F | 4000°F |
| Density, lb/ft$^3$ | 91.8 | 94.9 | 63.7 | 71.2 | 73.0 | 55.2 | 54.9 | 52.2 | 40.7 |
| Porosity, percent | 21.6 | 25.8 | 58.4 | 50.0 | 21.7 | 32.6 | 23.5 | 25.4 | 28.2 |
| Residue, Wt. percent | 72.0 | 74.1 | 91.3 | 85.4 | [a]69.0 | [a]71.5 | [a]100 | [a]100 | [a]100 |
| Carbon, Wt. percent | 23.4 | 24.7 | 8.7 | 14.6 | b- | b- | b- | b- | b- |
| Hydrogen, Wt. percent | 1.2 | 0.0 | 0.0 | 0.0 | 1.2 | 0 | 0 | 0 | 0 |
| Nitrogen, Wt. percent | 0.0 | 0.0 | 0.0 | 0.0 | 0.0 | 0.0 | 0.0 | 0.0 | 0.0 |
| [c]Oxygen, Wt. percent | 3.4 | 0.0 | 0.0 | 0.0 | - | - | - | - | - |
| Residue Compositions[d] | | | | | | | | | |
| SiO2 | Present | Present | Present | Present | | | | | |
| SiC | | | Present | Present | | | | | |
| Al ppm | 2400 | 2300 | 2450 | 2400 | | | | | |
| Ca ppm | 2 | 2 | 1 | 2 | | | | | |
| K ppm | 6 | 7 | 7 | 3 | | | | | |
| Li ppm | 2 | 1 | 2 | 2 | | | | | |
| Mg ppm | 1 | 1 | 1 | 1 | | | | | |
| Na ppm | 22 | 33 | 62 | 34 | | | | | |
| Ti ppm | 2700 | 2750 | 2600 | 2600 | | | | | |

[a]Estimated from TGA data.

[b]Because of graphite reinforcement, it is impractical to determine directly the carbon content of the resin alone.

[c]By difference.

[d]These results for graphite-phenolic were not obtained because of funding limitations.
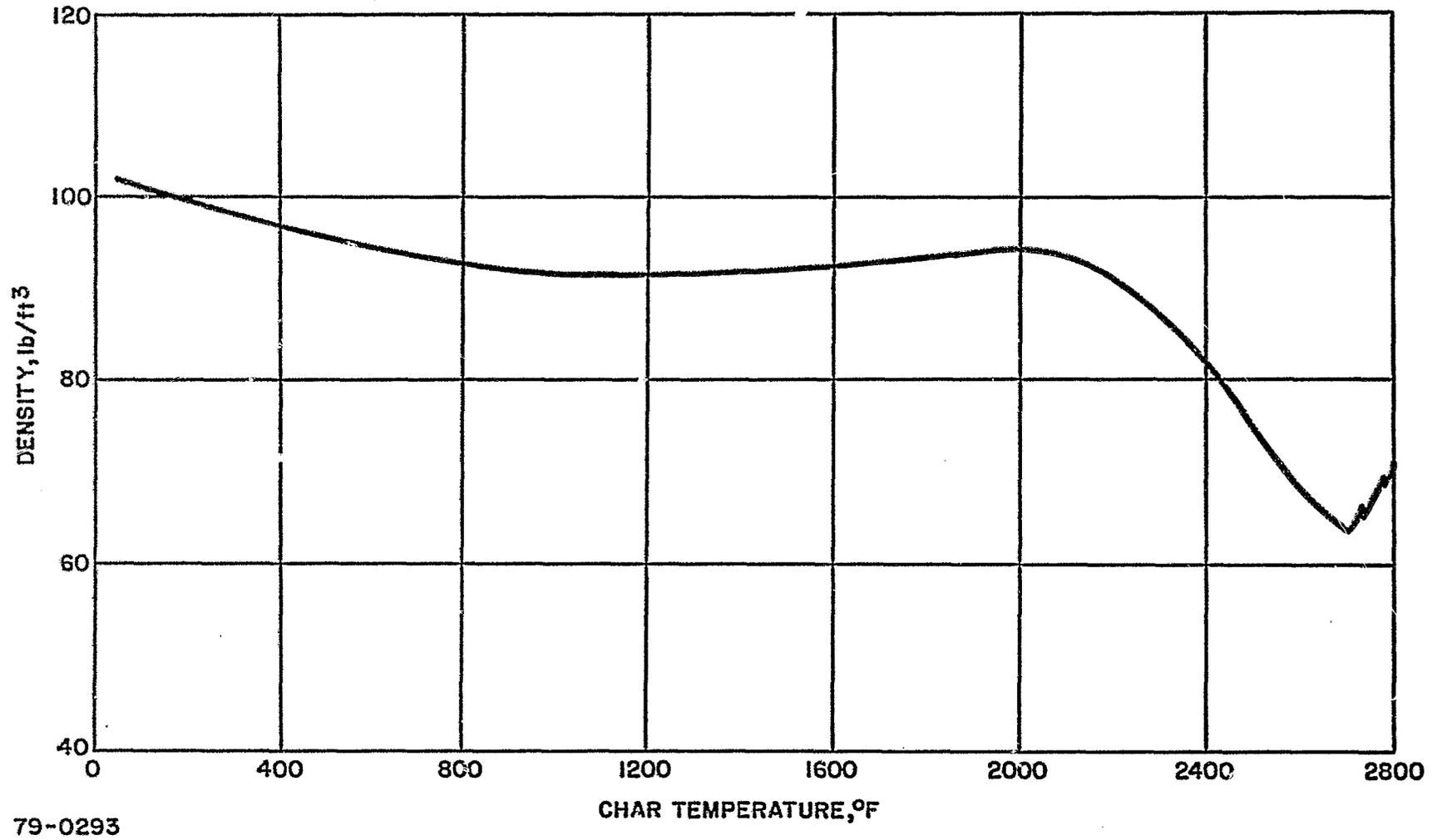
Figure 29  SILICA PHENOLIC MXS-89, DENSITY VERSUS CHAR TEMPERATURE
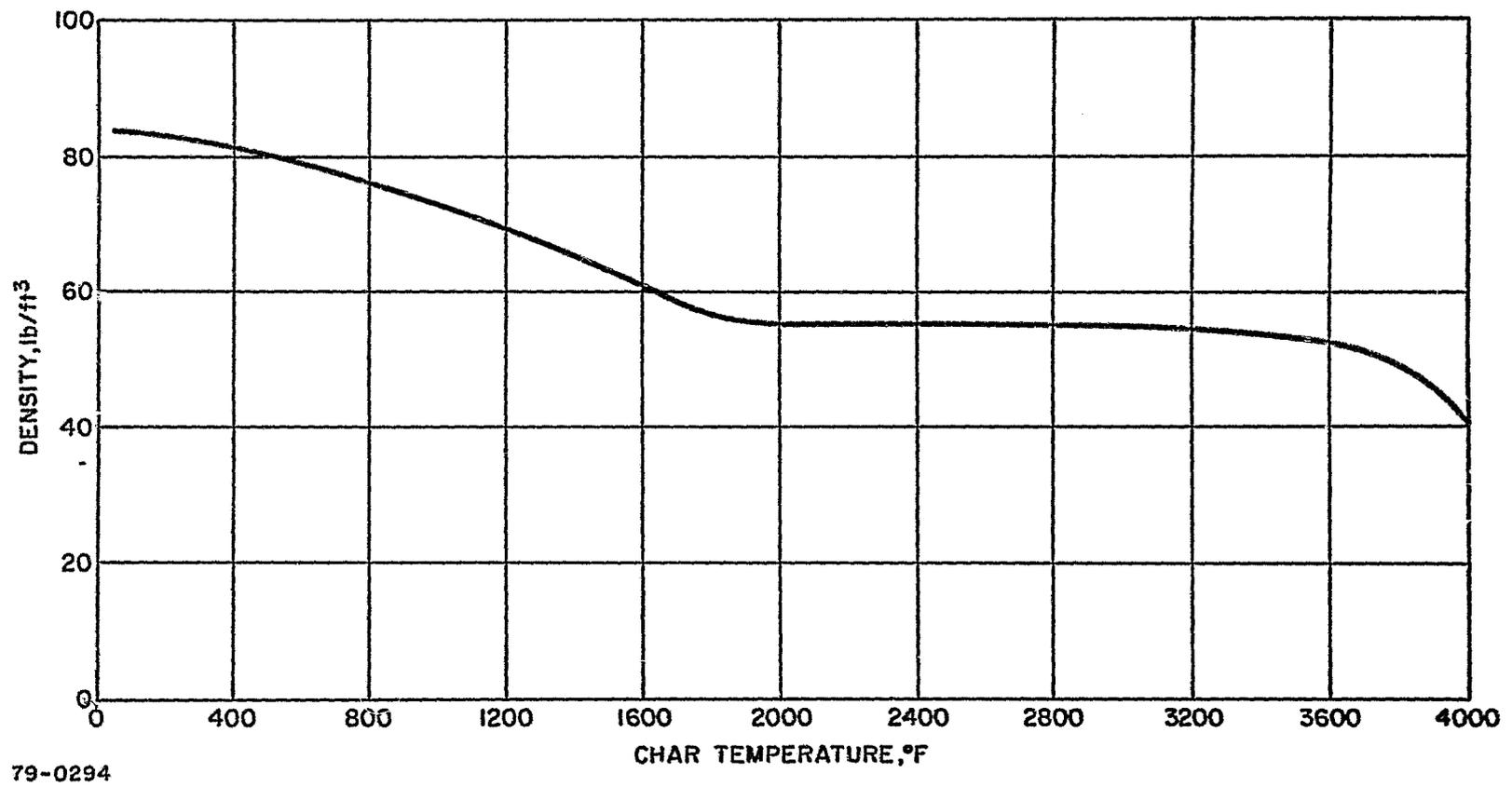
79-0293

Figure 30 GRAPHITE MX4501, DENSITY VERSUS CHAR TEMPERATURE
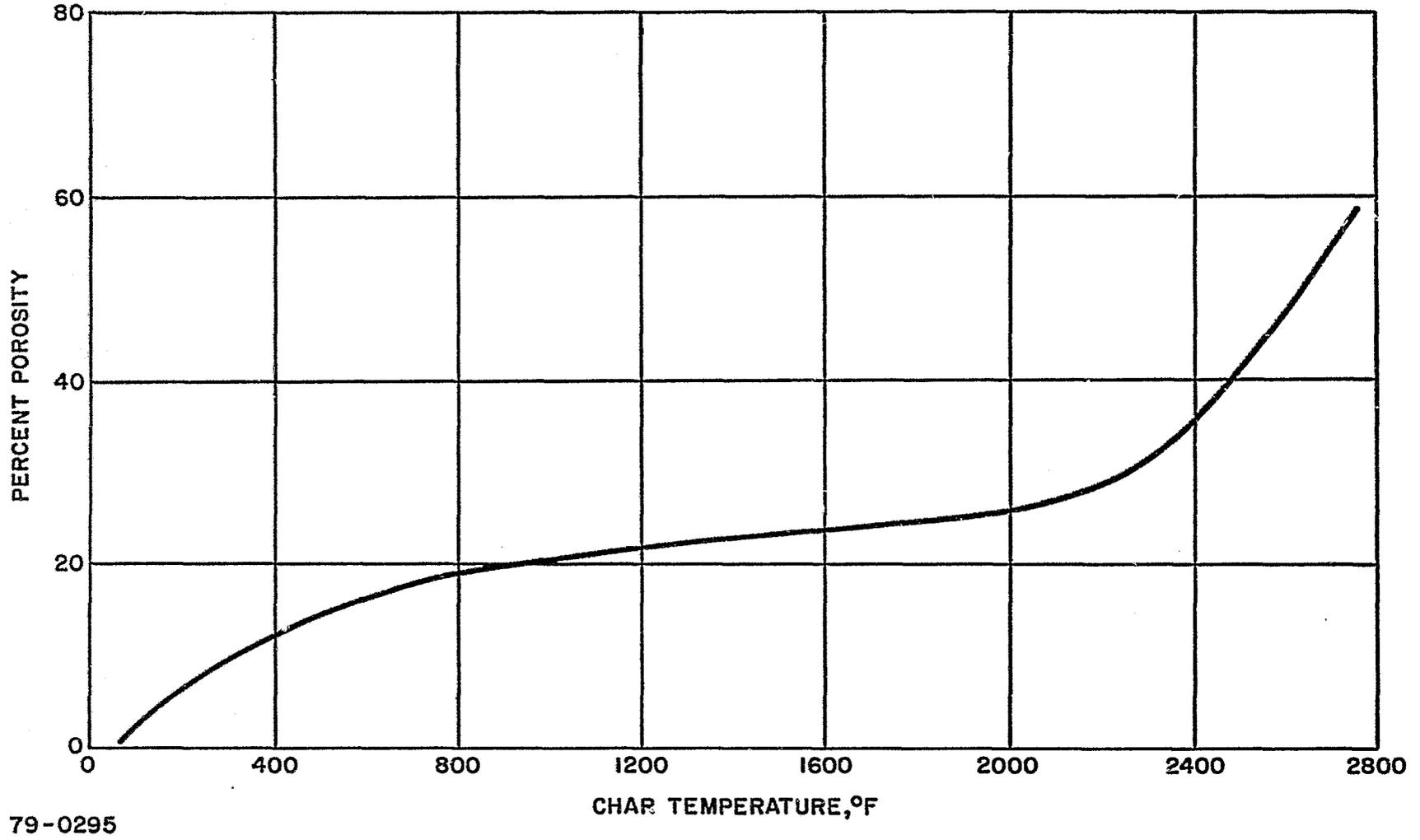
79-0294

Figure 31  SILICA PHENOLIC MXS-89, PERCENT POROSITY VERSUS
CHAR TEMPERATURE
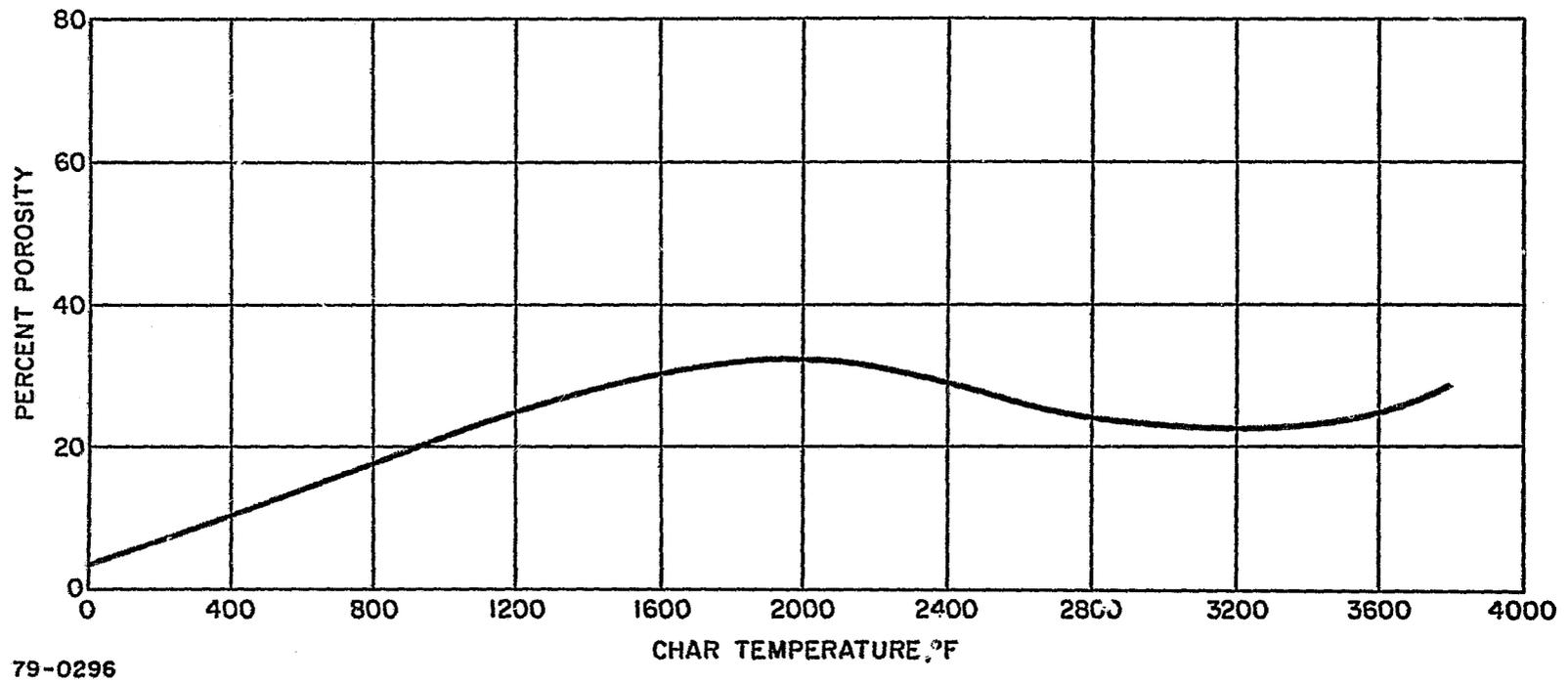
79-0295

Figure 32 GRAPHITE PHENOLIC MX4501, PERCENT POROSITY VERSUS
CHAR TEMPERATURE

79-0296

values determined for the 2800° F silica-phenolic char were not consistent with those for the 2700° F char. It was learned that this difference reflects a shorter "soak" time at temperature experienced by the 2800° F char.

In general, there was good similarity in the effect of temperature on both silica- and graphite-filled chars. To illustrate, both 1000° F char samples dropped to 1.2 percent hydrogen, and all higher temperature chars had no hydrogen. As Table IV shows, the residue values estimated for the 1000° and 2000° F graphite-phenolic chars from TGA data, 69.0 and 71.5 percent, were in good agreement with those values found for the corresponding silica-phenolic chars, 72.0 and 74.1 percent, respectively.

2)  Thermogravimetric Analysis (TGA)

    a)  Virgin Materials -- TGA curves were obtained for both the silica-phenolic and graphite-phenolic materials at heating rates of approximately 9°, 18°, and 36° F per minute in helium and air. These are attached as composite TGA curves in Figures 33 through 36.

A comparison of the curves obtained on heating silica-phenolic and graphite-phenolic in helium indicated that both materials decompose in a similar manner. Pyrolysis studies, discussed below, bear out this observation. Extensive degradation of the phenolic resin occurred in the 750° to 1470° F range with a char yield of slightly greater than 50 percent. Variation of heating rate from 9° to 36° F per minute had little effect on the dynamic weight loss at any one temperature.

It was noted that there was a (slightly) lower content of material volatilized in the 200° to 570° F range for the graphite-phenolic. This difference is attributed to the way the virgin billets from which these samples taken were cured. An NDT survey (Ref. 2) showed that although exposed to the same curing cycle, the silica billet cured from the outside-in whereas the graphite billet was cured from the inside-out. This may be attributed to the difference in thermal conductivity between the two types of fillers: apparently, the higher thermal conductivity of graphite filler allowed heat to reach the center of the billet before curing began. Conversely, the curing reaction in the silica-filled billet may have begun before heat could reach the center. In this case, it is likely that this billet contained small amounts of entrapped water. Further evidence for this was found during pyrolysis studies. At the 1110° F pyrolysis temperature, water was found to comprise 63 mole percent of the volatile products found for the silica-phenolic, whereas for graphite-phenolic, water made up 26 mole percent of the volatile products.

The decomposition of both silica- and graphite-filled phenolic resins appears to have been similar in air, also, as comparison of the curves show. Extensive degradation occurs in the range of 570° to 1290° F. With the graphite-phenolic material, a major difference is the oxidation of the reinforcement which was well under way by 1290° F.

It was noted for both materials that there was a weight gain from 390° to 570° F which is characteristic of phenolic resin degradation
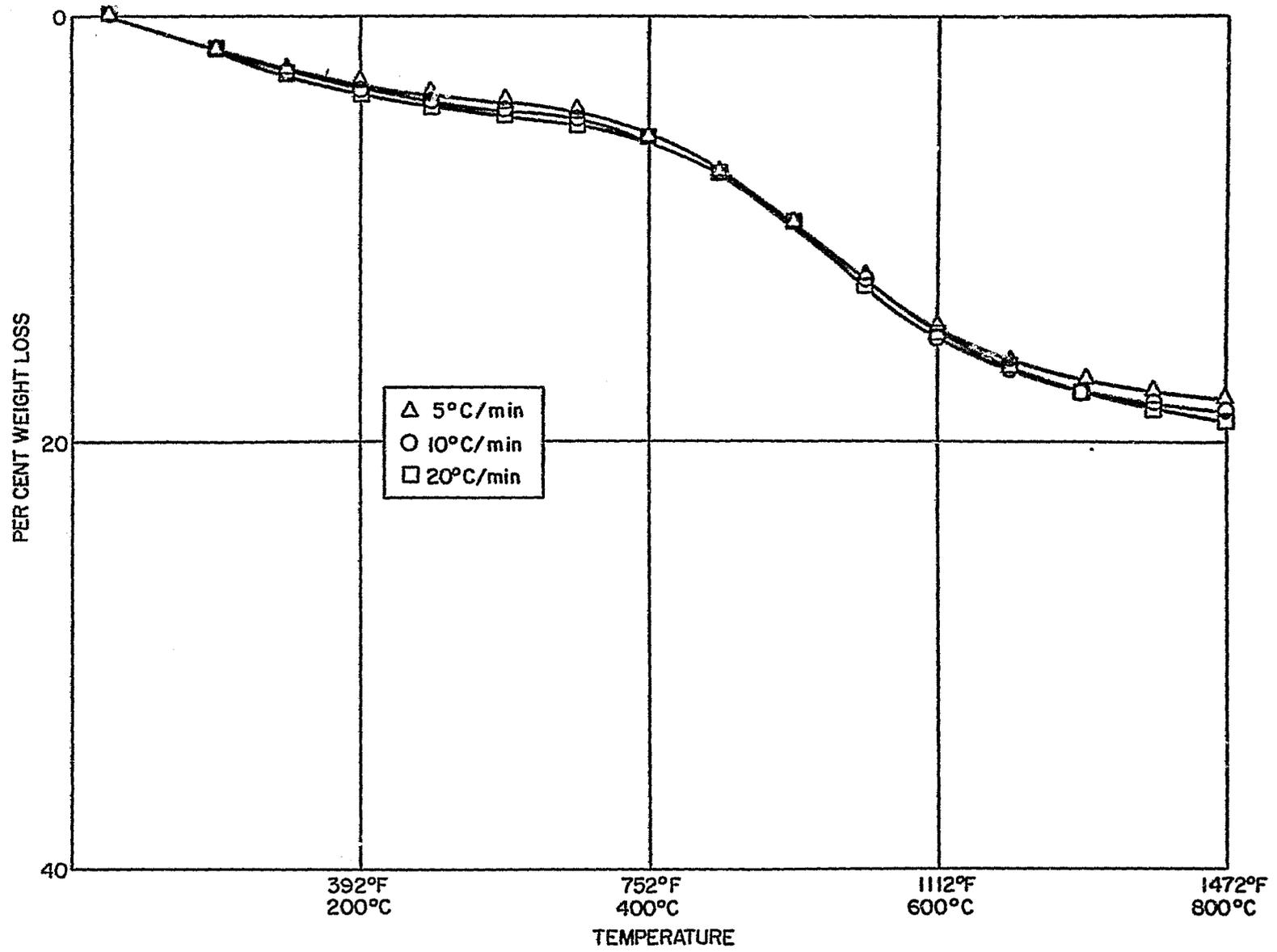
Figure 33  TGA CURVES FOR SILICA-PHENOLIC IN HELIUM
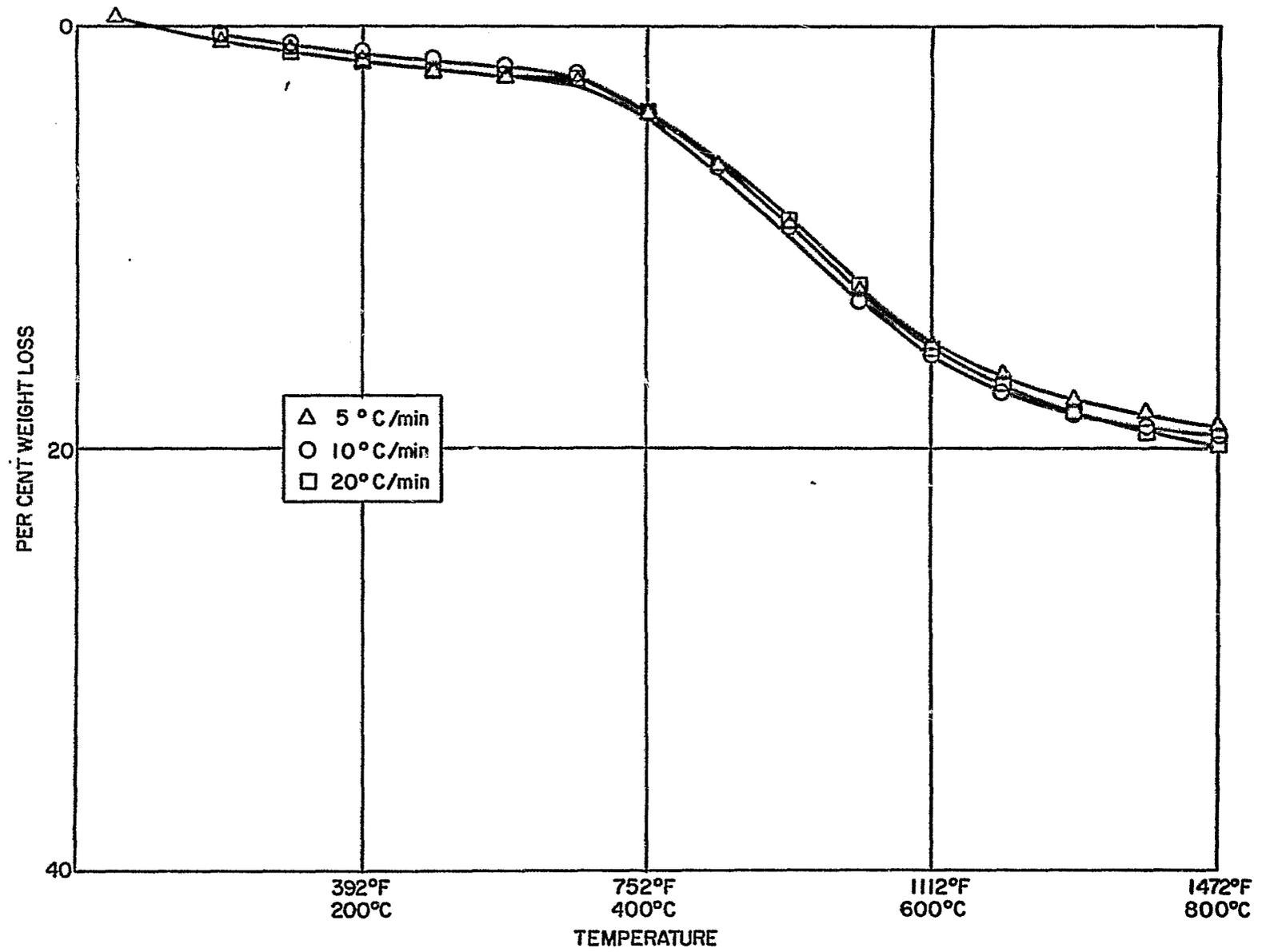
78-1482

Figure 34  TGA CURVES FOR GRAPHITE-PHENOLIC IN HELIUM
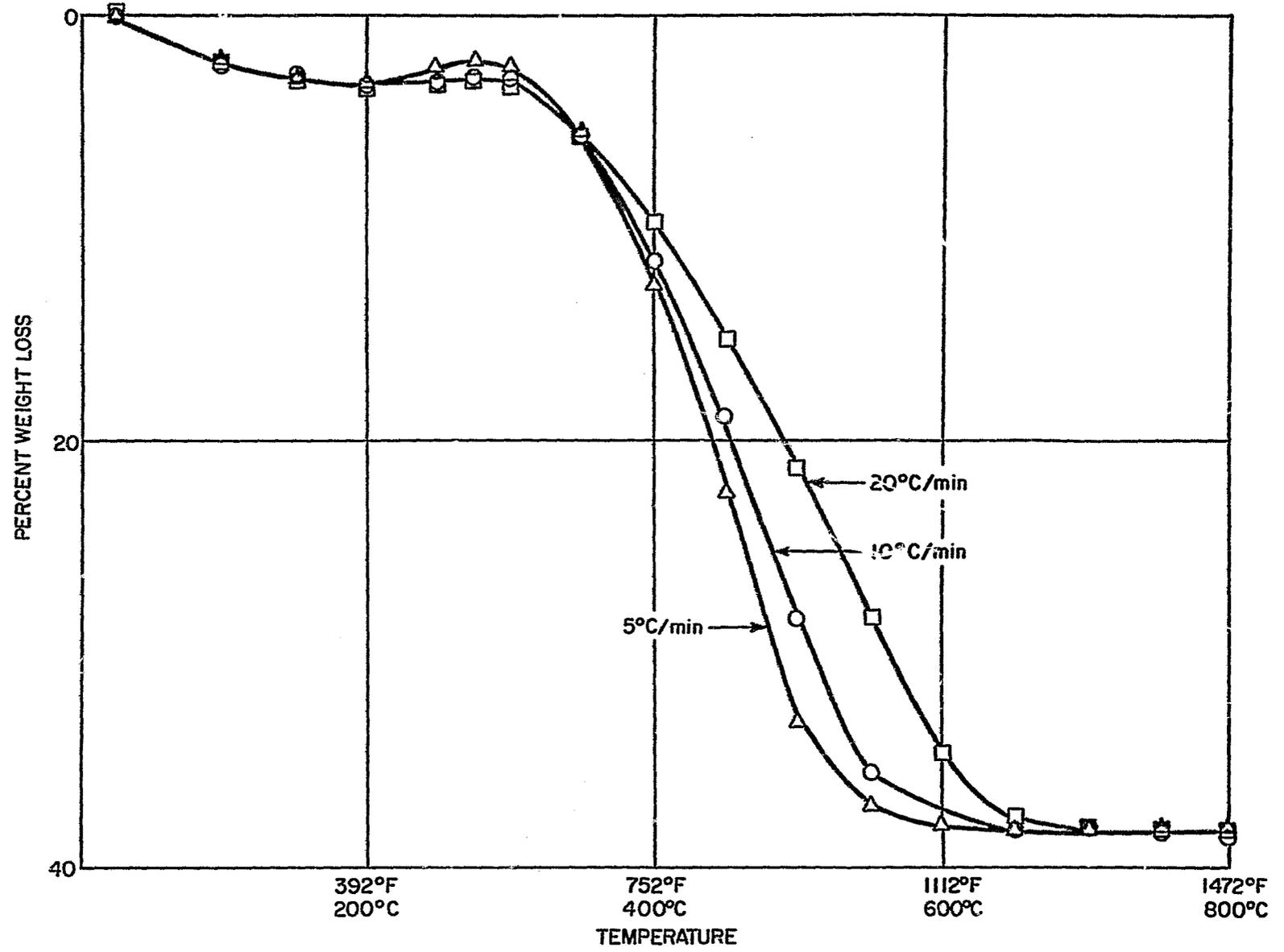
78-1483

78-1484

Figure 35  TGA CURVES FOR SILICA-PHENOLIC IN AIR
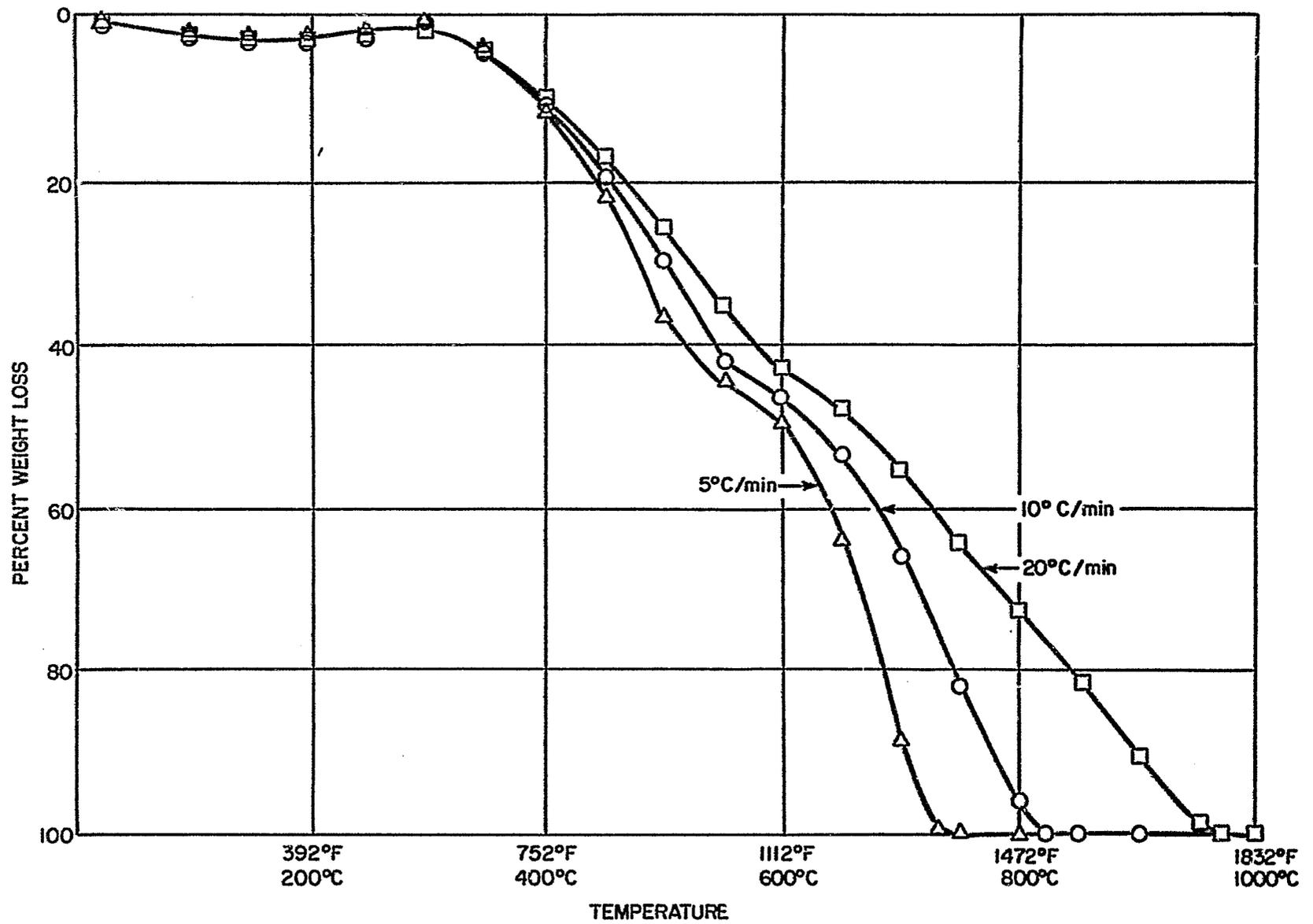
Figure 36 TGA CURVES FOR GRAPHITE-PHENOLIC IN AIR

78-148'

and postulated (Ref. 2) to be due to the oxidation of methylene bridges to form dihydroxybenzophenone linkages,

$$\text{(phenol-CH}_2\text{-phenol)} \xrightarrow{[O]} \text{(phenol-CO-phenol)}$$
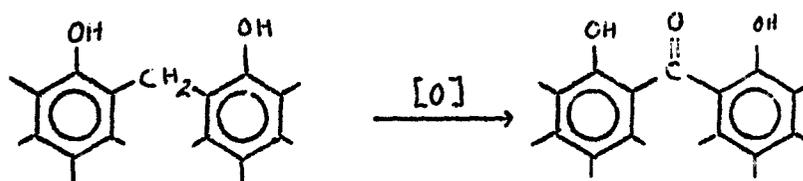
and to the oxidation of methylol groups to acid groups.

$$\text{(phenol-CH}_2\text{OH)} \xrightarrow{[O]} \text{(phenol-COOH)}$$
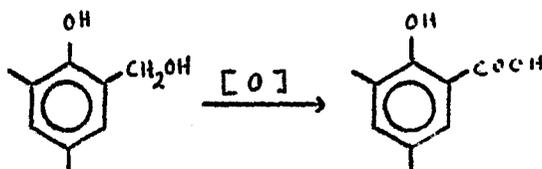
### b) Oven Reference Chars

<u>1 Silica Phenolic</u> -- Four oven chars, 1000°, 2000°, 2700°, and 2800° F, were heated in helium to 1470° F at 18° F per minute to ascertain whether they had picked up moisture or gases during their handling prior to chemical and physical test. The results are shown in Figure 37.

Less than one percent weight loss occurred for each of the 2000°, 2700°, and 2800° F chars, showing that insignificant amounts of moisture and/or absorbed gases were present. The 1000° F char contained about 1.0 percent moisture and lost an additional 3.5 percent which consisted most likely of small amounts of high boiling residues and, above 1000° F, additional resin loss due to charring reactions.

<u>2 Graphite-Phenolic</u> -- Five reference chars, 1000°, 2000°, 3000°, 3650° and 4000° F, were heated in helium at 18° F per minute and in air at 9° F per minute. The tests in helium were conducted for the same reason the silica-phenolic reference chars were run. All chars except the 1000° F lost no weight to 1650° F. The 1000° F char showed no weight loss to 1110° F but lost 2.5 percent between 1100° and 1470° F. The curves are not included.

Figure 38 depicts the TGA curves obtained for these chars in air. These tests were made to ascertain whether the amount of graphite filler remaining in the chars could be determined. As indicated in Figure 36, the curve of graphite-phenolic heated in air at 9° and 18° F per minute exhibits a distinct change in slope at about 1020° F. This change implies the onset of oxidation of the graphite filler. At this point, the loss in weight reflects closely the resin content determined by another method.

As Figure 38 shows, similar slope changes were observed for the 1000° and 2000° F chars. These changes corresponded to a graphite content of 69.0 and 71.5 percent, respectively. Curves obtained for the other chars indicate only graphite to be present. For this reason, it was interesting to note that the higher the char preparation temperature, the higher the temperature required to initiate oxidation of the graphite.

The increased oxidation resistance could be due to an increase in the crystallinity of the carbon deposited on the graphite by the degrading resin during char preparation. Increased oxidation resistance could result also from the removal of impurities in the graphite filler by volatilization or other reactions taking place during char preparation.
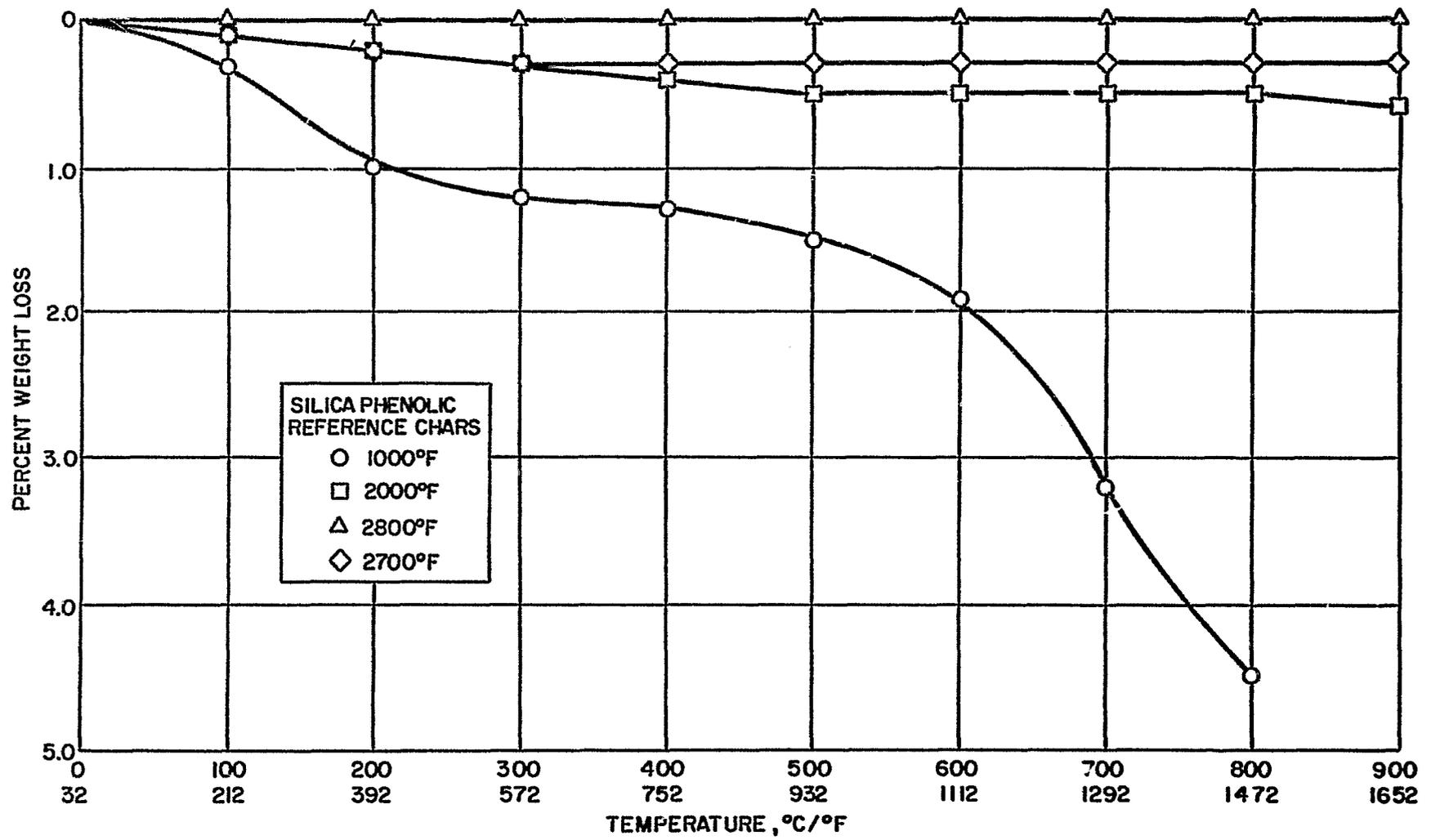
Figure 37 TGA IN HELIUM AT 10° C/MIN -- SILICA-PHENOLIC REFERENCE CHARS
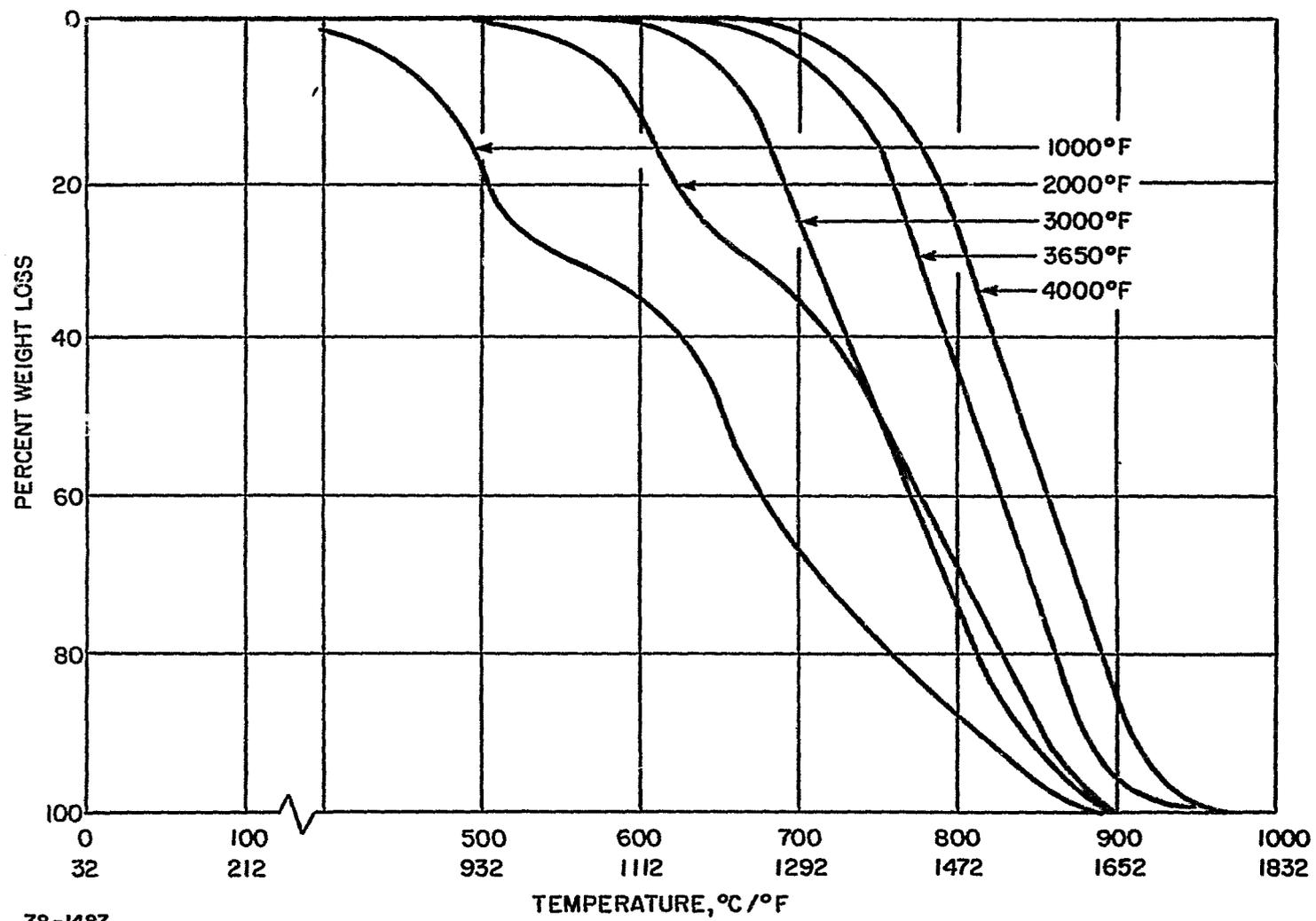
78-1486

Figure 38 GRAPHITE PHENOLIC THERMOGRAVIMETRIC ANALYSIS IN AIR
AT 5° C/MIN

78-1487

3) <u>Pyrolysis Studies</u> -- Table V gives the volatile product distribution from the pyrolyses of both materials at 1110°, 1470°, and 1830°F. Included for each composite are 1) total weight of recovered pyrolysis products (as weight-percent of resin); 2) the measured weight loss (as weight-percent of the resin); and 3) the mole percent of each product based on the total moles of volatile products.

Figures 39 through 42 more clearly illustrate the data in Table IV by showing the effect of temperature on the distribution of hydrogen, carbon monoxide, water, and hydroxyl-containing aromatics. (A new sample was pyrolyzed for each temperature studied.) Figure 39 shows the weight percents of these products versus pyrolysis temperature for both composites. Figures 40 and 41 show mole percent of the products versus temperature for silica-phenolic and graphite-phenolic, respectively. Figure 42 shows the moles of volatile products yeilded by 100 grams of composite.

For both composites the agreement between the measured resin weight-percent loss and the total sum of the individual products identified and measured is very good at 1832°F (58.9 versus 59.6 percent for silica-phenolic and 57.9 versus 59.5 percent for graphite-phenolic), and then becomes more divergent at the lower temperatures. The inability to account for all decomposition products at the lower pyrolysis temperatures would be compatible with an assumption of the formation of a greater proportion of nonvolatile tarry material, consisting of low-molecular weight, partially-degraded resin and high-boiling polynuclear hydrocarbon, which most likely condenses at the inlet of the gas chromatographic column.

Figures 39 through 42 show that the overall distribution patterns are similar for both materials, but several differences are apparent in the levels of the product distribution curves. The amount of water produced at each temperature is greater for the silica-phenolic material. This is strikingly evident at 1110°F where water is 63 mole percent of the volatile products (Figure 41). An NDT survey (Ref. 2) of both composites used in this study showed that the silica-reinforced billet cured from the outside-in whereas the graphite-phenolic billet cured from the inside-out. The difference in curing may be attributed to the difference in thermal conductivity between the graphite- and silica-fabric fillers. Apparently when the graphite-phenolic billet was being heated at the curing temperature, the higher thermal conductivity of the graphite filler allowed heat to reach the center of the billet before curing began. Conversely, the curing reaction may have begun in the silica-filled billet before heat could be conducted to the center. Probably, therefore, the silica material contained entrapped water. Thermogravimetric analysis (Figures 33 through 36) has shown that the silica-phenolic composite loses more weight in the room temperature to 660°F range than the graphite-filled material does.

The amount of carbon monoxide and hydroxyl-containing aromatic compounds, phenol, o-cresol, etc. is higher at each temperature for the graphite-reinforced phenolic. This may imply that more energy can be utilized by this material to break the resin into smaller fragments because no energy is consumed in the volatilization of entrapped water.

-54-

## TABLE V

### PRODUCT DISTRIBUTION FROM DECOMPOSITION OF PHENOLIC RESIN AT VARIOUS TEMPERATURES

| Product Distribution | Silica Reinforcement | | | | | | Graphite Reinforcement | | | | | |
|---|---|---|---|---|---|---|---|---|---|---|---|---|
| | 1110° | | 1470° F | | 1830° F | | 1110° F | | 1470° F | | 1830°F | |
| | Weight (percent) | Mole (percent) | Weight (percent) | Mole (percent) | Weight (percent) | Mole (percent) | Weight (percent) | Mole (percent) | Weight (percent) | Mole (percent) | Weight (percent) | Mole (percent) |
| Ethanol | 0.52 | 0.87 | 0 | 0 | 0 | 0 | 1.42 | 2.37 | 0 | 0 | 0 | 0 |
| 2-Propanol | 0.66 | 0.84 | 0 | 0 | 0 | 0 | 0.70 | 0.89 | 0 | 0 | 0 | 0 |
| Benzene | 0 | 0 | 2.44 | 0.91 | 4.52 | 1.32 | 0 | 0 | 2.60 | 1.04 | 5.42 | 1.84 |
| Toluene | 0.29 | 0.24 | 1.80 | 0.57 | 0.06 | 0.01 | 0.20 | 0.17 | 1.72 | 0.58 | 0.09 | 0.02 |
| m-Xylene | 0.24 | 0.17 | 0.55 | 0.15 | 0 | 0 | 0.21 | 0.15 | 0.48 | 0.14 | 0 | 0 |
| Benzaldehyde | 0 | 0 | 0.10 | 0.03 | 0 | 0 | 0 | 0 | 0.12 | 0.04 | 0 | 0 |
| Phenol | 3.01 | 2.45 | 3.68 | 1.14 | 0 | 0 | 5.86 | 4.80 | 5.61 | 1.86 | 0 | 0 |
| o-Cresol | 3.37 | 2.39 | 1.17 | 0.31 | 0 | 0 | 4.37 | 3.13 | 1.29 | 0.37 | 0 | 0 |
| 2,6 Dimethylphenol | 0.82 | 0.52 | 0.08 | 0.02 | 0 | 0 | 0.85 | 0.54 | 0.08 | 0.02 | 0 | 0 |
| m- and p-Cresol | 1.96 | 1.39 | 0.92 | 0.25 | 0 | 0 | 3.24 | 2.31 | 1.20 | 0.35 | 0 | 0 |
| 2,4 Dimethylphenol | 1.37 | 0.86 | 0.18 | 0.04 | 0 | 0 | 2.00 | 1.26 | 0.20 | 0.05 | 0 | 0 |
| 2,3 and 3,5 Dimethylphenol | 0.18 | 0.11 | 0 | 0 | 0 | 0 | 0.18 | 0.11 | 0 | 0 | 0 | 0 |
| Napthalene | -- | -- | -- | -- | 1.05 | 0.19 | -- | -- | -- | -- | 1.01 | 0.21 |
| Water | 14.8 | 63.0 | 15.0 | 24.3 | 7.17 | 9.12 | 6.16 | 26.3 | 8.56 | 14.8 | 5.12 | 7.55 |
| Carbon Monoxide | 6.14 | 16.8 | 17.6 | 18.3 | 36.2 | 29.6 | 12.1 | 33.3 | 24.7 | 27.5 | 36.7 | 34.8 |
| Carbon Dioxide | Trace | -- | 1.06 | 0.70 | 1.32 | 0.69 | Trace | -- | 1.47 | 1.04 | 0.87 | 0.53 |
| Methane | 0.96 | 4.60 | 6.14 | 11.2 | 7.15 | 10.2 | 1.46 | 7.02 | 5.61 | 11.0 | 7.04 | 11.7 |
| Hydrogen | 0.08 | 5.75 | 1.45 | 42.1 | 2.13 | 48.8 | 0.23 | 17.7 | 1.32 | 41.2 | 1.63 | 43.3 |
| Total as Weight Percent of Resin | 34.4 | | 52.2 | | 59.6 | | 39.0 | | 55.0 | | 57.9 | |
| Measured Weight Percent of Resin Lost during Pyrolysis | 44.5 | | 56.2 | | 58.9 | | 52.4 | | 58.6 | | 59.1· | |
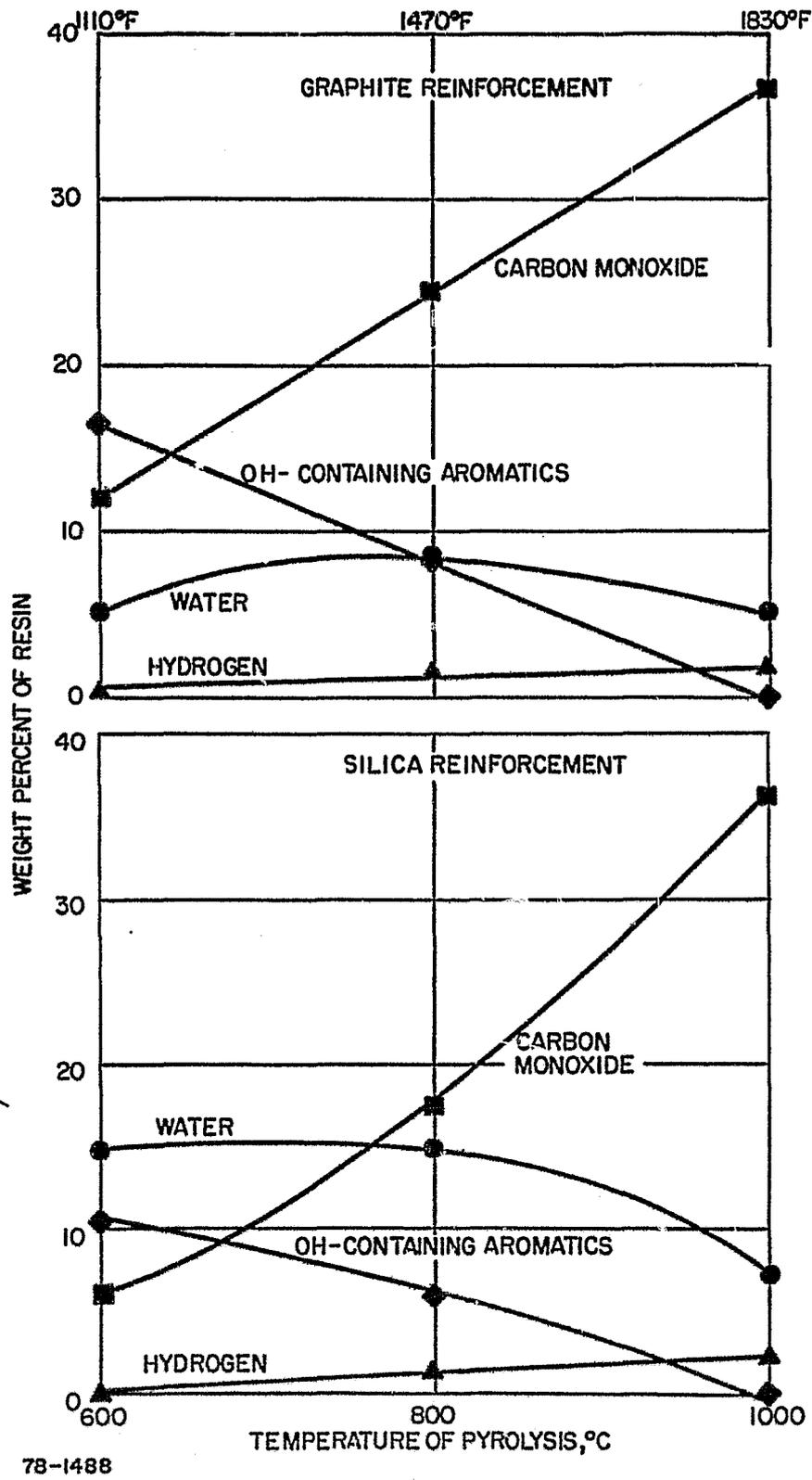
Figure 39 PRODUCT DISTRIBUTION FROM DECOMPOSITION OF PHENOLIC RESIN

78-1488
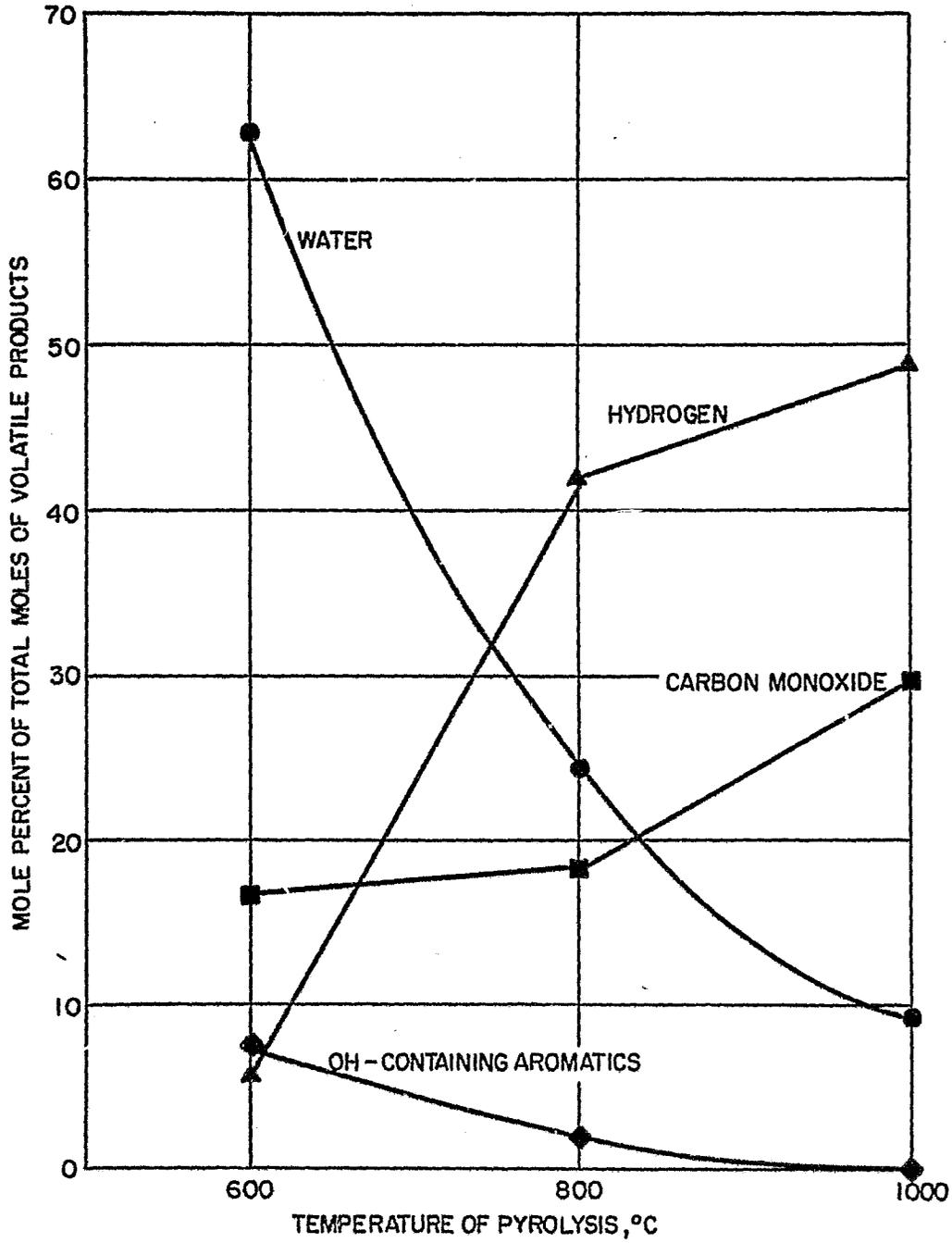
Figure 40 PRODUCT DISTRIBUTION FROM DECOMPOSITION OF SILICA
REINFORCED PHENOLIC RESIN

87-1489
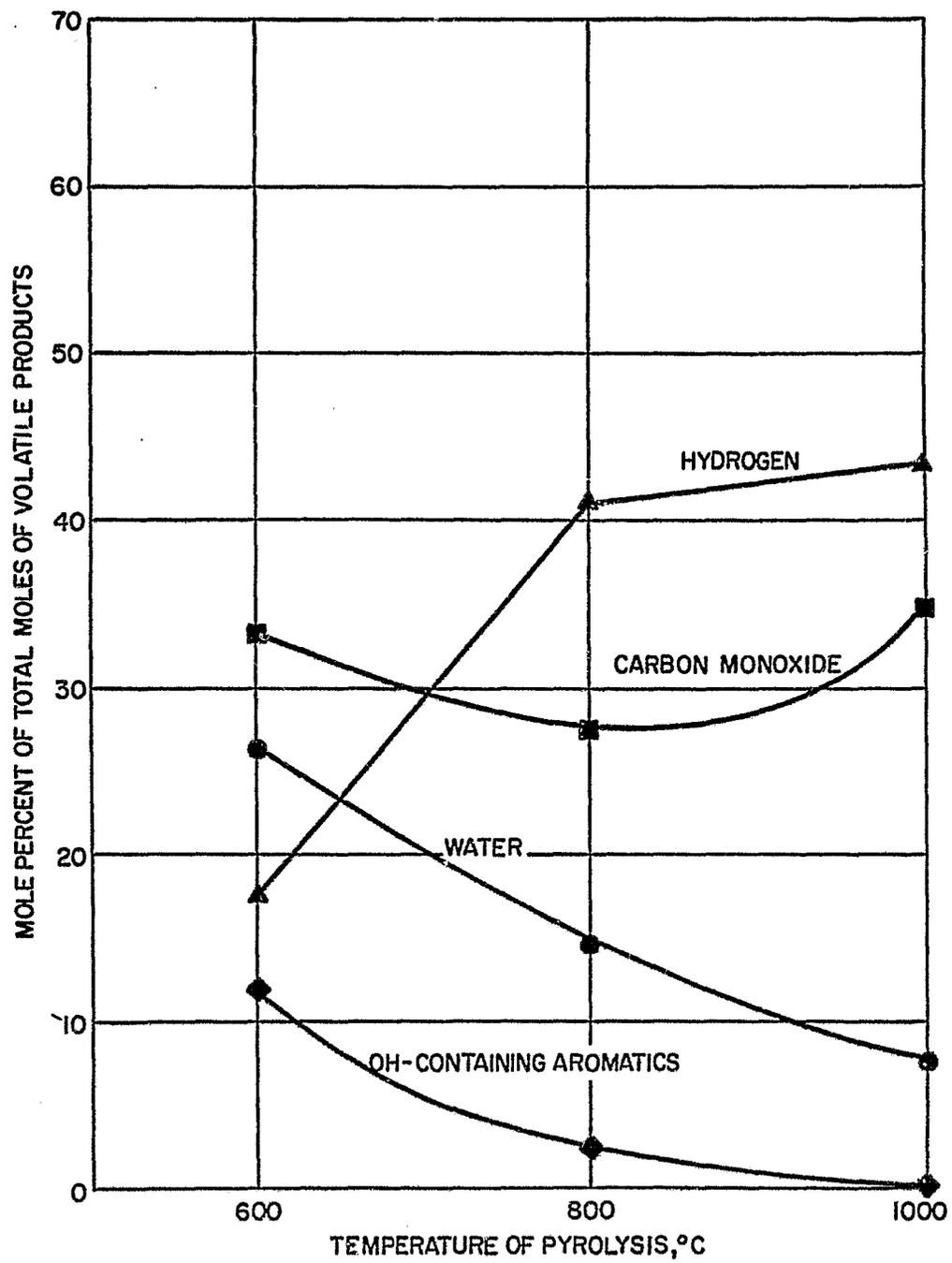
Figure 41  PRODUCT DISTRIBUTION FROM DECOMPOSITION OF GRAPHITE
REINFORCED PHENOLIC RESIN

87-1490
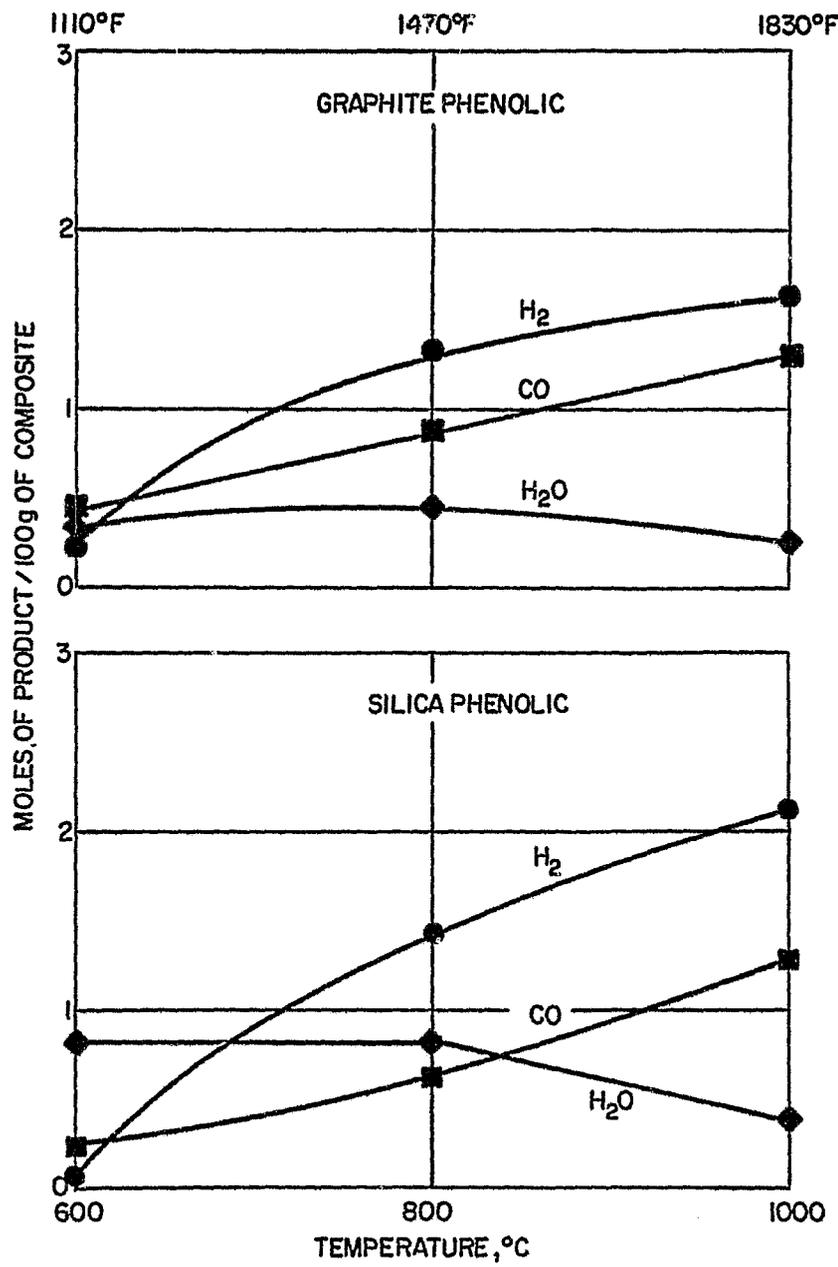
Figure 42  PRODUCT DISTRIBUTION FROM DECOMPOSITION OF REINFORCED
PHENOLIC RESINS

78-1491

For both materials, the amounts of water and hydroxyl-containing aromatics decrease with increasing temperature. Conversely, carbon monoxide and hydrogen production increase rapidly. Over the temperature range studied, both composites undergo two simultaneously occurring reactions: depolymerization and oxidation. At $1110^{\circ}F$, depolymerization predominates as evidenced by the presence of hydroxy-aromatics. However, as Table IV indicates, the weight relationship among these products for the silica-phenolic differs from that for the graphite-phenolic. This is more clearly illustrated by Figure 43 in which typical chromatograms show that the differing weight ratios of the hydroxy-aromatics form a pattern or "fingerprint" unique to the composite being pyrolyzed. This fact suggests that the depolymerization mechanism is different for each composite and depends upon both the type of reinforcement and possibly the manner by which the composite cured. At the higher temperatures, oxidation predominates, the oxygen source being the hydroxyl groups in the original polymer. This is made evident by the complete disappearance of hydroxyl-containing compounds and the increased production of carbon monoxide, carbon dioxide, and benzene.

Table VI shows the distribution of carbon, hydrogen, and oxygen in the $1830^{\circ}F$ pyrolysis products for both composites. The data are presented as a "material balance". For both composites, recovery is essentially complete; i.e., the weight percents of the products plus the char total almost 100 percent. For both composites the amount of oxygen recovered between the products and char is higher than the amount present in the starting materials. Some of this difference may result experimentally from air entering the system as a sample is pushed into the hot zone (see Appendix E). The remainder of the difference is probably due to the fact that oxygen in the starting materials and chars is determined by difference. For the silica-phenolic, the recovered hydrogen value is high also. This is attributed to experimental error although good agreement is obtained in the case of the graphite-phenolic. There is good agreement also for carbon recovery in the silica composite. A similar determination was not possible for the graphite-phenolic char.

It will be noted from Table VI that more than the theoretical oxygen was accounted for in the analysis of the pyrolysis products. This error is attributed to an accumulated error which results both from the use of instrumental methods of analysis having a tolerance of ± 5 percent and from the calculation of oxygen by difference.

4) <u>Optical Properties of Oven-Charred Silica and Graphite-Phenolic</u> — Specimens were prepared from the oven-charred material for optical reflectance measurements in order to test the relationship between char temperature level and total reflectance for use in confirming nozzle char temperature profile postulations. The measurements were conducted on a Beckman Model DK-2 spectrophotometer adapted for use with a magnesium oxide-coated integrating sphere. The principle of operation is given in Appendix B. Data were taken over the wavelength range 0.22 to 2.7 microns. Char temperatures of the test specimens were: silica-phenolic MXS-89- $1000^{\circ}$, $2000^{\circ}$, $2700^{\circ}$, and $2800^{\circ}F$; graphite-phenolic MX 4501 - $1000^{\circ}$, $2000^{\circ}$, $3000^{\circ}$, $3650^{\circ}$ and $4000^{\circ}F$. The virgin materials were measured for reference purposes.
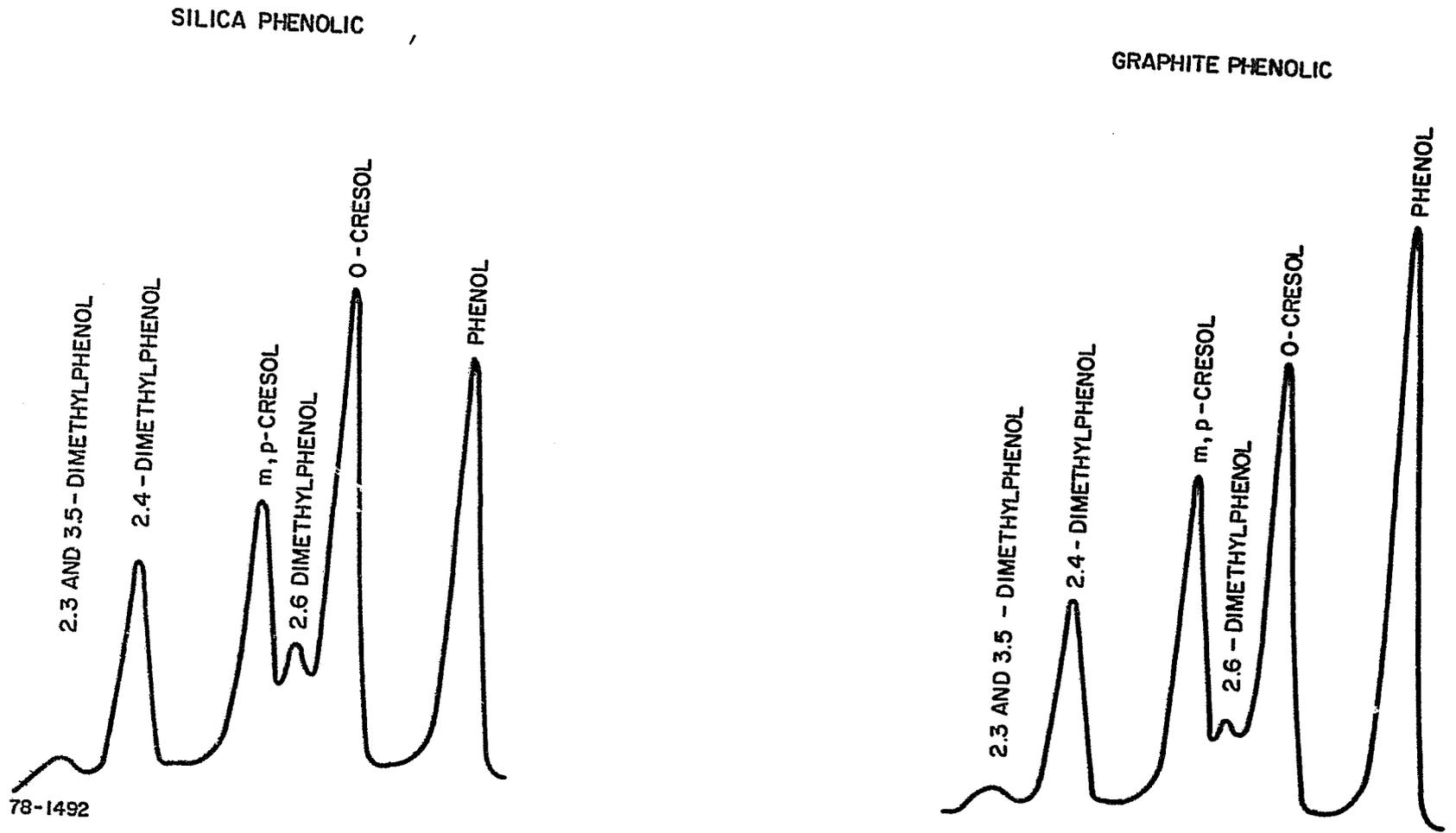
Figure 43  TYPICAL CHROMATOGRAMS OF HYDROXYL-CONTAINING AROMATIC
COMPOUNDS YIELDED BY 600°C PYROLYSIS

## TABLE VI

## DISTRIBUTION OF C, H, O IN 1830°F PYROLYSIS PRODUCTS

| | Silica-Phenolic Weight Percent | | | | | Graphite-Phenolic Weight Percent | | | |
|---|---|---|---|---|---|---|---|---|---|
| | Weight Percent | C | H | O | Ash | Weight Percent | C | H | O |
| Benzene | 1.70 | 1.57 | 0.13 | – | – | 2.38 | 2.20 | 0.18 | – |
| Toluene | 0.02 | 0.016 | 0.004 | – | – | 0.04 | 0.03 | 0.01 | – |
| Napthalene | 0.32 | 0.30 | 0.02 | – | – | 0.44 | 0.41 | 0.03 | – |
| Water | 2.23 | – | 0.25 | 1.98 | – | 1.61 | – | 0.18 | 1.43 |
| Carbon Monoxide | 13.56 | 5.82 | – | 7.74 | – | 16.17 | 6.94 | – | 9.23 |
| Carbon Dioxide | 0.49 | 0.13 | – | 0.36 | – | 0.38 | 0.10 | – | 0.28 |
| Methane | 2.67 | 2.00 | 0.67 | – | – | 3.09 | 2.31 | 0.78 | – |
| Hydrogen | 0.80 | – | 1.60 | – | – | 0.72 | – | 1.44 | – |
| Total | 21.79 | 9.84 | 2.67 | 10.08 | – | 24.83 | 11.99 | 2.62 | 10.94 |
| Char | 77.88 | 17.18 | 0.12 | 2.5 | 80.2 | 74.00 | 97.85 | 0 | 2.15 |
| Total | 99.67 | 27.00 | 2.79 | 12.6 | | 98.83 | | 2.62 | 13.09 |
| Starting Material (Table I) | | 26.6 | 2.2 | 8.6 | | | 31.4 | 2.6 | 10.00 |
| Difference | | +0.4 | +0.6 | +4.0 | | | | 0.0 | +3.1 |

The results of the optical tests, as shown in Figure 44, indicate for the silica-phenolic composite that the major optical sensitivity occurs between the virgin material condition and 1000°F char level. Beyond that temperature only a slight change in reflectance in the near infrared region occurs up to 2000°F and remains virtually unchanged at higher temperature levels. The greatest asset which the optical reflectance technique appears to offer for degradation temperature assessments is from room temperature to near 1000°F. The tests performed on the graphite-phenolic material from virgin to 4000°F char level indicated a rather gross insensitivity between reflectance and char temperature. This technique was determined to be inadequate for use with graphite-phenolic type materials.

Since the reference standard material against which the various total reflectance measurements were made was vapor-deposited magnesium oxide, it is suggested that using the virgin nozzle materials as reference standards (at a critical wavelength) will provide greater sensitivity of measurements at the various char levels and as a result will strengthen the reflectance-temperature relationship.

   5) X-Ray Diffraction Analysis of MXS-89 and MX 4501 Oven Chars -- Using the Debye-Scherer X-ray diffraction analysis technique, both phenolic composites were analyzed for crystal phases present in the material as a result of being subjected to the high charring temperatures. In preparation for the analyses, the various char specimens were removed from the corings and ground to a homogeneous powder. Only 20 to 80 milligrams of each material were required for the X-ray tests, and since the procedure is nondestructive in nature these materials were returned for future use in various other experimental evaluations.

The test results showed the 1000° and 2000°F charred MXS-89 material were quite similar, each yielding X-ray patterns consisting of slightly crystalline carbon and amorphous material such as $SiO_2$ and carbon. Neither char gave any indications of the presence of SiC. In a similar fashion, both the 2700° and 2800°F chars indicated nearly identical X-ray results; i.e., heavy quantities of SiC, slight amounts of alpha crystobalite, and amorphous material such as carbon. Since the transition in SiC content between the 2000°F prechars was very abrupt, an additional coring of the MXS-89 billet was charred at an intermediate temperature of 2400°F. As was expected, an intermediate crystalline state existed consisting of smaller quantities of SiC, some slightly crystalline carbon, slight traces of alpha crystobalite, and amorphous material.

The graphite-phenolic X-ray results were unique in that there was insignificant difference in crystal phases between any of the char specimens regardless of char temperature. The more pertinent observations were scant traces of crystalline carbon, which increased in density (crystallinity) only slightly as a function of char temperature, and amorphous material.

Table VII summarizes the X-ray findings of the two charred materials.

CHAR TEMP: MXS 89:1000,2000,2700,2800°F
MXS 4501:1000,2000,3000,3650,4000°F

MXS 89 VIRGIN

MXS 89 1000°F CHAR

MXS 89:2000,2700,2800°F CHAR

MX4501 ALL CHARS & VIRGIN

REFLECTANCE, percent

WAVELENGTH, microns
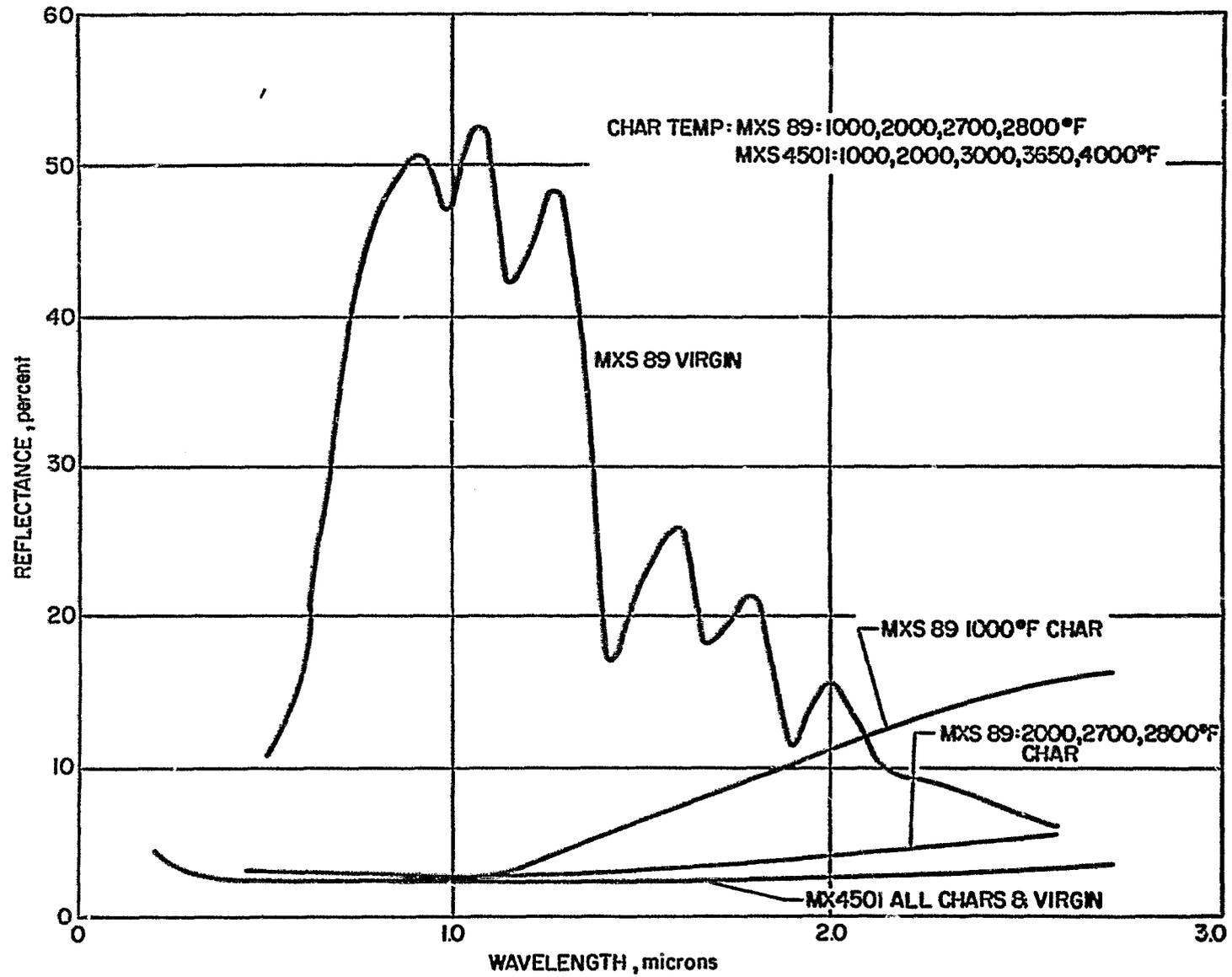
87-1493

Figure 44  SILICA-PHENOLIC MXS-89 AND GRAPHITE-PHENOLIC MX4501
CHAR OPTICAL PROPERTIES

## TABLE VII

### SUMMARY OF X-RAY DIFFRACTION ANALYSIS DATA
### FOR OVEN REFERENCE CHAR RESULTS

| Charring Temperature, (°F) | Silica-Phenolic | Graphite-Phenolic |
|---|---|---|
| 1000 | Amorphous silica and carbon<br>Poorly crystalline carbon | Amorphous carbon-Graphite |
| 2000 | Same as 1000 | Same as 1000°F, but an increase in graphite crystallinity |
| 2400, 2700, and 2800 | Amorphous silica and carbon<br>Poorly crystalline carbon<br>Silicon carbide<br>Alpha-crystobalite | -<br><br>No chars prepared. |
| 3000, 3650, and 4000 | No chars prepared. | Same as before except that degree of graphite crystallinity increases slightly with increasing temperature. |

e.  Thermal Properties Determinations

1) <u>Thermal Conductivity Measurements</u> -- Thermal conductivity measurements of the virgin and charred corings were conducted using the "cut-bar" experimental test method.  This method was selected because of its appropriateness to the post-test analyses of rocket nozzles, both from a limited-materials point of view and thermal conductivity profiling scheme.  This scheme is discussed later in the report.  The cut-bar test method used for oven char series is illustrated in Figure C-5 of Appendix C.  A 1-inch-diameter by 1-inch-long material specimen is placed between two similarly shaped reference standard materials.  Heat is caused to flow one-dimensionally through each of the three cylindrical elements.  Since the thermal properties of the reference standard material are well established, this information, the temperature gradients, and the geometries of the elements are used in the determination of the thermal conductivity of the test material.  A fuller explanation and certification of the test technique is presented in Appendix C.

Figures 45 and 46 show the results obtained from tests on both MXS-89 and MX4501 virgin materials.  These data are also tabulated in Table VIII.  Since these data are presented in a graphical format unique to thermal profiling experiments, and explanation is presented to aid in comparing this information with that obtained from actual nozzle char specimens.

-65-
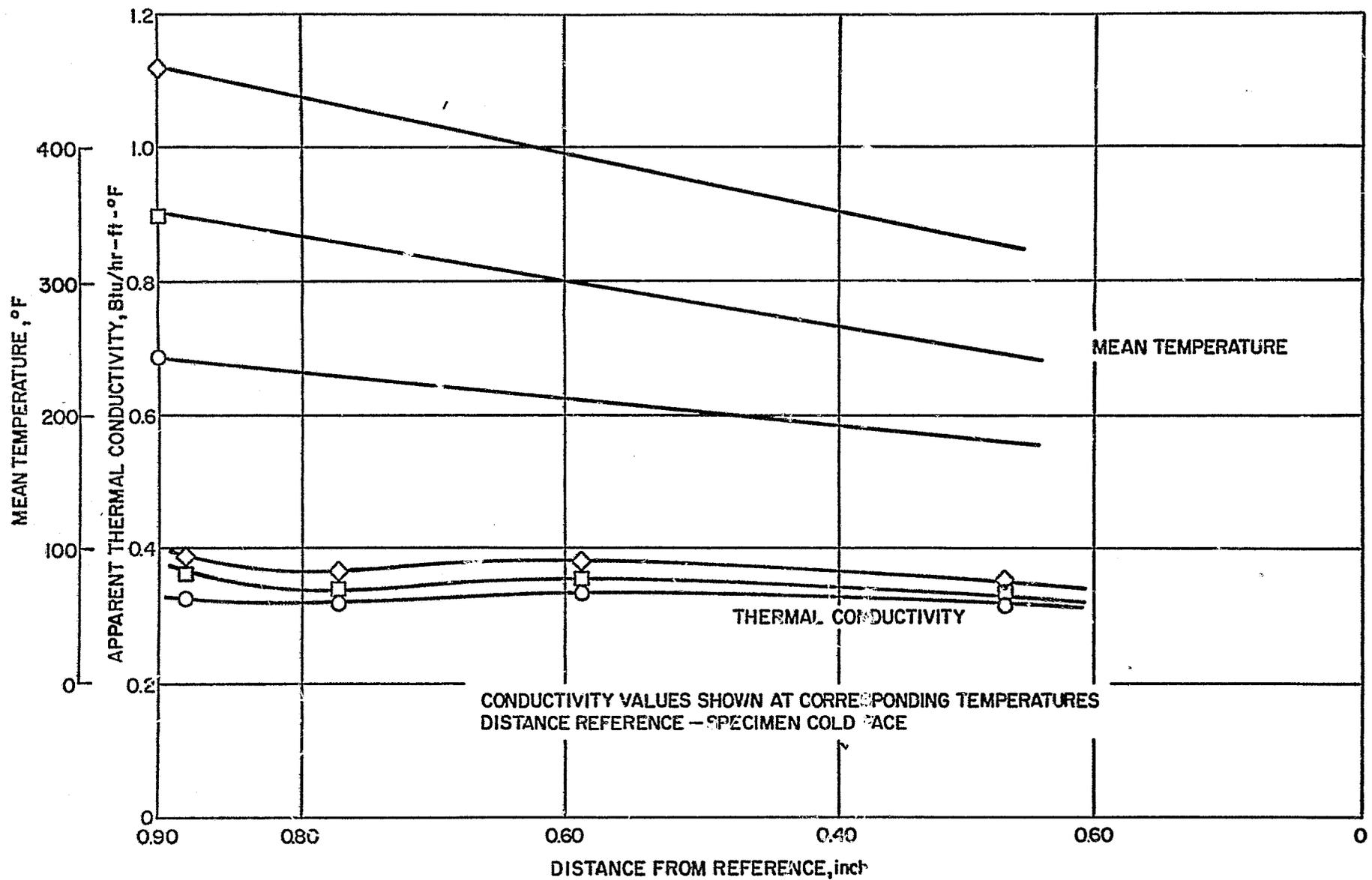
78-1494

Figure 45  SILICA–PHENOLIC BILLET MXS–89 THERMAL CONDUCTIVITY PROFILE
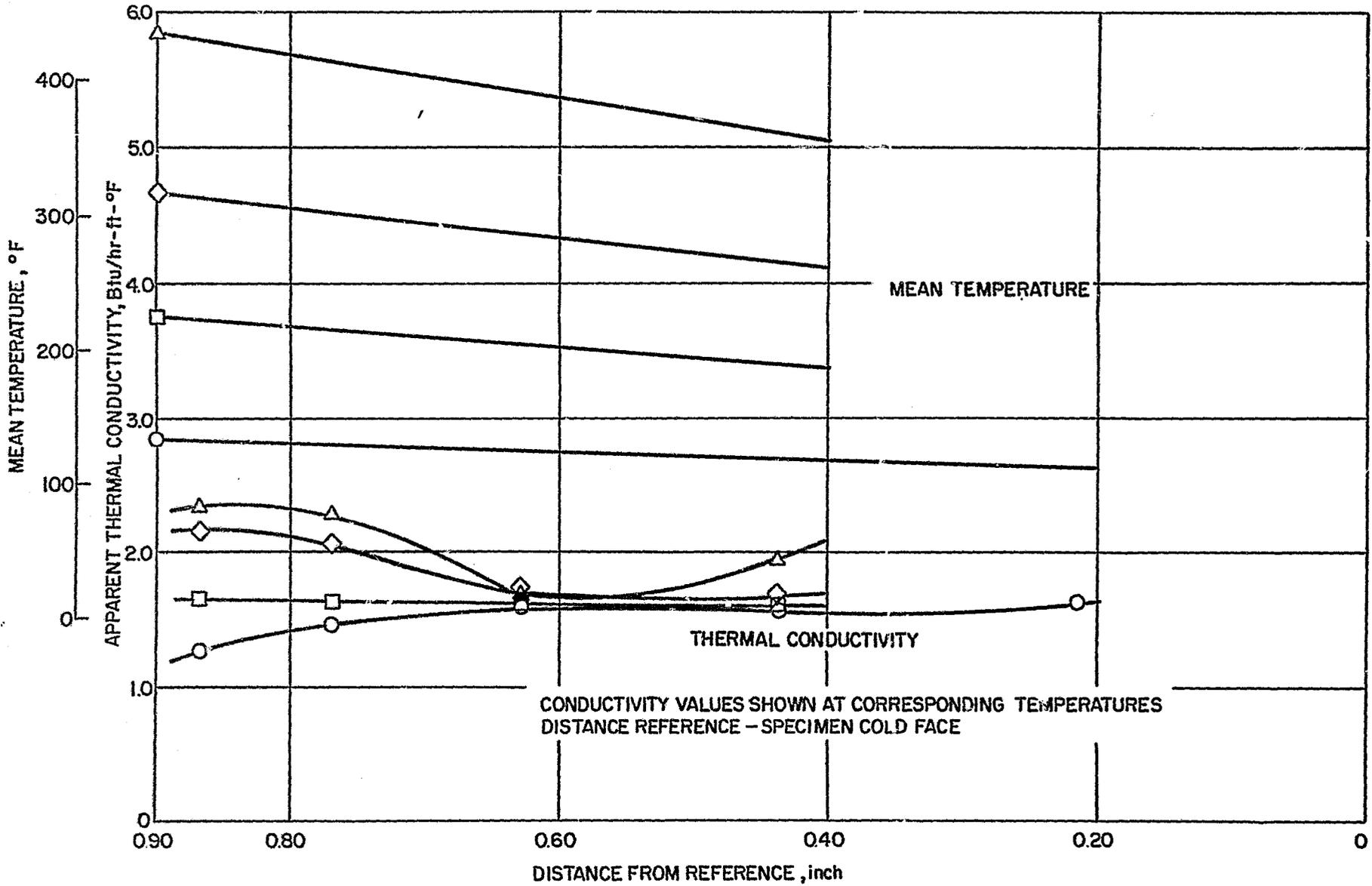
Figure 46 GRAPHITE-PHENOLIC BILLET MX4501 THERMAL CONDUCTIVITY PROFILE

78-1495

# TABLE VIII

## THERMAL DATA TABULATION OF AS RECEIVED BILLETS
## THERMAL CONDUCTIVITY TESTS

| Silica-Phenolic MXS-89 Density = 102.36 lb/ft$^3$ | | | | Graphite-Phenolic MX4501 Density = 83.21 lb/ft$^3$ | | | |
|---|---|---|---|---|---|---|---|
| Distance From Cold End (in.) | Section | Temperature (°F) | Conductivity, K (Btu/hr-ft-°F) | Distance From Cold End (in.) | Section | Temperature (°F) | Conductivity, K (Btu/hr-ft-°F) |
| 0.265 | T1 | 179 | 0.314 | 0.216 | T1 | 114 | 1.63 |
| 0.384 | T2 | 213 | 0.332 | 0.436 | T2 | 120 | 1.54 |
| 0.765 | T3 | 232 | 0.319 | 0.627 | T3 | 125 | 1.59 |
| 0.880 | T4 | 243 | 0.325 | 0.770 | T4 | 129 | 1.47 |
| | T1 | 245 | 0.322 | 0.868 | T5 | 132 | 1.27 |
| | T2 | 300 | 0.351 | | T2 | 189 | 1.60 |
| | T3 | 331 | 0.335 | | T3 | 203 | 1.65 |
| | T4 | 350 | 0.363 | | T4 | 213 | 1.62 |
| | T1 | 325 | 0.340 | | T5 | 221 | 1.66 |
| | T2 | 397 | 0.381 | | T2 | 265 | 1.67 |
| | T3 | 436 | 0.365 | | T3 | 287 | 1.72 |
| | T4 | 460 | 0.387 | | T4 | 302 | 2.08 |
| | | | | | T5 | 312 | 2.17 |
| | | | | | T2 | 361 | 1.92 |
| | | | | | T3 | 392 | 1.65 |
| | | | | | T4 | 415 | 2.29 |
| | | | | | T5 | 427 | 2.34 |

Five thermocouples were installed at specific axial locations on each virgin specimen. Temperature data were monitored at each of these locations during a normal test. Once the proper test conditions were achieved, thermal conductivity values were computed from the temperature gradient between each in-line pair of thermocouples, and plotted as a function of their mean location along the length of the specimen. The average temperature obtained from each pair of thermocouples was also plotted as a function of axial location. This procedure was repeated at three different test temperature levels. Referring to Figures 40 and 41 the thermal conductivity profile curves shown in the lower grouping are related to corresponding average temperature profiles having identical symbols. One merely has to replot vertically to obtain a thermal conductivity versus temperature relationship for any given specimen location. The data shown at the various distances indicated in the figures have been assigned distance-locations symbols and these are indicated in Table VIII as T1, T2, T3, etc. The distances are given with respect to the "cold" end surface of the test specimen cylinders.

Table IX lists the thermal conductivity data results from tests performed on silica-phenolic MXS-89 corings which were charred at 1000° and 2000°F. The tabulation includes the direction of heat flow with respect to the laminate layup direction, char density, and mean test temperature at which the conductivity values were determined. These data have been plotted and are presented in Figures 47 and 48. Unlike the previous virgin tests, the conductivity values were based on temperature measurement from two thermocouples located near each end of the test specimen as is customary in cut-bar testing techniques. In this manner a bulk conductivity value is obtained for the material at its average temperature. Reference standard material for these tests was an Avco proprietary material calibrated against NBS certified material. Because of the extreme fragility of the 2700° and 2800°F charred specimens, it was not possible to test for thermal conductivity on these materials.

## TABLE IX

## THERMAL CONDUCTIVITY DATA TABULATION

| Laboratory Pre-Charred Samples Silica-Phenolic MXS-89 Measurements taken parallel to laminates | | | |
|---|---|---|---|
| Pre-Char Temperature (°F) | Density (lb/ft³) | Test Temperature (°F) | Conductivity (Btu/hr-ft-°F) |
| 1000 | 92.17 | 152 | 0.330 |
|  |  | 200 | 0.355 |
|  |  | 285 | 0.372 |
|  |  | 330 | 0.391 |
| 2000 | 99.6 | 152 | 0.501 |
|  |  | 233 | 0.520 |
|  |  | 337 | 0.546 |
|  |  | 434 | 0.570 |

$\rho \approx 102.4 (\text{VIRGIN}) 92.17 (\text{CHAR}) \text{lb/ft}^3$

REMARKS = 1000°F CHAR
HEAT FLOW PARALLEL TO LAYUP
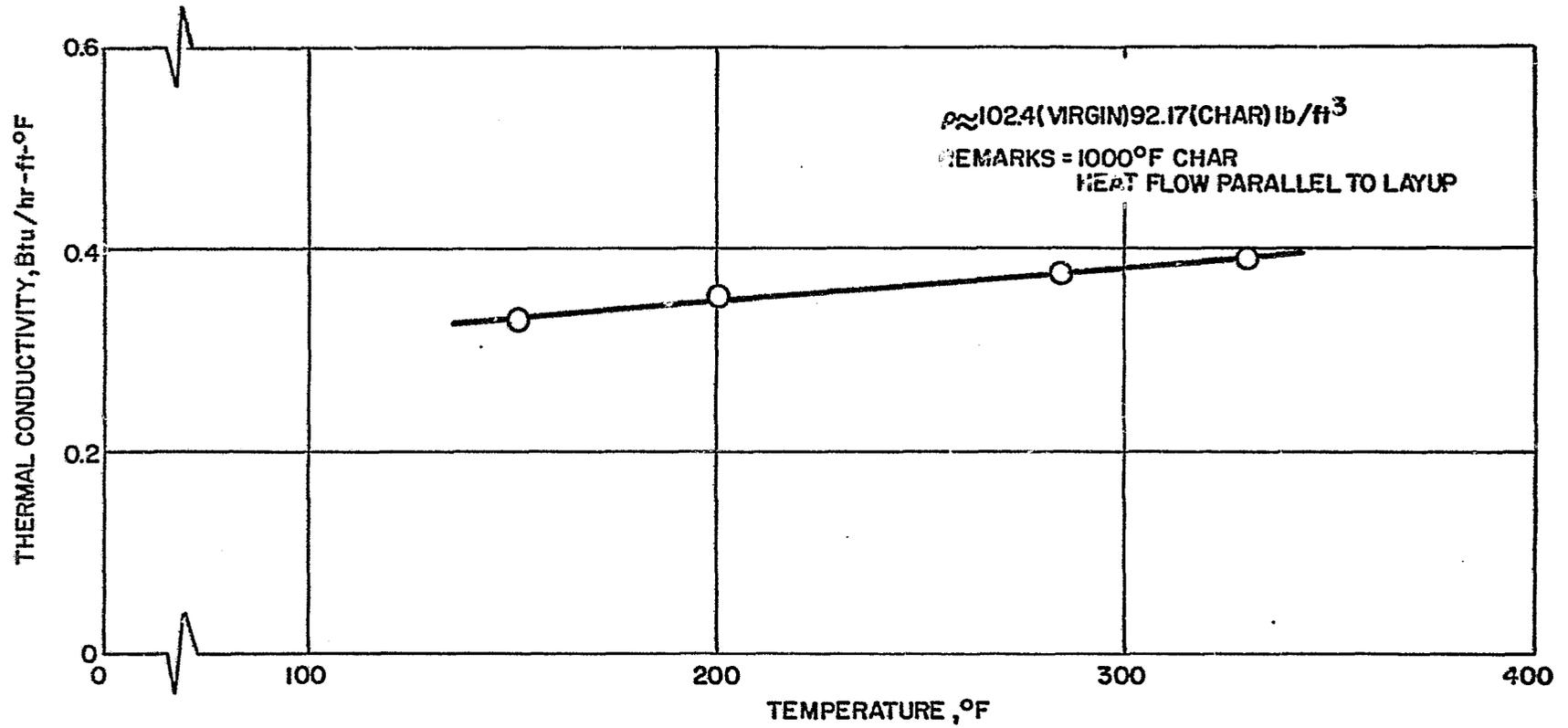
Figure 47  SILICA-PHENOLIC MXS-89, 1000°F PRECHARRED, THERMAL
CONDUCTIVITY VERSUS TEMPERATURE
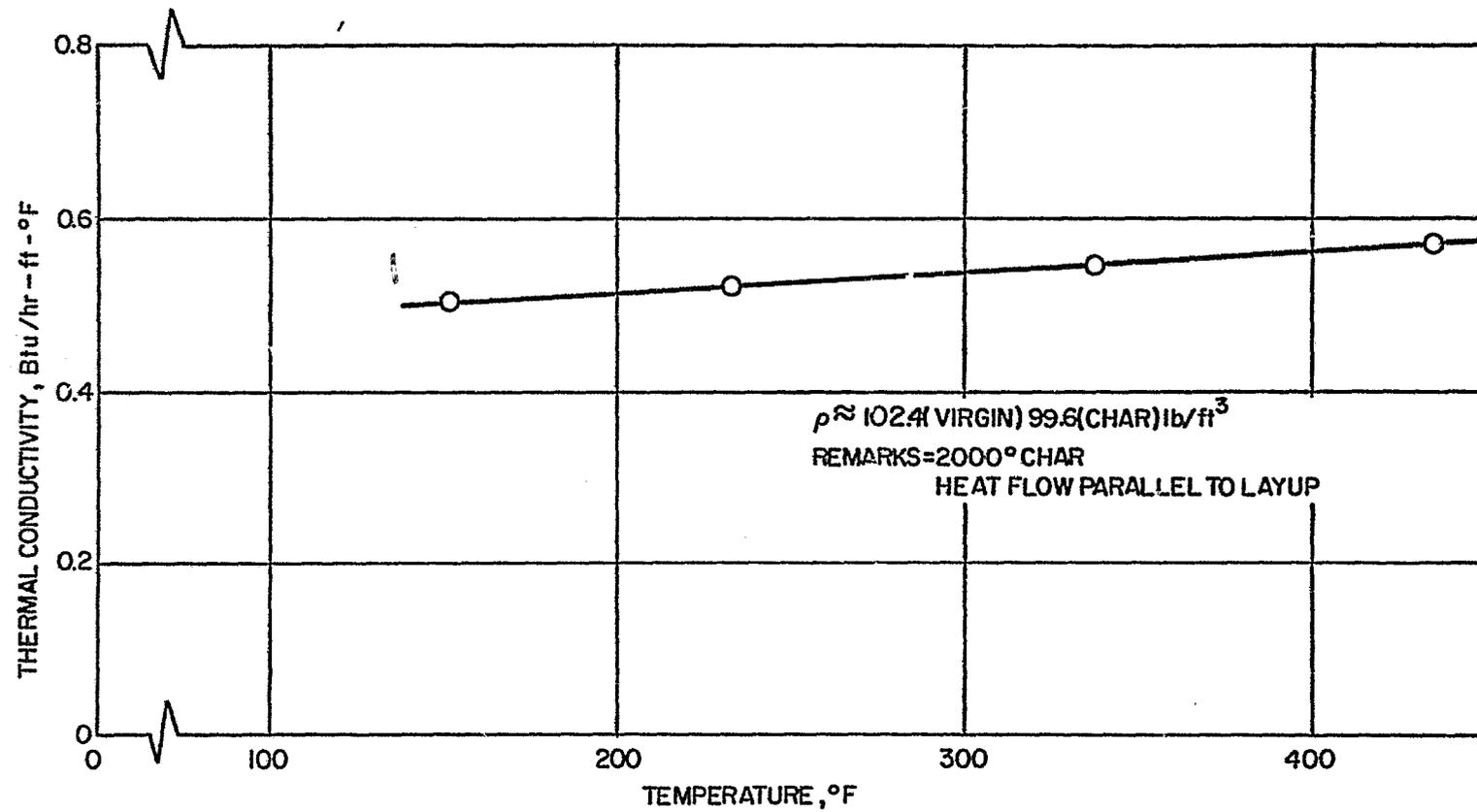
78-1496

Figure 48 SILICA-PHENOLIC MXS-89, 2000°F PRECHARRED, THERMAL
CONDUCTIVITY VERSUS TEMPERATURE

78-1497

$\rho \approx 102.4($VIRGIN$)$ 99.6$($CHAR$)$ lb/ft$^3$

REMARKS=2000°CHAR
HEAT FLOW PARALLEL TO LAYUP

THERMAL CONDUCTIVITY, Btu/hr — ft - °F

TEMPERATURE, °F

-71-

Table X lists the results of the thermal conductivity measurements on the graphite-phenolic MX4501 charred material. These were performed in the same fashion as the MXS-89 material. Similarly the tabulation contains pertinent data related to heat flow direction, density and mean test temperature, and char temperature level. These data have been plotted and are shown in Figures 49 through 53. Reference standard material for this series was Pyroceram 9606, a product of Corning Glass Company, whose thermal properties have been well established by NBS and others. The data from Figures 45 through 53 were rearranged to provide a conductivity (at temperature) versus char temperature relationship. These are shown in Figures 54 and 55 as based on data extracted at 200° and 400°F. The knee of the curve appearing in Figure 55 at approximately 3000°F is felt to be attributed to the graphitization of the charred phenolic matrix which tends to increase overall conductivity level. Although the conductivity-char temperature relationship for the MXS-89 materials is limited to the 2000°F char level, it clearly illustrates the increasing conductivity relationship as a function of char temperature level.

## TABLE X

## THERMAL CONDUCTIVITY DATA TABULATION

| Laboratory Pre-charred samples Graphite-Phenolic MX4501 Measurements taken parallel to laminates | | | |
|---|---|---|---|
| Pre-Char Temperature (°F) | Density (lb/ft$^3$) | Test Temperature (°F) | Conductivity (Btu/hr-ft-°F) |
| 1000 | 72.46 | 155 | 2.40 |
|  |  | 289 | 3.10 |
|  |  | 422 | 3.96 |
| 2000 | 72.07 | 151 | 3.82 |
|  |  | 296 | 4.63 |
|  |  | 400 | 5.31 |
| 3000 | 70.48 | 159 | 4.64 |
|  |  | 278 | 6.37 |
|  |  | 414 | 7.88 |
| 3650 | 74.4 | 152 | 10.67 |
|  |  | 284 | 13.61 |
|  |  | 398 | 15.22 |
|  |  | 527 | 18.15 |
| 4000 | 76.24 | 146 | 15.54 |
|  |  | 220 | 16.28 |
|  |  | 290 | 17.17 |
|  |  | 409 | 20.55 |
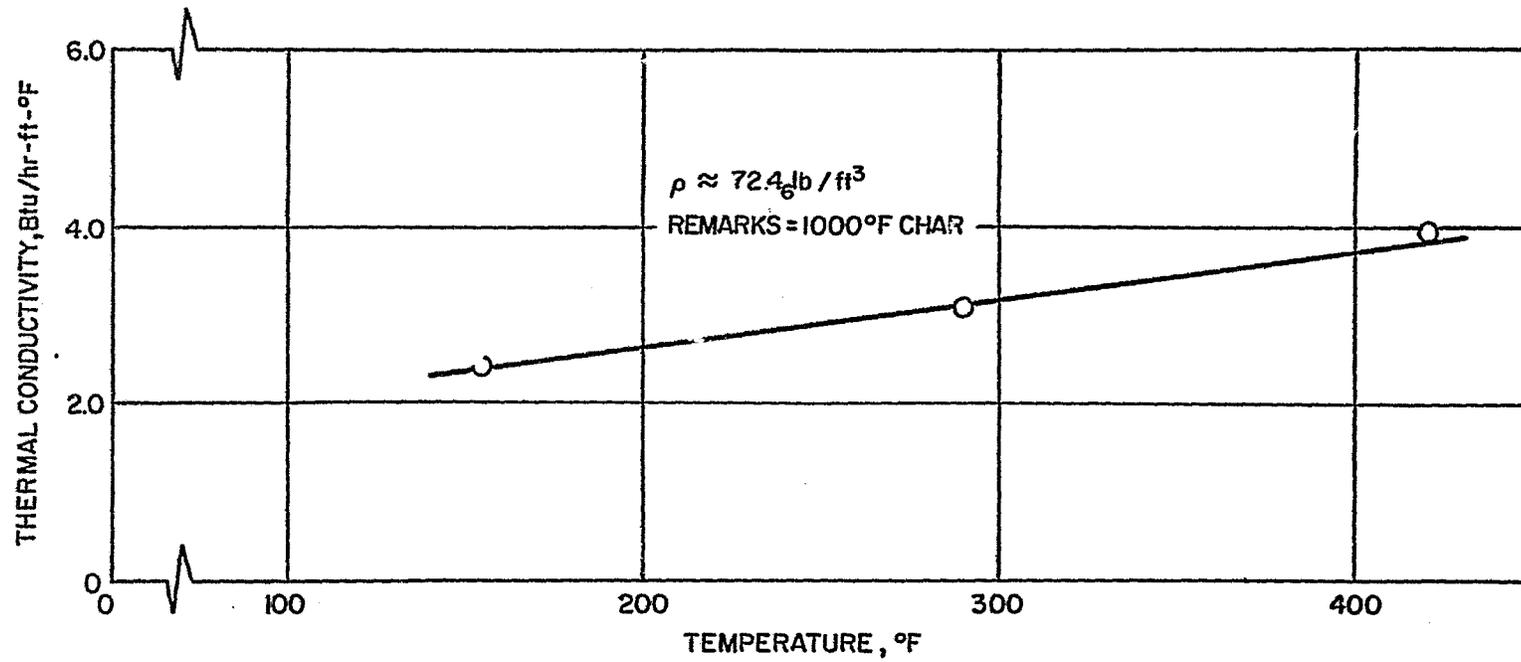
Figure 49 GRAPHITE-PHENOLIC MX4501, 1000°F PRECHARRED, THERMAL
CONDUCTIVITY VERSUS TEMPERATURE
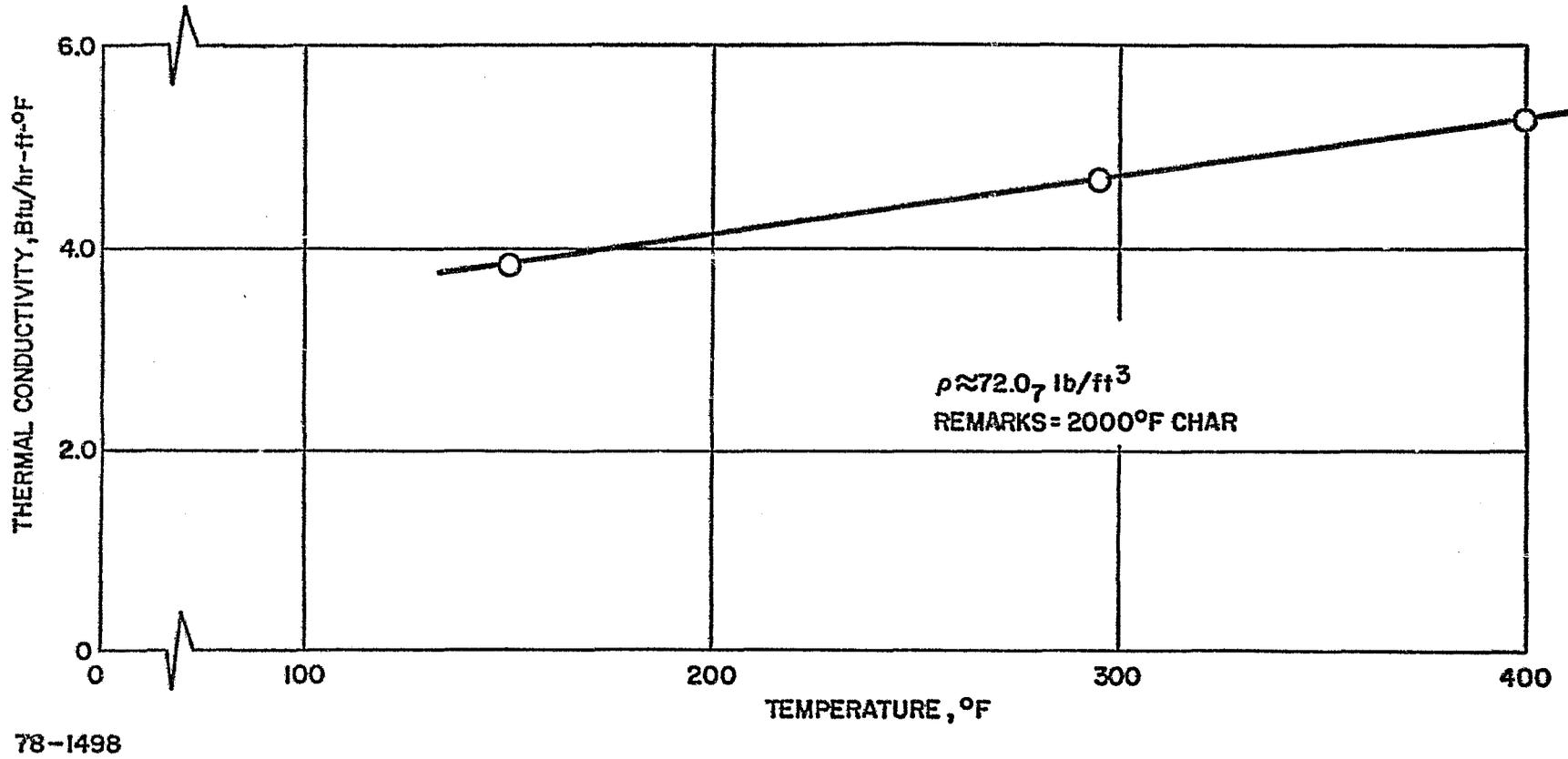
78-1497

78-1498

Figure 50 GRAPHITE-PHENOLIC MX4501, 2000°F PRECHARRED, THERMAL
CONDUCTIVITY VERSUS TEMPERATURE
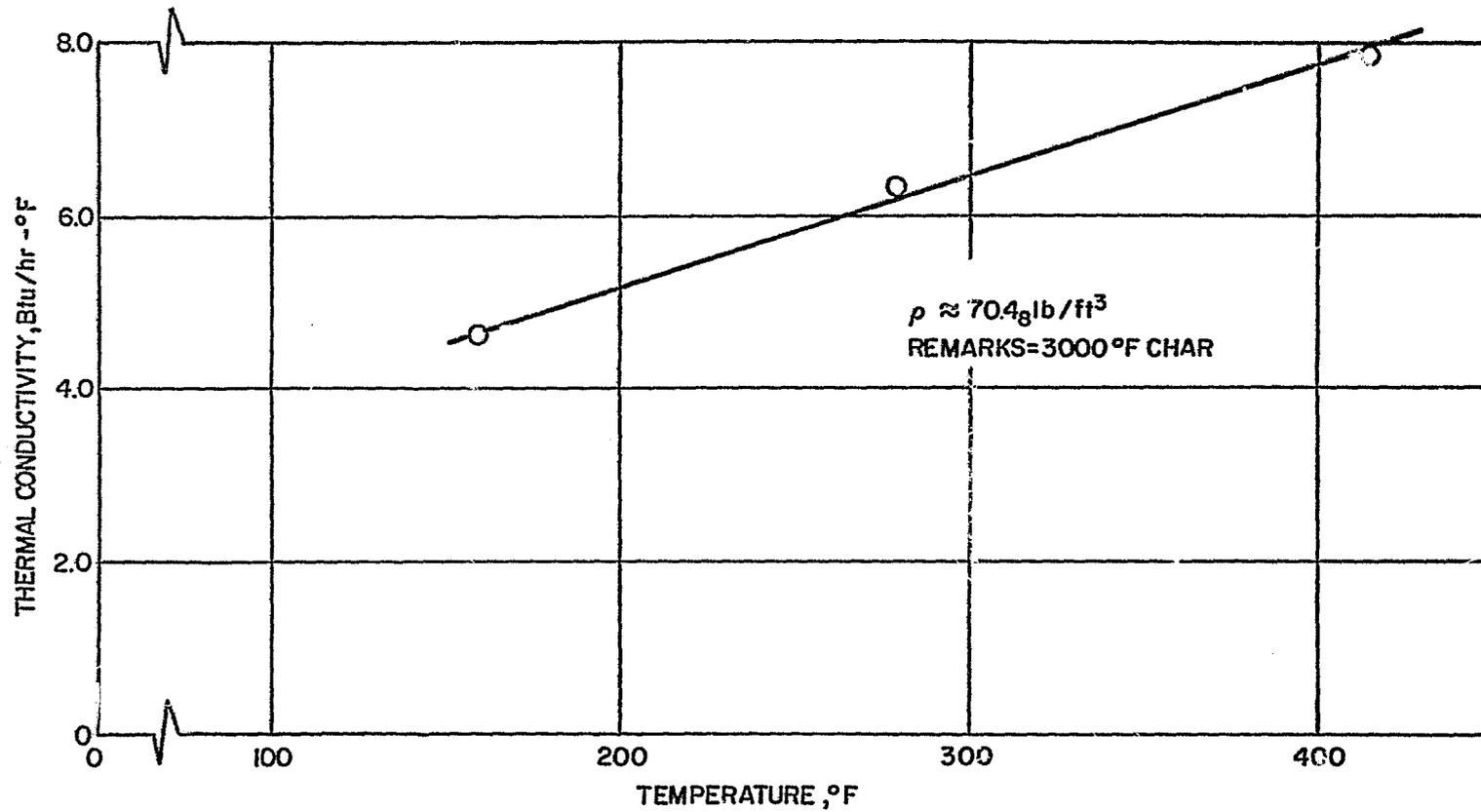
Figure 51 GRAPHITE-PHENOLIC MX4501, 3000°F PRECHARRED, THERMAL
CONDUCTIVITY VERSUS TEMPERATURE

The figure plots THERMAL CONDUCTIVITY, Btu/hr - °F (y-axis, 0 to 8.0) versus TEMPERATURE, °F (x-axis, 0 to 400). Annotation on plot:

$\rho \approx 70.4_8 \, lb/ft^3$
REMARKS = 3000°F CHAR
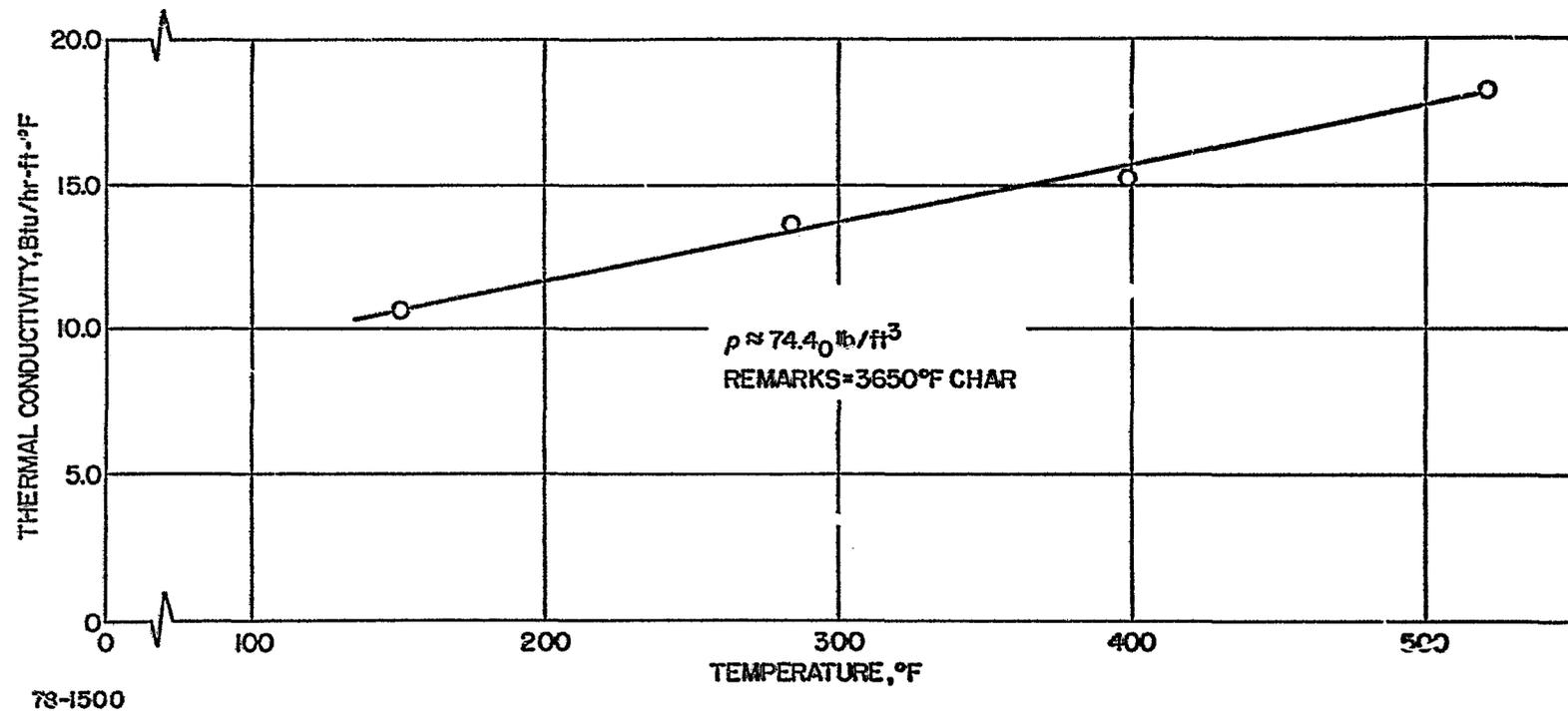
Figure 52  GRAPHITE-PHENOLIC MX4501, 3650°F PRECHARRED, THERMAL
CONDUCTIVITY VERSUS TEMPERATURE

-76-
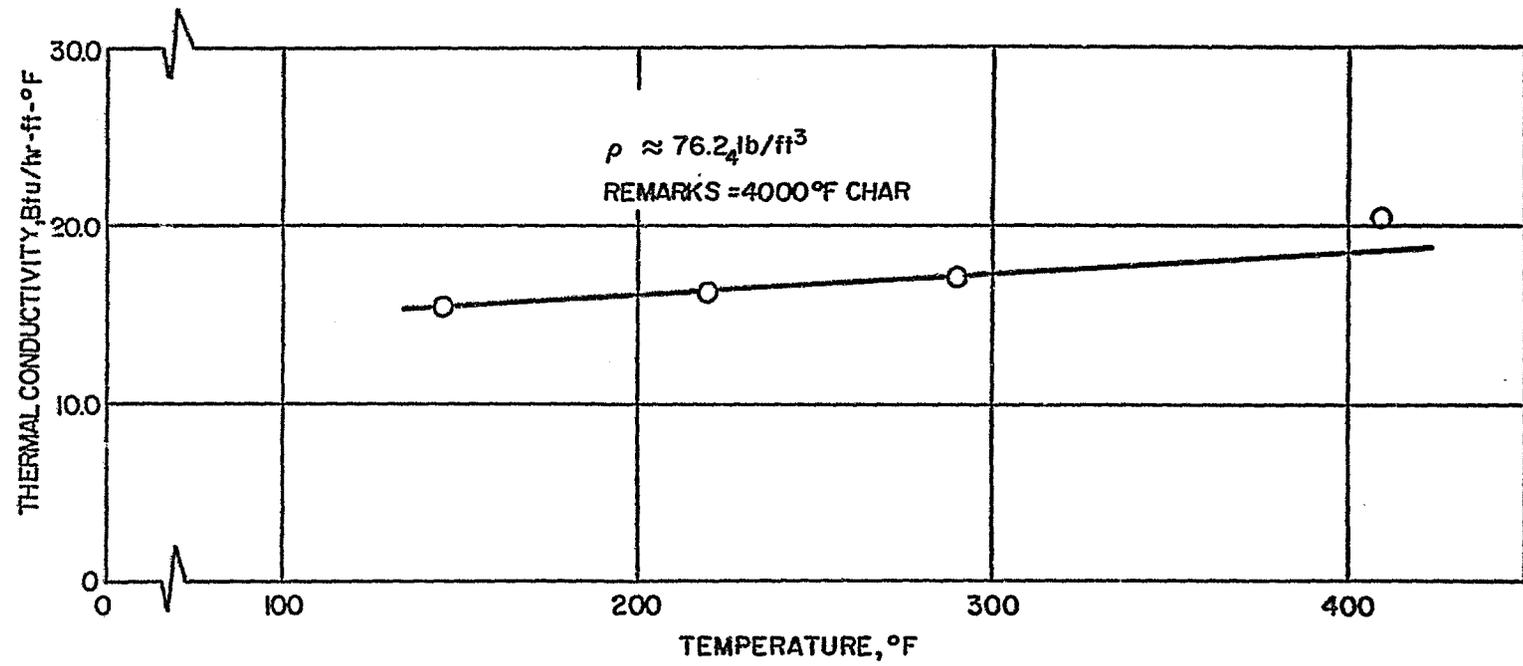
Figure 53  GRAPHITE-PHENOLIC MX4501, 4000°F PRECHARRED, THERMAL CONDUCTIVITY VERSUS TEMPERATURE

78-1501

SPECIMENS CHARRED IN HELIUM ATMOSPHERE
CONDUCTIVITY TEST TEMPERATURES NOTED ON CURVES

400°F

200°F

THERMAL CONDUCTIVITY, Btu/hr-ft-°F
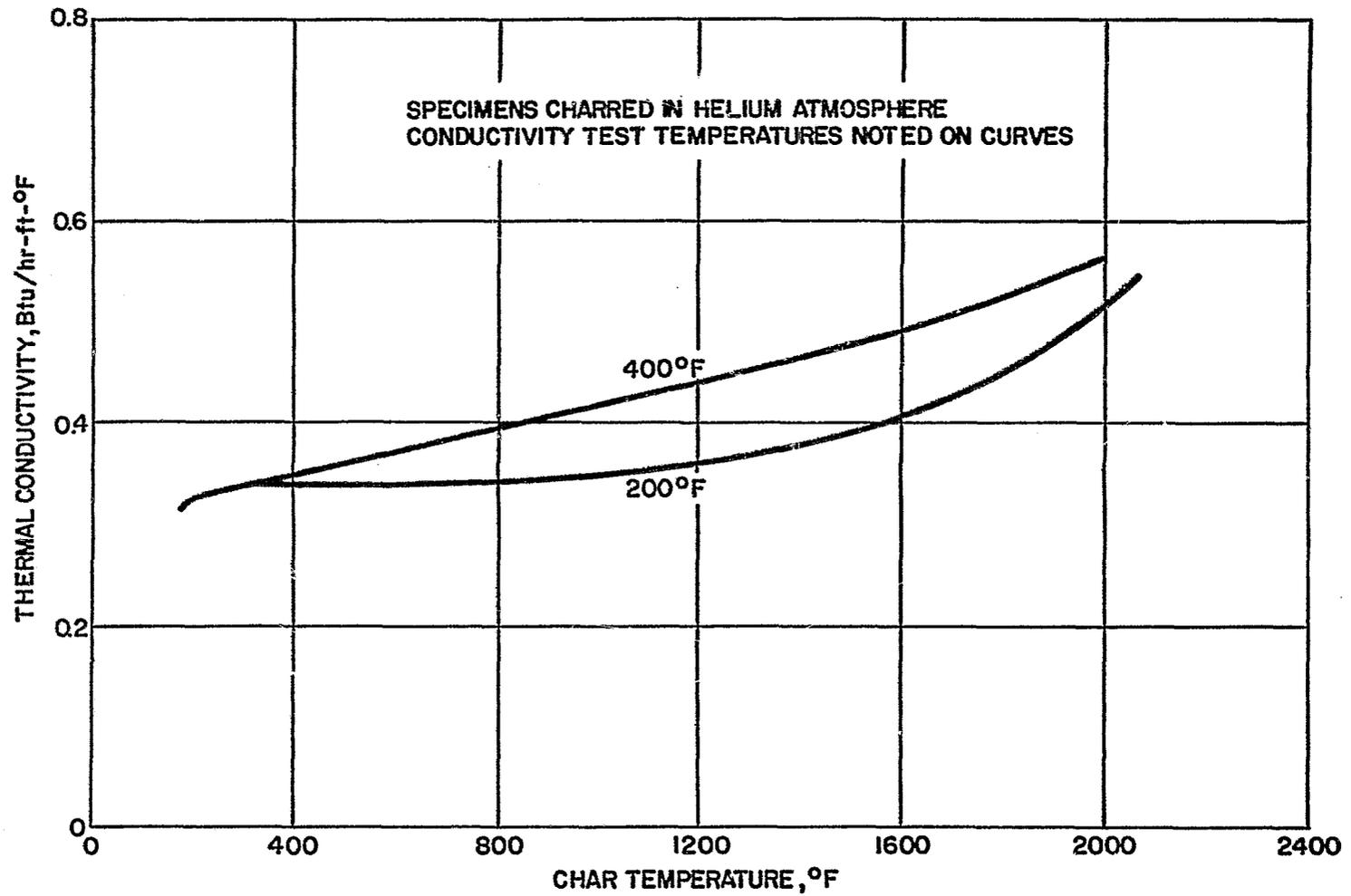
CHAR TEMPERATURE, °F

78-1502

Figure 54  SILICA-PHENOLIC MXS-89, THERMAL CONDUCTIVITY (AT
TEMPERATURE) VERSUS CHAR TEMPERATURE

78-1503
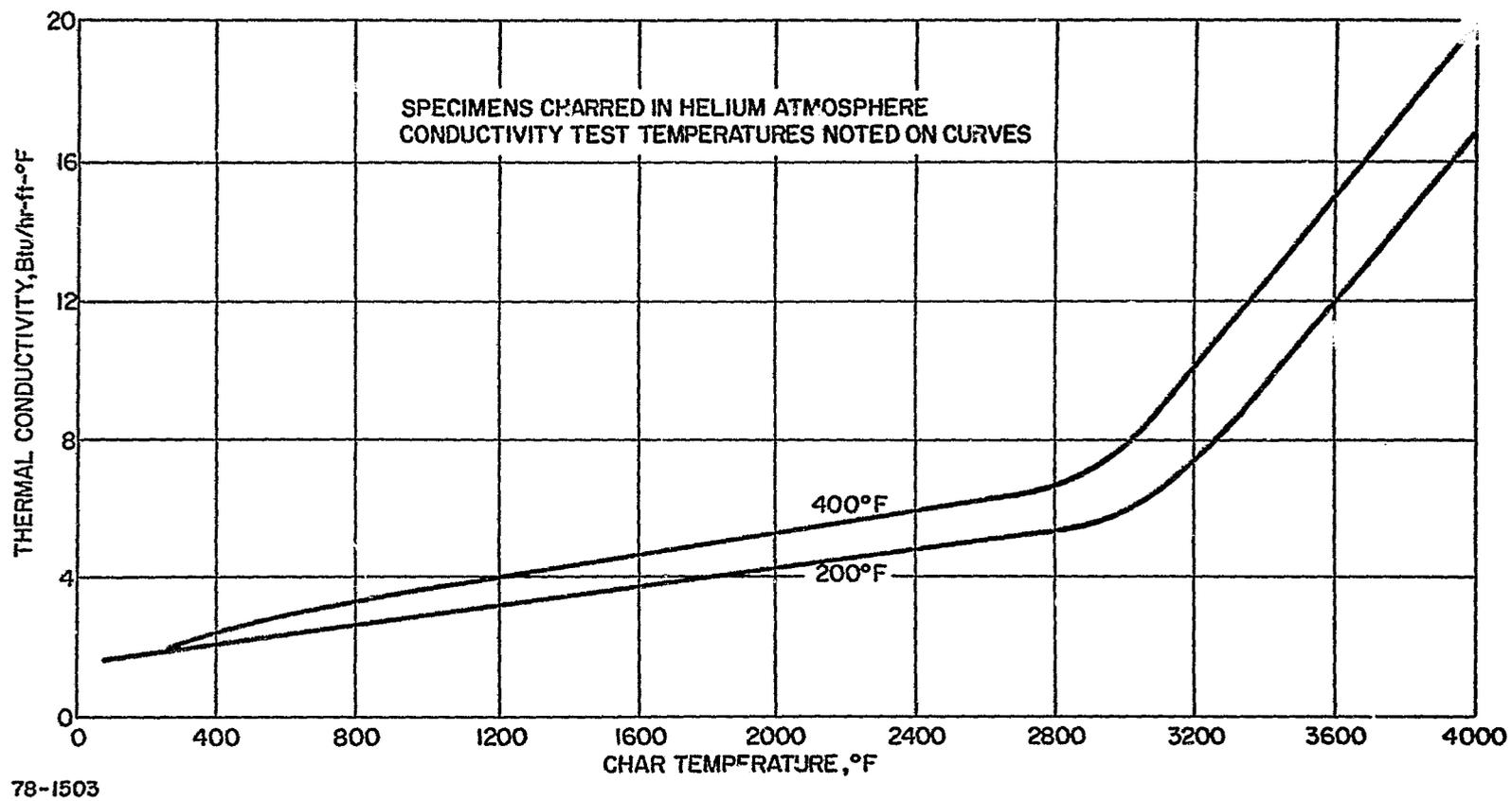
Figure 55  GRAPHITE PHENOLIC MX4501, THERMAL CONDUCTIVITY (AT
TEMPERATURE) VERSUS CHAR TEMPERATURE

2)  Specific Heat Measurements of Oven Chars -- The measurements of specific heat were performed using two distinct experimental techniques, 1) Method of Mixtures (M/M) and 2) Differential Scan Calorimetry (DSC). A full explanation of the two methods is presented in Appendix D.  The purpose of performing the measurements in this double fashion was to qualify the DSC method by comparing results thus obtained with those obtained by the Method of Mixtures.  The M/M tests are conducted in accordance with ASTM Specification C351-61.  In both methods, synthetic sapphire reference standards are used as calibration materials.  The DSC method has the advantage of requiring sample sizes in the order of 20 milligrams and as such is uniquely appropriate for the characterization of nozzle char specific heat profiles.  The M/M sample requirements are in the order of six specimens of 3/8-inch diameter x 1-inch length -- rendering it inappropriate for profiling techniques.  The DSC tests yield direct measurements of specific heat as a function of temperature and by integrating this function produces an enthalpy-temperature relationship.  On the other hand, the M/M yields enthalpy-temperature functions which upon differentiation produce specific heat-temperature relationships.

Specimens for the specific heat tests of the virgin material were furnished for both methods of testing.  All subsequent tests on charred materials were performed on the DSC apparatus.  Six corings having dimensions as previously stated were machined from each virgin billet to provide M/M specimens and a 1/2-inch cube of each billet was ground to a powder and tumbled to provide DSC specimens.  The powdering of a relatively large specimen and subsequent tumbling are essential procedures to ensure that the sample tested is representative of the subject material.  This is of particular importance when testing laminated composite materials such as MXS-89 and MX4500, since it is theoretically possible to select powdered specimens containing a disproportionate amount of fabric or phenolic constituents and thereby giving the measured property a weighted bias.

Figures 56 and 57 are the results of the virgin material measurements. Note there is excellent agreement between the two methods of testing. Note also that the data obtained from the DSC is reported at every 18° F interval.  Table XI includes the raw data obtained during the M/M tests.

Using the enthalpy versus temperature relationship is a more significant mode of comparing the two test methods over a specific heat versus temperature function because the potential variation in specific heat values obtained upon differentiation of the M/M enthalpy function may result in an unrealistic comparison which is due to the arbitrary power of the data fit and the extreme sensitivity of the functions derivative ($C_p$ = dh/dt). Therefore, it is more reasonable to use the less deceptive integration of the DSC's direct measurements of specific heat.

In addition to the enthalpy curve, each graph includes specific heat data at several arbitrary temperatures.

Having suitably qualified the measurements performed on the DSC, the four oven-charred MXS-89 materials were tested over the temperature 100° F to 930° F.  The results of these tests are shown in figures 58 through 61. The data were replotted to provide a specific heat (at temperature) versus
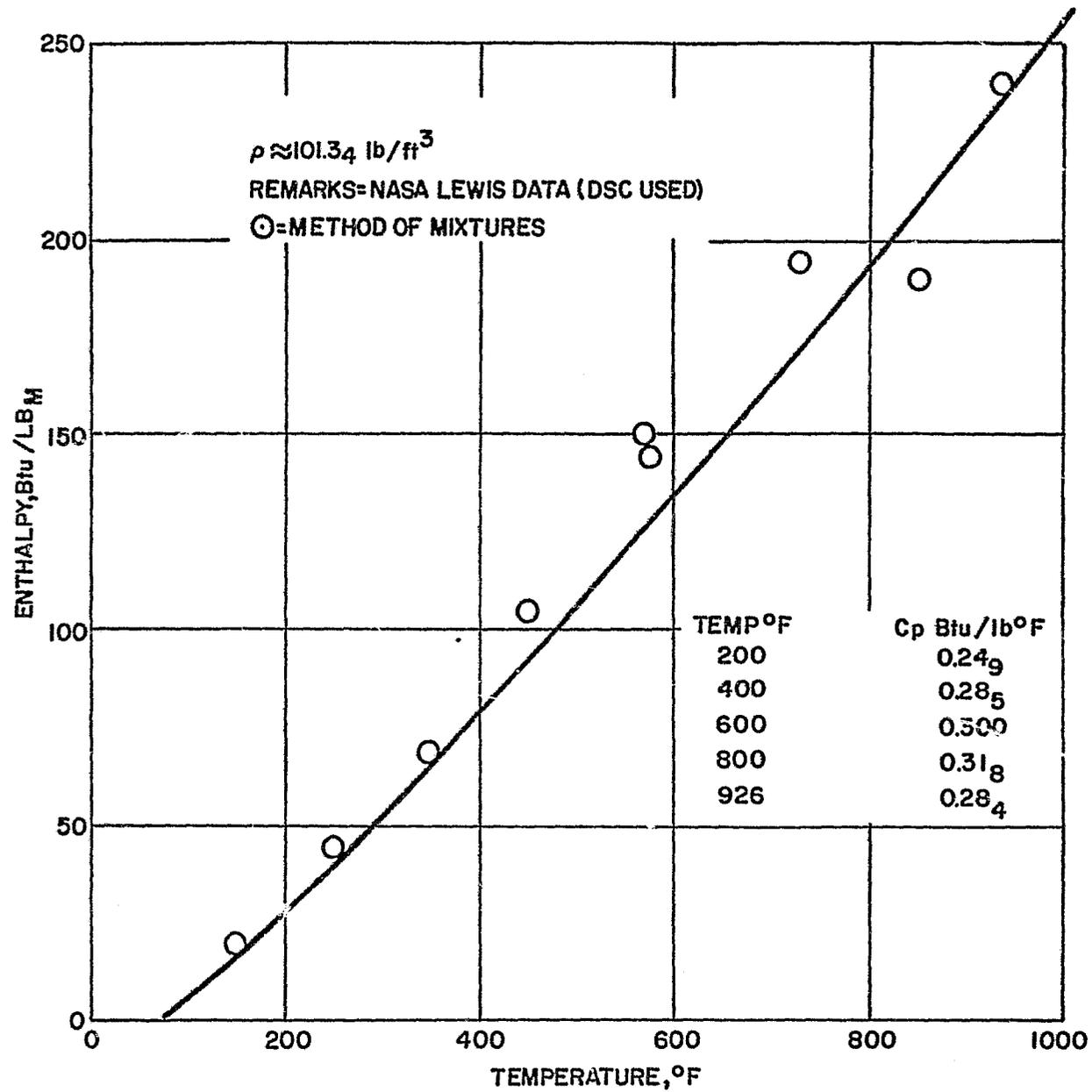
Figure 56  SILICA-PHENOLIC BILLET MXS-89, ENTHALPY VERSUS TEMPERATURE
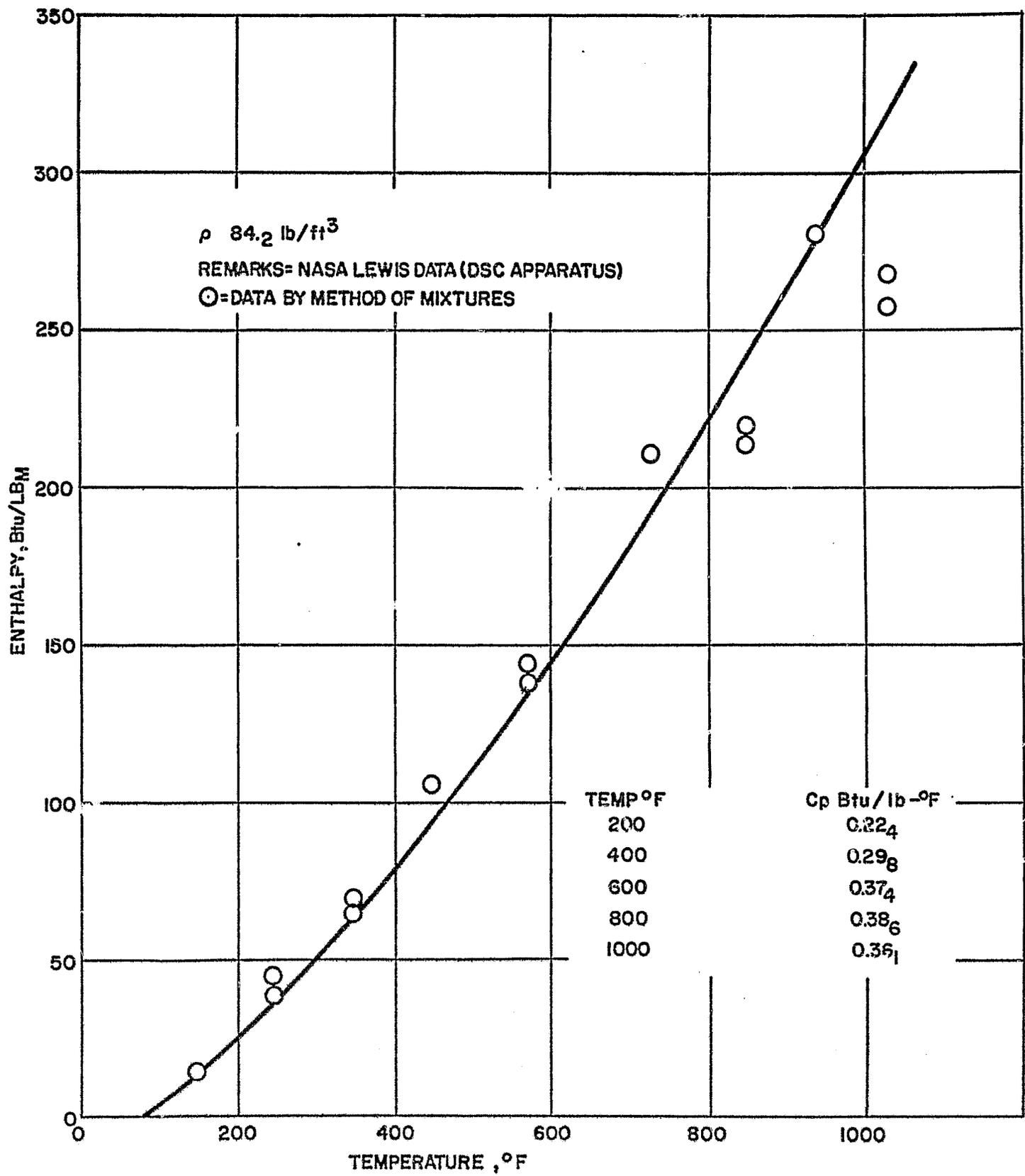
Figure 57 GRAPHITE-PHENOLIC BILLET MX4501, ENTHALPY VERSUS TEMPERATURE

The figure is an enthalpy versus temperature plot with the following annotations:

- $\rho$ 84.2 lb/ft$^3$
- REMARKS= NASA LEWIS DATA (DSC APPARATUS)
- $\odot$=DATA BY METHOD OF MIXTURES

Y-axis: ENTHALPY, Btu/LB$_M$ (0 to 350)
X-axis: TEMPERATURE, °F (0 to 1000)

| TEMP °F | Cp Btu/lb-°F |
|---------|--------------|
| 200     | $0.22_4$     |
| 400     | $0.29_8$     |
| 600     | $0.37_4$     |
| 800     | $0.38_6$     |
| 1000    | $0.36_1$     |

78-1505

-82-

## TABLE XI

## THERMAL DATA TABULATION OF AS-RECEIVED BILLETS
## SPECIFIC HEAT

| Silica-Phenolic MXS-89 Density = 101.34 lb/ft$^3$ | | | Graphite-Phenolic MX4501 Density = 84.25 lb/ft$^3$ | | |
|---|---|---|---|---|---|
| Temperature ($^{\circ}$F) | Enthalpy, $\Delta H$ (Btu/lb) | Specific Heat, $C_p$ (Btu/lb-$^{\circ}$F) | Temperature ($^{\circ}$F) | Enthalpy, $\Delta H$ (Btu/lb) | Specific Heat, $C_p$ (Btu/lb-$^{\circ}$F) |
| 147 | 20.49 | | 147 | 15.39 | |
| 200 | | 0.249 | 200 | | 0.224 |
| 244 | 45.24 | | 244 | 39.38 | |
| 349 | 68.06 | | 349 | 70.91 | |
| 400 | | 0.285 | 400 | | 0.298 |
| 453 | 107.96 | | 453 | 107.64 | |
| 147 | 19.56 | | 147 | 15.66 | |
| 244 | 45.53 | | 244 | 45.86 | |
| 349 | 68.47 | | 349 | 67.77 | |
| 453 | 105.63 | | 453 | 107.64 | |
| 575 | 151.24 | | 575 | 139.37 | |
| 600 | | 0.281 | 600 | | 0.374 |
| 727 | 195.34 | | 727 | 211.10 | |
| 800 | | 0.318 | 800 | | 0.386 |
| 855 | 191.75 | | 855 | 214.07 | |
| 926 | | 0.284 | 926 | | 0.361 |
| 940 | 240.30 | | 940 | 283.83 | |
| | | | 1036 | 268.62 | |

-83-
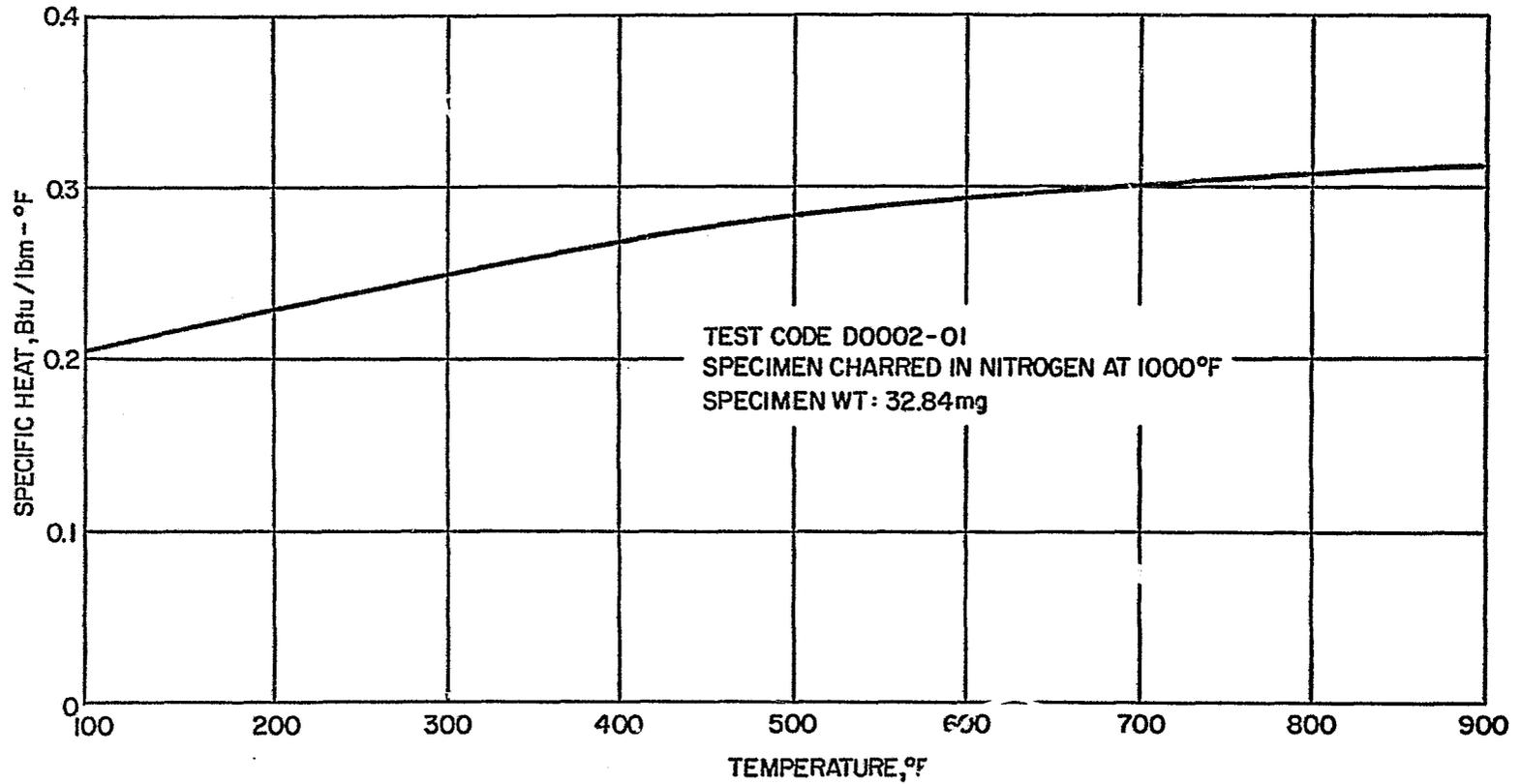
Figure 58  SILICA-PHENOLIC MXS-89, 1000°F PRECHARRED, SPECIFIC HEAT VERSUS TEMPERATURE
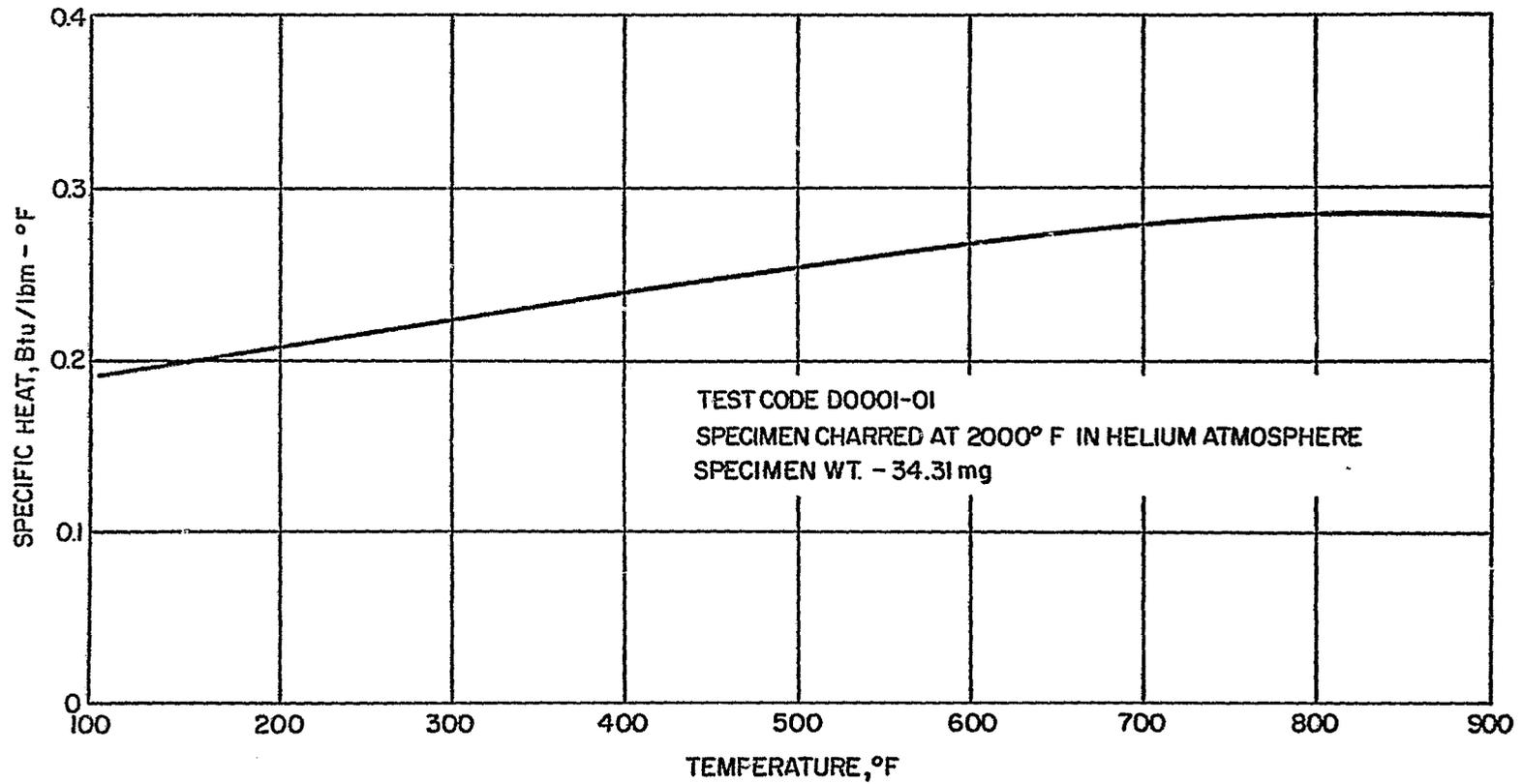
78-1506

Figure 59 SILICA-PHENOLIC MXS-89, 2000°F PRECHARRED, SPECIFIC
HEAT VERSUS TEMPERATURE
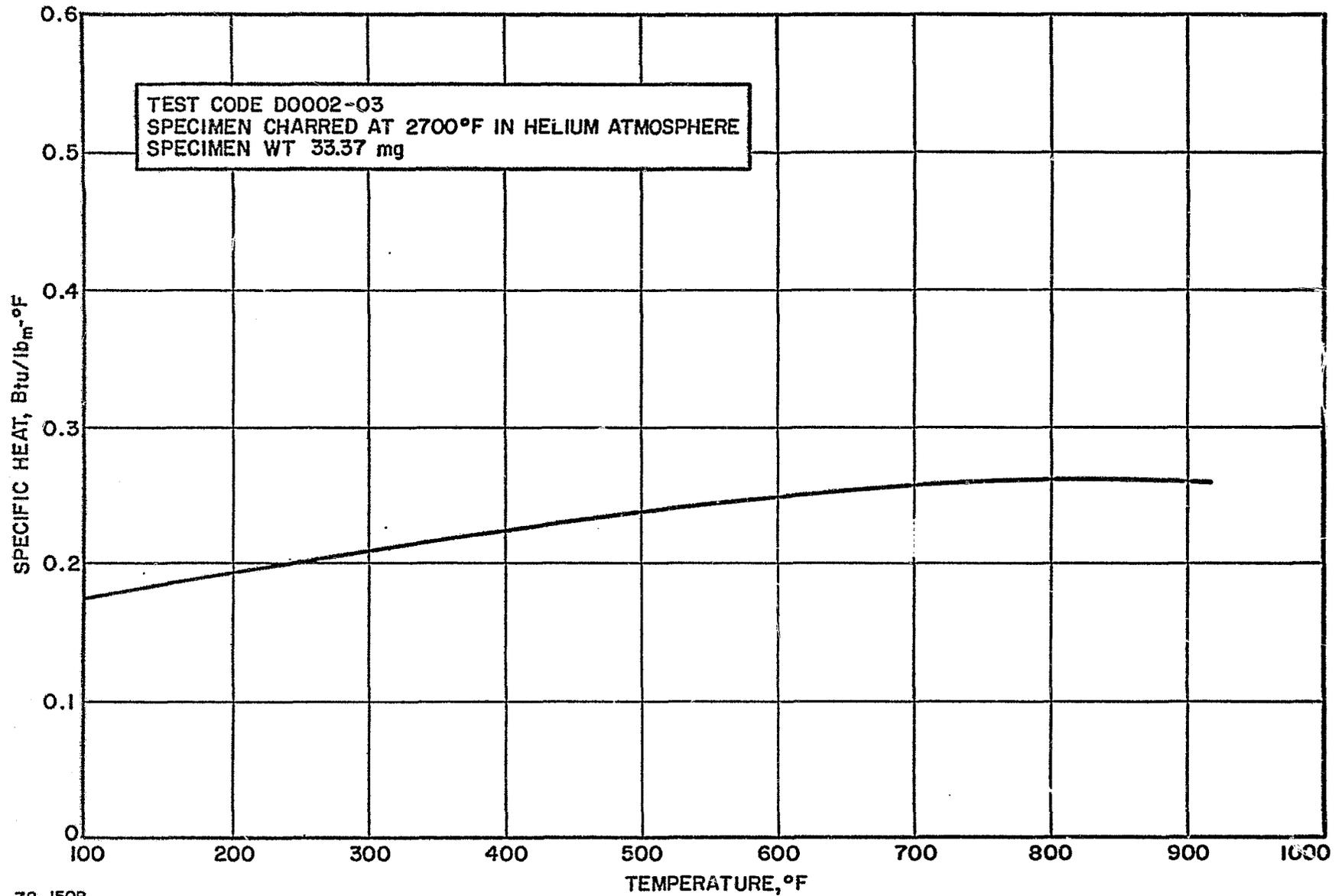
78-1507

Figure 60 SILICA-PHENOLIC MXS-89, 2700°F PRECHARRED, SPECIFIC
HEAT VERSUS TEMPERATURE

78-1508

-86-
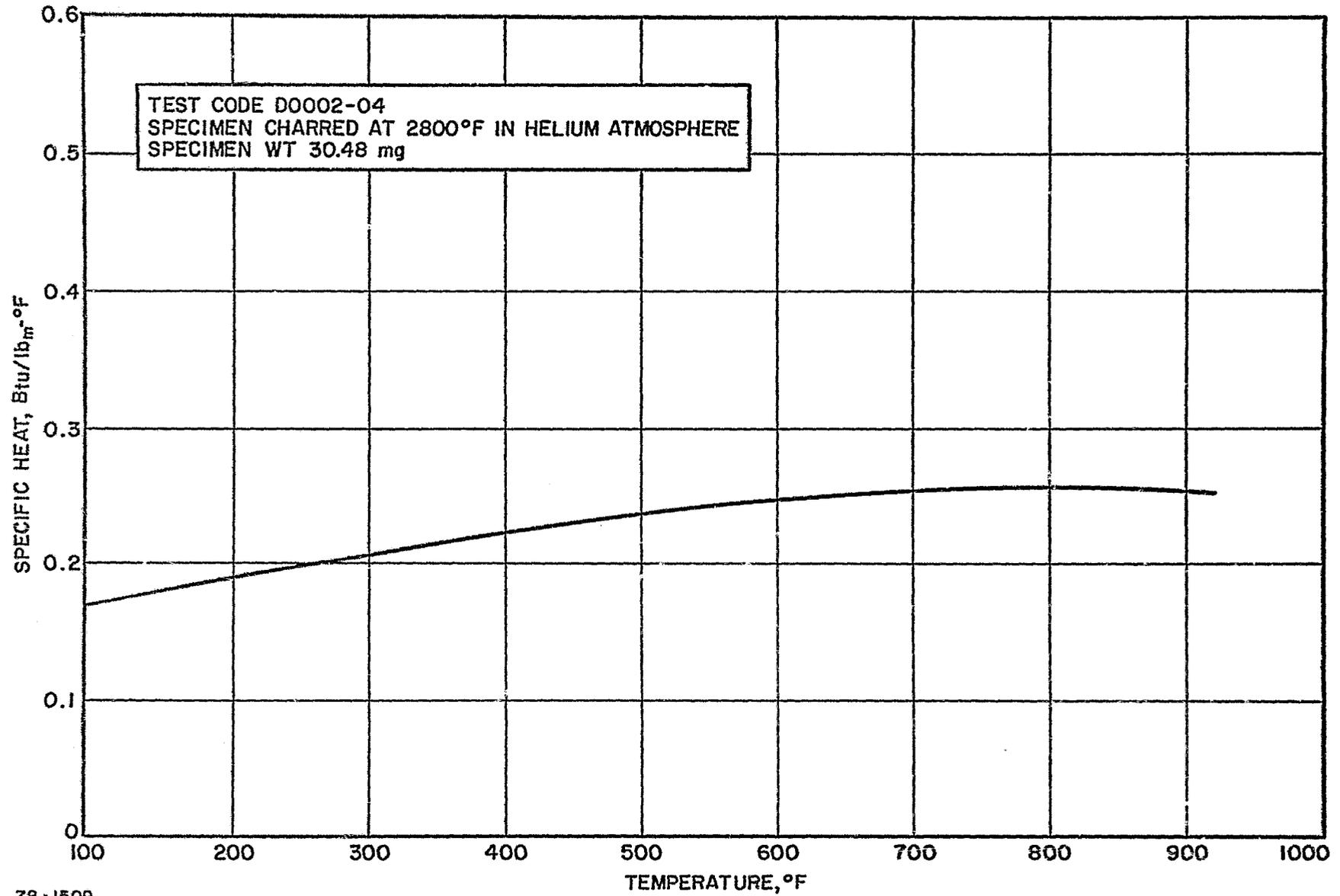
Figure 61  SILICA-PHENOLIC MXS-89, 2800°F PRECHARRED, SPECIFIC
HEAT VERSUS TEMPERATURE

78·1509

char temperature relationship as shown in Figures 54 through 62. Note, that, in contrast to the thermal conductivity measurements, data were obtained from the 2700° and 2800° F charred specimens owing to the small sample size requirement and the absence of a restrictive specimen geometry. Data were extracted from the $C_p$ versus temperature curves only at 200°, 500°, and 900° F for clarity of presentation. Any intermediate temperature can be similarly treated. From Figure 62 the specific heat-temperature relationship for any char temperature, within the range tested, can be postulated. It can be observed that the specific heat at any given temperature decreases with char temperature, suggesting a corresponding variation in composition as was indicated in both the microscopic and X-ray analyses.

Figures 63 through 67 show the results of the specific heat tests on the graphite-phenolic oven chars as performed on the DSC at 18° F intervals. These data were also replotted to provide specific heat versus char temperature data as shown in Figure 68.

The data in Figure 68 show that the specific heat at any given test temperature is not a strong function of char temperature, and since the specific heat is sensitive to material composition, the figure infers a similar composition of the MX4501 material at all char temperatures. This inference also supports the observations made during the 500X microscopic analysis of the material and the X-ray diffraction analyses.

2. Characterization of Post-Fired Nozzles

    a. Photomicrographic Observations of Post-Fired Nozzles

The post-fired nozzles, MXS-89 and MX4500, underwent extensive microscopic analysis. A careful examination of the char zones of each nozzle was conducted after the nozzles had been cut in half (Figures 2 and 3). The initial visual observations were that the basic char structure was similar over the entire length of the nozzle except at the zones immediately adjacent to the nozzle entrances where the char depth decreased abruptly. The abrupt change in char depth is attributed to the effect of whatever mounting jigs were used during the nozzle firing. The most notable difference between the two nozzles was that the char depth of the graphite-phenolic was greater -- presumably due to its higher thermal diffusivity. The following table summarizes the comparison between the two nozzle materials based on the initial cross-section visual examination:

Graphite-Phenolic Nozzles                          Silica-Phenolic Nozzles

In-Depth Char Zone

1. Apparent char depth -- 0.5 inches    1. Apparent char depth -- 0.3 inches

2. No signs of fabric layer separa-     2. Extensive fabric layer separation
   tion in the char zone                   in the char zone.
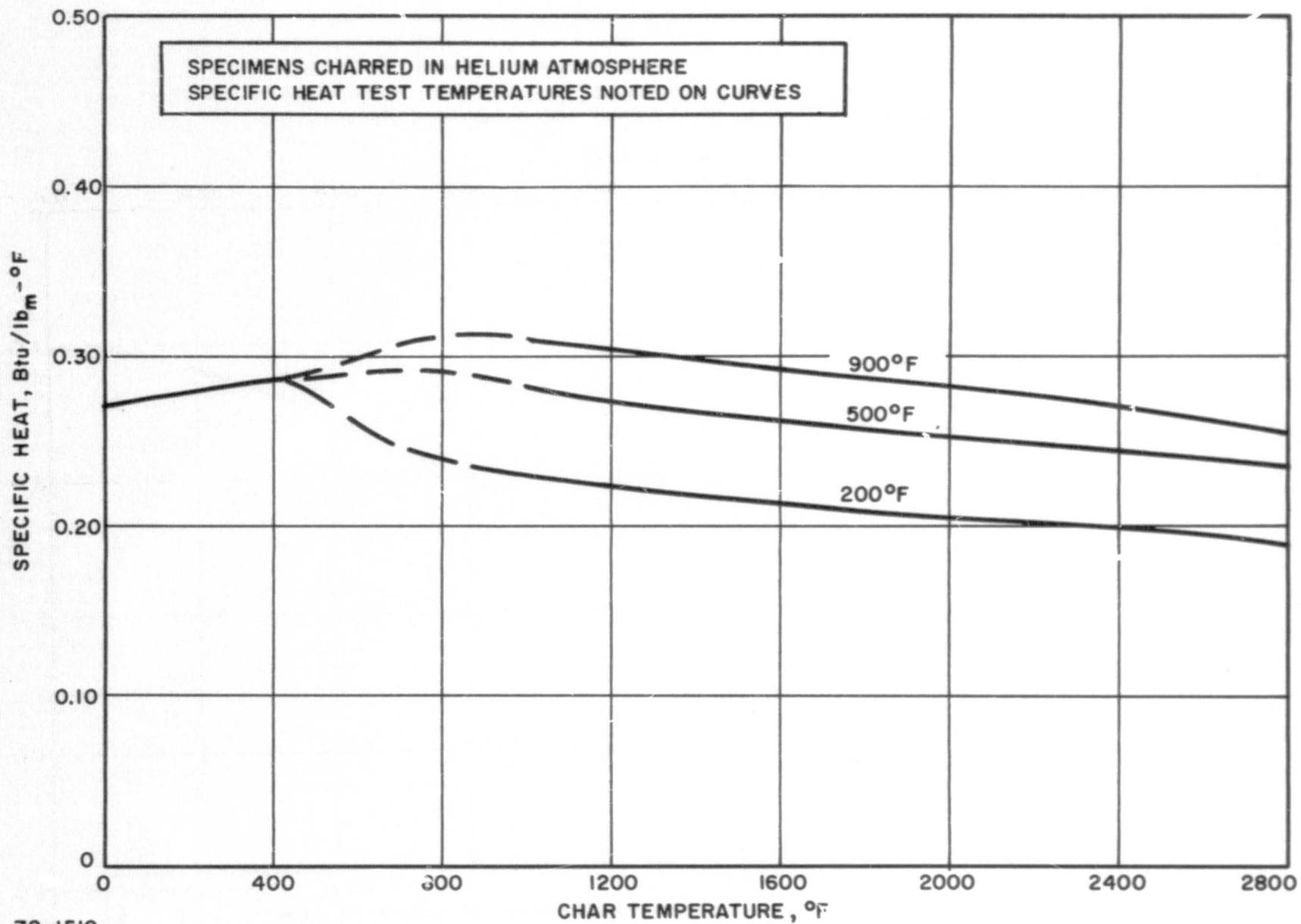
Figure 62  SILICA PHENOLIC MXS-89, SPECIFIC HEAT (AT TEMPERATURE)
VERSUS CHAR TEMPERATURE
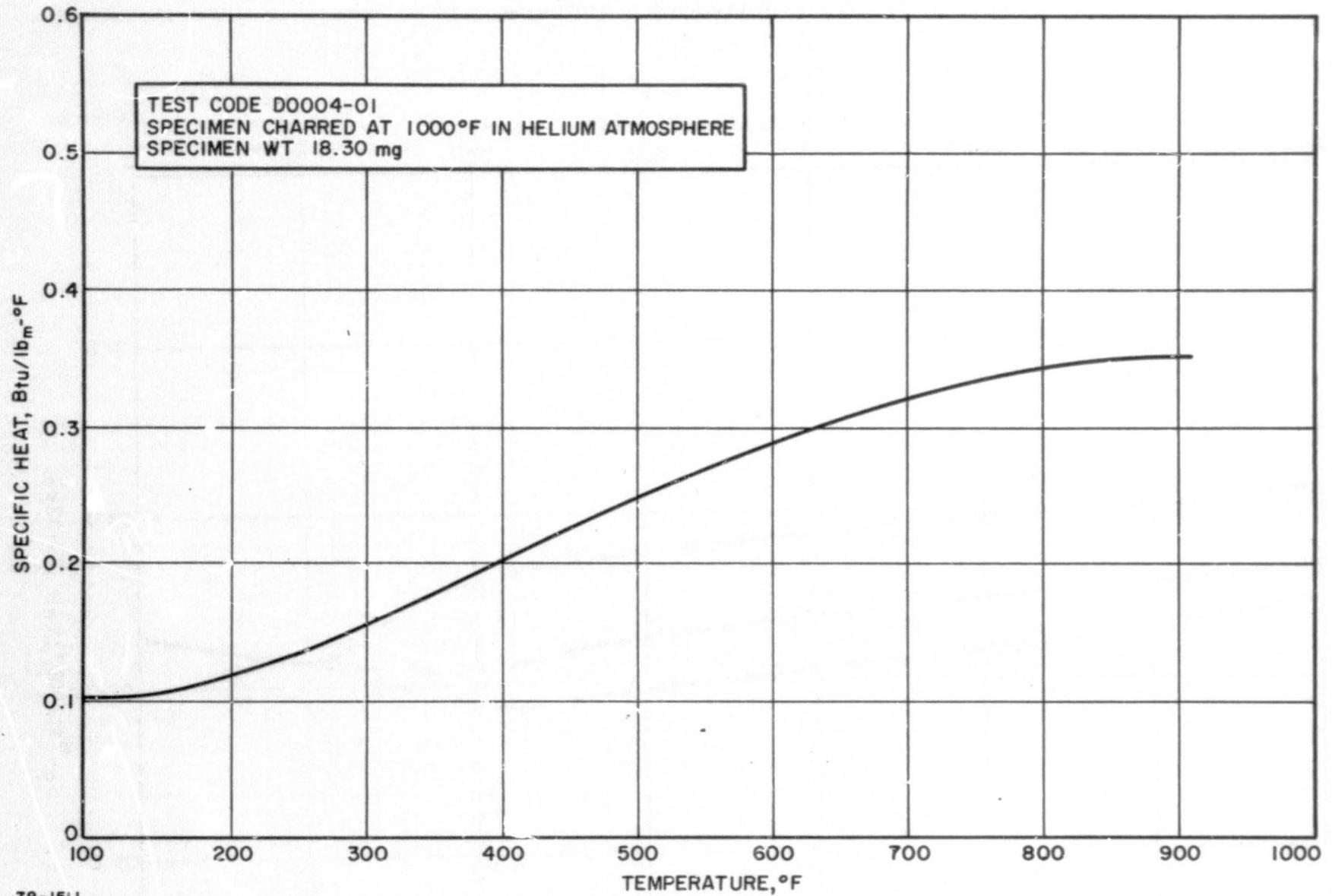
78-1510

Figure 63 GRAPHITE-PHENOLIC MX4501, 1000°F PRECHARRED, SPECIFIC
HEAT VERSUS TEMPERATURE

TEST CODE D0004-02
SPECIMEN CHARRED AT 2000°F IN HELIUM ATMOSPHERE
SPECIMEN WT 21.16 mg
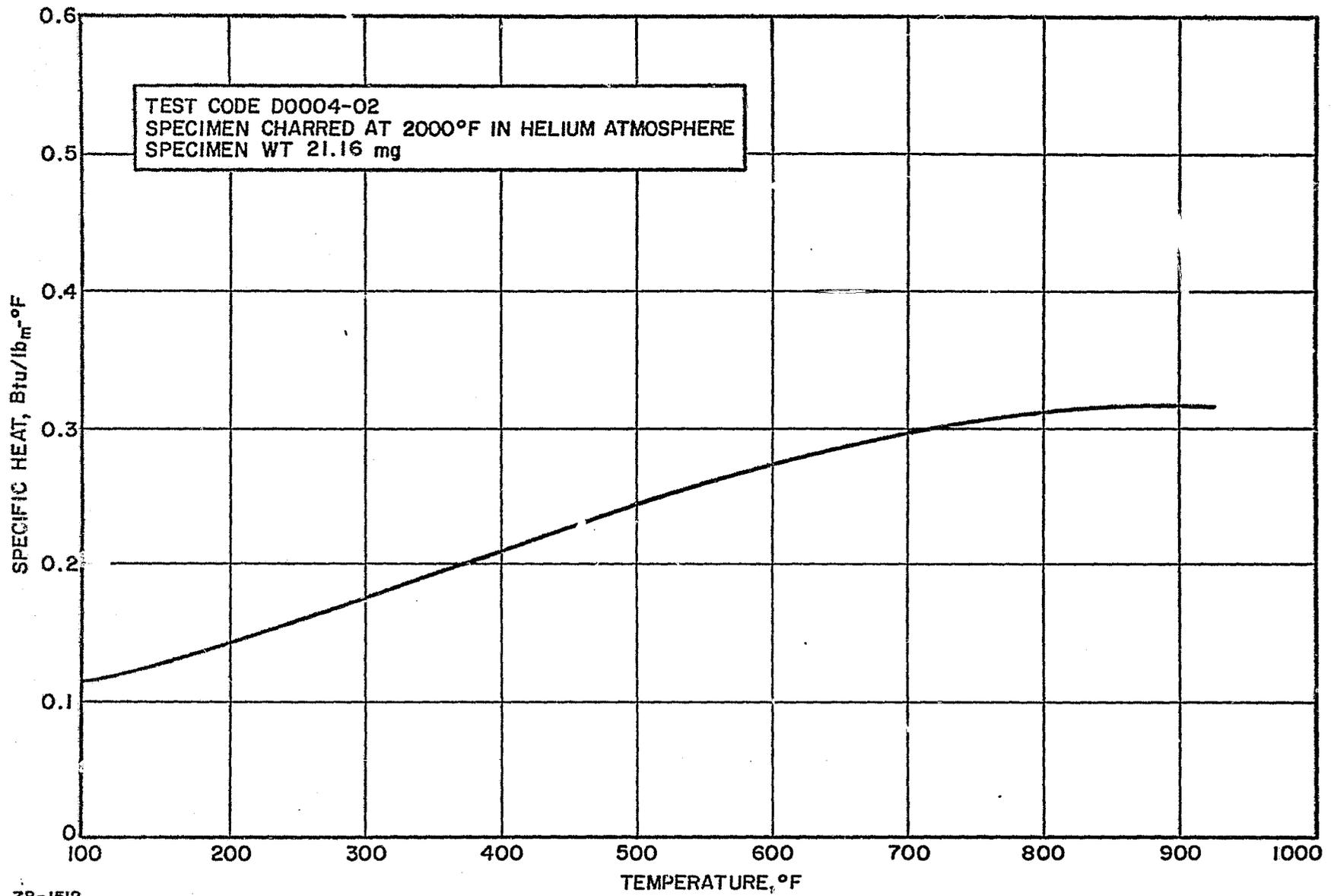
78-1512

Figure 64  GRAPHITE-PHENOLIC MX4501, 2000°F PRECHARRED, SPECIFIC
HEAT VERSUS TEMPERATURE
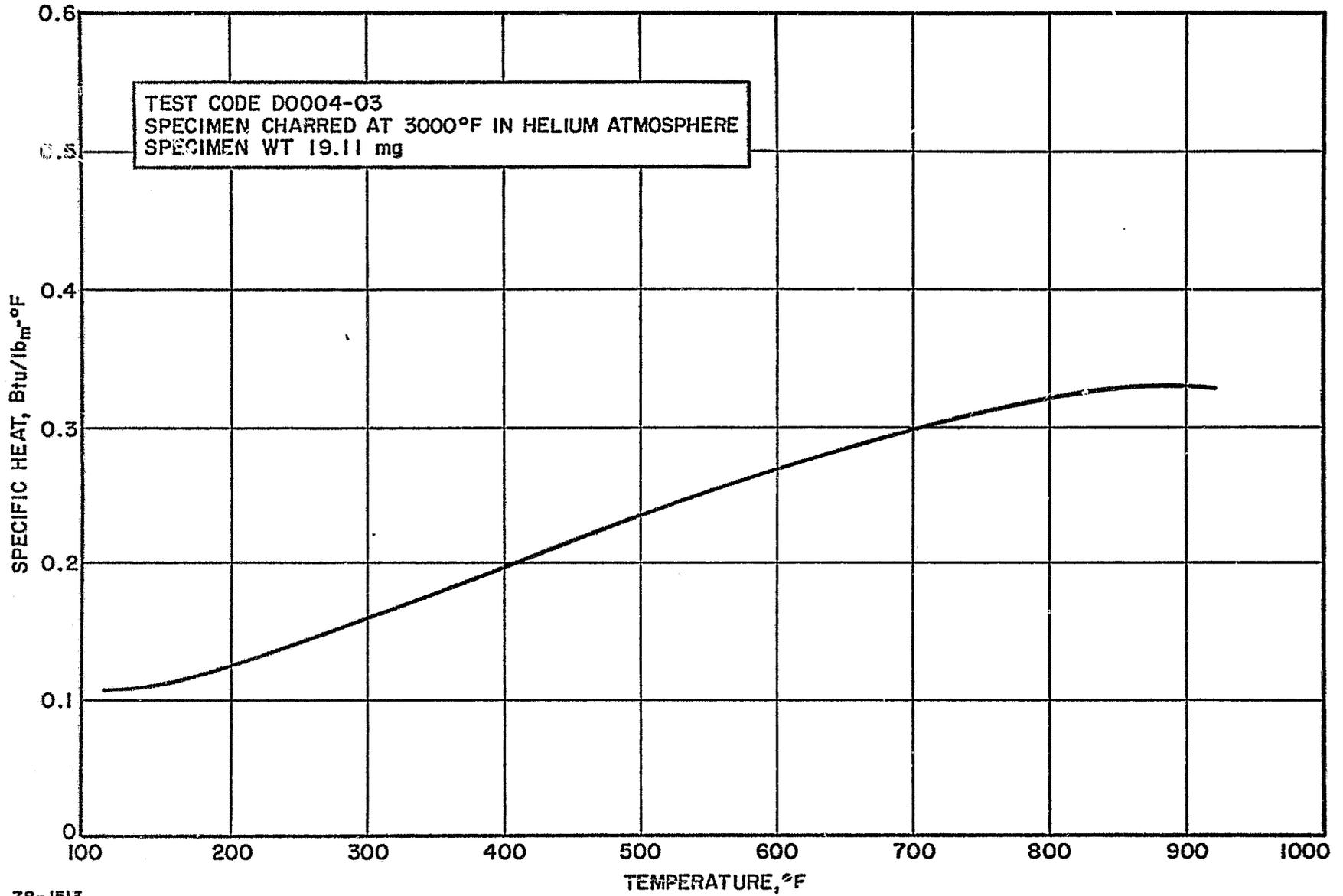
Figure 65 GRAPHITE-PHENOLIC MX4501, 3000°F PRECHARRED, SPECIFIC
HEAT VERSUS TEMPERATURE
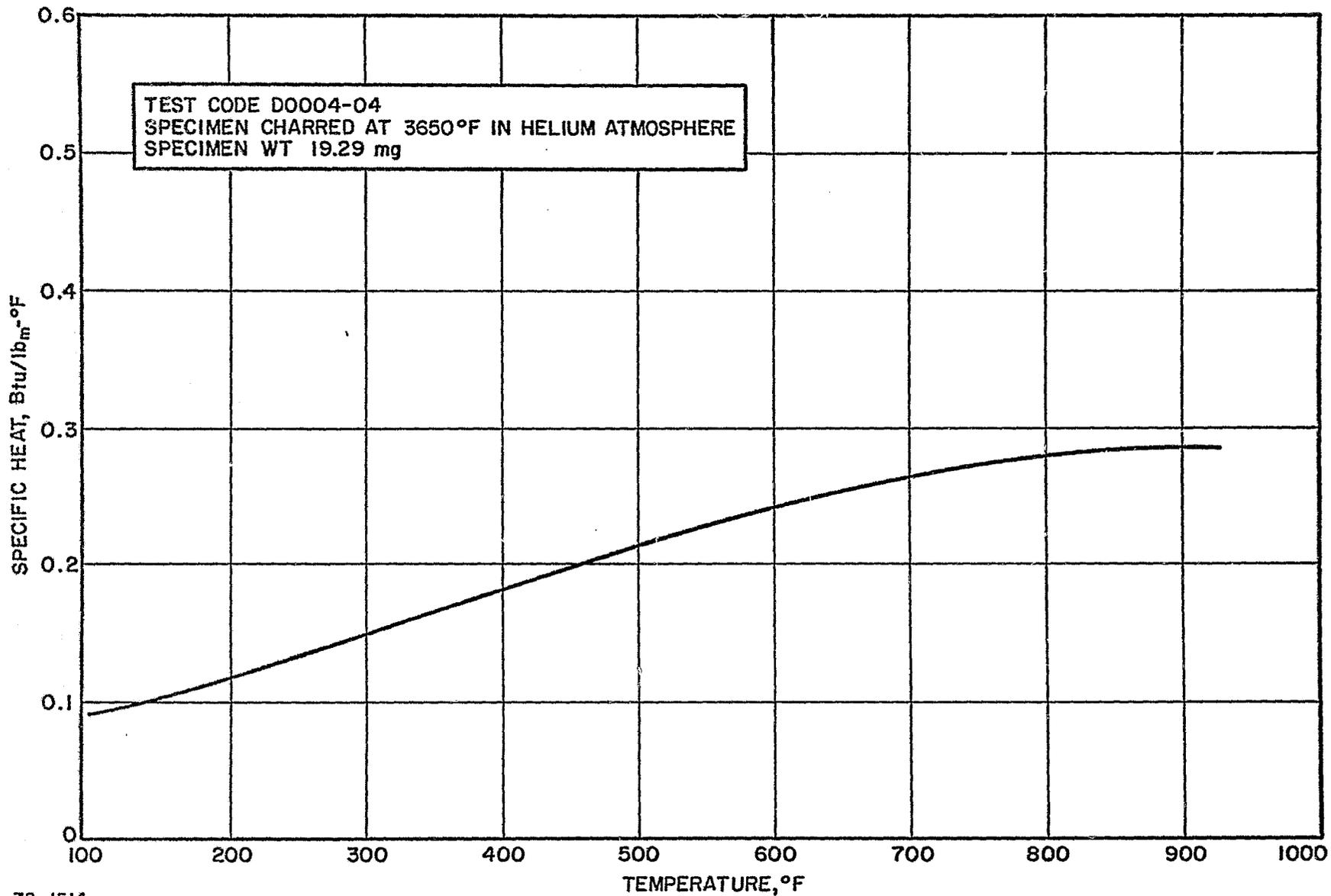
78-1513

78-1514

Figure 66  GRAPHITE PHENOLIC MX4501, 3650°F PRECHARRED, SPECIFIC
HEAT VERSUS TEMPERATURE
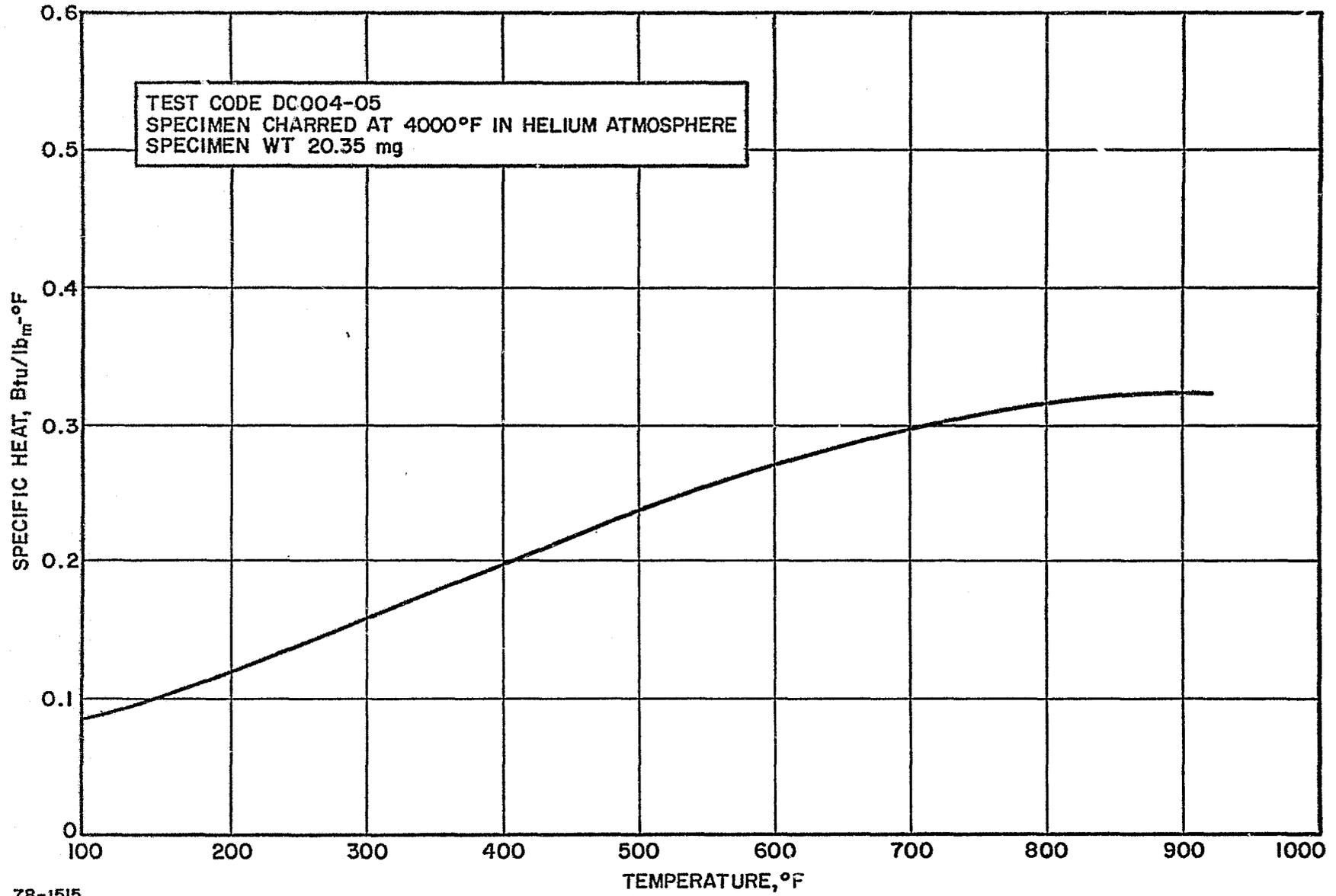
Figure 67 GRAPHITE-PHENOLIC MX4501, 4000°F PRECHARRED, SPECIFIC
HEAT VERSUS TEMPERATURE
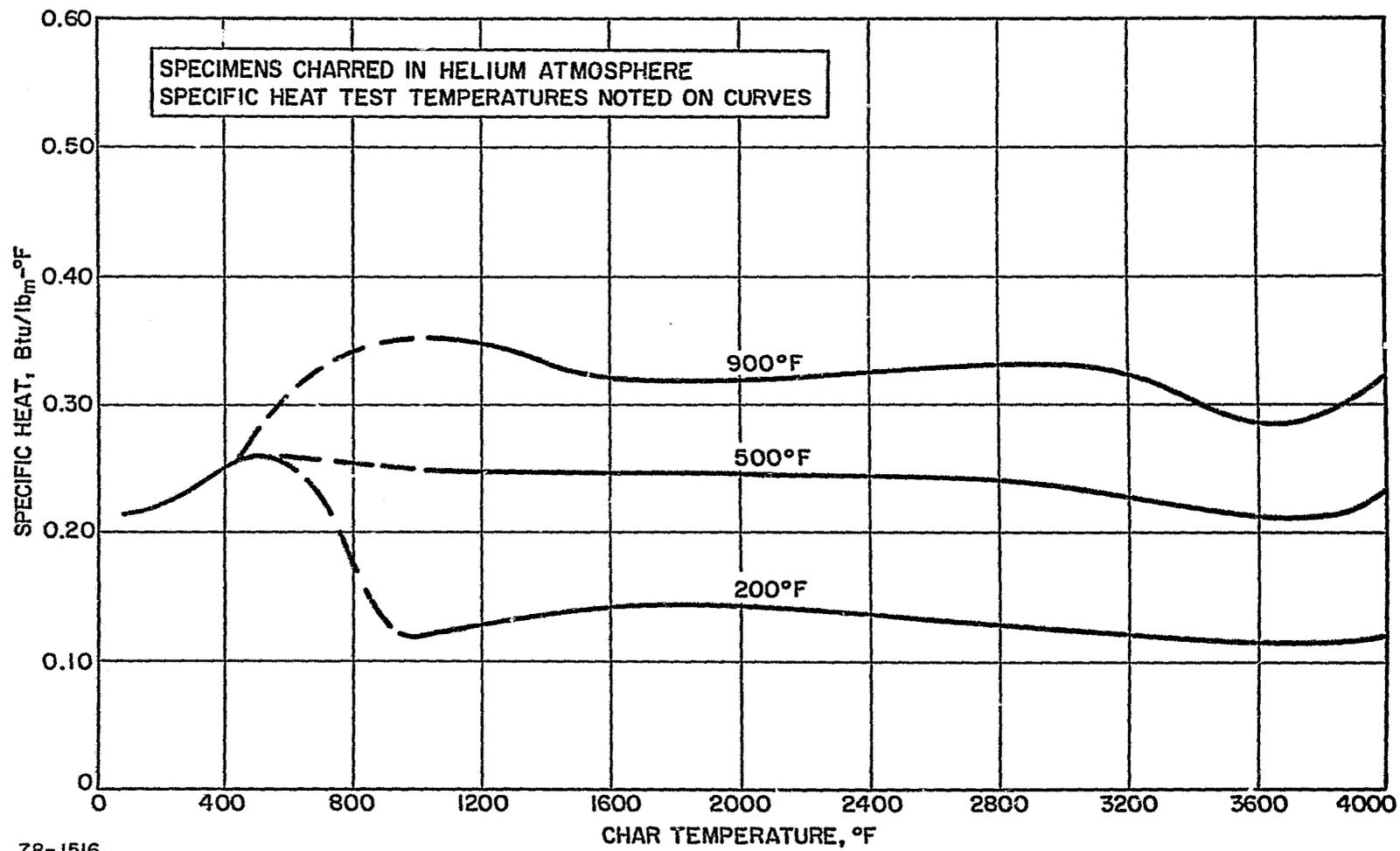
78-1515

78-1516

Figure 68  GRAPHITE PHENOLIC MX4501, SPECIFIC HEAT (AT
TEMPERATURE) VERSUS CHAR TEMPERATURE

3.  Resin degradation not apparent. Virgin to char texture grades from hard friable solid to soft granular coke.

3.  Resin degradation obvious. Virgin to char texture grades from hard resin, through charred resin to empty voids.

4.  No apparent percolation or re-deposition of resins.

4.  Resin percolation apparent -- redeposition of charred resins onto fabric and molten silica apparent.

## Interior Nozzle Surface

1.  Interior nozzle surface contains no signs of a molten product.

1.  Interior nozzle surface contains much molten material.

2.  Relatively smooth surface appears to have been formed by mechanical erosion-surface texture influence by the presence of fabric weave forming what looks like minute eddies.

2.  Surface appears to be composed chiefly of molten silica which has been dragged downstream in the form of tenaceous globules. The glassy silica is apparently coated with the percolating resins which have been charred to form a black glassy coating. A layer of soot overlays the glassy globules.

3.  Apparent erosion of the surface at the nozzle entrance altering the nozzle divergency.

3.  Clear glassy silica present at nozzle entrance -- grades into darker color downstream -- no apparent erosion of the nozzle entrance.

Sections were removed from the entrance, throat, and exit regions of each nozzle. These were subsequently mounted and polished for metallographic examinations. 5X magnification photographs were taken at each section to document the overall extent of the nozzle degradation. It was decided that the 100X and 500X microscopic examinations would be concentrated at the nozzle throat section because of the overall char similarity at the various sections.

1)  Silica Phenolic -- Figures 69, 70 and 71 show the 5X magnification photographs of the silica-phenolic MXS-89 nozzle chars taken at the three zones previously mentioned. Each photograph includes brief descriptions of the most pertinent observations that can be made at that magnification. In examining the two nozzles it was noted that the char structures were composed of four definable zones: charred, transition, degradation, and virgin zones. These zones are indicated in each of the three figures. However a more precisely dimensioned zone identification is shown in Figure 72 as prepared from 100X microscopic observations of the throat area and includes brief descriptions of the various regions. The regions identified as void areas were characterized by splitting of the laminates, the appearance of void pockets, and the presence of pyrolytic graphite.
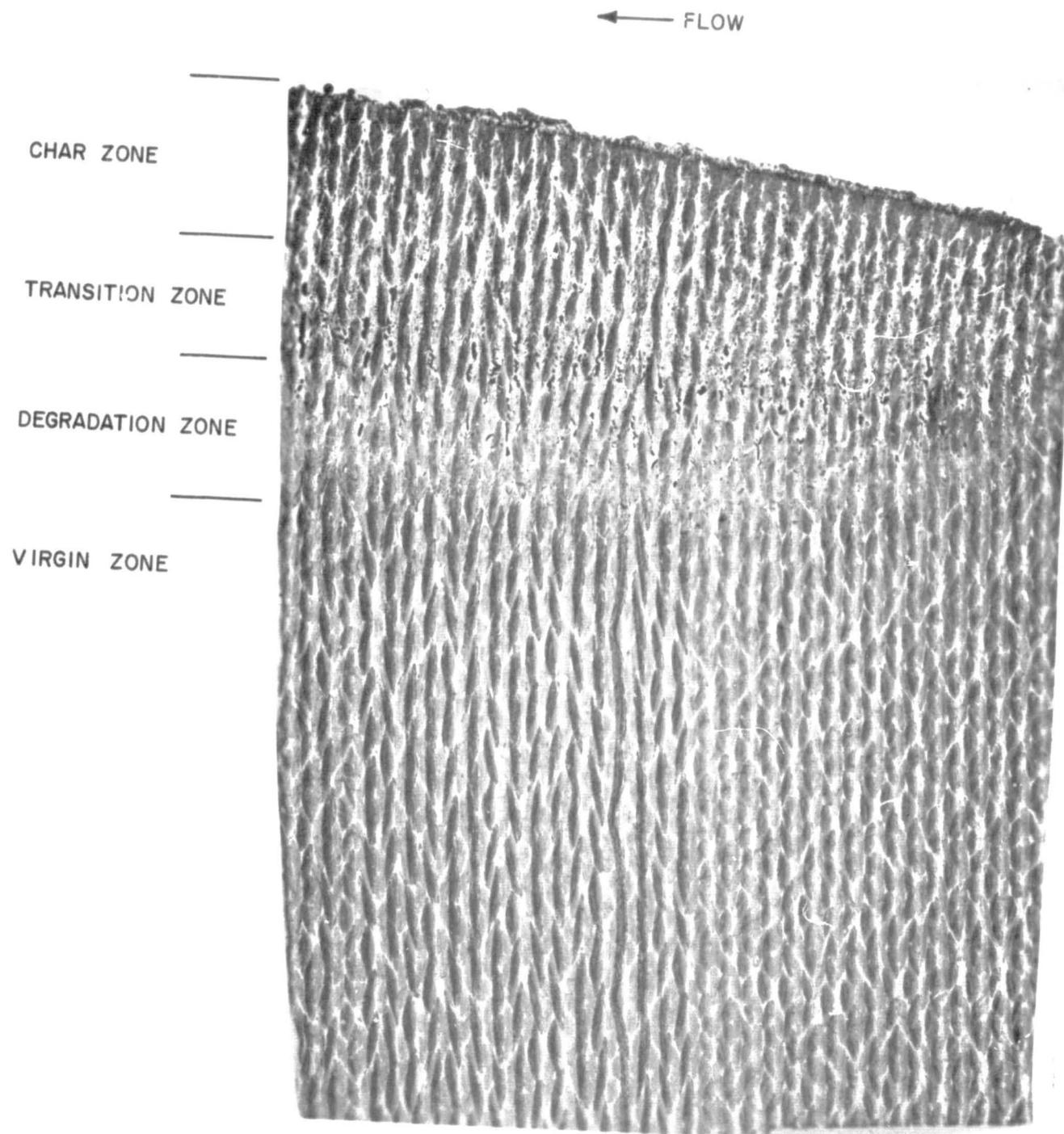
Figure 69 CUTAWAY VIEW OF SILICA-PHENOLIC MXS-89 ENTRANCE SECTION OF POST-FIRED ROCKET NOZZLE (5X MAGNIFICATION)

78-1517

FLOW

CHAR ZONE

TRANSITION ZONE

DEGRADATION ZONE

VIRGIN ZONE

MONTAGE
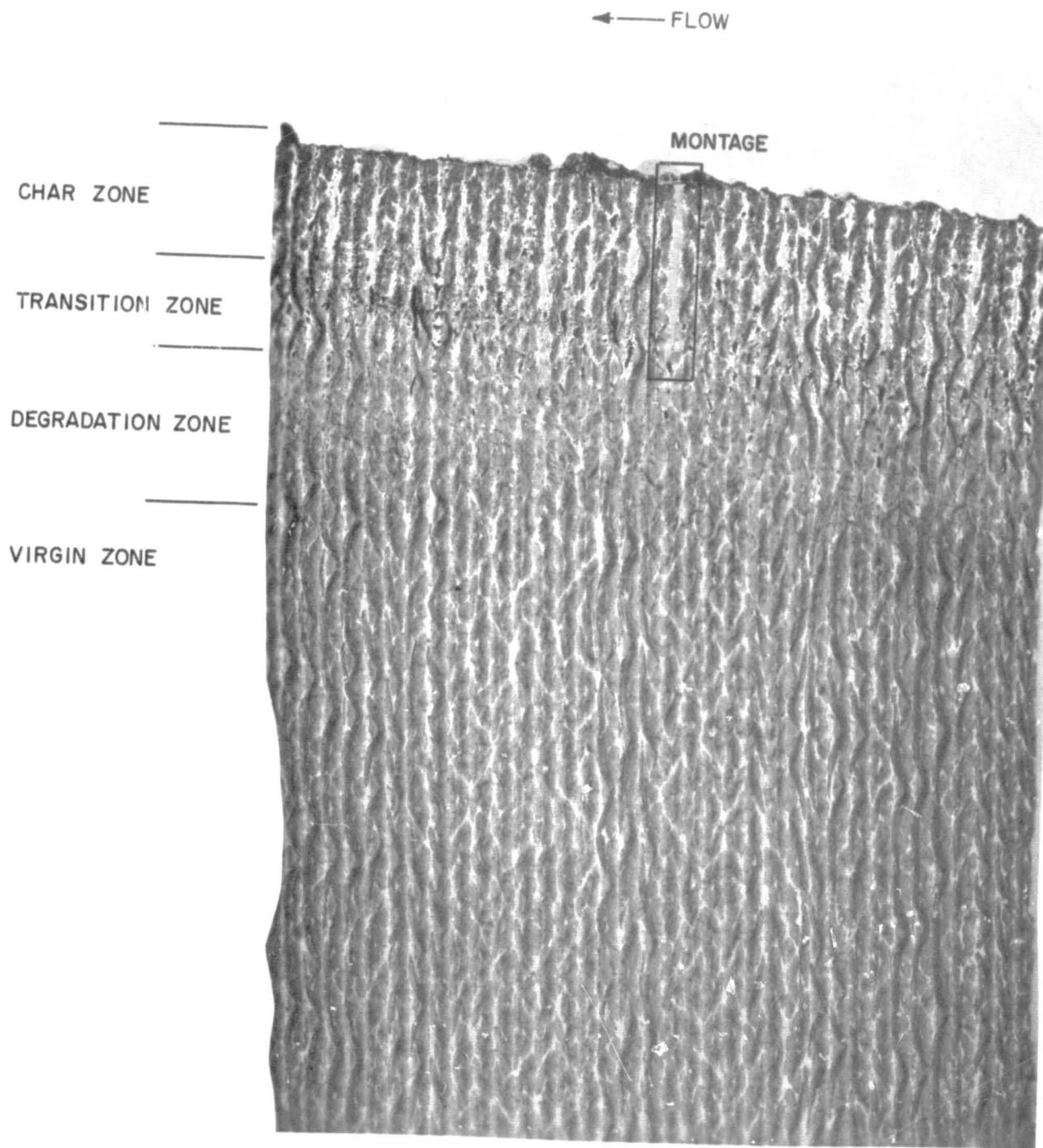
78-1518

Figure 70 CUTAWAY VIEW OF SILICA-PHENOLIC MXS-89 THROAT SECTION OF
POST-FIRED ROCKET NOZZLE (5X MAGNIFICATION)

← FLOW



CHAR ZONE

TRANSITION ZONE

DEGRADATION ZONE

VIRGIN ZONE
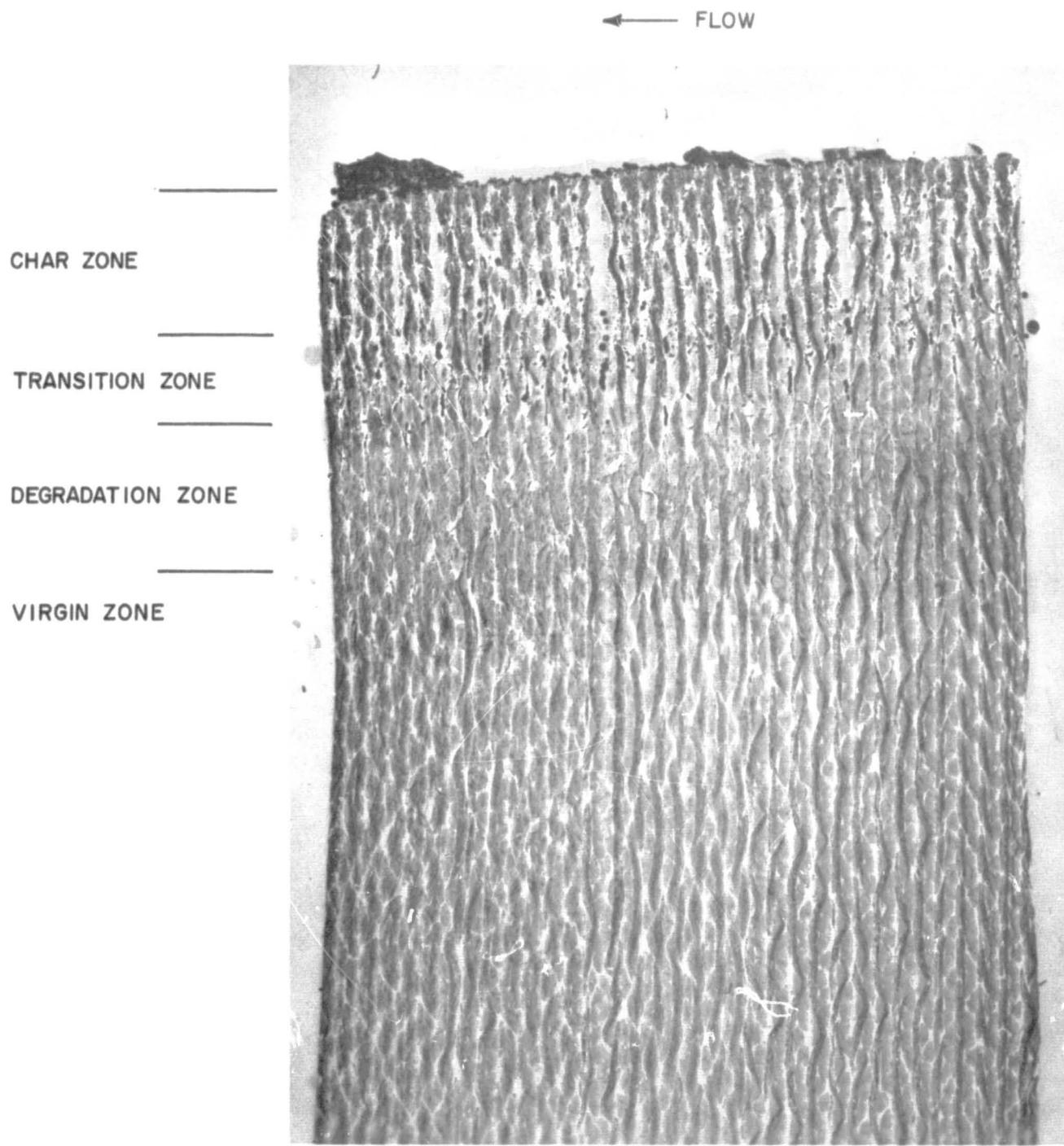
78-1519

Figure 71  CUTAWAY VIEW OF SILICA-PHENOLIC MXS-89 EXIT SECTION OF
POST-FIRED ROCKET NOZZLE (5X MAGNIFICATION)

0.020 in.

$S_1 O_2$

PYROLYTIC GRAPHITE

PHENOLIC CRACK AREA

CHARRED ZONE

VOID AREA

0.127 in.

0.070 in.

0.637 in.

BLACK TRANSITION ZONE

0.078 in.

DEGRADED (DISCOLORED)

0.362 in.

VIRGIN
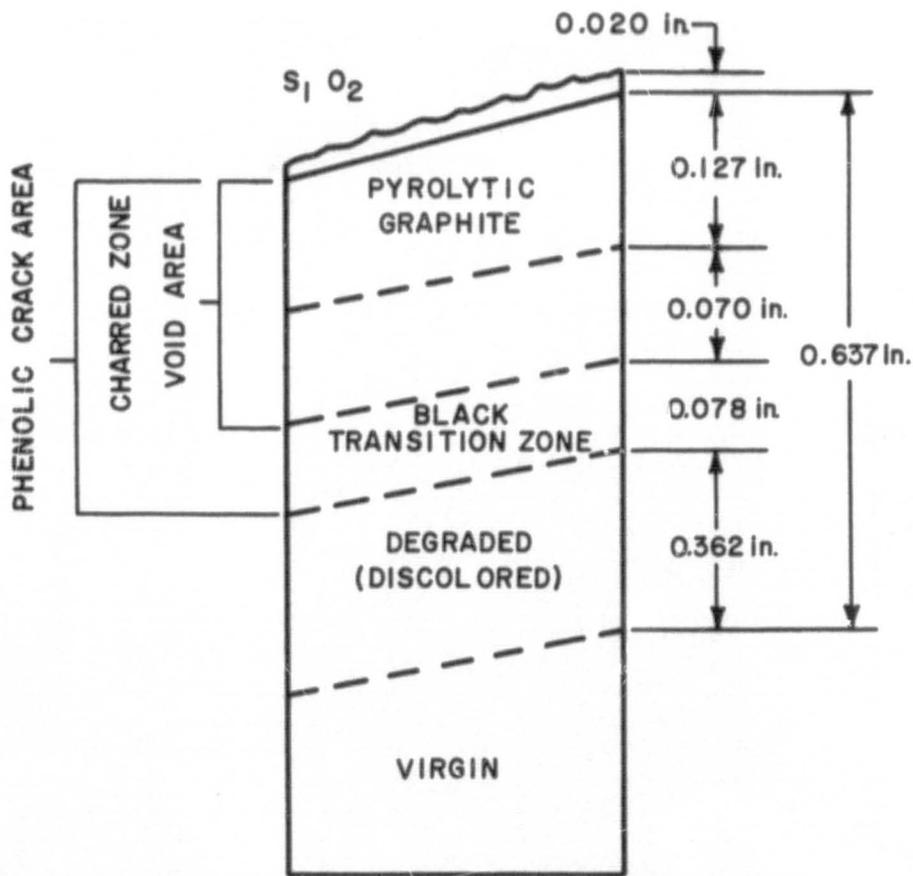
78-1520

Figure 72 CRITICAL ZONE LOCATIONS OF SILICA-PHENOLIC NOZZLE MXS-89-2
(THROAT SECTION)

The void area graded into a region in which the phenolic matrix contained vast amounts of cracking which were held to be the result of severe thermal stresses.

The transition zone was characterized by a more amorphous graphitic state associated with the breakdown of the phenolic matrix. The degraded zone was noted to be composed chiefly of a dark brown discoloration of the phenolic, apparently attaining temperatures insufficient to convert to a more charred state.

A 100X montage (Figure 73) using polarized lighting was constructed from a series of photographs of the area indicated in Figure 70. It clearly demonstrates the extent of the splitting which prevailed in the MXS-89 nozzle char. The top of the figure corresponds to the internal nozzle surface. The length of the montage corresponds to a char depth of approximately 1/4 inch. The most notable observations were the tight weave pattern of the silica fibers, the bright lining along the walls of the fissure indicating the extent of pyrolytic graphite deposition, and the predominance of a heavy silica layer at the mouth of the crack. The dispersion of the pyrolytic graphite indicated by the bright regions is clearly seen not only along the fissure walls but also surrounding the individual fibers in the adjacent regions.

During the 500X microscopic study at the throat section, four photographs were taken at different char levels. These are shown in Figures 74 through 77. The figures are arranged in consecutive order starting at the surface and continuing in-depth. The orientation of each view with respect to the char surface has been included in each figure.

Figure 74 shows the immediate surface layer. Melting and fusion of the silica fibers can be seen at the lower left corner. The overcoating immediately adjacent to the fibers is considered to be silicon carbide. The rounded buildup (light gray) of material along the walls of the split (slightly to the right of the photo vertical centerline) is pyrolytic graphite while the underlayment is fully charred phenolic. Molten surface silica is shown in the top-center region of the photo and contains many voids and cracks. Above that region and throughout various sections of the photograph (dark gray areas) is the epoxy used in the metallographic mountings.

The center of Figure 75 is located at a depth of 0.027 inch from the char surface. The dark gray areas are the mounting epoxy. The buildup of pyrolytic graphite is clearly demonstrated, and no apparent melting of the fibers has occurred at this depth. The absence of phenolic cracks in the areas of the fiber bundles is also notable. There does appear to be some evidence of reactions around the periphery of the fibers in the top half of the photo. The pyrolytic graphite appears to have been built up at different rates (or perhaps times) by the stratification of the layers. Charred phenolic is shown as the light gray regions surrounding the fibers.

Figure 76 was taken in the transition zone at a depth of 0.238 inch (photo center). The dark gray areas are the mount epoxy. Typical of the transition zone are the many cracks throughout the charred phenolic matrix.

MELTED SILICA

INTERLAMINATE FISSURE

PYROLYTIC GRAPHITE

SILICA FIBERS END VIEW

SILICA FIBERS SIDE VIEW

SURFACE CHAR ZONE

CHARRED PHENOLIC WITH P.G. DEPOSITION

78-1521
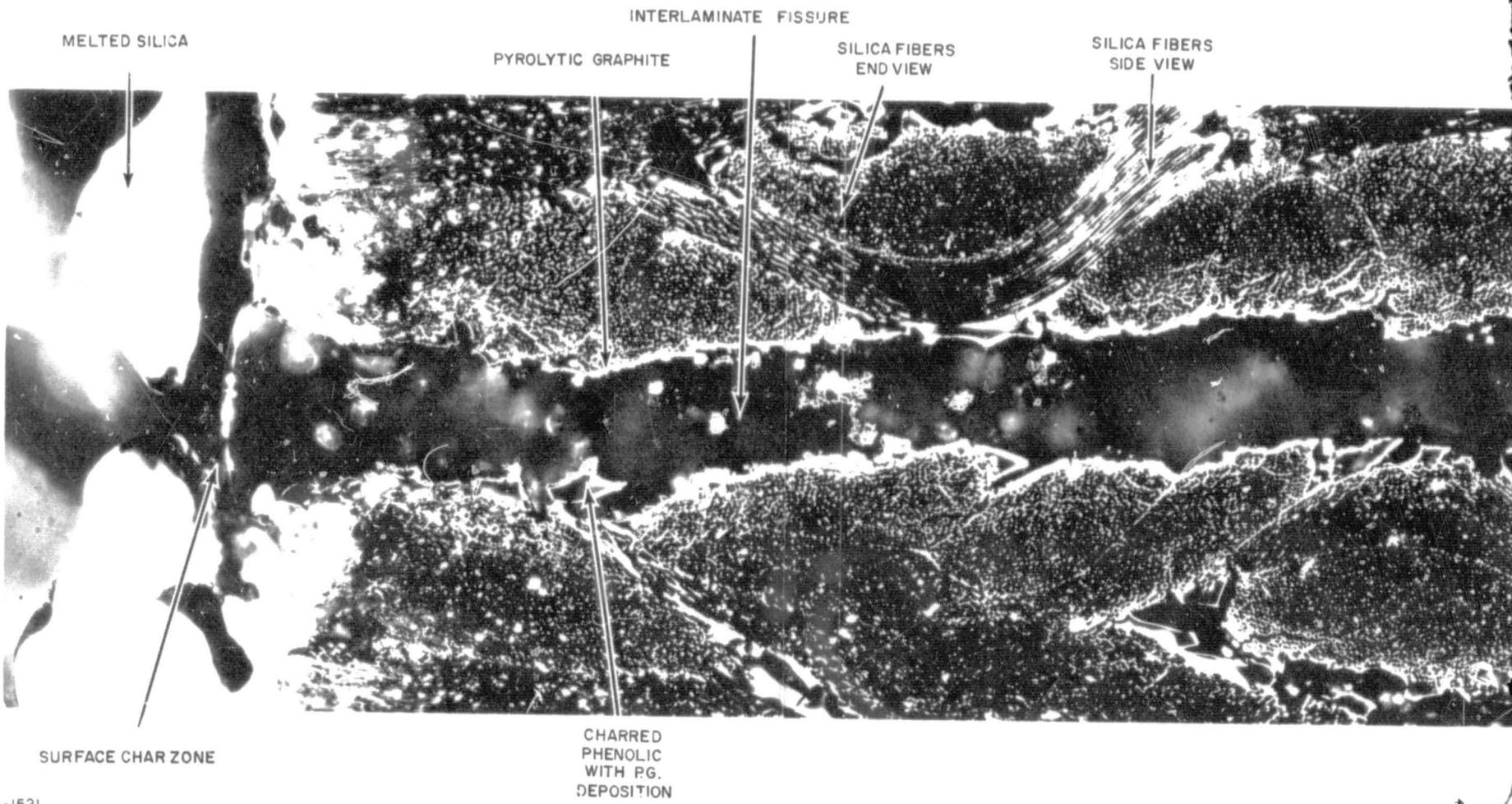
Figure 73  SILICA-PHENOLIC MXS–
MONTAGE (
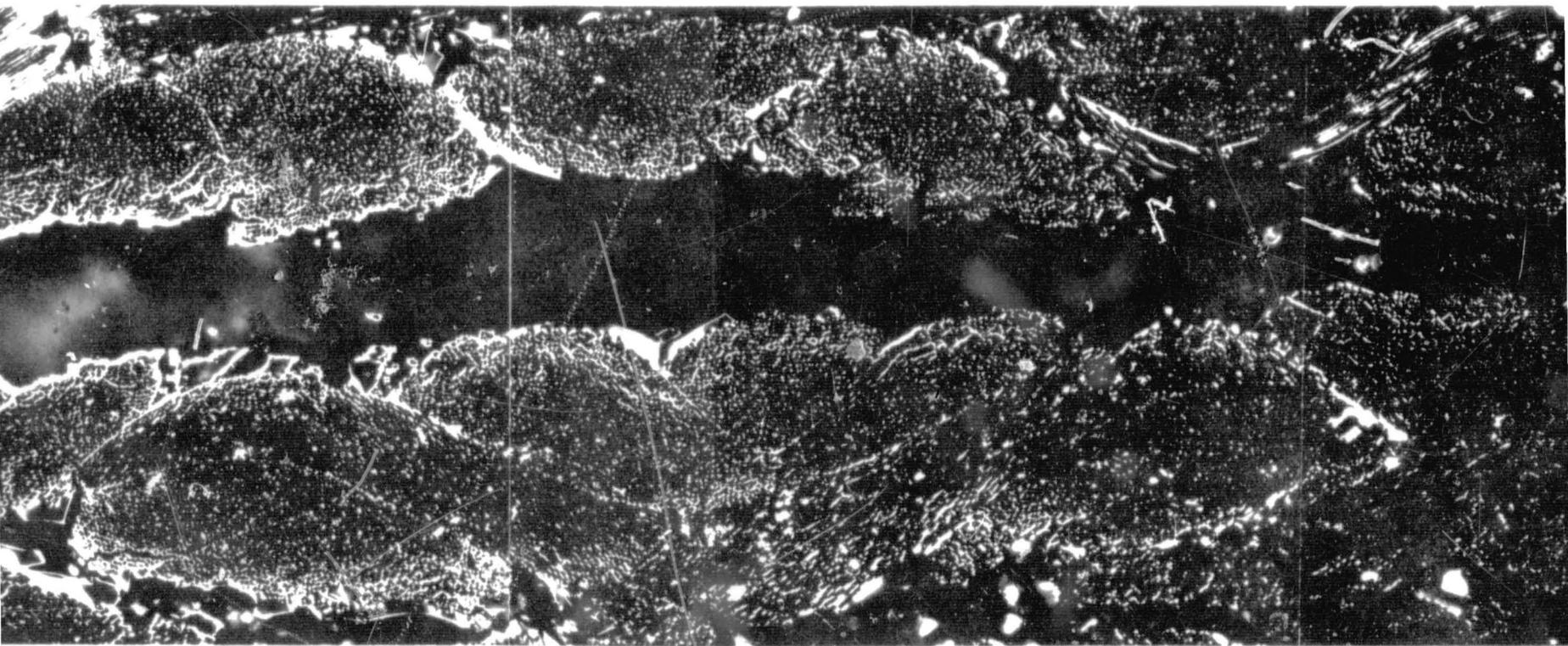
Figure 73 SILICA-PHENOLIC MXS-89 POST-FIRED ROCKET NOZZLE CHAR ZONE
MONTAGE (100X MAGNIFICATION)
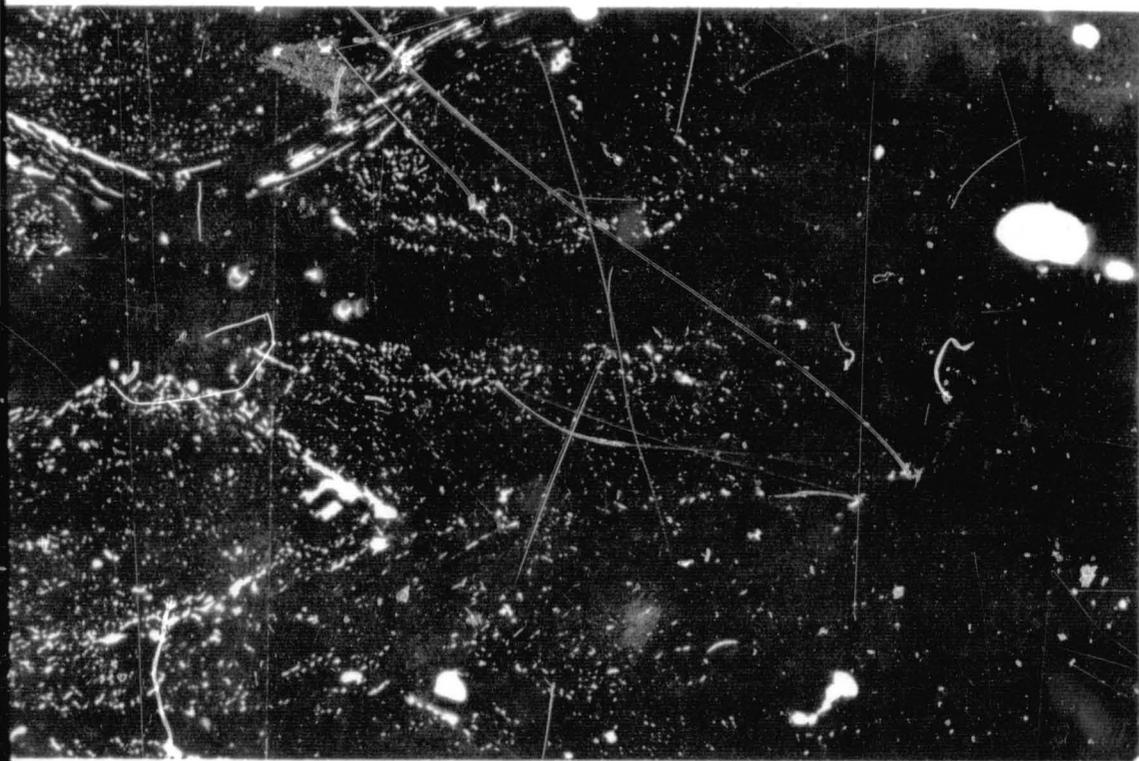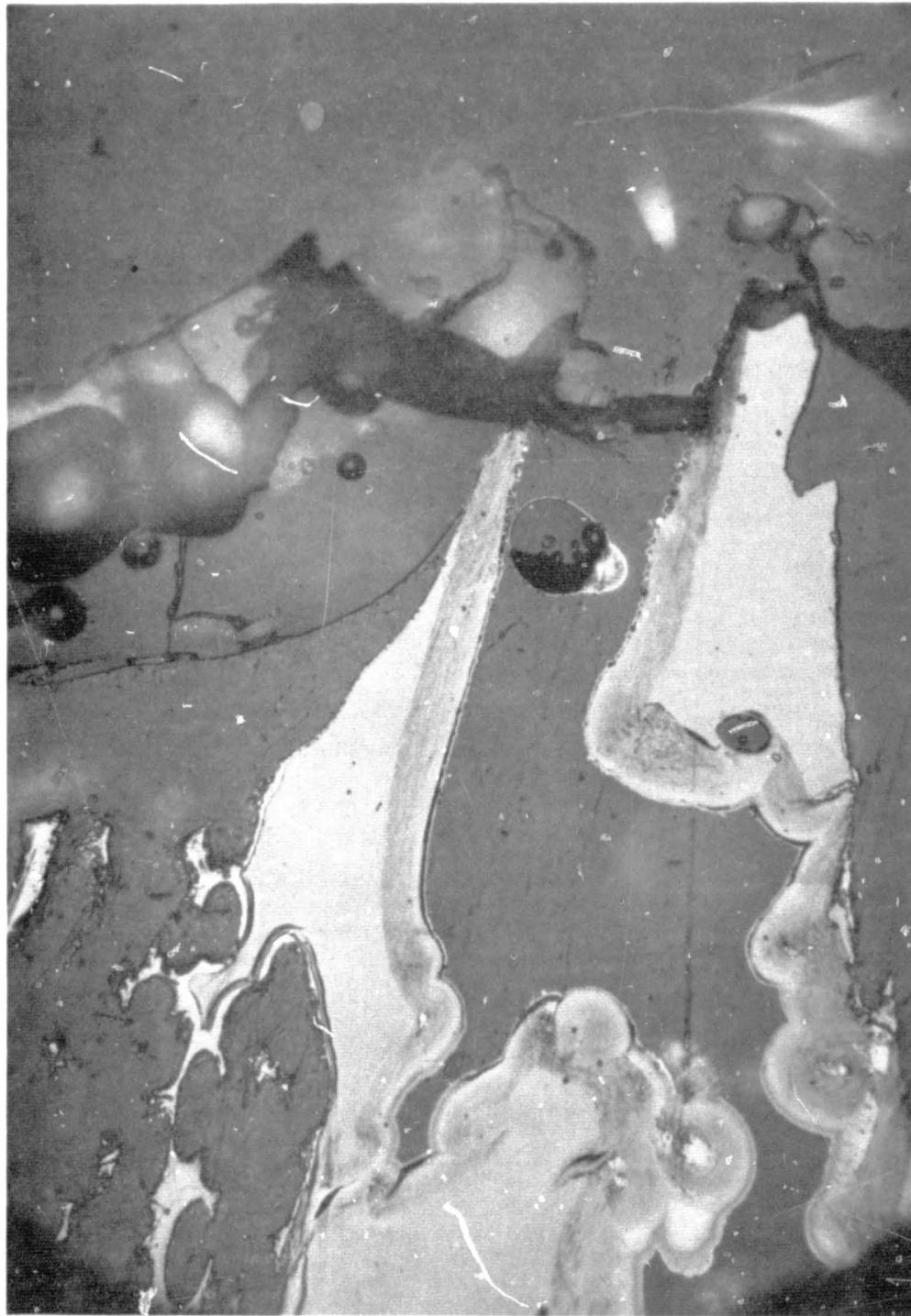
Figure 74 POST-FIRED SILICA-PHENOLIC MXS-89 NOZZLE SURFACE CHAR
(500X MAGNIFICATION)

NOZZLE CHAR SURFACE
⟶
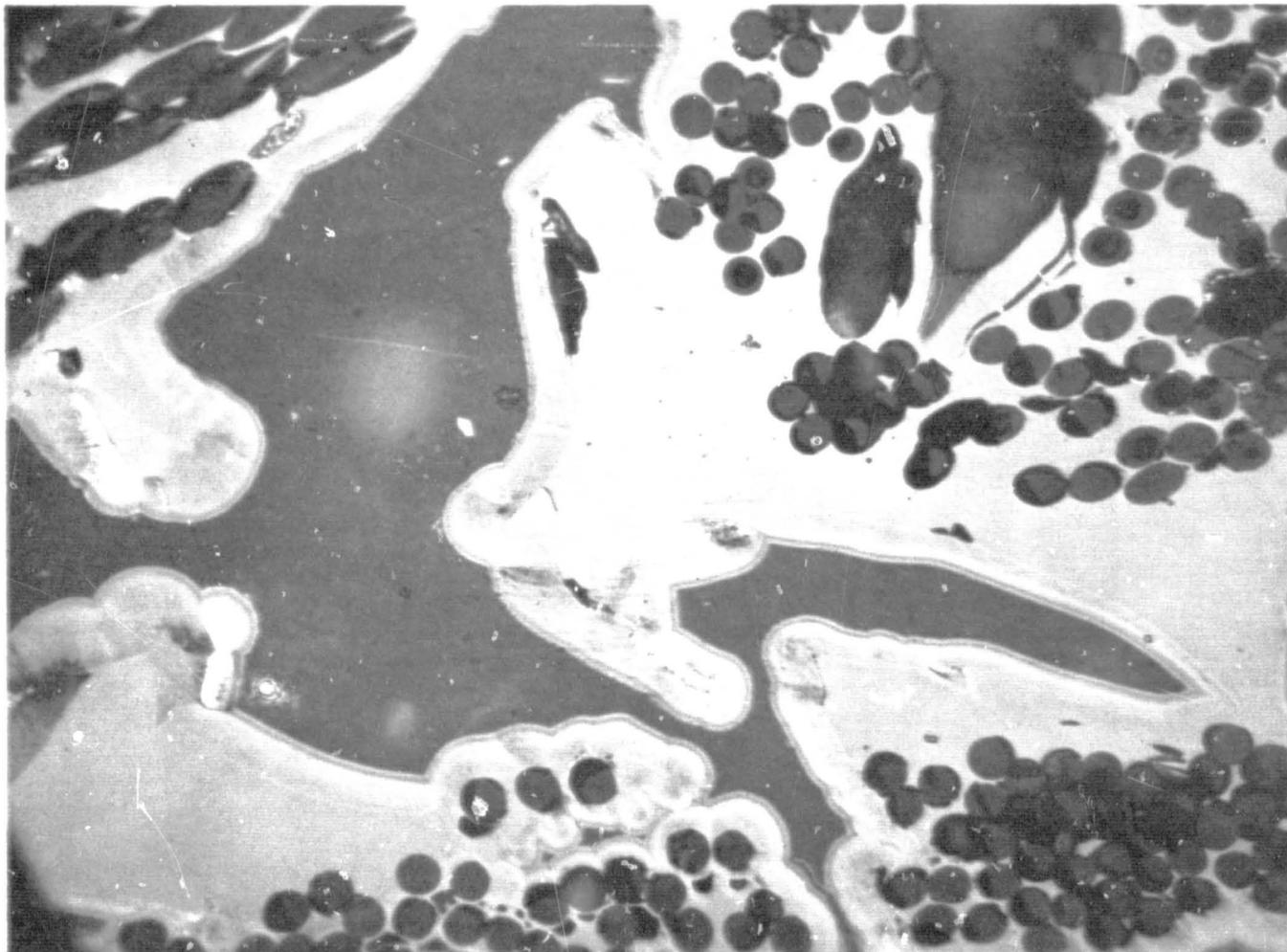


|← ——— 0.027 inches FROM CHAR SURFACE ———→

78-1522

Figure 75  POST-FIRED SILICA-PHENOLIC MXS-89 NOZZLE CHAR, 0.027-INCH
CHAR DEPTH (CHAR ZONE) (500 MAGNIFICATION)

NOZZLE CHAR SURFACE

→
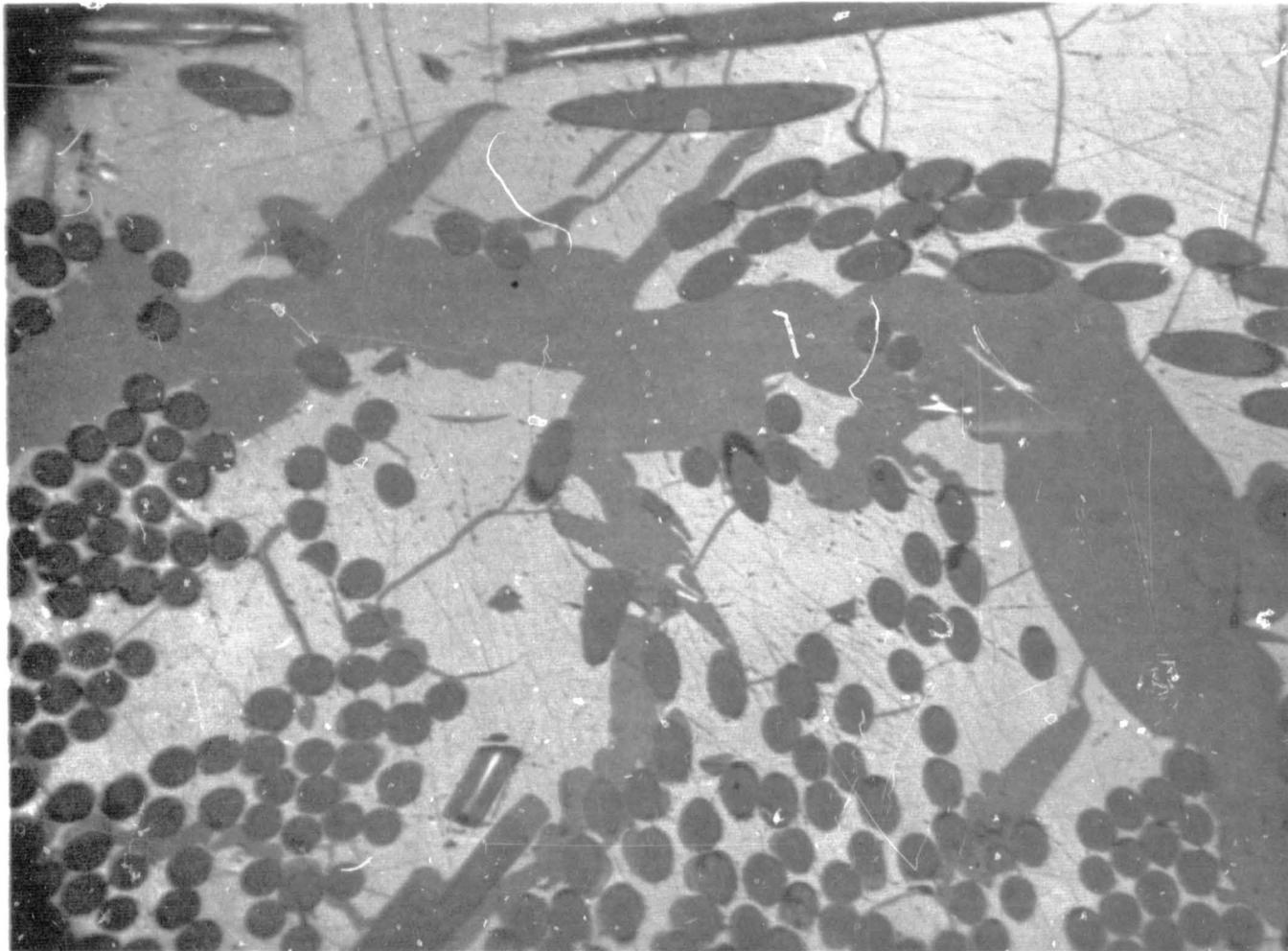


←──── 0.238 inches FROM CHAR SURFACE ────→

78-1523

Figure 76   POST-FIRED SILICA-PHENOLIC MXS-89 NOZZLE CHAR, 0.238-INCH
CHAR DEPTH (TRANSITION ZONE) (500X MAGNIFICATION)

NOZZLE CHAR SURFACE
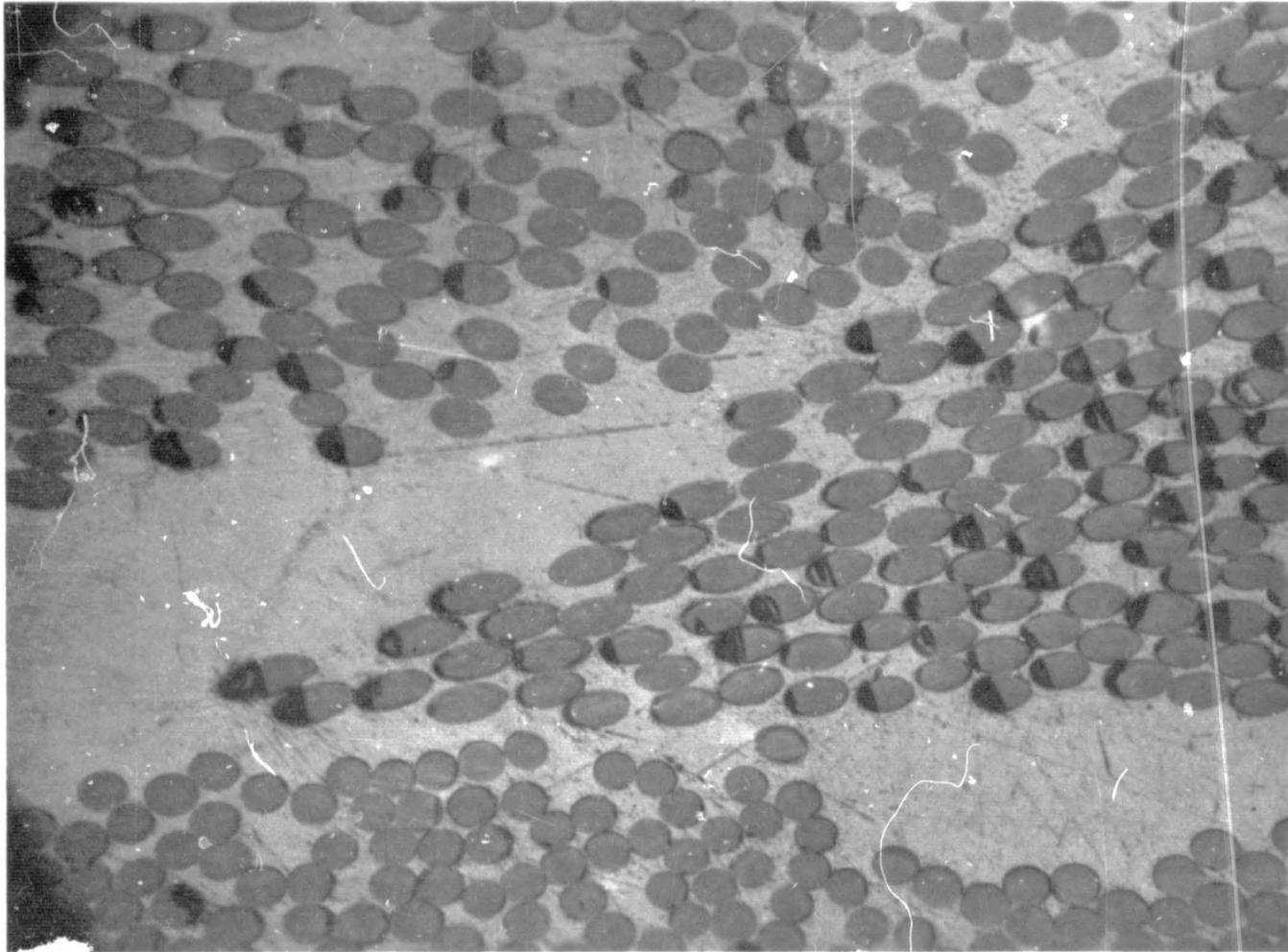


← 1 inch FROM CHAR SURFACE →

78-1524

Figure 77 POST-FIRED SILICA-PHENOLIC MXS-89 NOZZLE CHAR, 1-INCH DEPTH
(VIRGIN ZONE) (500X MAGNIFICATION)

There was no evidence of any deposition of pyrolytic graphite, and the silica fibers are intact and unreacted upon.

Figure 77 was taken in the virgin zone at a depth of approximately 1 inch from the char surface. There are no thermal stress cracks present, and the fibers are intact. Notice the clarity and grain free condition of the phenolic matrix.

2) Graphite-Phenolic -- Figures 78 through 80 show the 5X magnification views of the entrance, throat, and exit sections of the graphite-phenolic MX4500 nozzle. As with the MXS-89 nozzle the chars contained the four zones previously identified. These are indicated in the figures. Although the photo contrast is less for the MX4500 sections, these figures show the degree of splitting in the char zone which is much less than that which appear in the silica-phenolic material except for one major fissure shown in Figure 79. The charred regions are characterized by a large percentage of void or char pockets, an eroded char surface, and the presence of pyrolytic graphite (not observable on the 5X views), and extensive cracking and splitting of the graphite filler material. The transition zone which appears on the photo as a blanched band is relatively free of the extensive fissuring existing in the char zone. Likewise, the degradation zone is relatively free of interlaminar and fiber splitting. However the virgin region is dominated by much splitting of the graphite fibers, many of which are across the fiber grains. The splitting stopped toward the degraded zone apparently coalescing to form continuous strands throughout the rest of the char zone. The latter comments were made as a result of a 100X microscopic examination of the throat section mounting and is not evident from the 5X views. The dimensions of the various zones within the nozzle char are shown in Figure 81. These dimensions were established during the 100X examination.

Figure 79 shows the area which was covered in the construction of the 100X montage illustrated in Figure 82. Like the silica-phenolic montage, the depth of coverage is approximately 1/4 inch. The photographs arranged in the mosaic were taken using polarized lighting to aid in describing the extent of pyrolytic graphite deposition. This is shown as the bright areas which are predominant along the fissure walls and in general permeate the entire structure. As expected, the deposition of graphite diminishes toward the in-depth regions. The surface portion of the top photograph shows the pyrolytic graphite buildup extending out beyond the char layer. The latter indicates the mechanical effect of material erosion from the surface by the subsequent and sudden removal of material immediately adjacent to the graphite spike.

The four photographs shown in Figures 83 through 86 were taken at several char depths during the 500X microscopic study. Figure 83 was taken at the surface. Again the dark gray areas are the mounting epoxy. The buildup of pyrolytic graphite along the fissure wall is obvious. It is interesting to note the absence of pyrolytic graphite on the individual fibers near the surface. It is felt that the sweeping away action of the shearing combustion gases does not allow a buildup at this point. Areas, such as the fissure channel shown which extend further down into the char, experience large volume flow rates from the materials decomposing in depth and thus are not appreciably influenced by the gas shear action. The availability

FLOW $\longrightarrow$



CHAR ZONE

TRANSITION ZONE

DEGRADATION ZONE

VIRGIN ZONE
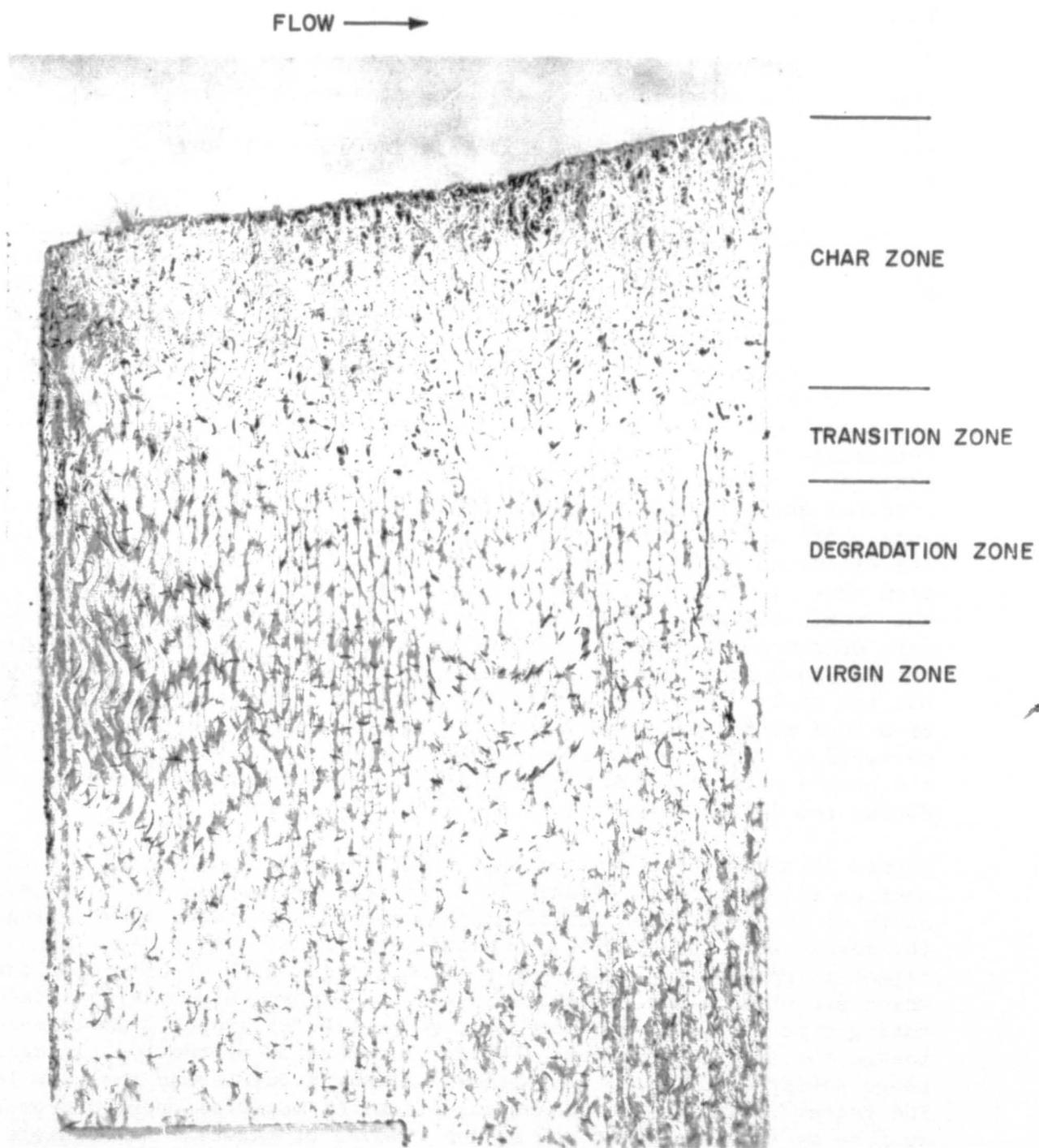
78-1525

Figure 108 GRAPHITE-PHENOLIC NOZZLE EXIT, SURFACE CHAR, SPECIFIC HEAT
VERSUS TEMPERATURE

FLOW

MONTAGE

CHAR ZONE

TRANSITION ZONE

DEGRADATION ZONE

VIRGIN ZONE
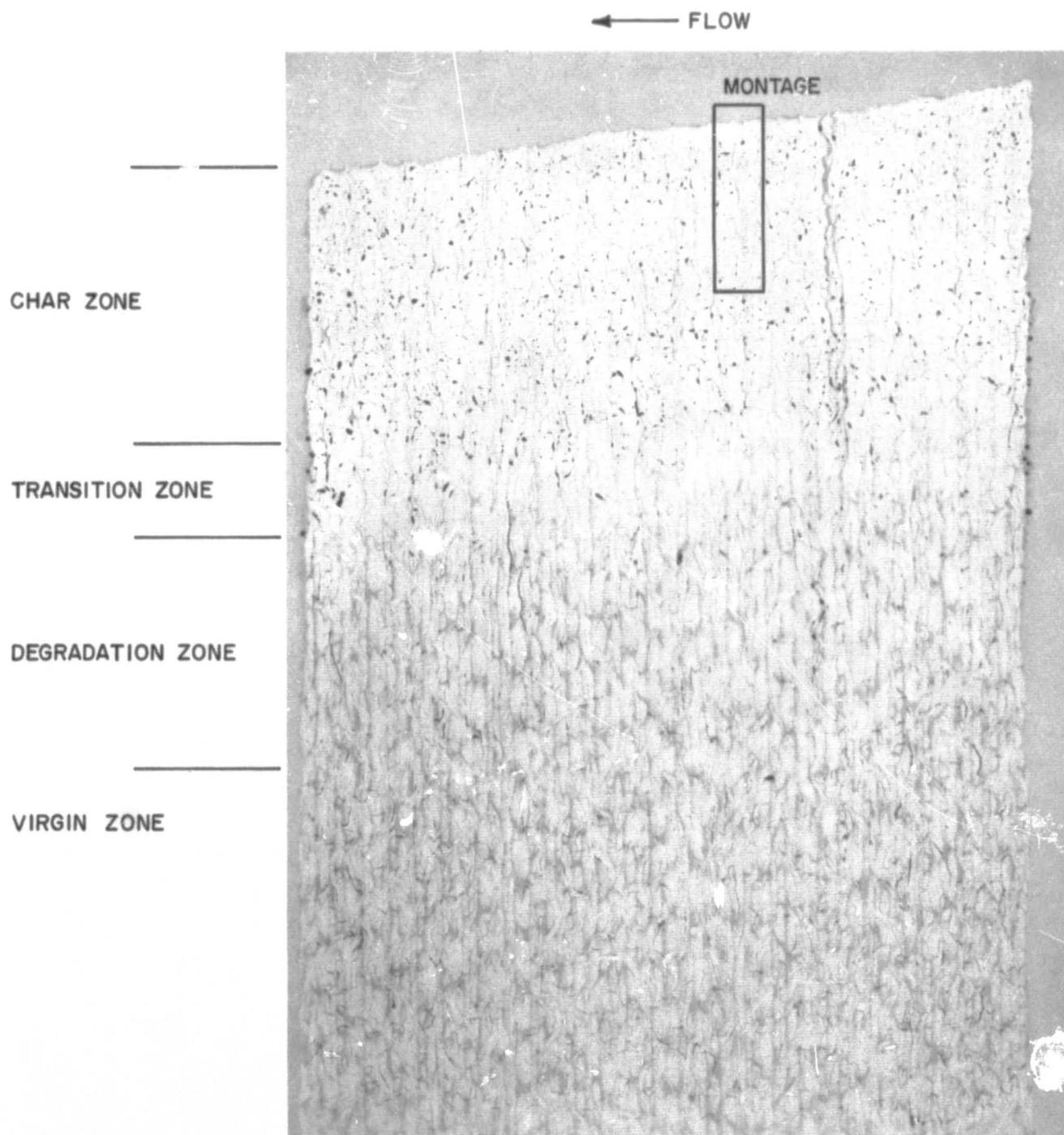
78-1526

Figure 79 CUTAWAY VIEW OF GRAPHITE-PHENOLIC MX4500 THROAT SECTION
OF POST-FIRED ROCKET NOZZLE (5X MAGNIFICATION)

CHAR ZONE

TRANSITION ZONE

DEGRADATION ZONE

VIRGIN ZONE
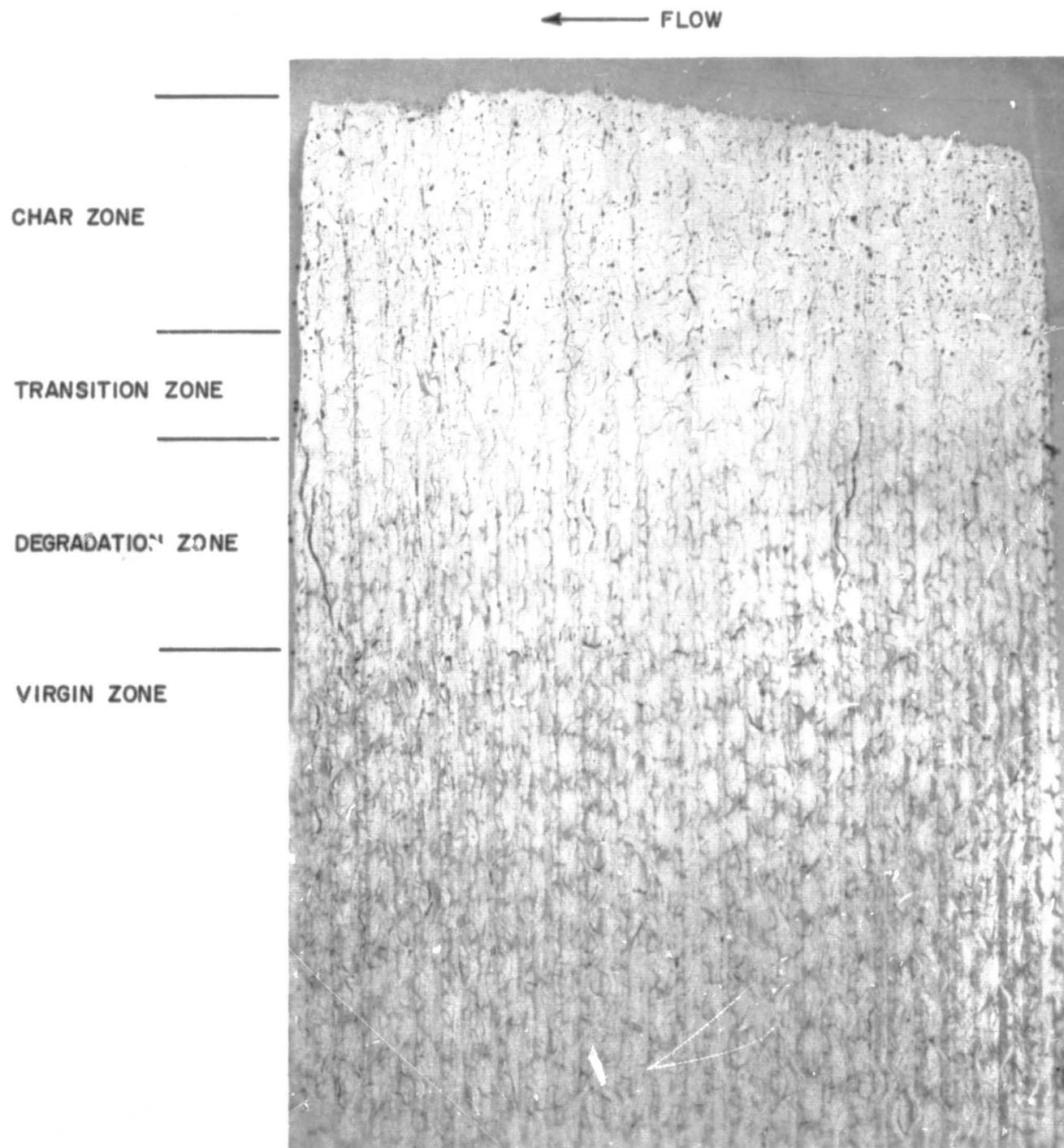
78-1527

Figure 80 CUTAWAY VIEW OF GRAPHITE-PHENOLIC MX4500 EXIT SECTION OF
POST-FIRED ROCKET NOZZLE (5X MAGNIFICATION)
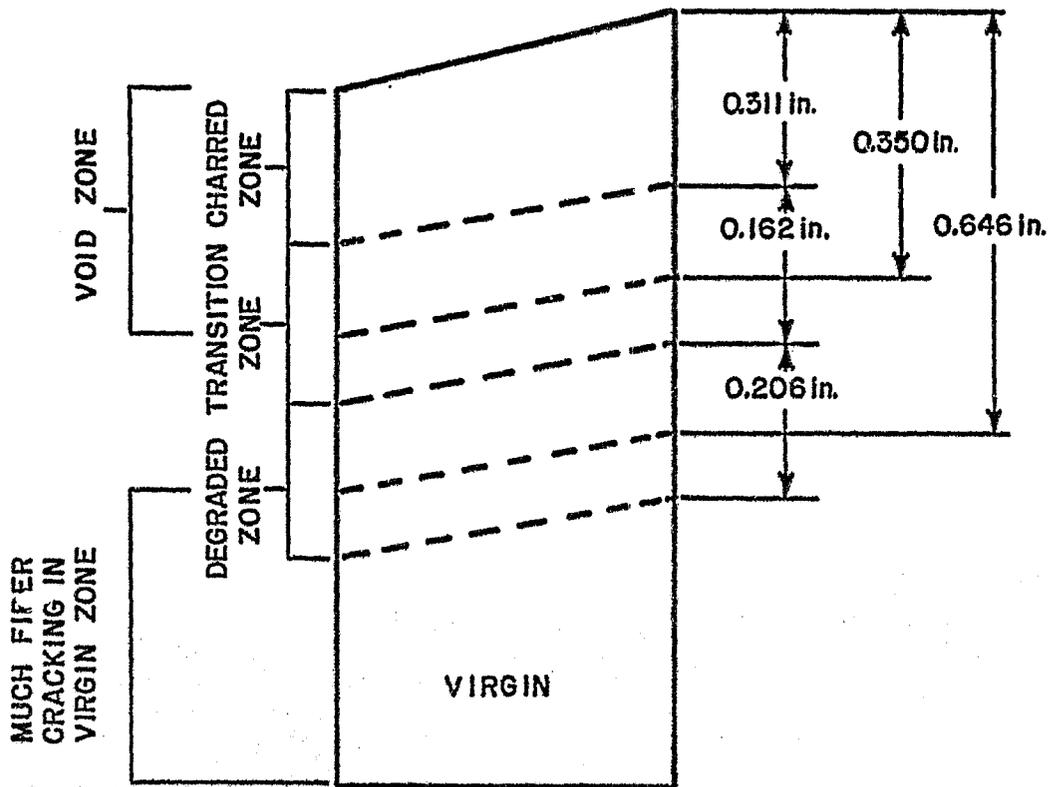
78-1528

Figure 81 CRITICAL ZONE LOCATION OF GRAPHITE-PHENOLIC NOZZLE MX4500-2
(THROAT SECTION)

-111-

PYROLYTIC GRAPHITE SPIKE  PYROLYTIC GRAPHITE DEPOSIT  GRAPHITE FIBERS END VIEW  INTERLAMINATE FISSURE  CHAR SURFACE
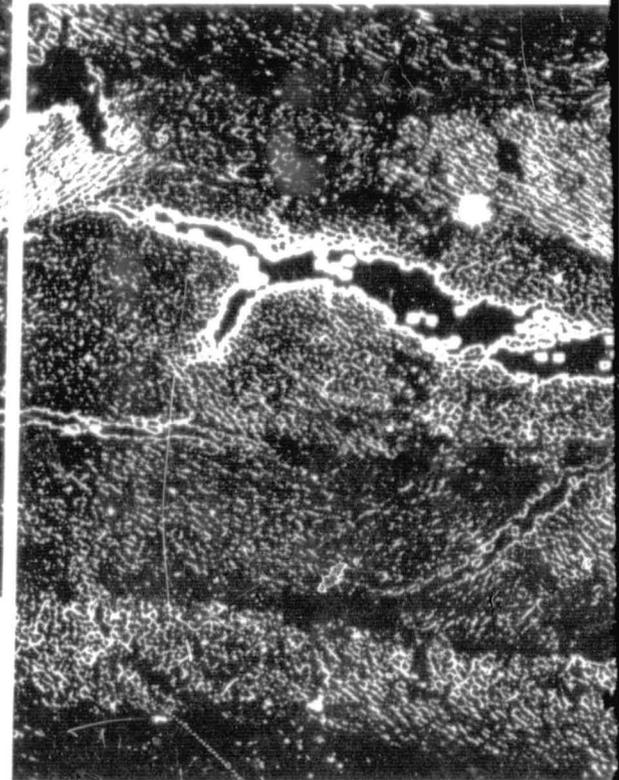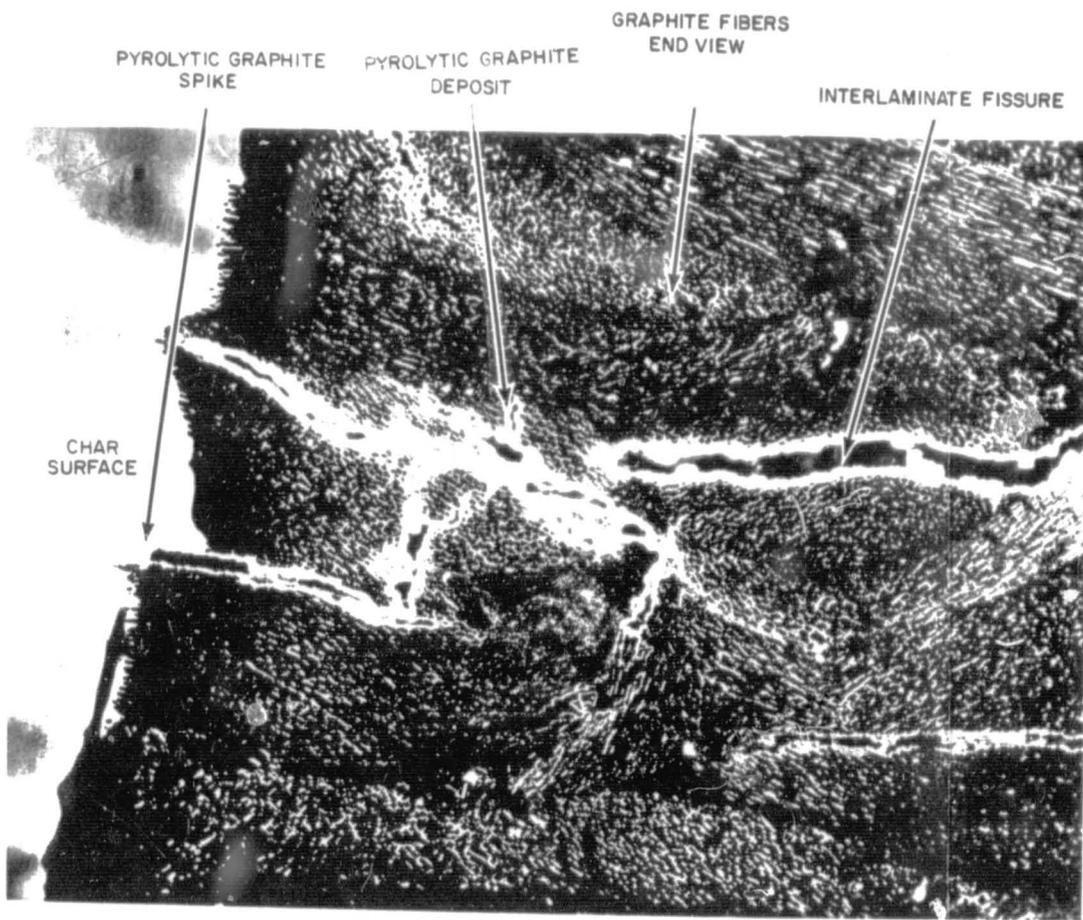
Figure 82 GRAPHITE-PH

GRAPHITE FIBERS
SIDE VIEW
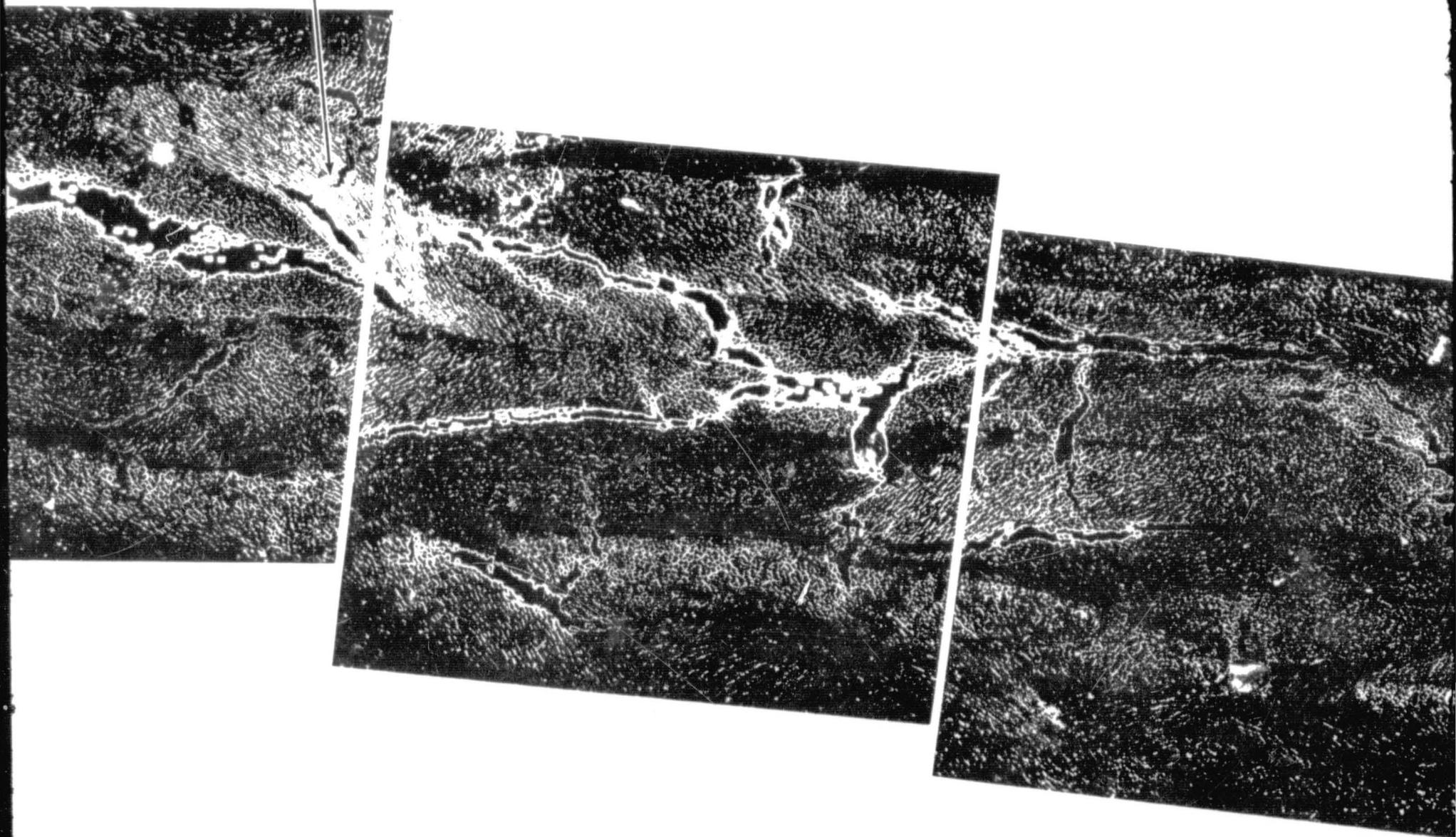
Figure 82  GRAPHITE-PHENOLIC MX4500 POST-FIRED ROCKET NOZZLE CHAR ZONE
MONTAGE (100X MAGNIFICATION)
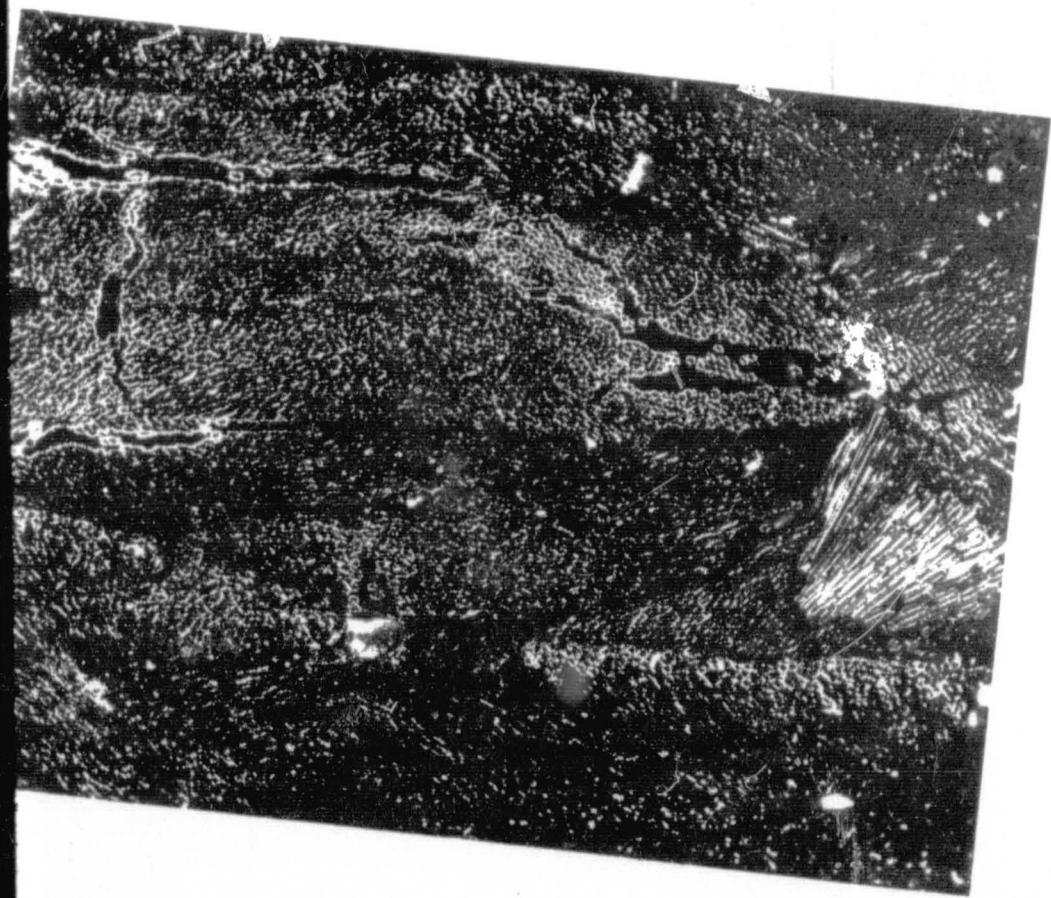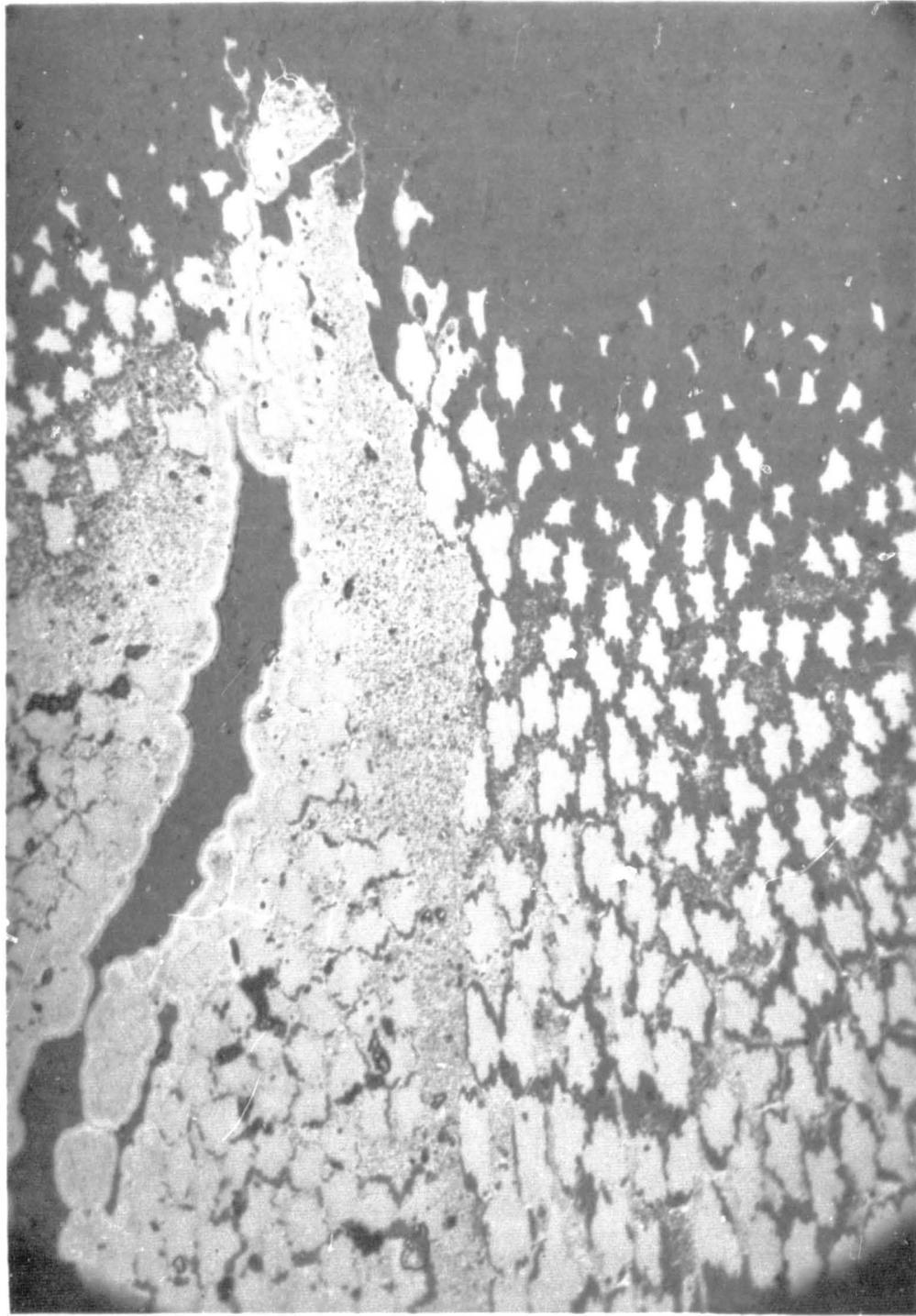
Figure 83  POST-FIRED GRAPHITE-PHENOLIC MX4500 NOZZLE CHAR (SURFACE
CHAR) (500X MAGNIFICATION)
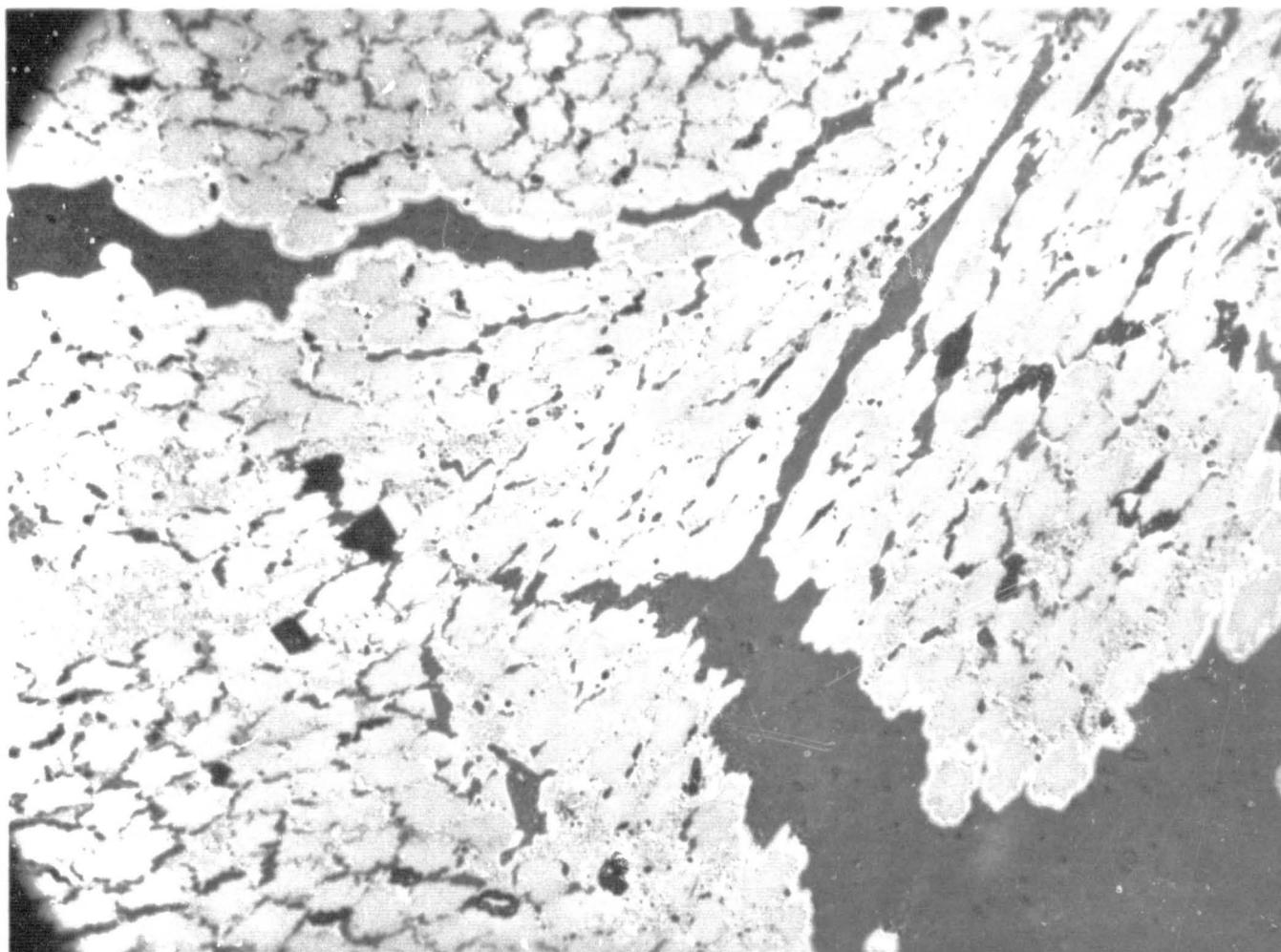
0.059 inches FROM CHAR SURFACE.

78-1530

Figure 84 POST-FIRED GRAPHITE-PHENOLIC MX4500 NOZZLE CHAR, 0.059-INCH
CHAR DEPTH (CHAR ZONE) (500X MAGNIFICATION)

NOZZLE CHAR SURFACE



← 0.174 inches FROM CHAR SURFACE →

78-1531

Figure 85   POST-FIRED GRAPHITE-PHENOLIC MX4500 NOZZLE CHAR, 0.174-INCH
CHAR DEPTH (CHAR ZONE) (500X MAGNIFICATION)
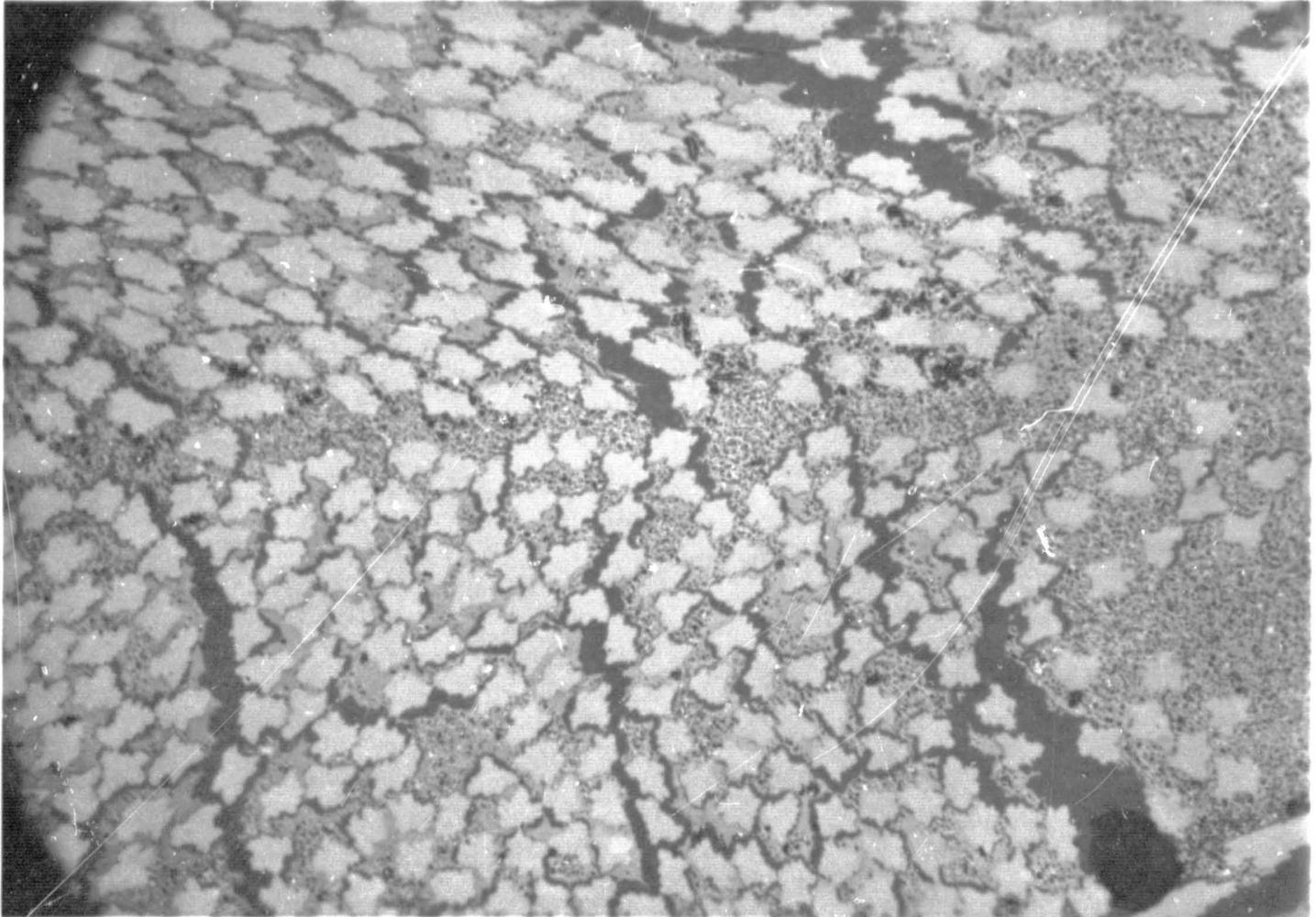
|← 0.421 inches FROM CHAR SURFACE →|

Figure 86  POST-FIRED GRAPHITE-PHENOLIC MX4500 NOZZLE CHAR, 0.421-INCH
CHAR DEPTH (TRANSITION ZONE) (500X MAGNIFICATION)

of the cracking tar products is great, therefore, the conditions for graphite deposition are enhanced. It can also be seen that the phenolic matrix material retained its grainy texture to the surface.

Figure 84 was taken at a depth of 0.059 inch (photo centerline) from the surface. The gross cracking of the material is shown. Also the pyrolytic graphite can be seen to have been deposited not only along the major fissures but around many of the individual fibers toward the top of the photo (closer to the surface).

Figure 85, taken 0.174 inch from the char surface, illustrates the diminishing deposition of the graphite in the regions of the fissure and the absence of deposition anywhere else. Also, local char zones are shown as black isolated bits. The dark egg-shaped object in the fissure channel is a void in the mounting epoxy.

Figure 86 was taken at a depth of 0.421 inch and demonstrates the many small thermal stress fissures which prevail. The phenolic matrix shows its typical graininess, and no sign of deposited graphite is indicated.

b. Physical and Chemical Characterization of Nozzle Chars

1) Silica-Phenolic -- Table XII presents the results of X-ray diffraction analysis on selected char layers. These data show that silicon carbide was present to a depth of about 0.050 inch from the char surface. Most of the layers were found to contain small amounts of iron. This is believed to have been introduced as the samples were homogenized before carbon, hydrogen, and ash analysis.

## TABLE XII

### SUMMARY OF X-RAY DIFFRACTION ANALYSIS DATA FOR SILICA-PHENOLIC NOZZLE THROAT CORE CHAR LAYERS

| Layer No. | Distance from Back of Core (inches) | Results |
|---|---|---|
| 00 | 1.75* | Silicon carbide, alpha-iron, amorphous silica and carbon, poorly crystalline carbon |
| 02 | 1.71 | Same except that there is less silicon carbide. |
| 03 | 1.68 | No silicon carbide. Alpha-iron, amorphous silica and carbon, and poorly crystalline carbon were observed. |
| 04, 06, 10 | 1.66, 1.60, 1.50 | Alpha-iron, amorphous silica and carbon, and poorly crystalline carbon. |
| 14 | 1.40 | Amorphous silica and carbon, and poorly crystalline carbon. |

*Front surface.

Figures 87 through 89 show the density, chemistry and porosity profiles, respectively, for this core specimen. The area of interest in these profiles begins with the virgin material, at a depth of about 1.4 inches, and proceeds toward the char surface, 1.75 inches from the back of the core.

The porosity profile fluctuates greatly from 10 to 60 percent and generally shows little correlation with the shape of the density and chemistry profiles. There is, however, a point of maximum porosity at 1.55 inches which corresponds to a point of minimum density due to the nearly complete loss of phenolic resin. Also, the next highest point of porosity, at 1.78 inches, corresponds to the next lowest point of density. A comparison of the density and chemistry profiles shows a similarity between these two properties, especially for the density and normalized carbon values. The procedure for calculating normalized values is given in Section III.B.5, Appendix E.

The density and chemistry profiles may be utilized together with information from thermogravimetric analyses, oven reference chars, carbon deposition and silicon carbide formation to construct a temperature profile through the char layer.

Figure 90 shows the postulated temperature profile for the silica-phenolic nozzle throat section plotted as a function of distance from the backface. The first temperature, 70° F at 1.40 inches, was established by assigning room temperature to the first layer encountered in the analysis having a virgin chemical composition. The next two temperature assignments, 570° F at 1.44 inches and 932° F at 1.55 inches, were established by assuming that TGA results in air, Figure 35, could be applied. Application of TGA results to temperature profile construction was suggested by DeSesa (Ref. 4) who found that weight losses obtained by heating samples of silica-reinforced phenolic resin isothermally in helium agreed quite well with the weight losses obtained during thermogravimetric analysis in helium up to 1470° F. In this case, TGA results in air were used because the nitrogen tetroxide -50/50 hydrazine/unsymmetrical dimethylhydrazine propellant mixture used to test the nozzles produces an oxidizing environment. The 570° F temperature at 1.44 inches is established from the TGA curve, Figure 35, as the beginning of degradation. In the char layer, initial decomposition is taken at the distance at which carbon, hydrogen, and oxygen first decrease. The next temperature, 932° F at 1.55 inches, was also determined from TGA data. The maximum rate of resin weight loss occurred during TGA analysis in air between 570° and 1112° F. The midpoint of the steepest slope was about 932° F. In the char layer, the steep drop-off in density, and carbon, hydrogen, and oxygen resembles the rapid weight loss in the TGA curves. For this reason, the steepest slope in the curves is labeled "Maximum Degradation Rate" and assigned a temperature of 932° F. Note that the normalized carbon, hydrogen, and oxygen values of the 1000° F oven reference chars fall on the respective curves in the chemistry profile in the region of the steepest slope. These are indicated by "x". The point at 1870° F is established from the initial carbon buildup responsible for the inversion in the density and carbon content profiles. The buildup of dense carbon is brought about by the cracking of carbonaceous, gaseous resin decomposition products on the hot char matrix. This deposition begins to occur at 1870° F in instrumented ablation samples tested at our facility
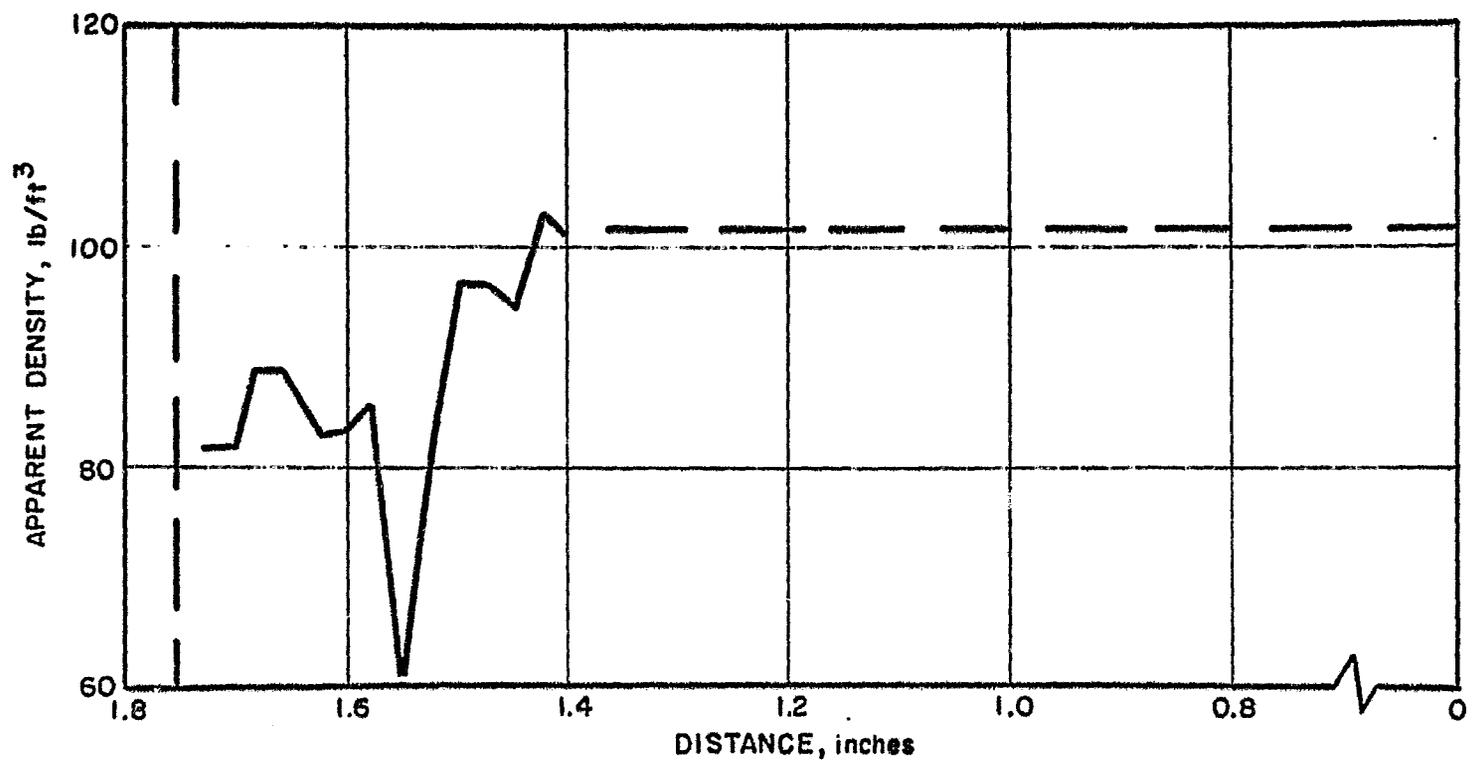
79-0300

Figure 87 SILICA-PHENOLIC NOZZLE MXS-89-2 POST-FIRED DENSITY PROFILE
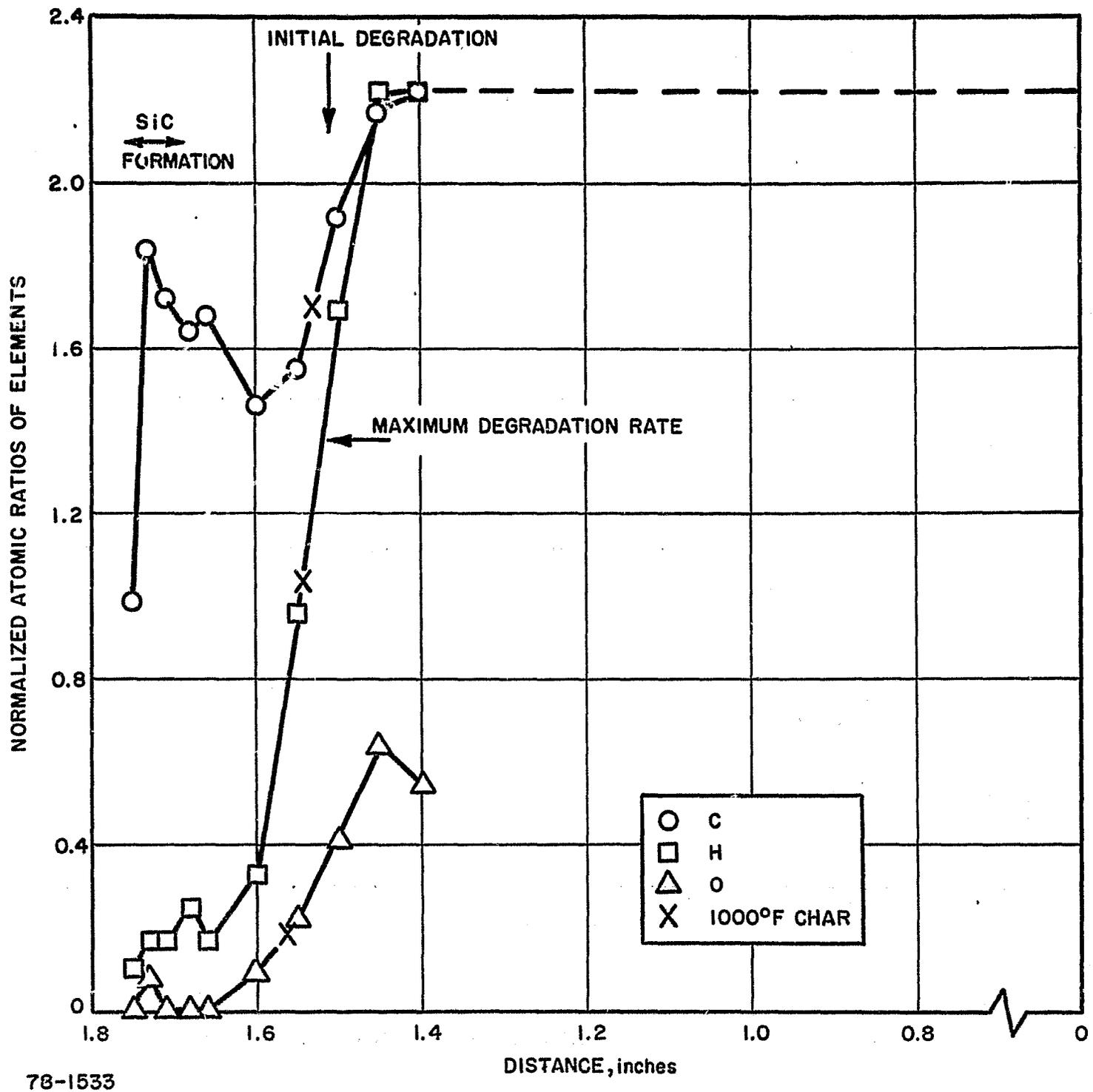
Figure 88 CHEMISTRY PROFILE OF THE SILICA-PHENOLIC NOZZLE MXS-89-2

78-1533
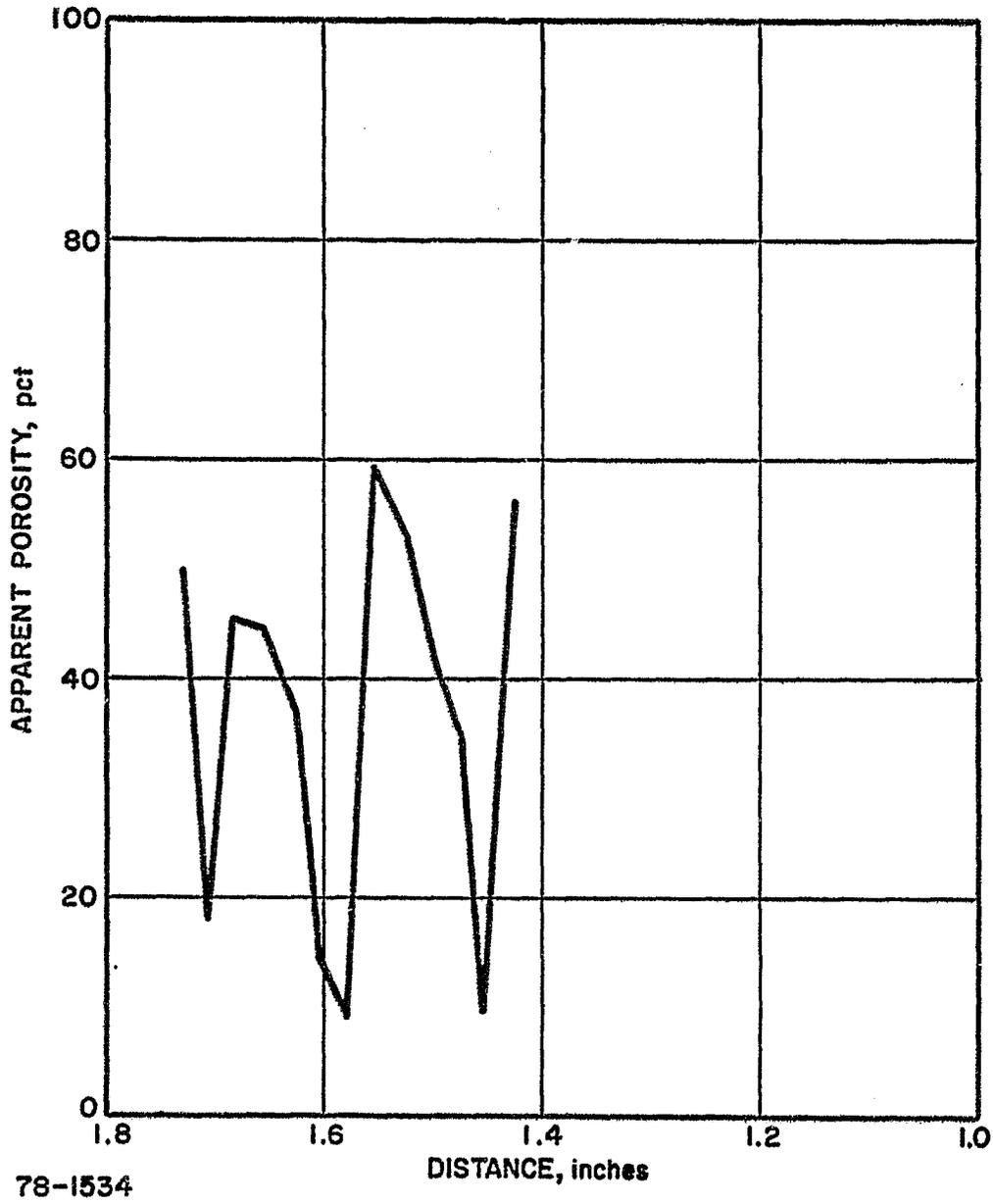
Figure 89  SILICA-PHENOLIC NOZZLE MXS-89-2 POST-FIRED POROSITY PROFILE
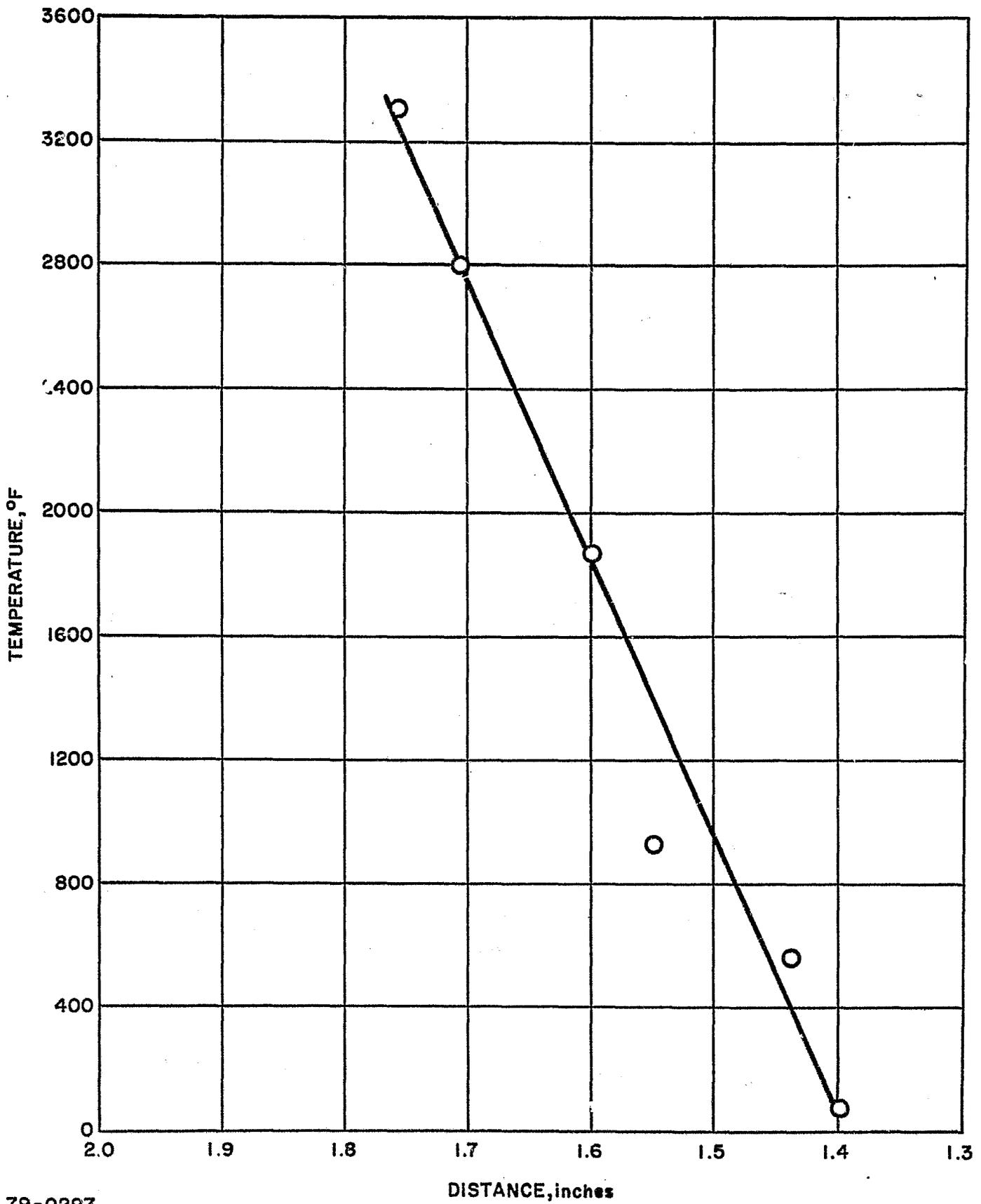
79-0297

Figure 90 POSTULATED TEMPERATURE PROFILE FOR THROAT SECTION OF
SILICA-PHENOLIC NOZZLE

in simulated high-temperature environments produced by plasma arcs. Normalizing the carbon and hydrogen content of the 2000° F oven reference char gives a value of 1.73 and 0.0 respectively. These values are in good agreement with the values of carbon and hydrogen found for the char layers in this region.

The next point, 2800° F at 1.71 inches from the backface is determined by the presence of silicon carbide. This compound is formed by the reaction of the silica reinforcement and carbon and was found also in the three oven reference chars prepared at 2400°, 2700°, and 2800° F. In this temperature region, three reactions between carbon and silica are most likely to occur (Ref. 5). These are as follows:

$$SiO_2 + 3C \rightarrow SiC + 2CO(g) \tag{1}$$

$$\Delta H_{2000° K (3140° F)} = 133 \text{ kcal}$$

$$SiO_2 + 2C \rightarrow Si(1) + 2CO(g) \tag{2}$$

$$\Delta H_{2000° K (3140° F)} = 157 \text{ kcal}$$

$$SiO_2 + C \rightarrow SiO(g) + CO(g) \tag{3}$$

$$\Delta H_{2000° K (3140° F)} = 147 \text{ kcal}$$

Reference 5 shows that of these reactions, reaction 1 is thermodynamically and kinetically the most favorable. Also shown is the temperature dependency of these reactions upon pressure. In rocket motors burning at 100 psia, the throat pressure is about 50 psia (Ref. 6). At this pressure, about the lowest temperature at which silicon carbide will form is 2800° F.

The temperature of 3300° F assigned to the outermost char layer at 1.76 inches was established by assuming that the silicon carbide further reacted with silica, Equation 4, to produce gaseous silicon monoxide and carbon monoxide.

$$SiC + 2 SiO_2 \rightarrow 3 SiO + CO \tag{4}$$

The net effect of reactions 1 and 4 would be one in which silica reacts with carbon to produce silicon monixide and carbon monoxide with the formation of silicon carbide as an intermediate (Ref. 7). The lowest temperature at which the sum of the equilibrium partial pressures of the silicon monoxide and carbon monoxide products is equivalent to 50 psia is 3300° F (Ref. 6).

Silicon monoxide gas (it remains solid at 3092° F) normally dissociates into elemental silicon and silicon dioxide unless cooled very quickly in its preparation (Ref. 8). Therefore, the presence of elemental silicon in the char layer could provide evidence for silicon monoxide formation during ablation. X-ray diffraction analysis did not show elemental silicon to be present. This result does not preclude silicon monoxide formation, however, for two reasons:

-123-

a) less than 5 weight percent of elemental silicon in the char layers analyzed would not be observed, and, more likely,

b) as the silicon monoxide formed, it was oxidized to silica before it could dissociate.

2) Optical Property Determinations -- As in the case of the oven-prepared chars, measurements of spectral reflectance were conducted on both types of post-fired nozzle chars using the Beckman DK2 Spectrophotometer. These measurements were performed at various char depth locations. The procedure for this phase of the study was typical of the other profiling techniques; that is, optical reflectances were determined first on the undisturbed char's surface. Following this, the specimens underwent, alternately, machine milling of the nozzle char to a predetermined depth, and subsequent reflectance determination from 0.4 micron to 2.7 microns wavelength. This procedure continued well into the virgin region. Machine milling was performed dry, and special attention was given to prevent the introduction of foreign matter into the nozzle char. No attempt was made to subsequently smooth each milled cut to avoid any contamination of the optical surface.

Figure 91 illustrates the results obtained on the silica-phenolic MXS-89 nozzle char. Included are the reflectances of the material at six different char depths. There is a definite difference between the reflectance characteristics of the undisturbed surface char and that of the region immediately beneath it. The difference is in magnitude rather than in the shape of the function. As measurements proceeded in depth, those determinations which were made within the char and transition zones were nearly identical both in magnitude and shape. Only upon reaching the zone corresponding to the transition-degradation region did the function shape change, as is shown in the figure (0.275-inch char depth trace). With reference to the 1000° F over char trace shown in Figure 44, a comparison between the oven char and nozzle char (0.275-inch depth) seems to infer that the boundary line region tested had experienced a test temperature in the neighborhood of 1000° F. By superimposing the 1000° F oven char curve and the virgin material curve, a trace similar to that which was produced in the nozzle char both in shape and magnitude would be obtained, with the exception of the region between 0.4 micron and 1.3 microns. Since the nozzle reflectance was obtained from a surface composed of both charred material and partially degraded material, it is likely that the degraded material composition attributed to the drop off in reflectance from 1.3 microns down to 0.4 micron. The scope of effort in the subject program did not allow a more detailed analysis of the silica-phenolic oven char reflectances for obtaining a clearer description of the optical differences in the material charred at temperatures above 1000° F. The properties obtained thus far, however, show excellent agreement between the high-temperature oven chars and the charred regions of the fired nozzle. This is demonstrated in the data for the 0.050-, 0.070-, and 0.108-inch-deep char measurements and the 2000°, 2700°, and 2800° F oven chars (the above depth is given with respect to the nozzle char surface). The molten silica which overlaid the nozzle interior surface was essentially transparent; therefore, the increase in magnitude of the reflectance trace is attributed to the highly reflecting black deposit which was observed covering the molten silica.
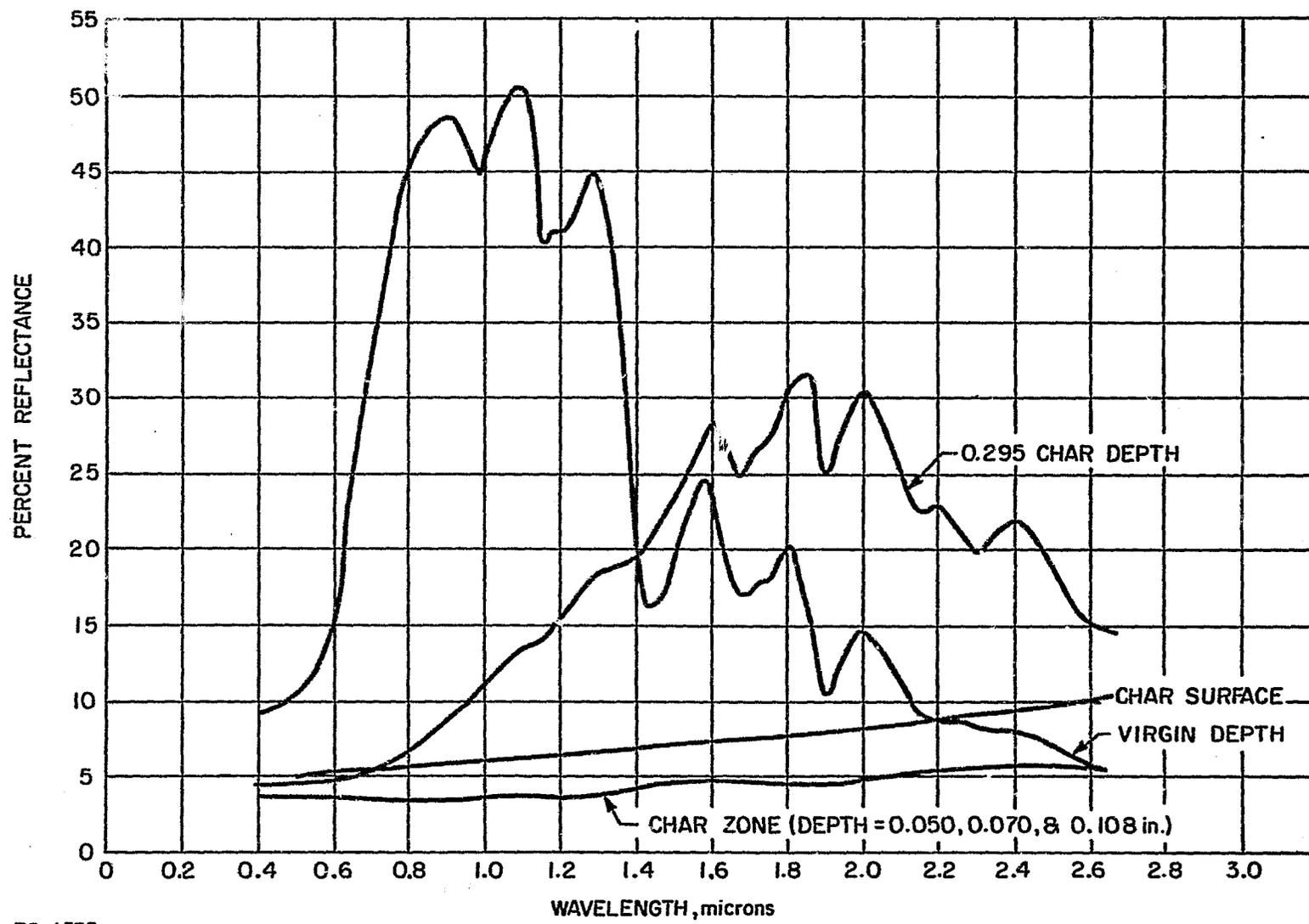
78-1535

Figure 91 MXS-89 SILICA-PHENOLIC NOZZLE CHAR OPTICAL PROPERTIES

3) <u>Graphite-Phenolic</u> -- X-ray diffraction analysis (Table XIII) of
selected char layers showed the presence of amorphous carbon, graphite,
and, as in the case of the silica-phenolic chars, some iron which was
probably introduced in sample preparation.

## TABLE XIII

### SUMMARY OF X-RAY DIFFRACTION ANALYSIS DATA FOR GRAPHITE-PHENOLIC NOZZLE THROAT CHAR LAYERS

| Layer No. | Distance From Back of Core (inches) | Results |
|---|---|---|
| 00, 03, 06, 10 | 1.70[a], 1.63, 1.55, 1.48 | Primarily graphite and amorphous carbon. No significant difference in degree of crystallinity of graphite. Minor amounts of alpha-iron. |
| 14, 16, 20 | 1.33, 1.28, 1.18 | Graphite and amorphous carbon. |

[a]Front surface.

Figures 92 and 93 show the density and chemistry profiles, respectively,
for the graphite-phenolic nozzle throat material. A porosity profile
could not be obtained for this specimen because it was so surface active
that consistent results were not determinable even when helium was sub-
stituted for air in the Beckman Air Comparison Pycnometer. It will be
noted that the chemistry profile is not as complete as the one obtained
for the silica-phenolic and contains only the hydrogen content of the
graphite-phenolic char layers versus char depth. This is due to the
inability to measure by usual methods the amount of carbon resulting from
resin degradation. However, hydrogen content serves to indicate the ex-
tent of resin decomposition occurring at the lower temperatures and takes
the place of a normalized atomic ratio plot such as that included for
the silica-phenolic. Included for comparison purposes are the hydrogen
contents of the silica-phenolic chars. The area of interest in the den-
sity and chemistry profiles proceeds from the virgin material at a depth
of 1.0 inch to the char surface at 1.70 inches.

As was done for the silica-phenolic, a temperature profile was postulated
for the graphite-phenolic nozzle throat by utilizing information from
density and chemistry profiles, TGA results (Figure 36) and carbon deposi-
tion. The temperature profile, Figure 94, was constructed as follows:
the first point, 1.13 inches, was established by assigning room tempera-
ture to the first virgin layer encountered in the analysis. The second
temperature, 570° F, is the initial decomposition temperature obtained
from TGA and was assigned to that point where hydrogen first decreases,
1.18 inches from the backface, as shown in Figure 93.
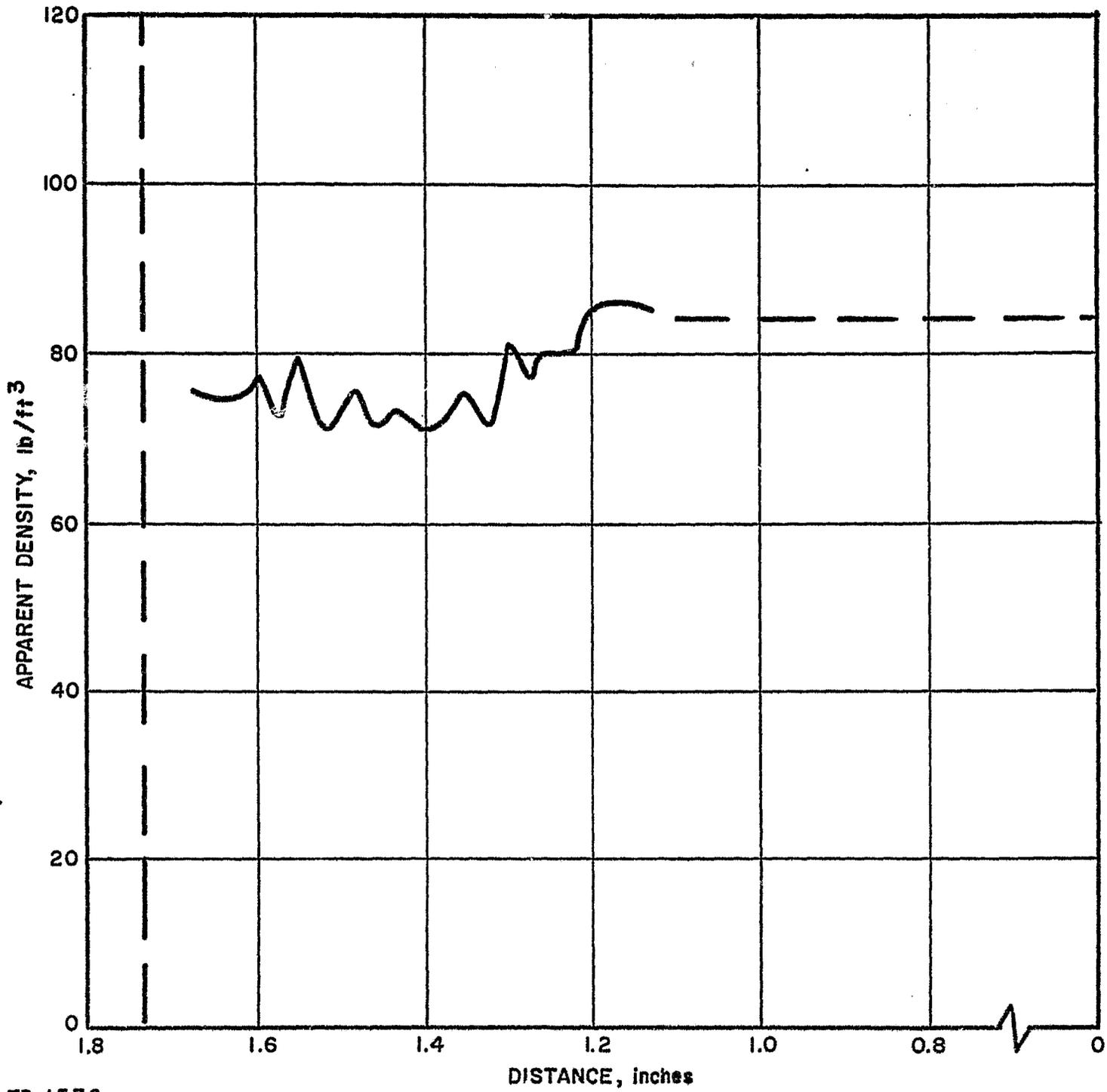
-126-

Figure 92  GRAPHITE-PHENOLIC NOZZLE MX4500-2 POST-FIRED DENSITY PROFILE
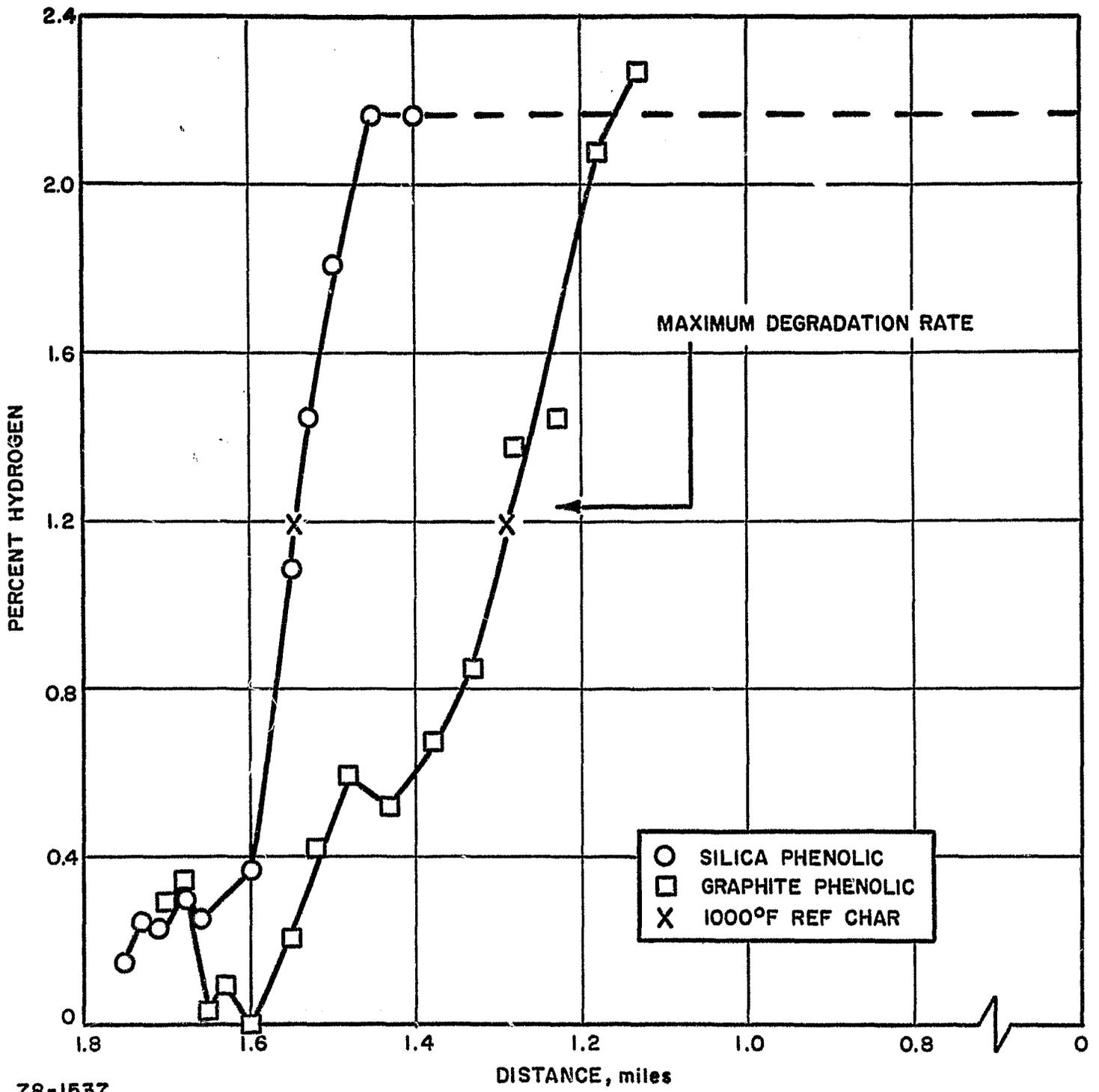
Figure 93  POST-FIRED NOZZLE DEGRADATION CHARACTERISTICS

78-1537
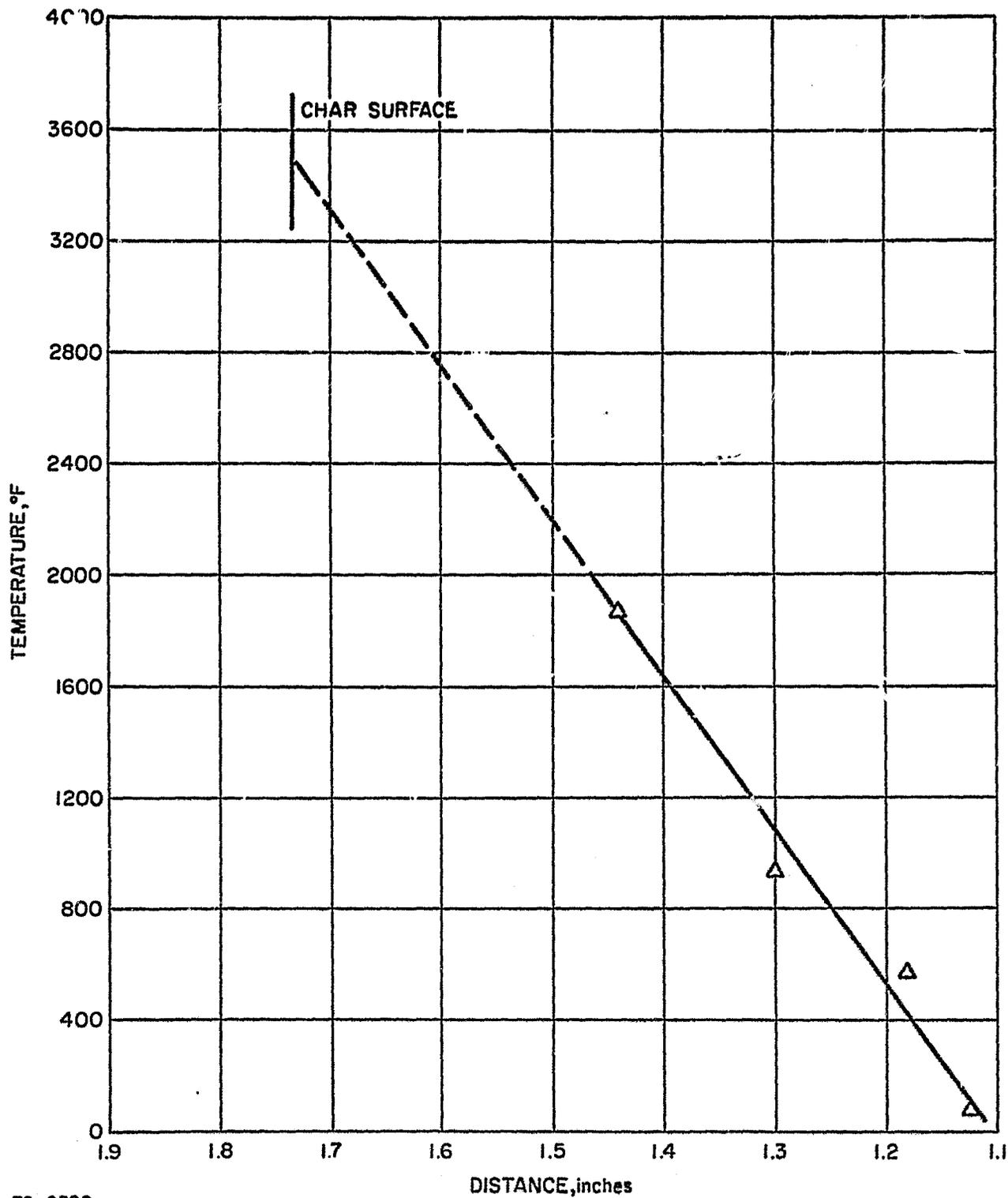
-128-

Figure 94 POSTULATED TEMPERATURE PROFILE FOR THROAT SECTION OF
SILICA-PHENOLIC NOZZLE

79-0298

The steep drop in hydrogen content is analogous to the steep drop in the TGA curves occurring in the region 660° to 1020° F. The midpoint of this slope is about 932° F. The hydrogen value of 1.2 percent, found for the 1000° F oven reference char and indicated by an "x" on the hydrogen curve is in good agreement with this temperature assignment. Note that the value of the hydrogen content of the 1000° F silica-phenolic reference char was also 1.2 percent and is indicated by an "x" on the silica-phenolic hydrogen curve in Figure 93 for comparison purposes.

The next temperature, 1870° F, at 1.44 inches from the backface was established from the density profile which shows a tendency to increase in density due to carbon buildup at this distance. It is interesting to note that the density profile of the graphite-phenolic does not display the prominent inversion of density observed in the silica-phenolic density profile. As stated in the section on silica-phenolic chars, the inversion of density is attributed to the buildup of dense carbon formed by the cracking of carbonaceous species on the hot char matrix. However, for the graphite-phenolic, the carbon being deposited does not differ greatly in density from that of the substrate, and consequently, the inversion is not as readily apparent.

Extrapolation of the graphite-phenolic temperature profile to the char surface gives a temperature of 3500° F, similar to that postulated for the silica-phenolic (3300° F).

The overall char depth of the graphite nozzle was greater than that of the silica-reinforced material. This was caused by greater heat penetration, which is consistent with the higher thermal diffusivity of the graphite-phenolic.

4) Optical Property Determinations -- All optical reflectance measurements conducted on all graphite-phenolic MX4500 nozzle material yielded the same value of reflectance (3 percent) regardless of char depth. Other than the fact that there was excellent agreement between nozzle and oven chars, there does not appear to be a reflectance-temperature correlation available.

Apparently the presence of the pyrolytic graphite deposits in the nozzle chars does not influence to any extent the optical reflectance property of these materials which, within the nozzle char regions particularly, can for all intents and purposes be represented by a laboratory oven char at related temperatures; however, the anisotropic nature of pyrolyzed graphite would undoubtedly be observed in reflectance measurements taken in a plane normal to the material laminates. It is unlikely that this slight change in interlaminate optical reflectance would significantly affect the existing ablation phenomenon models.

c.  Thermal Characterizatons of Nozzle Chars

1) Thermal Conductivity Profile Determinations -- The normal method of testing for thermal conductivity was modified in order to provide for generating a property profile as a function of char depth. (Details of these tests are given in Appendix C.) The modification was in two forms:

one dictated by the relatively complex geometry associated with the test
nozzles; the other by the added thermal guarding requirements associated
with the profiling technique.

As mentioned in a previous section, the nozzles were machined to provide
test material from four zones along the nozzle axis: entrance (Section
D), ramp (Section C), throat (Section B), and exit (Section A) -- see
Figure 5. Upon examining the nozzle section, it was decided that, con-
sistent with the scope of the study program, the best regions from which
to extract thermal conductivity specimens were the ramp (Section C) and/or
exit (Section A). These sections provided a good compromise between
proper test specimen geometry and representative nozzle chars. The mini-
mum throat section radius presented a somewhat excessive curvature not
only at the surface but also in the char layer as well. It was felt that
the curvature may tend to weaken the conductivity profiling precision
because the profile characterization assumes flat planar char regions.
The entrance sections of both types of nozzle materials contained char
depth variations, uneven mechanically eroded surfaces and only scant
quantities of molten silica which, as a whole was not consistent with
the rest of the nozzle surfaces.

The additional thermal guarding requirements which arise from post-test
graded char analyses are included in the discussion of Appendix C.

The silica-phenolic nozzle char was examined from specimens taken from
both ramp (C) and exit (A) sections. Test results are shown in Figures 95
and 96 which are presentations of thermal conductivity as a function of
char depth. Plots of the average temperatures at which the conductivity
values were computed are also included in the graphs. The distance coordi-
nates are given as a radius location from the outside nozzle surface.
This procedure has, in general, been kept fixed for all nozzle measurements
so that the various property determinations can be evaluated on the common
distance basis.

There is a marked similarity in the profiles of the two sections, not
only in their shapes but also in the magnitude of conductivity. Excellent
agreement was obtained between the conductivity measured in the nozzle
virgin zone and that measured on a separate virgin billet coring (Figure
40) shown on the curves as dashed lines.

The shape of the curves are influenced by many factors, the principal ones
being the material density, laminate splitting phenomena, char state, and
deposited degradation products. A comparison between density profile
(Figure 82 of Section 2.5) and the conductivity profiles shows the strong
interrelationship between the two properties, particularly in the regions
of the transition zones.

The rapid increase in conductivity near the char surface is strongly
influenced by the presence of silicon carbide and pyrolytic graphite,
whose conductivities are in the order of 25 to 100 Btu/hr-ft-$^{O}$F respec-
tively. The effect of the lowering of the surface density brought
about by the gross interlaminate splitting tends to suppress the effec-
tive conductivity of that zone. It is interesting to note that the

-131-
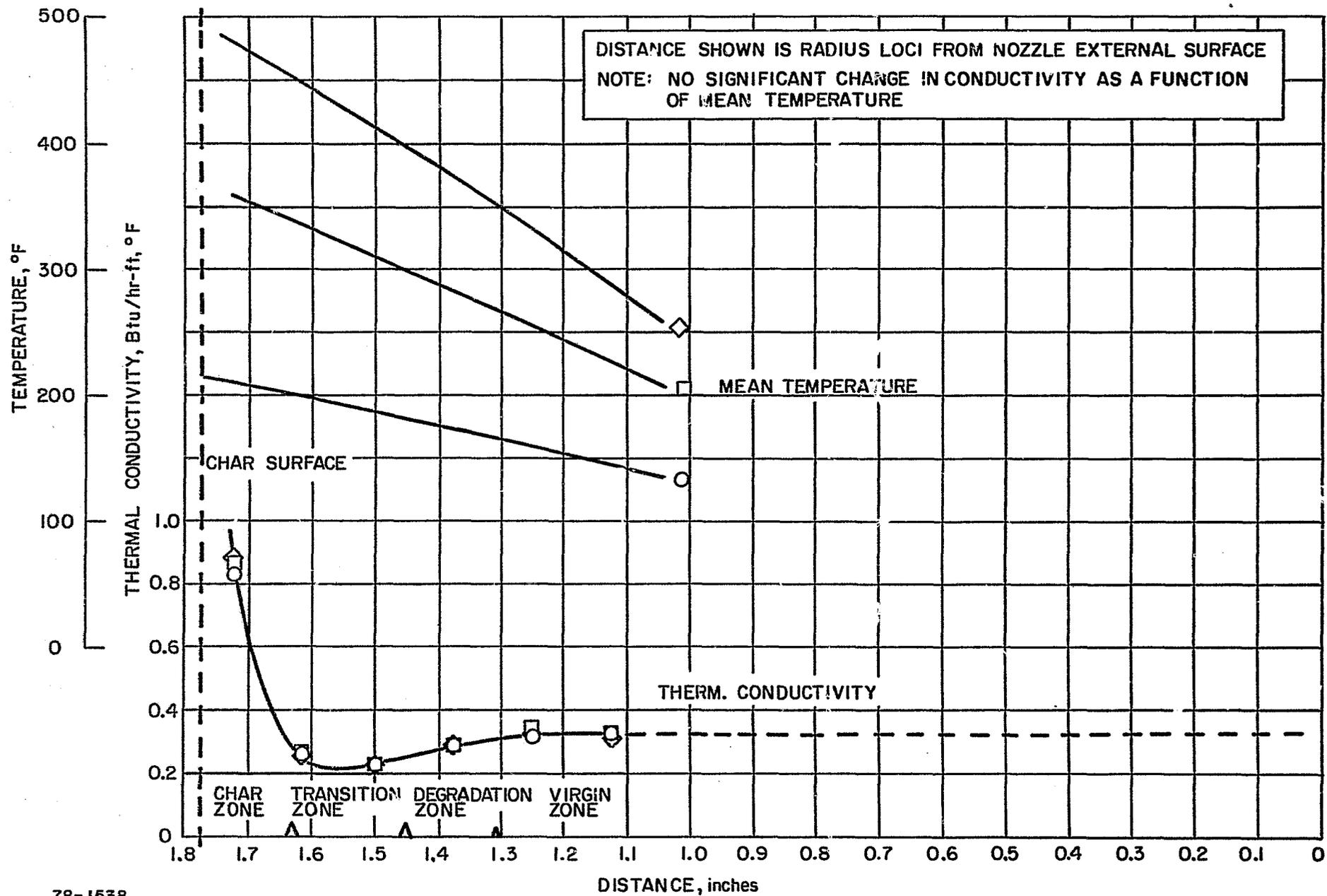
78-1538

Figure 95 SILICA-PHENOLIC NOZZLE EXIT, THERMAL CONDUCTIVITY VERSUS
CHAR DEPTH

DISTANCE SHOWN IS RADIUS LOCI FROM NOZZLE EXTERNAL SURFACE
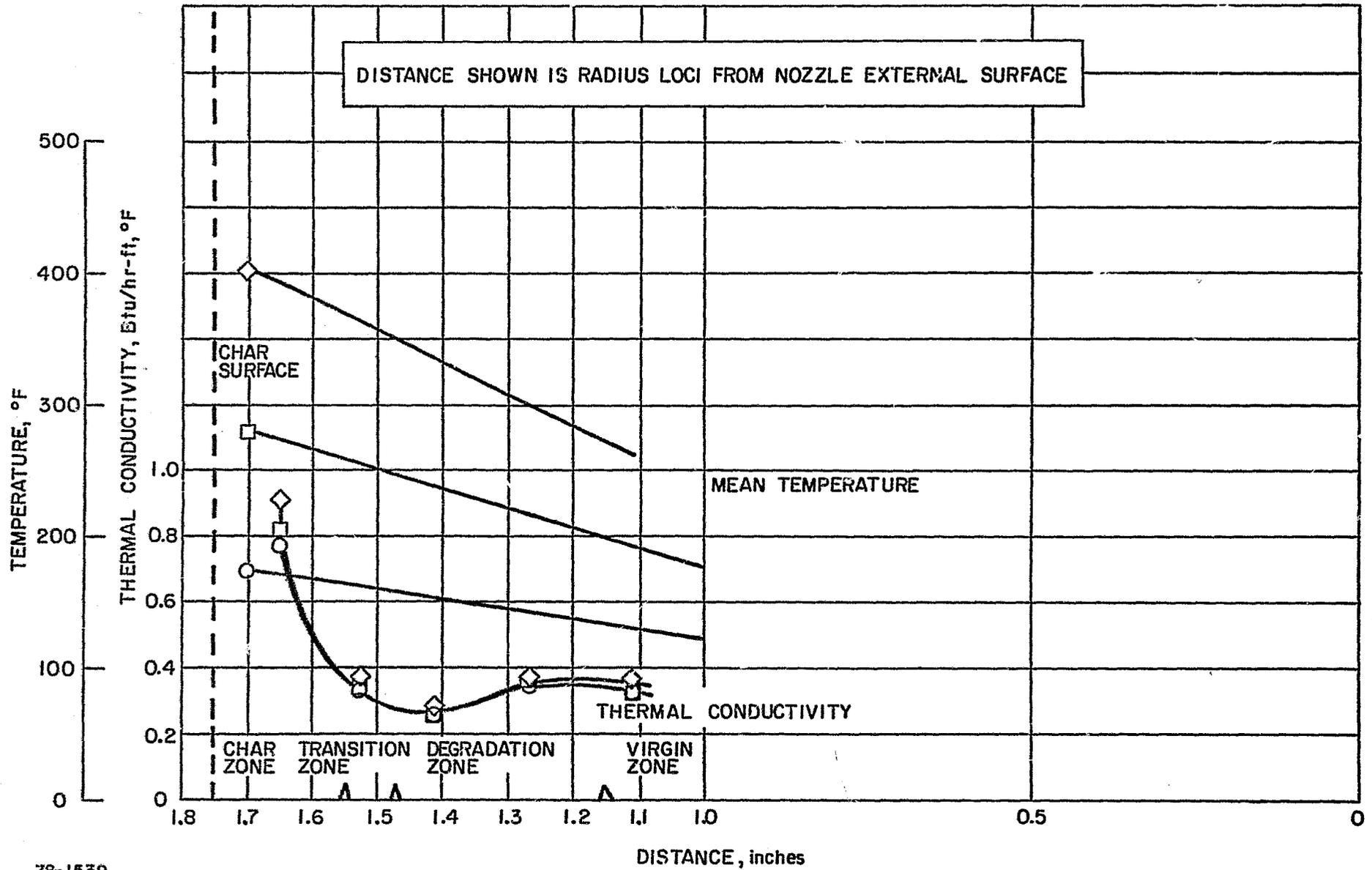
Figure 96 SILICA-PHENOLIC NOZZLE RAMP, THERMAL CONDUCTIVITY VERSUS
CHAR DEPTH

78-1539

-133-

major orientation of the deposited graphite is such that the high thermal conductivity plane (a-b) is parallel to the direction of conducted heat flow both in the fired test and thermal conductivity test.

The dip or low in the conductivity curve can be seen to occur in or near the transition zone (see Figure 76). This is the region which contains much cracking of the phenolic matrix, splitting of the fibers, and degraded material without the presence of either SiC or pyrolytic graphite, so a thermal conductivity lower than that of the virgin material can be expected.

The exit (A) section of the graphite-phenolic nozzle was treated for its thermal conductivity profile, and the results are shown in Figure 97. The coordinates are given in the same manner as the previous two figures. The characteristic dip in the curve has occurred in the region near the transition zone and was undoubtedly influenced by the decreasing presence of pyrolytic graphite and gross voids which existed in that region (see Figure 86). As with the silica-phenolic, the agreement between the results obtained in the virgin zone and those of a separate test of the virgin billet (Figure 46) was good.

The overall shape of the conductivity-char depth curve did not vary as drastically as did the MXS-89 curve. This is due in part to the nondrastic variation in density as noted in Figure 92. In addition the geometry of the conductivity test specimen did not allow measurements to be made at zones which were closer to the char surface and which contain proportionately larger quantities of deposited graphite. An assumed extrapolation in this region has been included in the graph as shown.

   2) _Specific Heat Profile Determinations_ -- Following the machine milling of the various nozzle char layers, the powders were collected. Portions of the powders were removed for specific heat determinations using the Perkin-Elmer Differential Scan Calorimeter. Tests were accomplished in the same manner as were the oven chars; the test procedure is included in Appendix D. The remaining portions of the powdered char material were examined for chemical, physical, and X-ray analyses. In this manner properties common to specific char layers were obtained.

The silica-phenolic nozzle specific heat results, obtained over the temperature range $100^{\circ}$ to $900^{\circ}$ F(+) for each layer, are presented in Figures 98 through 105. Each figure includes the location of the layer tested given with respect to the external nozzle surface, the mass of the specimen, and the weight loss determined at the conclusion of each test. The specific heat versus temperature data thus obtained were replotted as specific heat (at selected temperatures) versus char layer location to produce the profile that is shown in Figure 106. As can be seen the profiles include Cp data at $200^{\circ}$, $400^{\circ}$, $600^{\circ}$, and $800^{\circ}$ F. As in the case of the other profile measurements there is excellent agreement between the data in the virgin region of the nozzle char and those obtained from measurements of the raw billets (see Figure 56) which are represented on the profile curves as dashed lines. Since specific heat varies with material compositional changes, the profiles appear to suggest a similarity in composition from 1.5 inches to the char surface. However, even though the presence of SiC

($Cp \approx 0.3$ Btu/lb-°F) in the material would have a tendency to raise the apparent Cp of the material in the surface char regions. The predominance of amorphous silica, carbon, and pyrolytic graphite (whose $Cp \approx 0.15$ Btu/lb-°F) in those regions apparently suppress this tendency. The increase in resin or phenolic content within the degradation and virgin regions accounts for the corresponding increase in specific heat level.

Figure 107 is a curve of the weight loss resulting from the specific heat tests (maximum temperature = 930°F) plotted as a function of layer location. Within the char zone there was only a slight (1/2 percent) weight loss which may be attributed to included water absorbed during normal test handling or a very slight amount of degradation products which may have been redeposited from in-depth charring during the initial cool-down period of the nozzle firing. The latter would indicate a rather uniform deposition within the nozzle char. Further in-depth, the percent weight loss increases to a level of slightly over 8 percent in the virgin zone. This increasing percentage corresponds to the existence of degradation products which can vaporize out of the nozzle material at temperatures around 930°F. Interestingly, the sudden anomaly around the 1.5-inch region suggests a possible concentration of redeposited resins in that region. The 8-1/2 percent level in the virgin region agrees very well with TGA data discussed elsewhere in this report (Figure 33).

A similar series of specific heat determinations was performed on the MX4500 graphite-phenolic nozzle chars. The results of these tests are shown as specific heat versus temperature plots in Figures 108 through 119. Replotting these curves yielded the specific heat at temperature versus char depth profile shown in Figure 120. The correspondence between virgin billet data (see Figure 57) and virgin nozzle data can be seen as dashed continuations of the profile curves. There appears to be a suggestion of a gradual change in composition with char depth by the increase in specific heat with depth. It is possible that the slight traces of alpha iron which were observed during the X-ray profile studies of the nozzle layers (also discussed in another section) may have influenced (by suppression) the slope of the profiles in the char region. The slight traces of iron which were considered to have come from one of the machining processes in preparation of test specimens, appeared in decreasing quantities in depth.

Referring to the post-test weight loss profile (Figure 121) the 1/2 percent level throughout the char zone can be attributed to absorbed moisture or slight amounts of condensed degradation products in depth. The increase in weight loss toward the virgin region is attributed to an increasing percentage of degradable (at 930°F) products. The 6 percent level in the vicinity of the virgin region is consistent with TGA data (Figure 34).
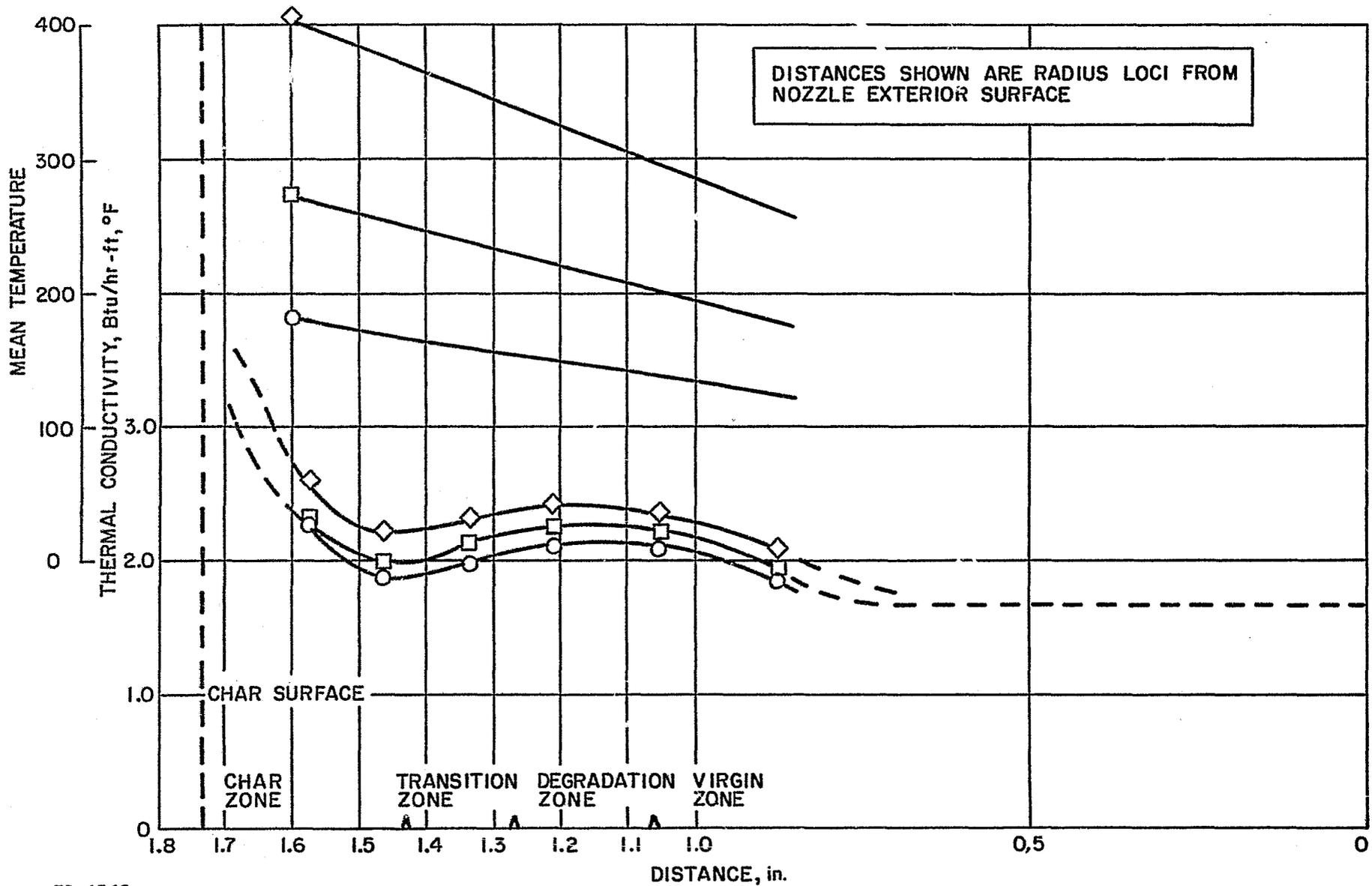
Figure 97 GRAPHITE-PHENOLIC NOZZLE EXIT, THERMAL CONDUCTIVITY VERSUS CHAR DEPTH

78-1540

-136-
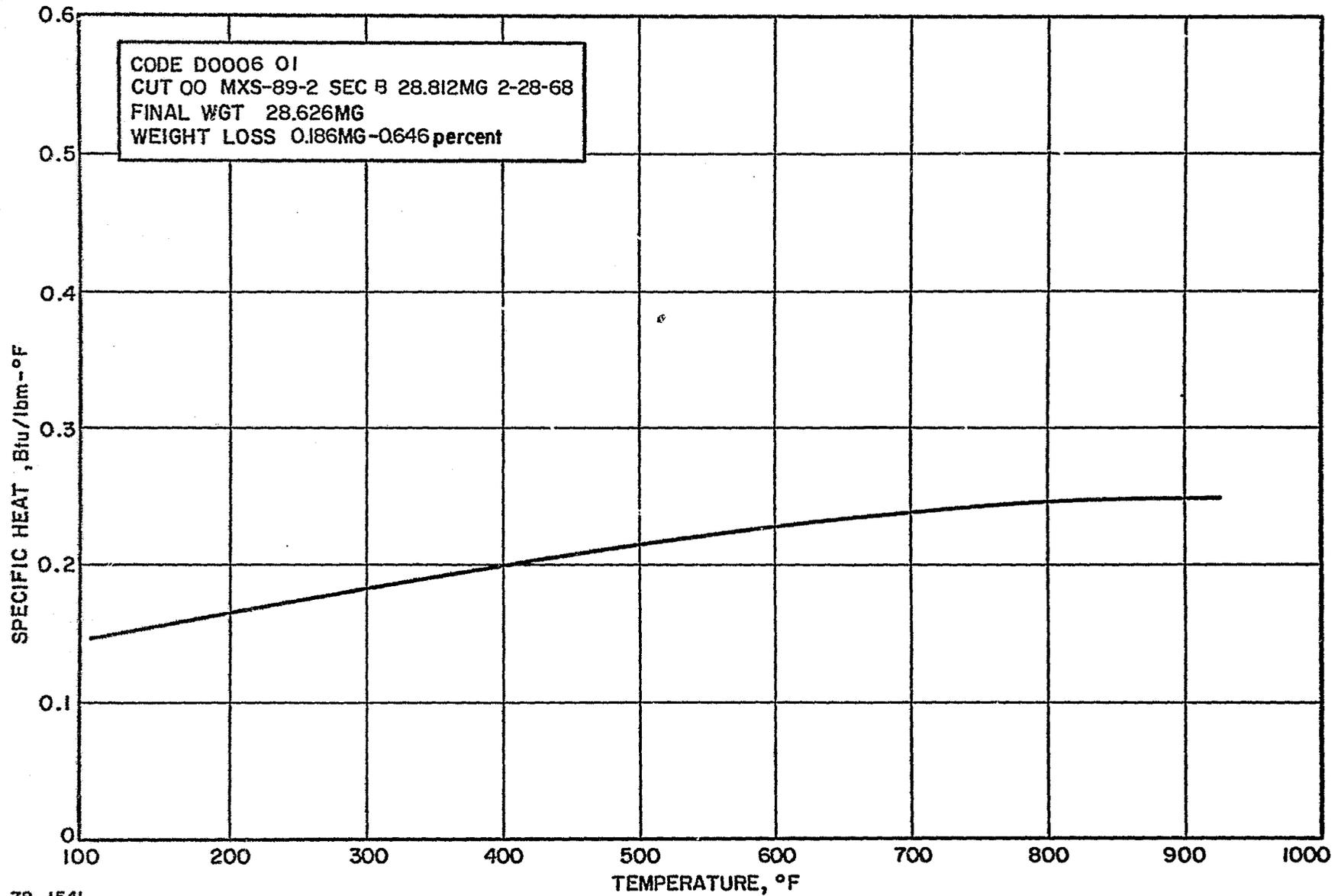
Figure 98 SILICA-PHENOLIC NOZZLE THROAT, SURFACE CHAR, SPECIFIC HEAT
VERSUS TEMPERATURE
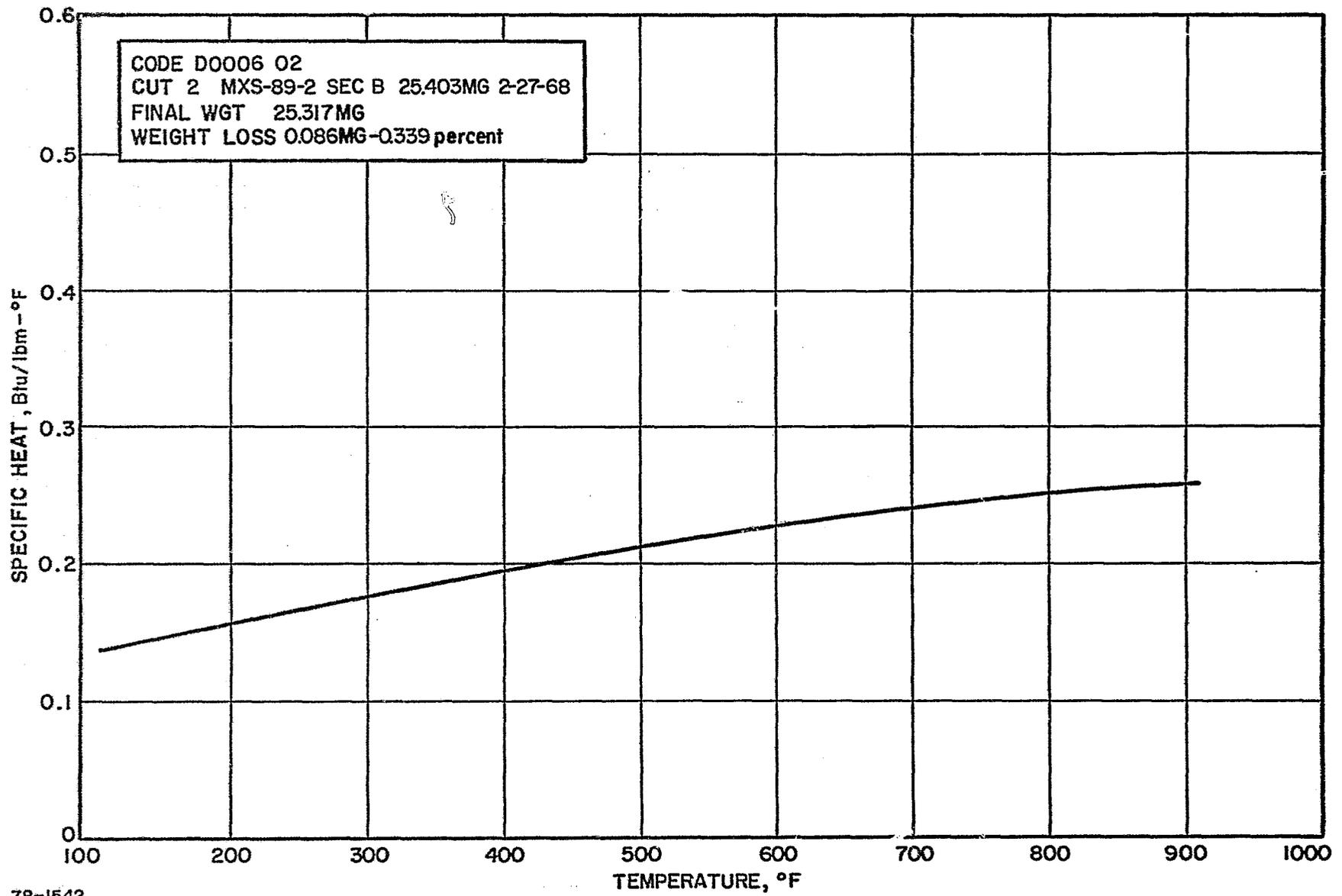
78-1541

Figure 99 SILICA-PHENOLIC NOZZLE THROAT, 1.707-INCH CHAR LAYER, SPECIFIC HEAT VERSUS TEMPERATURE

78-1542

CODE D0006 03
CUT 04 MXS-89-2 SEC B 26.782MG 2-29-68
FINAL WGT 26.654MG
WEIGHT LOSS 0.128MG—0.478 percent
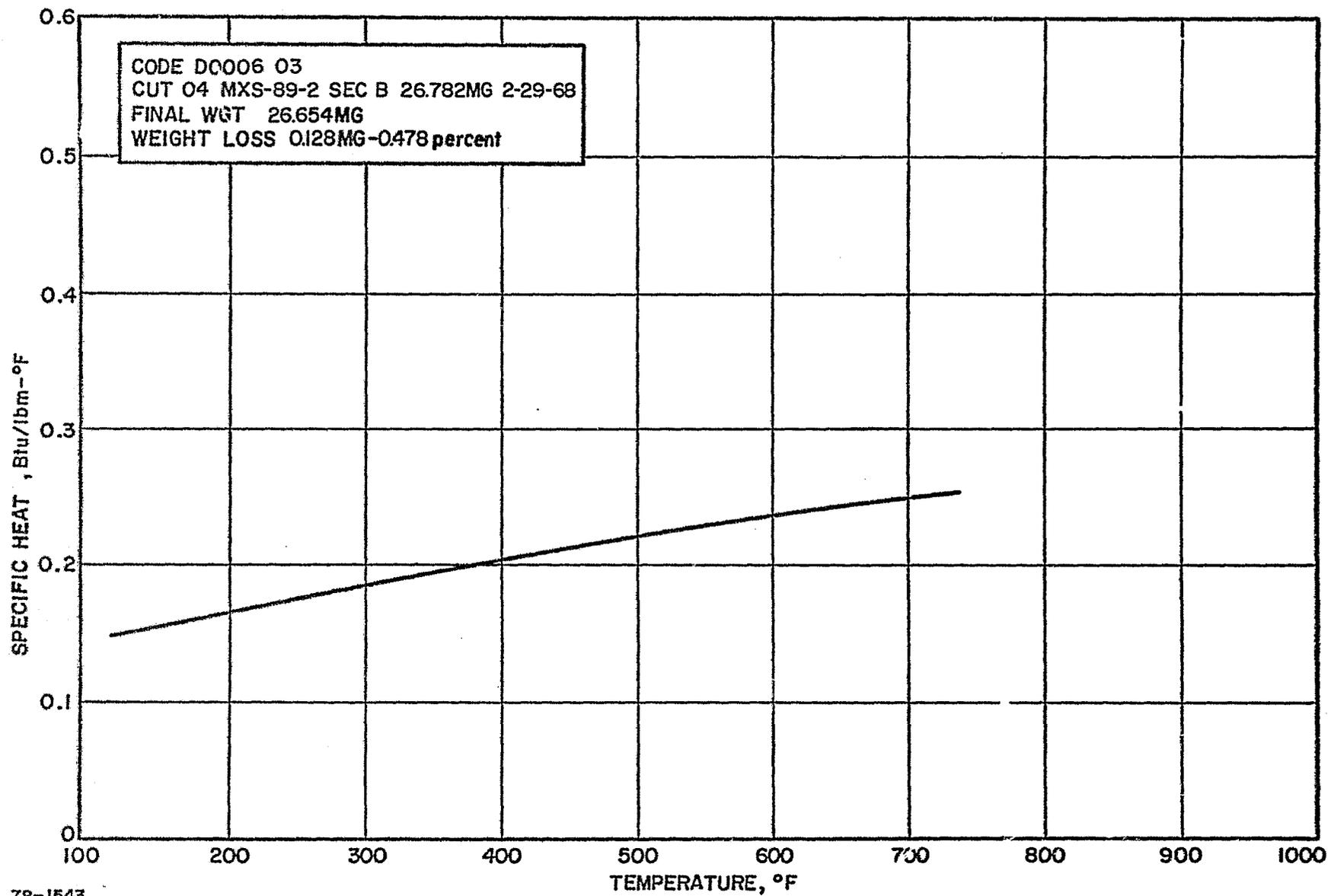
Figure 100 SILICA-PHENOLIC NOZZLE THROAT, 1.656-INCH CHAR LAYER,
SPECIFIC HEAT VERSUS TEMPERATURE
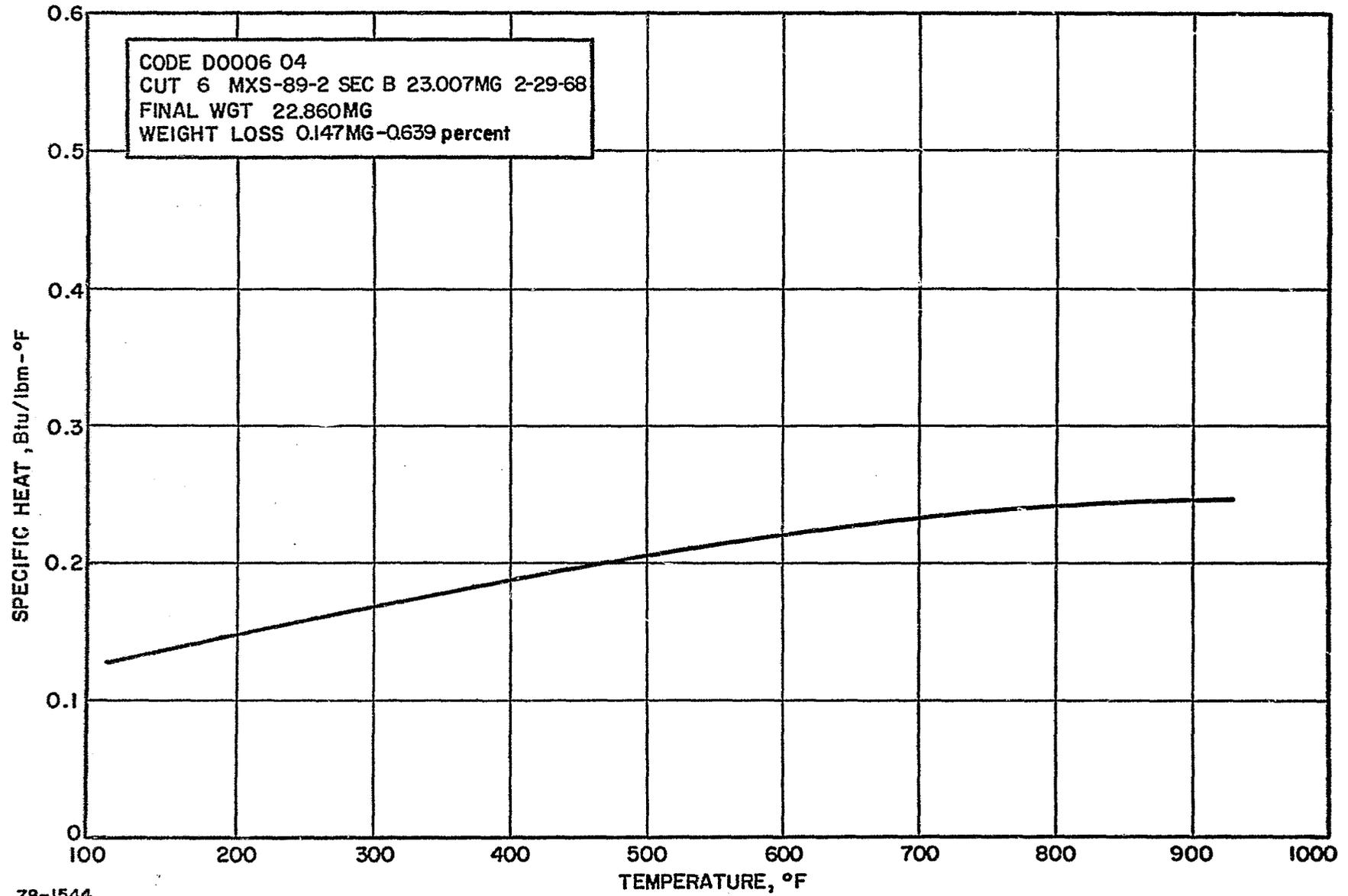
78-1543

Figure 101 SILICA-PHENOLIC NOZZLE THROAT, 1.604-INCH CHAR LAYER,
SPECIFIC HEAT VERSUS TEMPERATURE
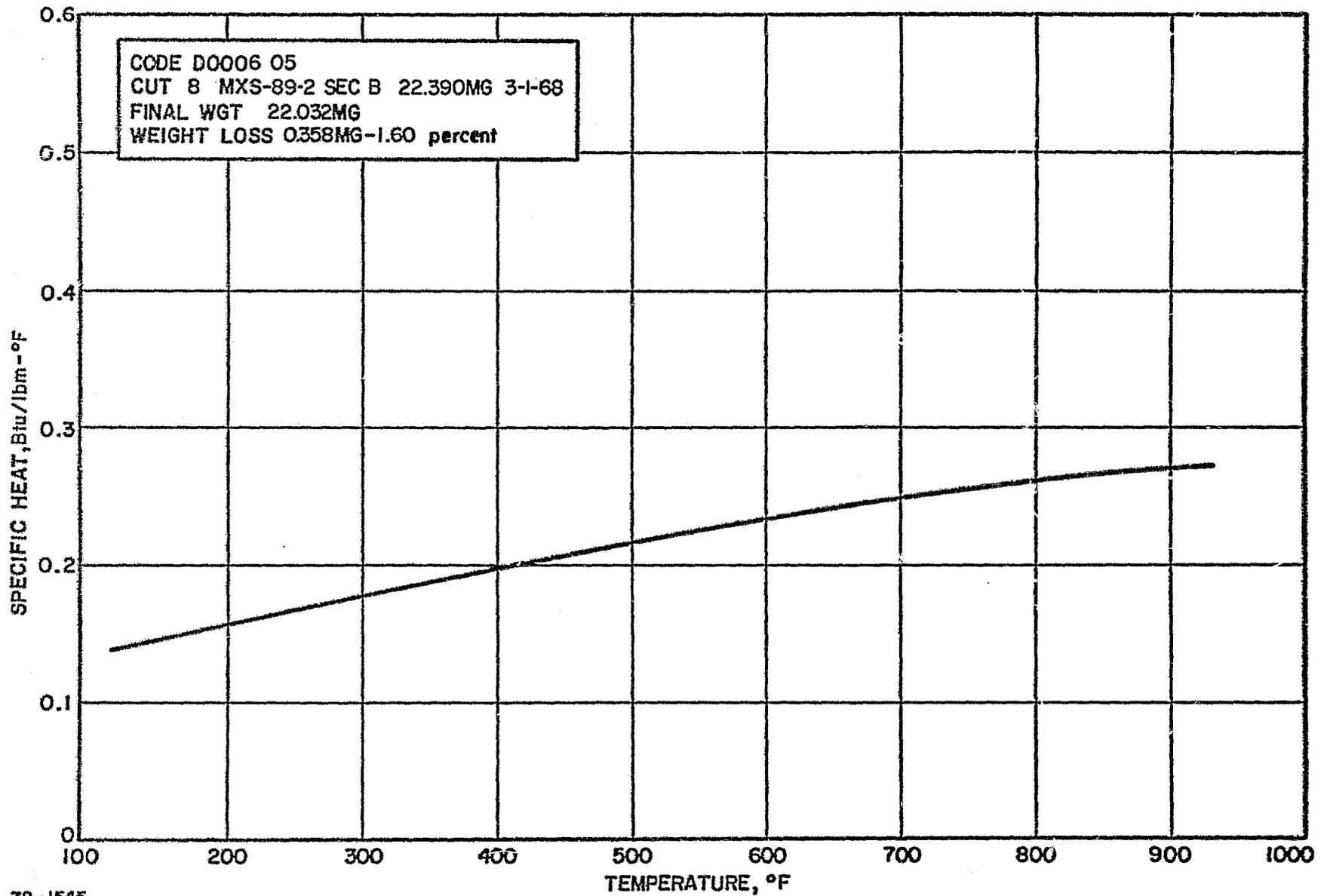
78-1545

Figure 102  SILICA-PHENOLIC NOZZLE THROAT, 1.552-INCH CHAR LAYER,
SPECIFIC HEAT VERSUS TEMPERATURE
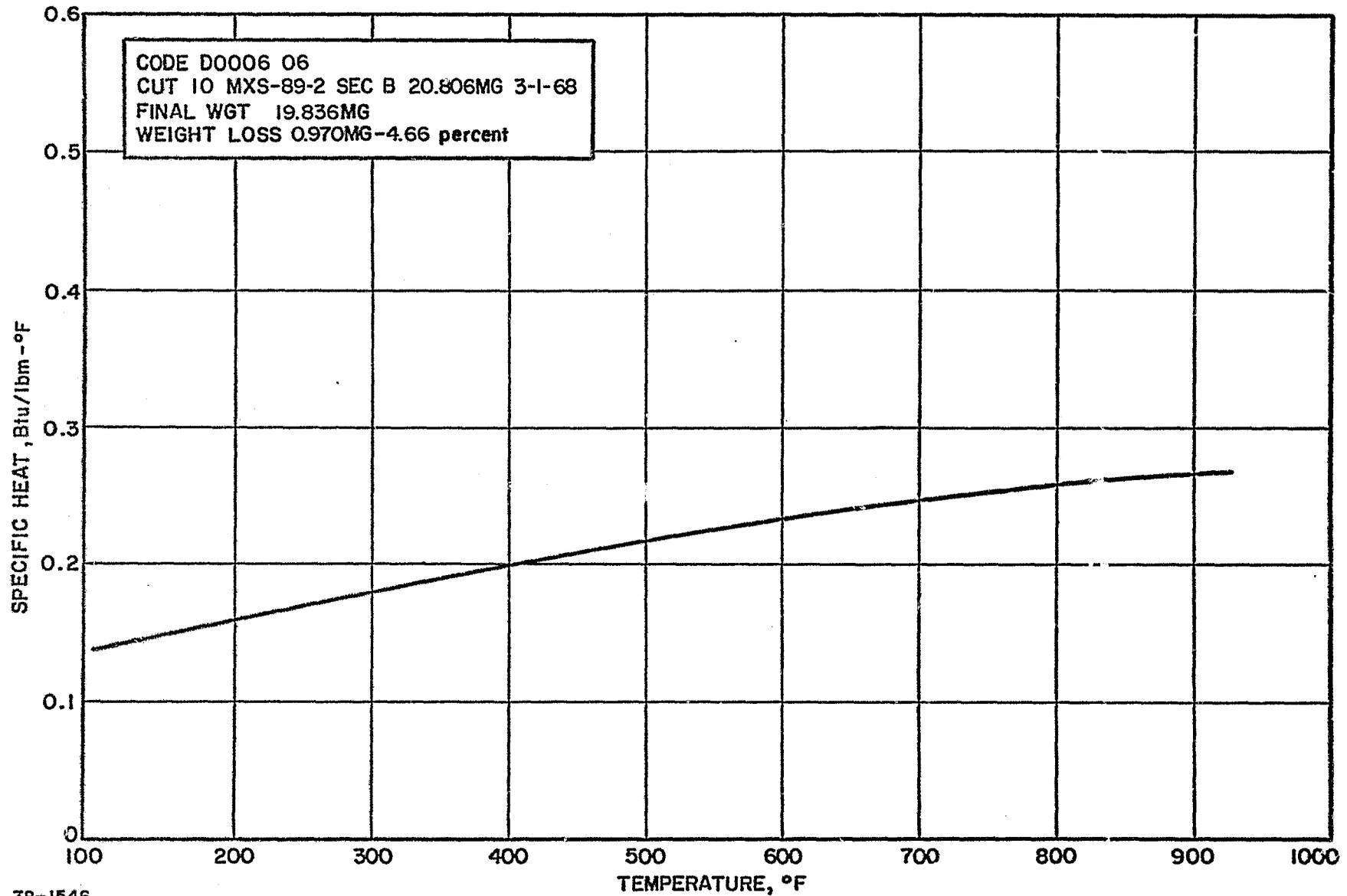
Figure 103 SILICA-PHENOLIC NOZZLE THROAT, 1.500-INCH CHAR LAYER, SPECIFIC HEAT VERSUS TEMPERATURE
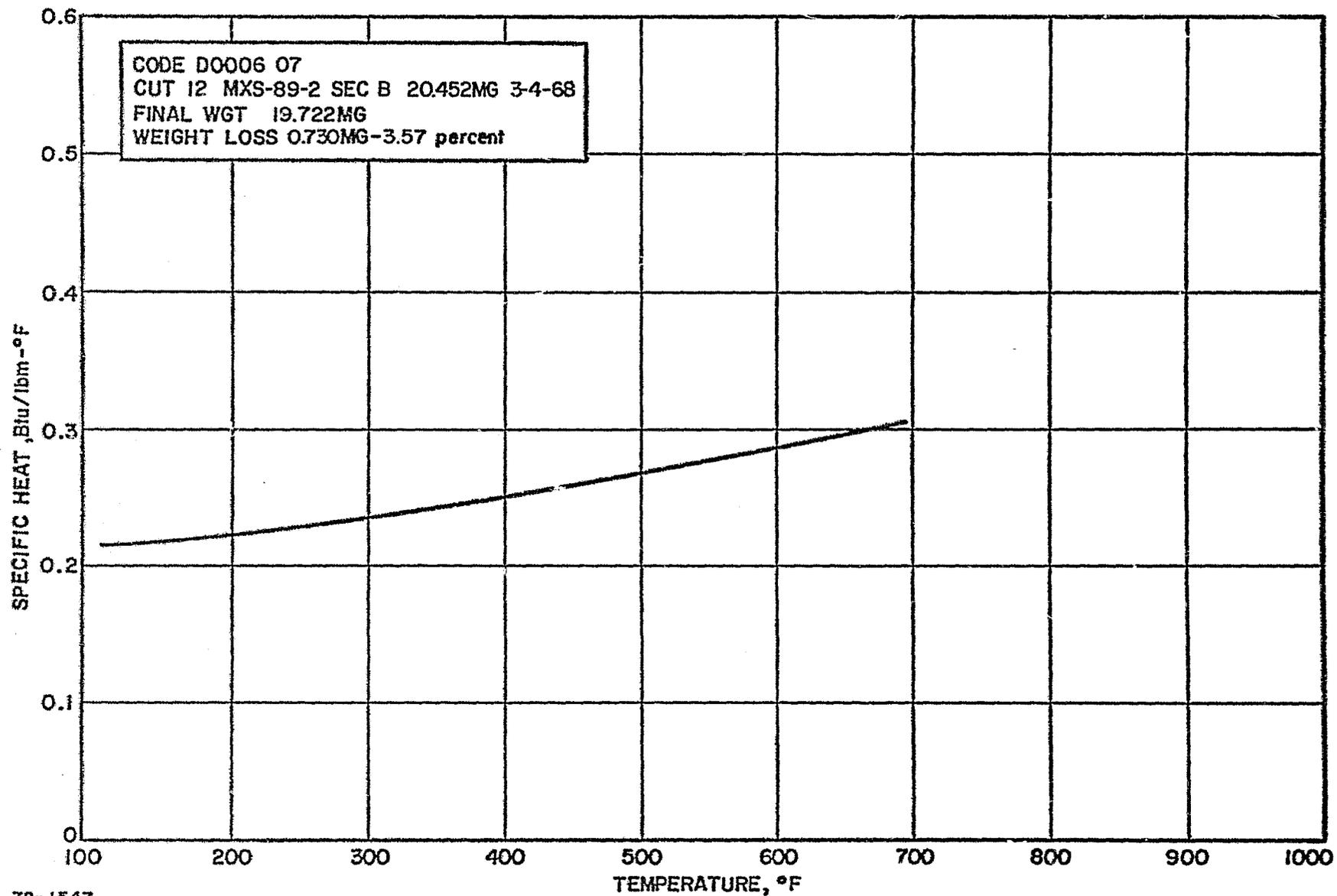
78-1546

Figure 104 SILICA-PHENOLIC NOZZLE THROAT, 1.451-INCH CHAR LAYER,
SPECIFIC HEAT VERSUS TEMPERATURE

78-1547

-143-
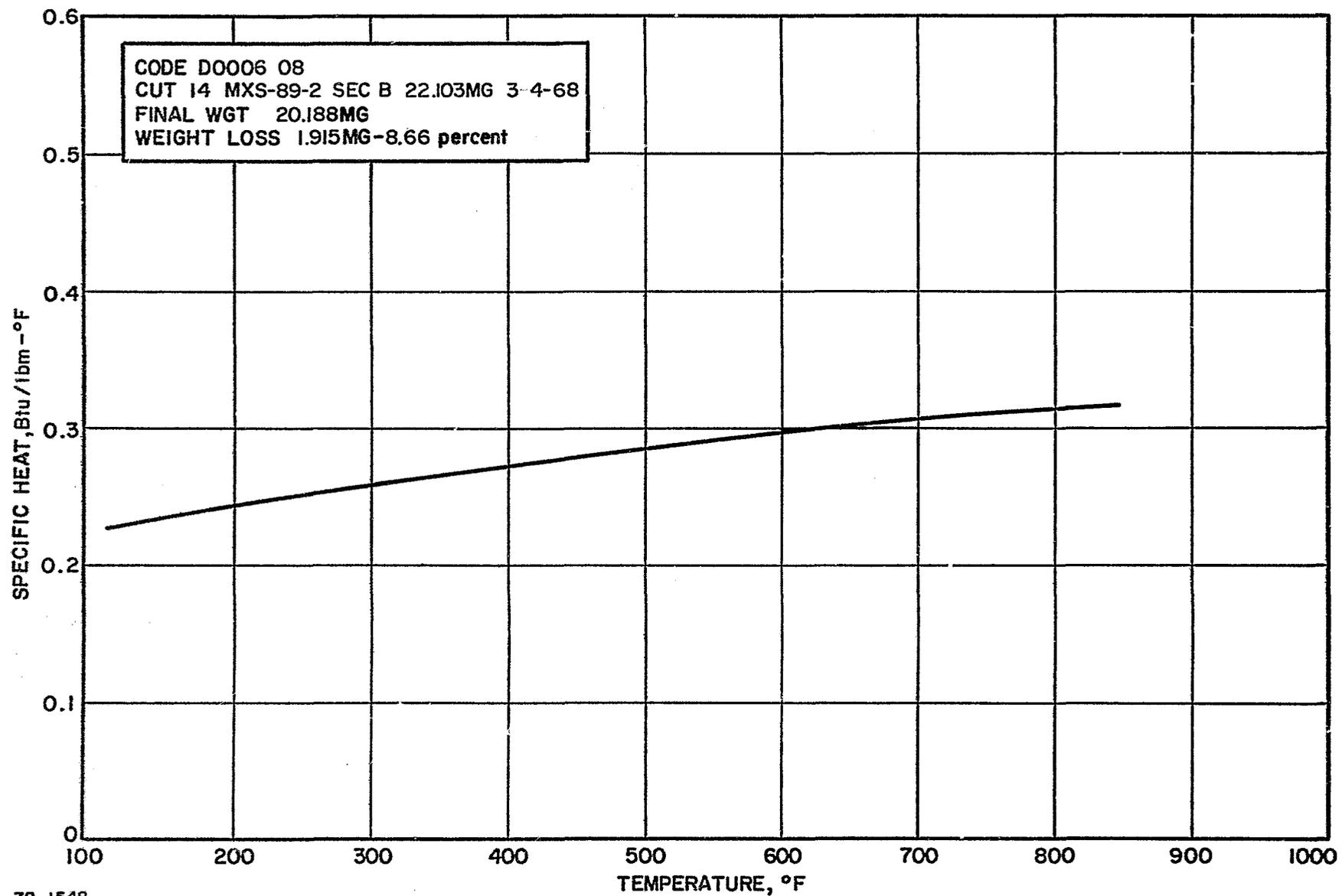
Figure 105 SILICA PHENOLIC NOZZLE THROAT, 1.404-INCH CHAR LAYER,
SPECIFIC HEAT VERSUS TEMPERATURE

78-1548

-144-
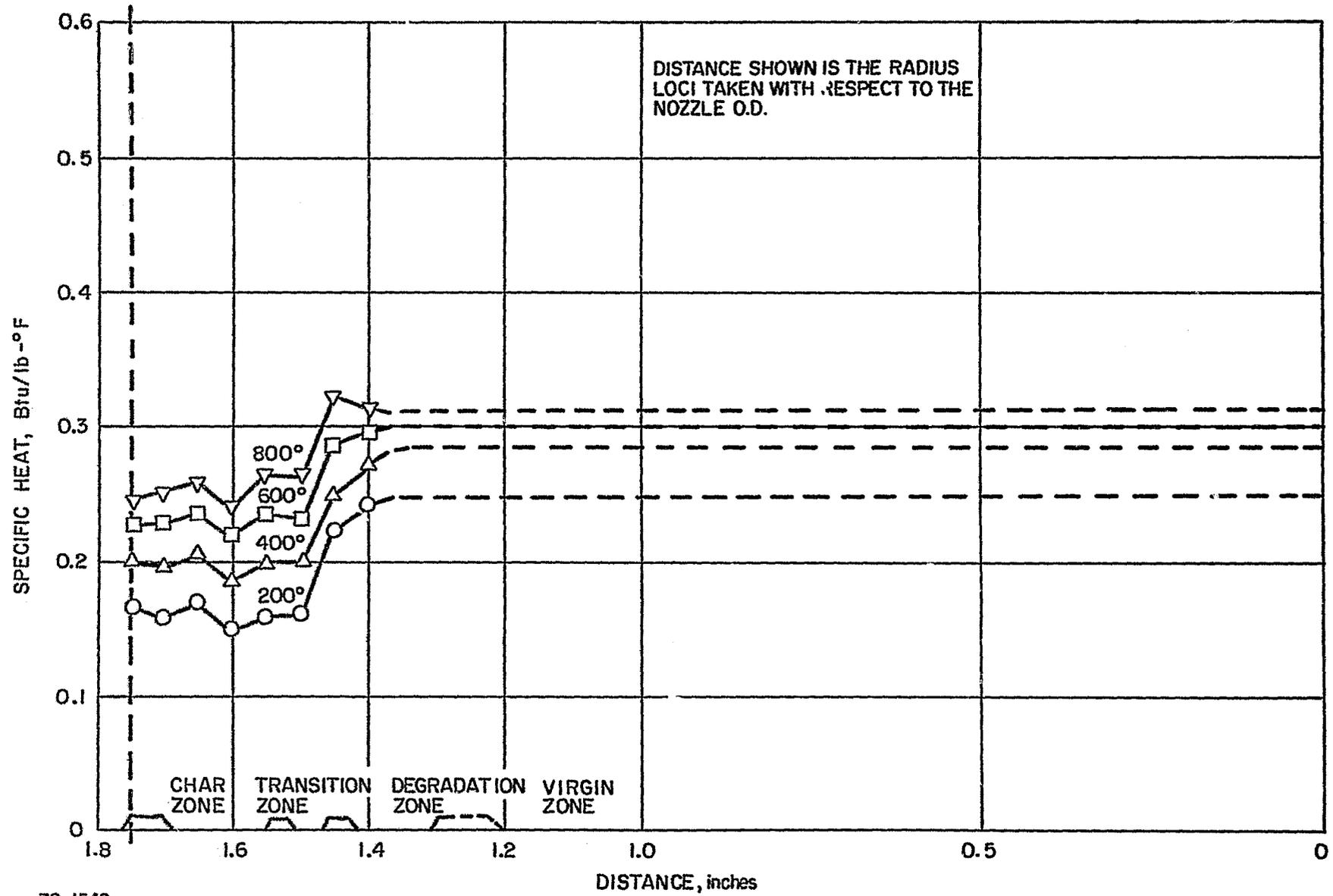
78-1549

Figure 106 SILICA-PHENOLIC NOZZLE THROAT, SPECIFIC HEAT (AT TEMPERATURE)
VERSUS CHAR DEPTH
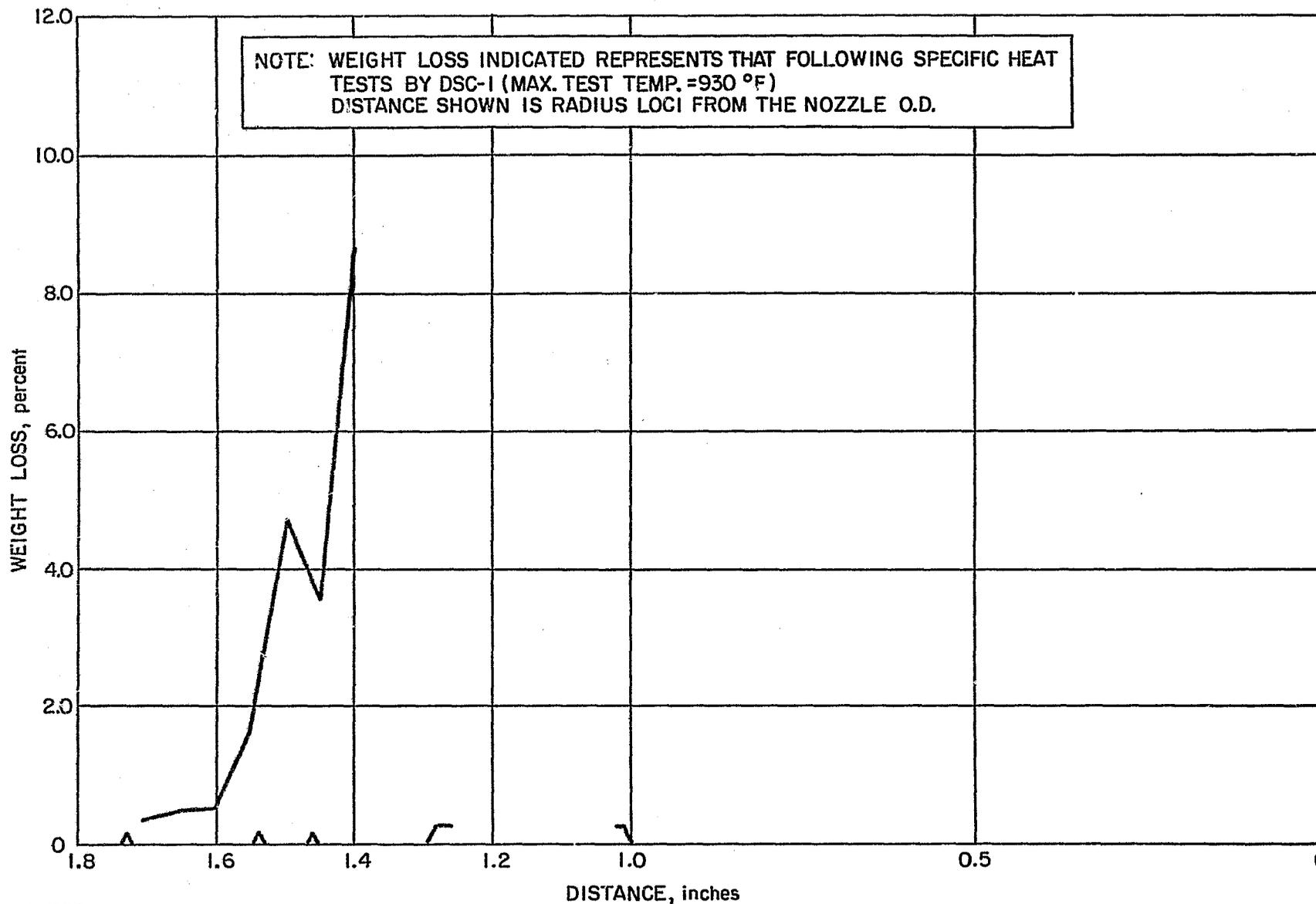
Figure 107 SILICA-PHENOLIC NOZZLE THROAT, POST DSC TEST WEIGHT
LOSS VERSUS CHAR DEPTH
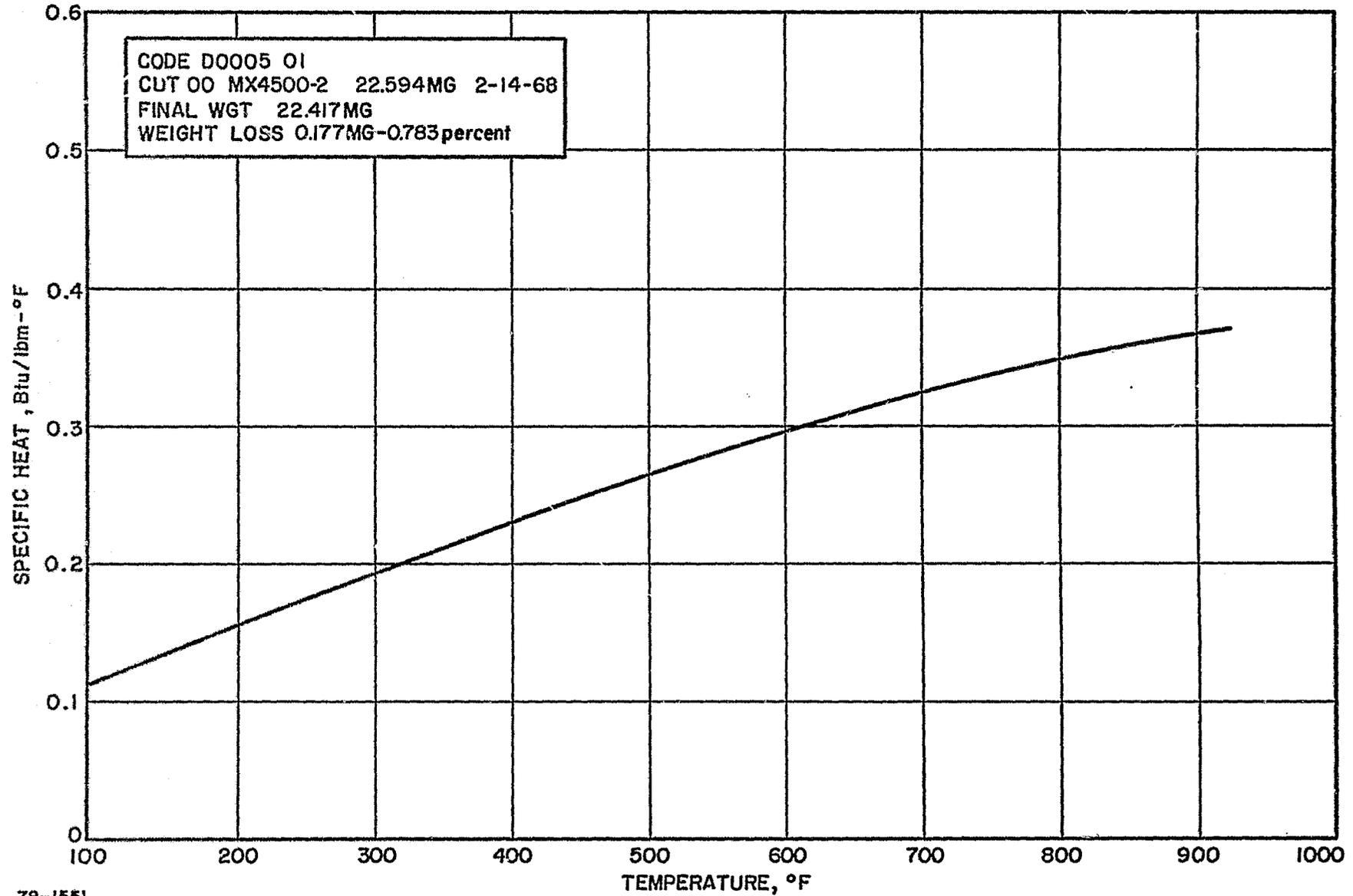
78-1550

Figure 108 GRAPHITE-PHENOLIC NOZZLE EXIT, SURFACE CHAR, SPECIFIC HEAT
VERSUS TEMPERATURE

78-1551

-147-
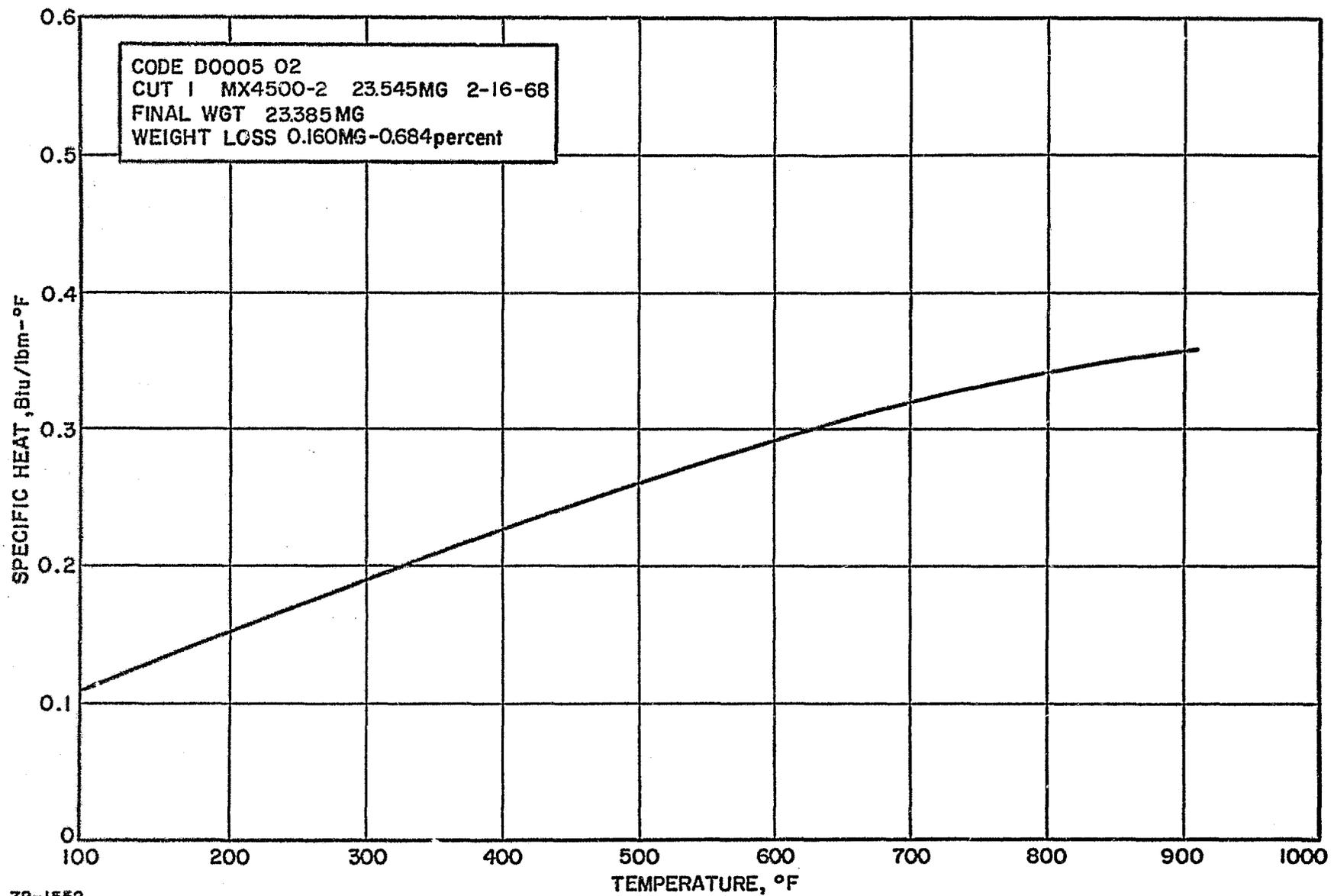
Figure 109  GRAPHITE-PHENOLIC NOZZLE EXIT, 1.678-INCH CHAR LAYER,
SPECIFIC HEAT VERSUS TEMPERATURE
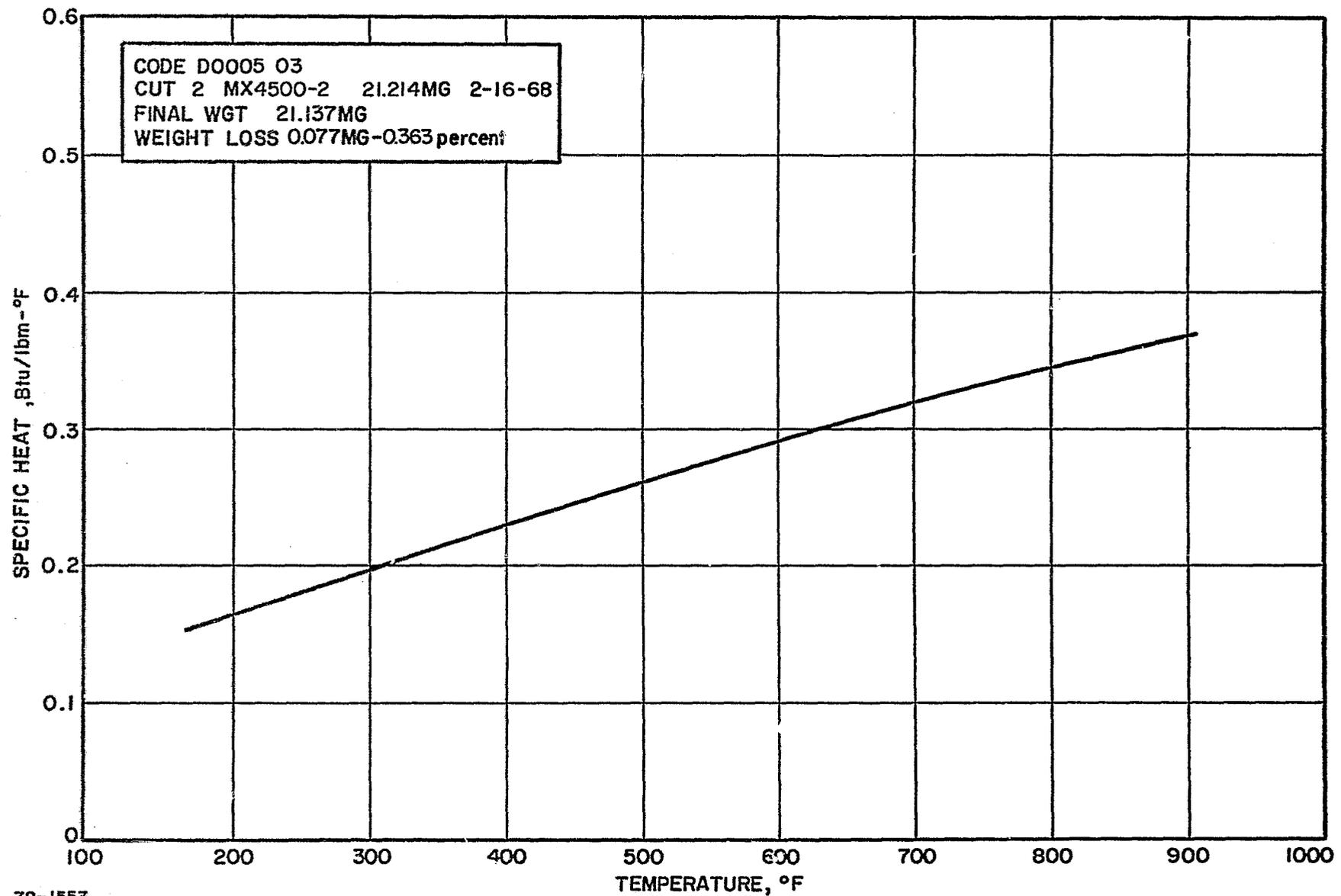
78-1552

Figure 110 GRAPHITE-PHENOLIC NOZZLE EXIT, 1.653-INCH CHAR LAYER,
SPECIFIC HEAT VERSUS TEMPERATURE
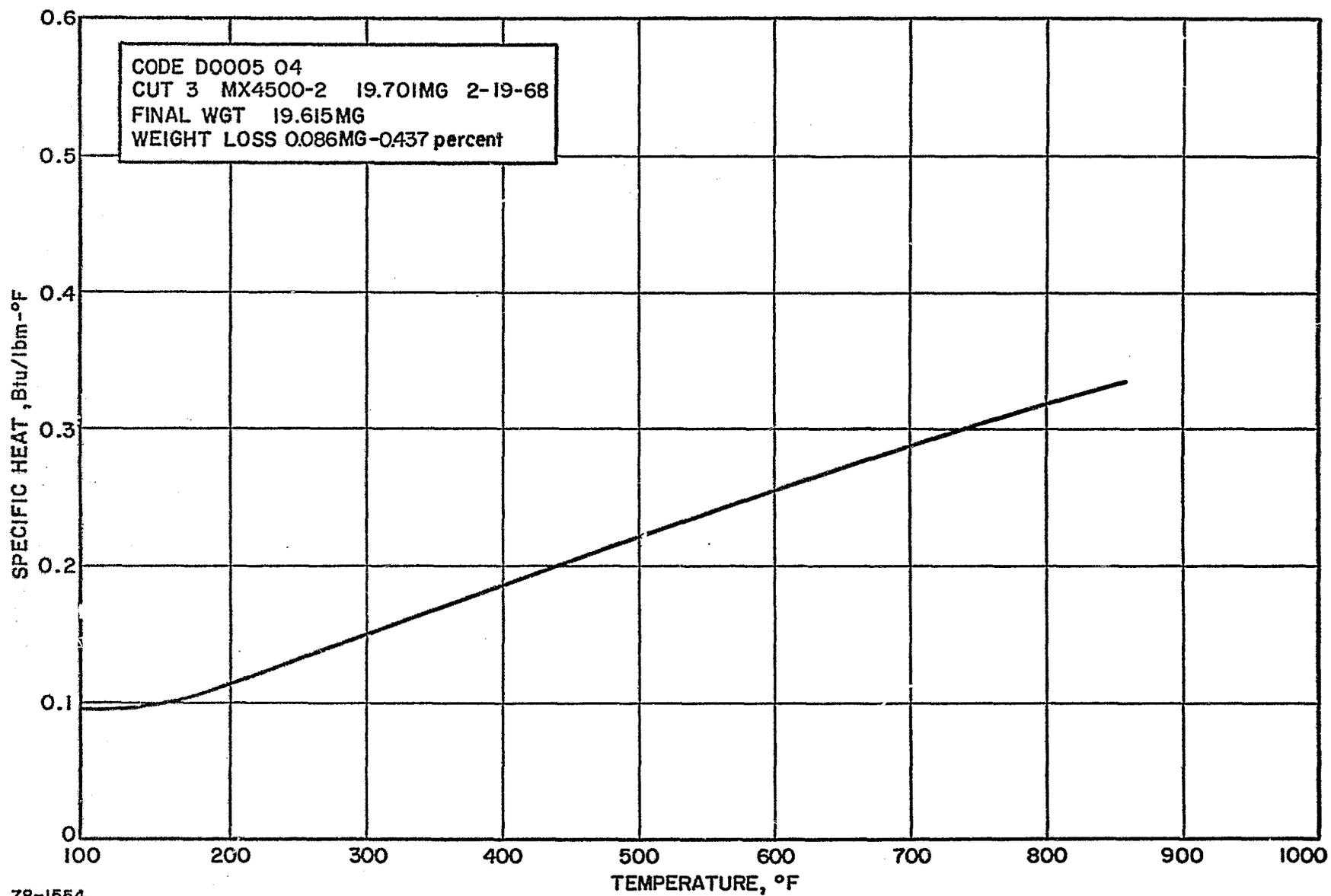
78-1553

Figure 111 GRAPHITE-PHENOLIC NOZZLE EXIT, 1.627-INCH CHAR LAYER, SPECIFIC HEAT VERSUS TEMPERATURE
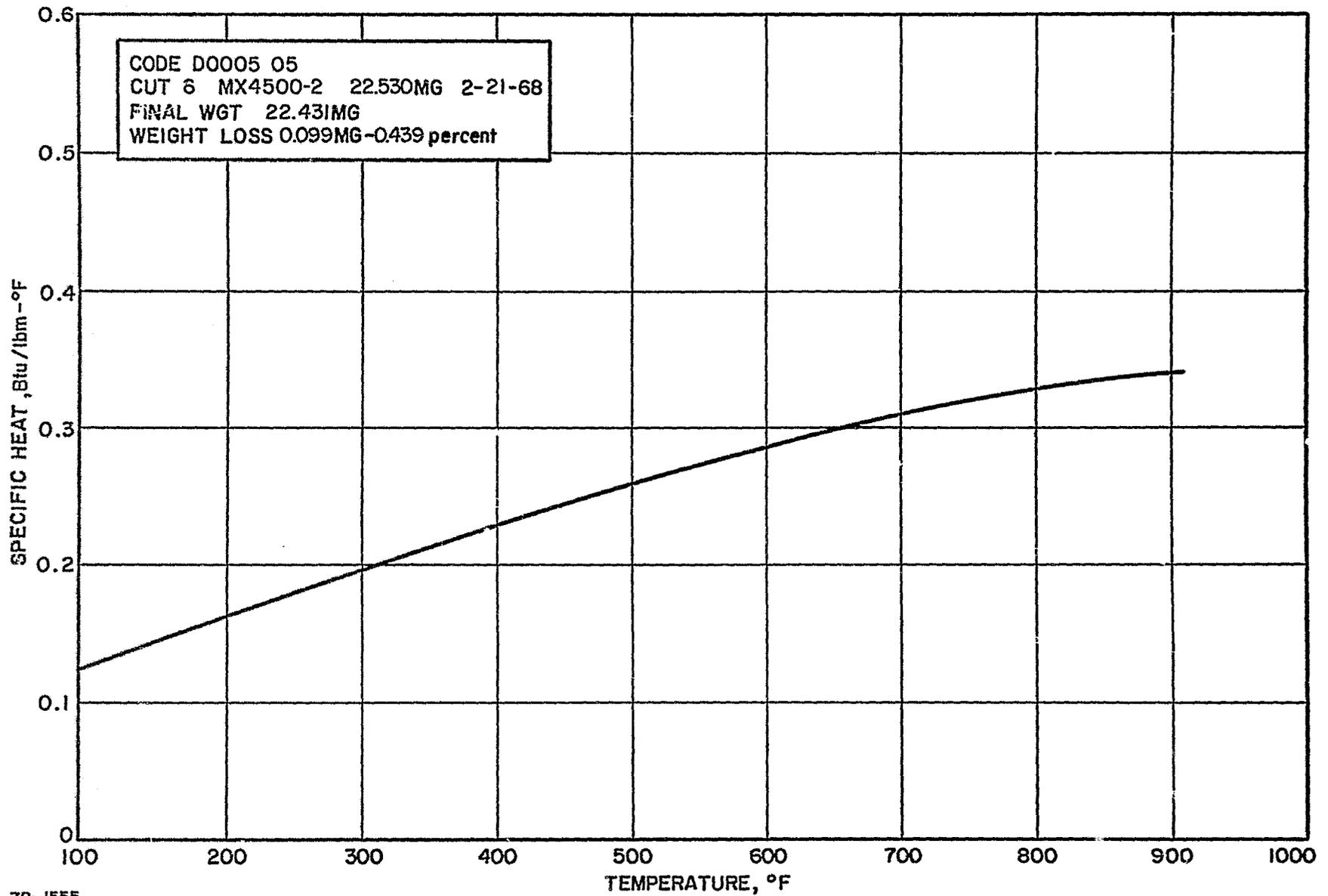
78-1554

Figure 112  GRAPHITE-PHENOLIC NOZZLE EXIT, 1.553-INCH CHAR LAYER,
SPECIFIC HEAT VERSUS TEMPERATURE

-151-
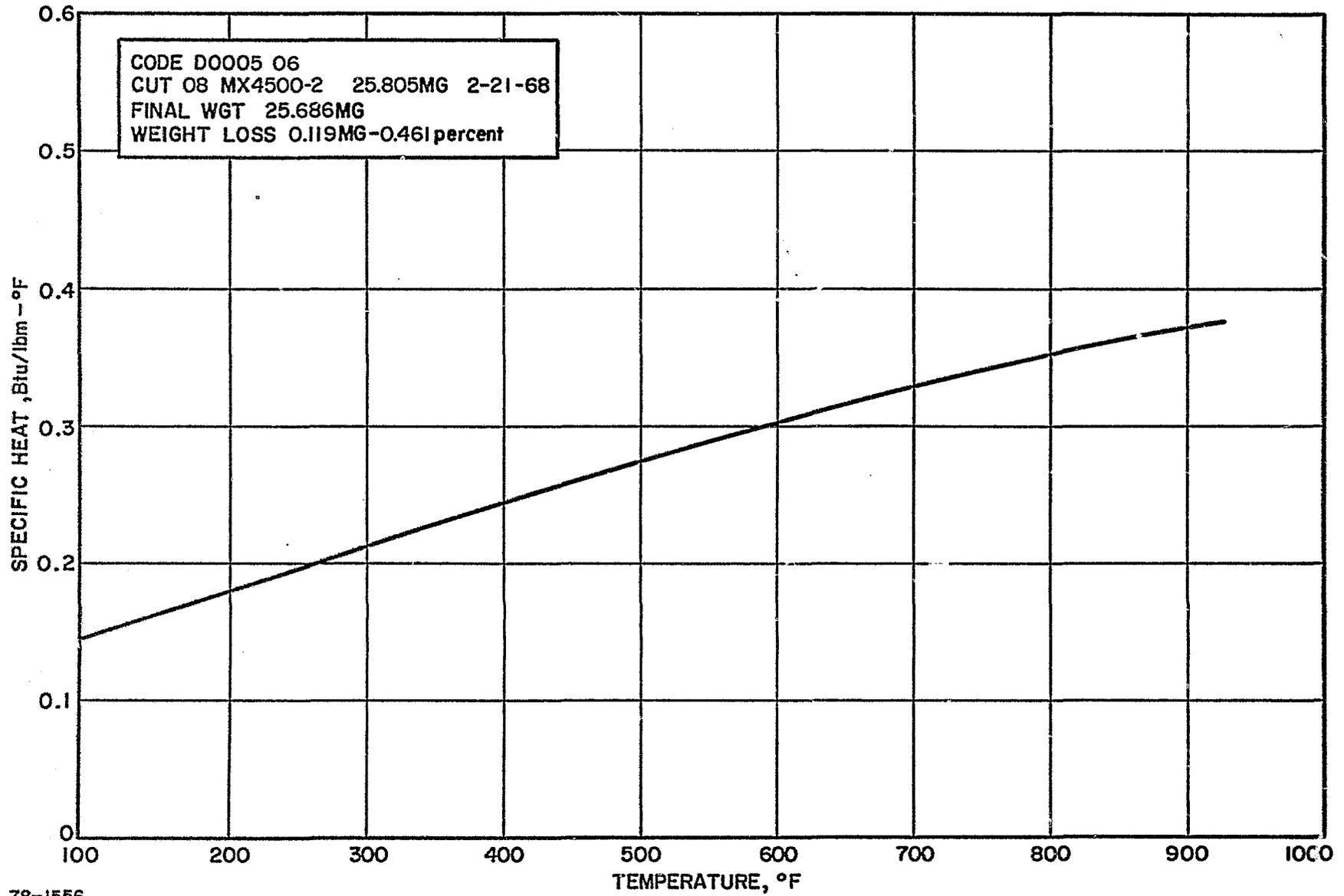
Figure 113 GRAPHITE-PHENOLIC NOZZLE EXIT, 1.483-INCH CHAR LAYER,
SPECIFIC HEAT VERSUS TEMPERATURE
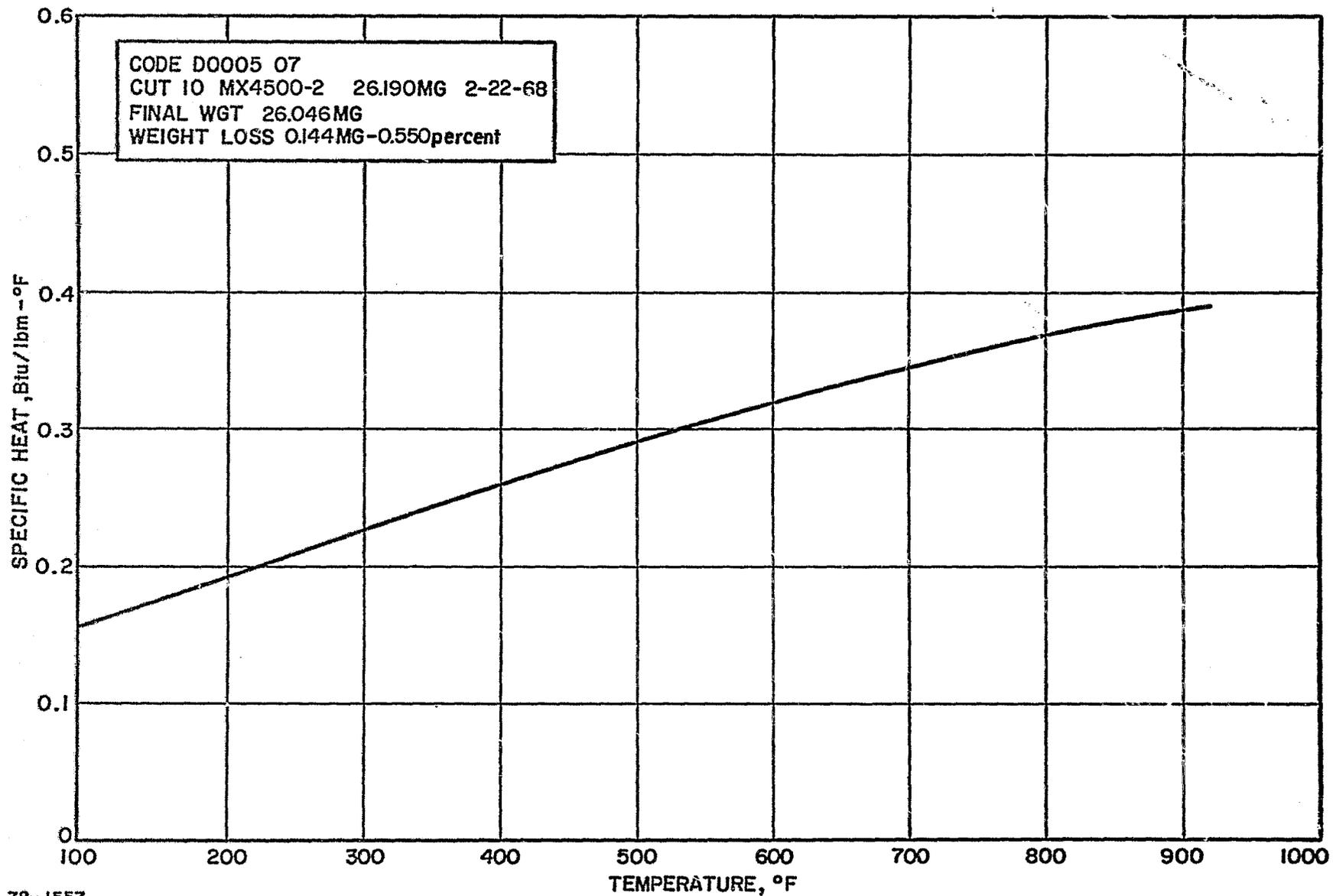
78-1557

Figure 114 GRAPHITE-PHENOLIC NOZZLE EXIT, 1.433-INCH CHAR LAYER,
SPECIFIC HEAT VERSUS TEMPERATURE
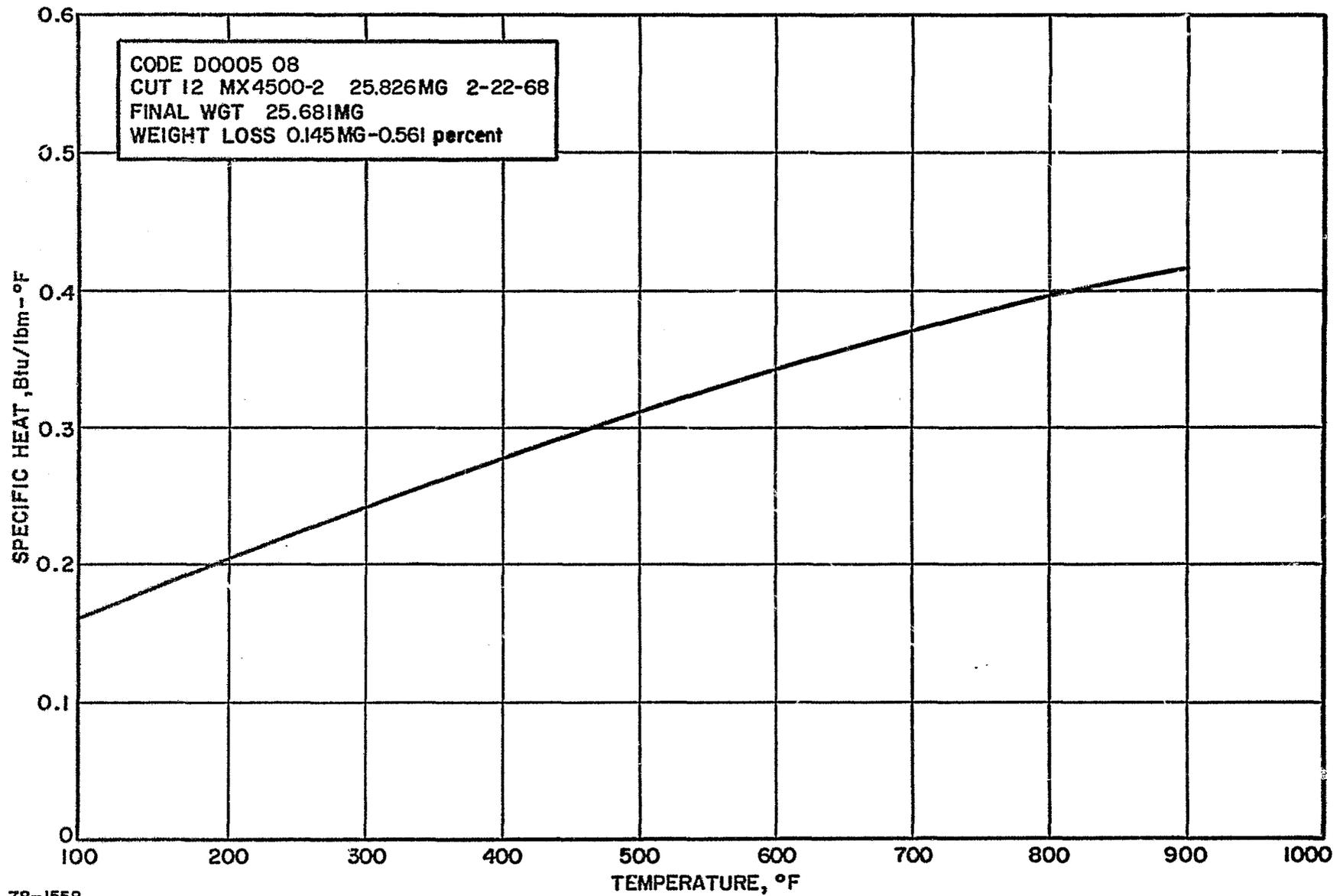
Figure 115  GRAPHITE-PHENOLIC NOZZLE EXIT, 1.377-INCH CHAR LAYER,
SPECIFIC HEAT VERSUS TEMPERATURE

The chart shows SPECIFIC HEAT, Btu/lbm-°F (y-axis, 0 to 0.6) versus TEMPERATURE, °F (x-axis, 100 to 1000).

Legend box:
CODE D0005 08
CUT 12  MX4500-2   25.826MG  2-22-68
FINAL WGT  25.681MG
WEIGHT LOSS 0.145MG-0.561 percent
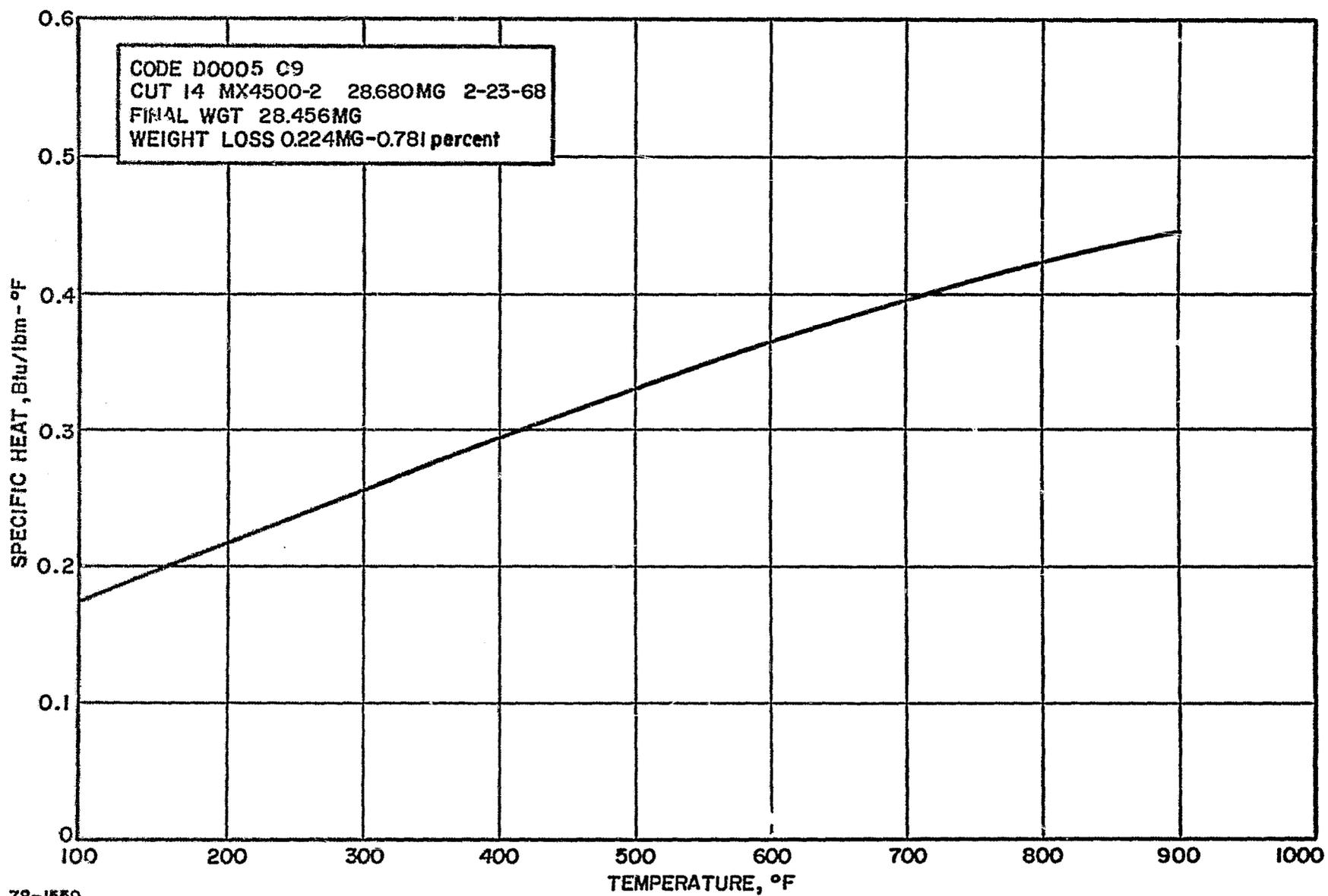
78-1558

Figure 116 GRAPHITE-PHENOLIC NOZZLE EXIT, 1.336-INCH CHAR LAYER,
SPECIFIC HEAT VERSUS TEMPERATURE

78-1559
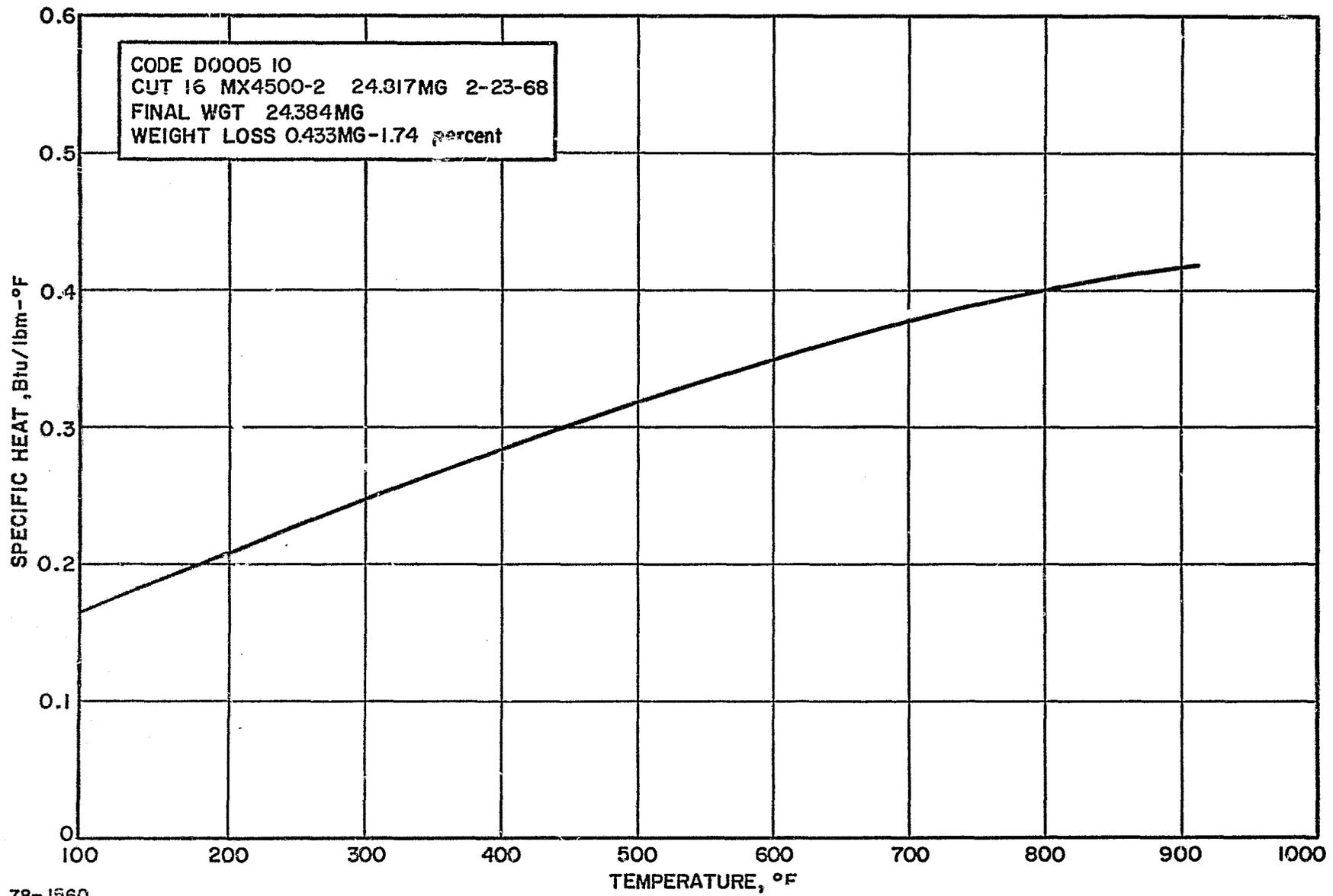
Figure 117  GRAPHITE-PHENOLIC NOZZLE EXIT, 1.276-INCH CHAR LAYER,
SPECIFIC HEAT VERSUS TEMPERATURE

78-1560

CODE D0005 II
CUT 18 MX500-2    28.240MG  2-26-68
FINAL WGT  27.198MG
WEIGHT LOSS 1.042MG-3.69 percent
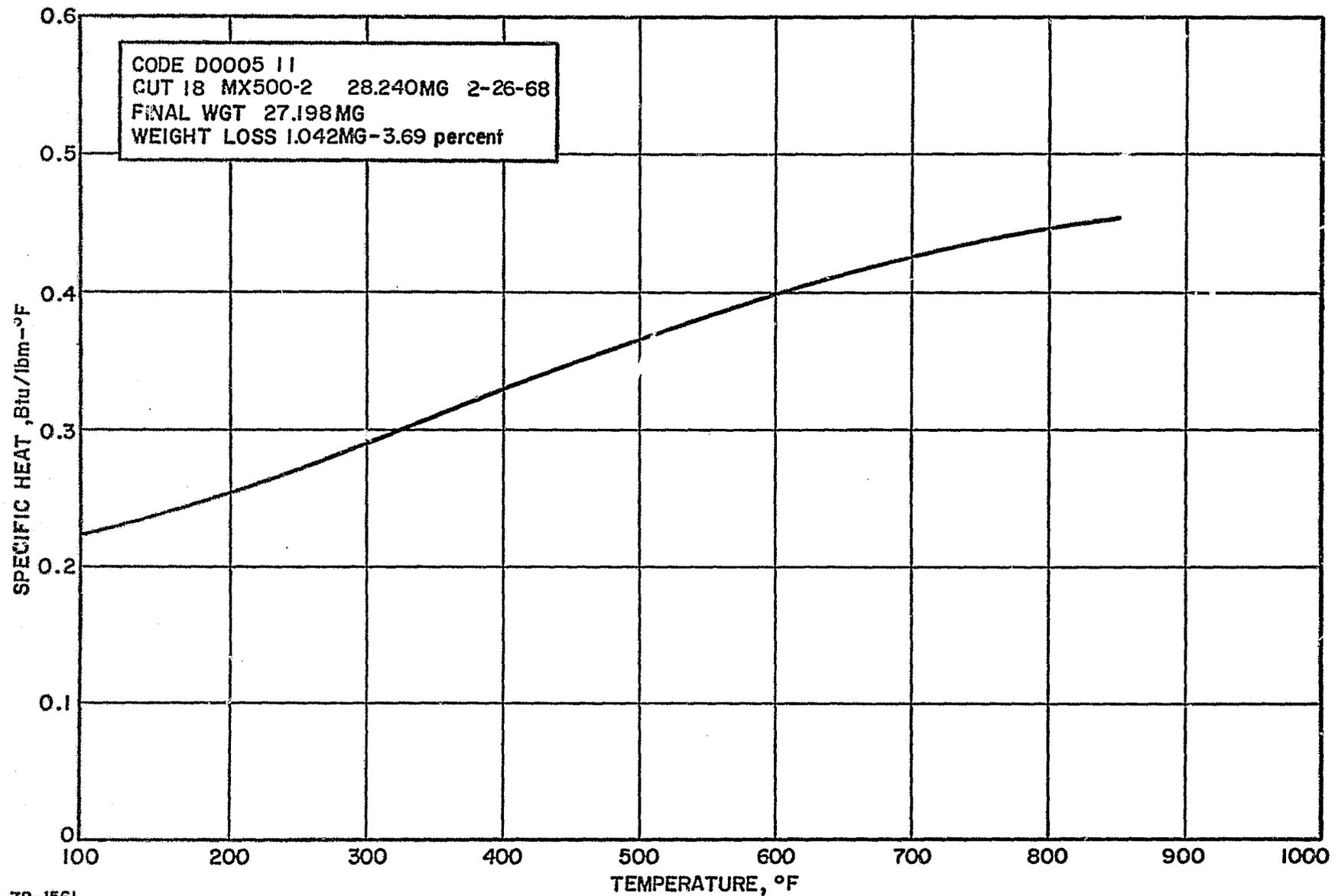
Figure 118  GRAPHITE-PHENOLIC NOZZLE EXIT, 1.228-INCH CHAR LAYER,
SPECIFIC HEAT VERSUS TEMPERATURE
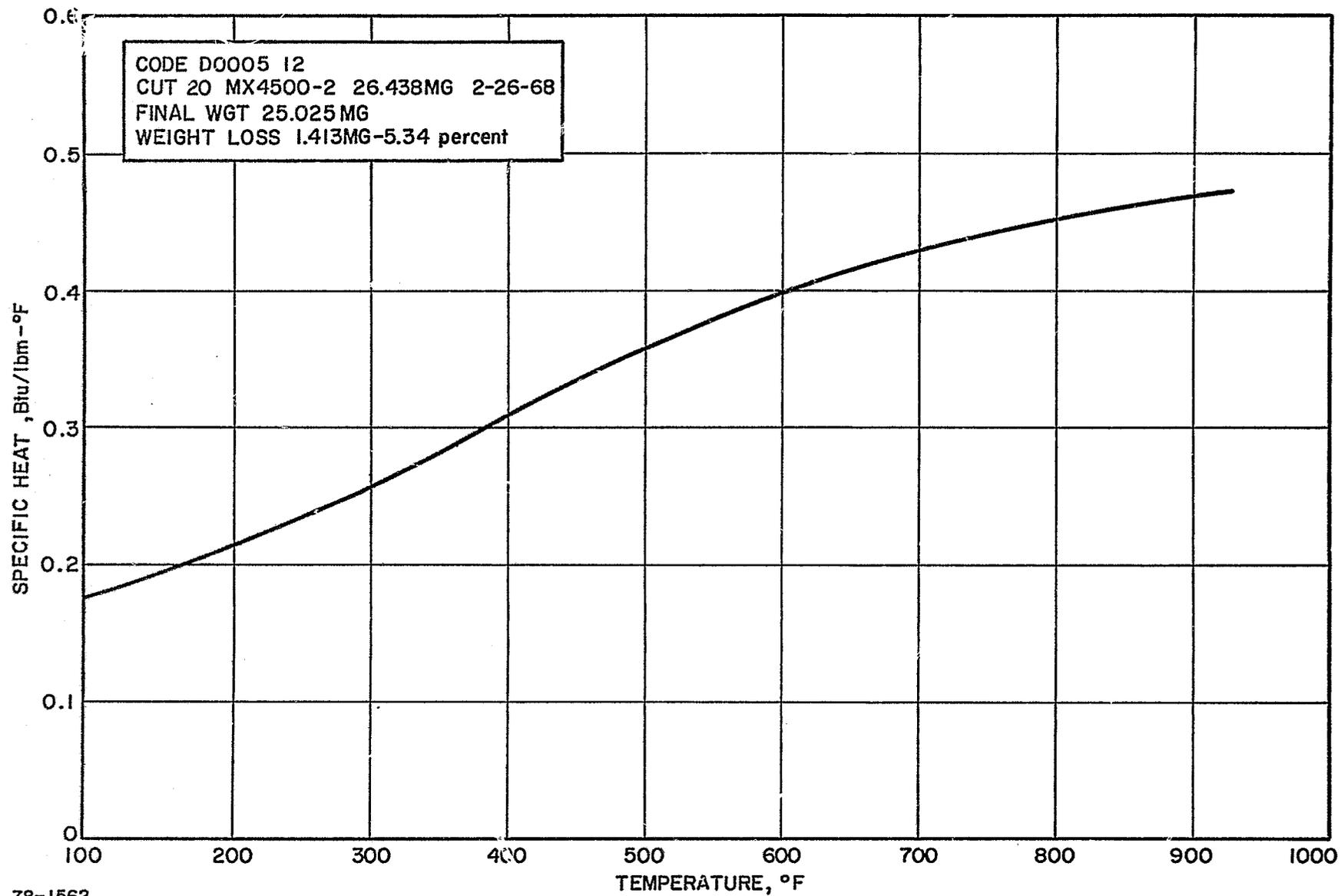
78-1561

Figure 119 GRAPHITE-PHENOLIC NOZZLE EXIT, 1.178-INCH CHAR LAYER,
SPECIFIC HEAT VERSUS TEMPERATURE
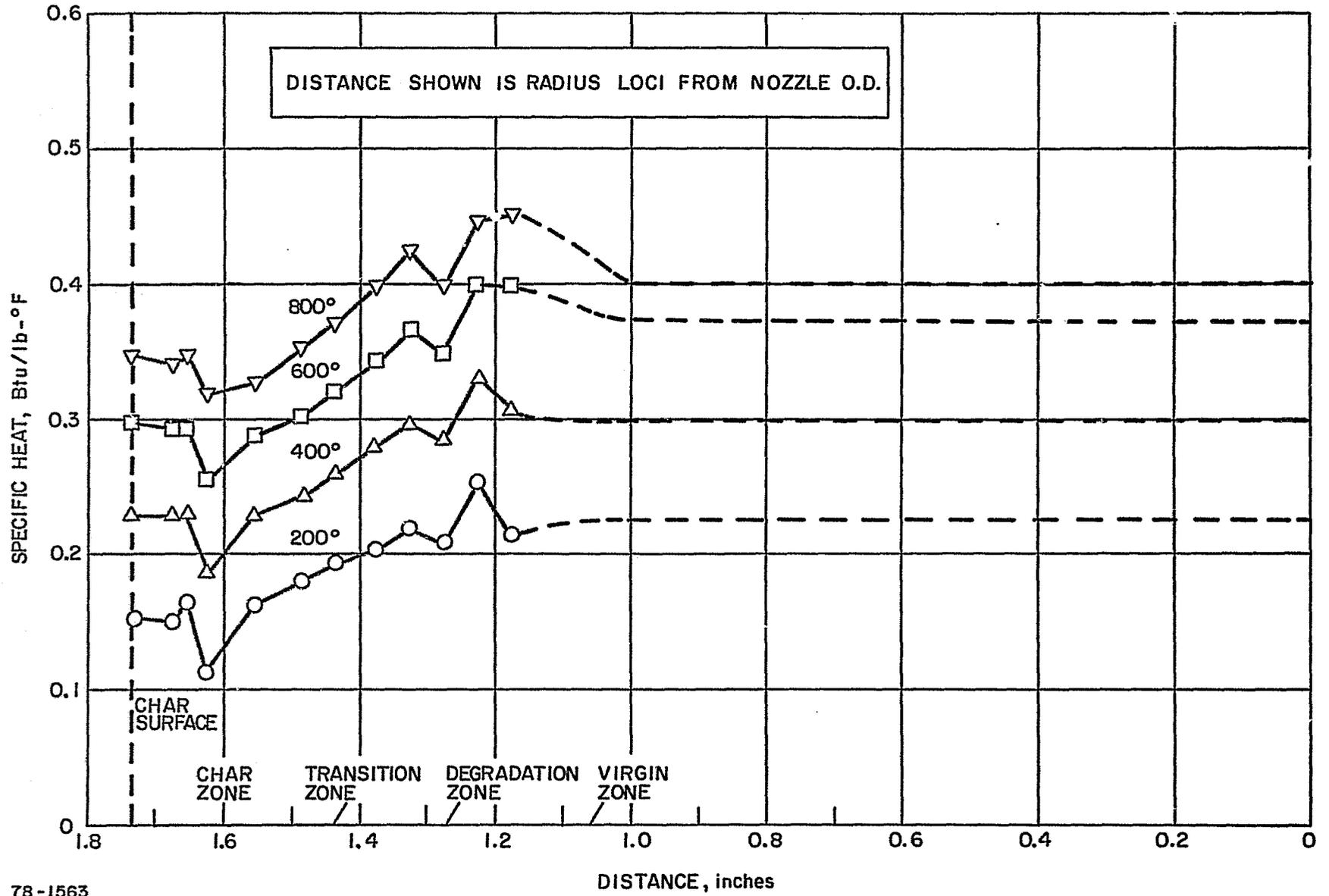
78-1562

Figure 120  GRAPHITE PHENOLIC NOZZLE EXIT, SPECIFIC HEAT (AT TEMPERATURE)
VERSUS CHAR LENGTH

78-1563

-159-
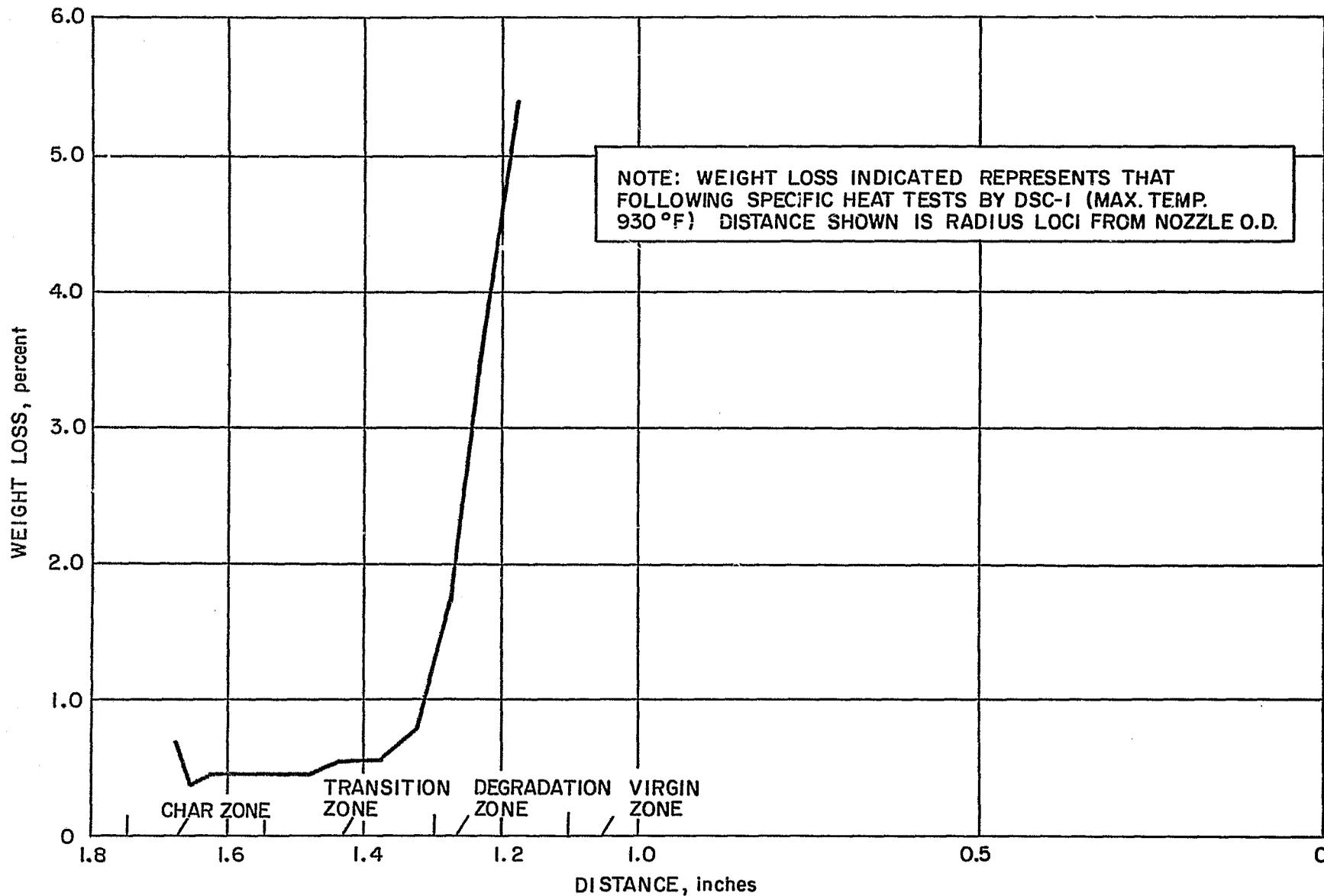
Figure 121 GRAPHITE PHENOLIC NOZZLE EXIT, POST-DSC TEST WEIGHT LOSS
VERSUS CHAR DEPTH

78-1564

# IV.  CONCLUSIONS

## A.  CHARACTERIZATION OF VIRGIN MATERIALS AND OVEN REFERENCE CHARS

### 1.  Virgin Billets

Virgin billet of MXS-89 was uniform in density except that an area of macroporosity was noted in the center of the billet.  This was due to trapped volatiles occurring as a result of nonuniform curing associated with its lower thermal conductivity.

The virgin billet of MX4501 density was greatest along the axis and decreased outward the circumference.  This was attributed to a rapid curing in the center than at the circumference, influenced mainly by the higher thermal conductivity of the graphite filler material.

### 2.  Oven Chars

For the oven-charred MXS-89 material:  (silica-phenolic)

a)  The greatest change in weight occurred near the $1000^{\circ}$ F level.

b)  The greatest shrinkage occurred across the fabric laminates and ranged from 0 to 6.9 percent, progressively increasing with temperature.

c)  The material decomposed extensively at temperatures around $2800^{\circ}$ F losing virtually all of its structural integrity.

d)  The density varies as a function of charring temperature as follows: from a room temperature value of 101.3 lb/ft$^3$ it steadily decreases to 92 lb/ft$^3$ at $1000^{\circ}$ F, rises uniformly to 94 lb/ft$^3$ at $2000^{\circ}$ F, and drops off sharply to 63.7 lb/ft$^3$ at $2700^{\circ}$ F.  The sharp drop off in density at the higher temperatures is attributed to the depletion of the specimens forming silicon carbide and gaseous silicon monxide and carbon monoxide.  The degree of drop off is felt to be a time-at-temperature dependent phenomenon which can lead to total depletion of the charring material.

For the oven-charred MX4501 material:  (graphite-phenolic)

a)  The greatest change in weight occurred near the $1000^{\circ}$ F level.

b)  The greatest shrinkage occurred across the fabric planes and ranged from 0 to 7.5 percent proportional to temperature.

c)  The material retained structural integrity after being precharred to $4000^{\circ}$ F with only an additional 3 percent weight loss above $1000^{\circ}$ F.

d)  The density varies as follows:  from a room temperature value of 84.2 lb/ft$^3$ it decreases to 55 lb/ft$^3$ at $2000^{\circ}$ F where it remains until $3000^{\circ}$ F, whereupon it drops uniformly through 52.8 lb/ft$^3$ at $3600^{\circ}$ F to a $4000^{\circ}$ F level of 40.7 lb/ft$^3$.

Both oven-charred materials experienced similar weight losses at $1000^o$ and $2000^o$ F char temperatures, indicating a basic similarity of the phenolic matrix and its decomposition mechanism.

   a.   Silica Phenolic MXS-89

The principal silica-phenolic degradation occurred at temperatures near $1000^o$ F continuing to near $2000^o$ F, and was attended by thermal stress cracking of the phenolic matrix.

No apparent visually observable reactions between the silica fibers and charred matrix occurred up to $2000^o$ F.

The oven chars prepared at $2400^o$, $2700^o$, and $2800^o$ F contained silicon carbide, however, formed by the oven charring process at any of the charring temperatures. This is felt to be due to the long and slow process of charring which does not present a mechanism to support cracking type reactions.

   b.   Graphite Phenolic

Although the phenolic matrix contained graphite powder, the principal decomposition occurred near $1000^o$ F as was the case for the silica-phenolic material.

The graphite fabric material was unreacted upon at all char temperatures, although thermal stress cracks prevailed throughout the specimens at all char temperatures. No pyrolytic graphite was produced through oven charring to $4000^o$ F.

A coarse-fine-coarse transition occurred in the phenolic matrix texture over the range $1000^o$ to $4000^o$F with the finest texture occurring at $3000^o$F.

B.   CHEMICAL AND PHYSICAL ANALYSIS OF VIRGIN MATERIAL AND OVEN CHARS

TGA studies and pyrolysis studies in helium indicated that both composites decompose in a similar manner, with extensive degradation of the phenolic resin occurring between $750^o$ and $1470^o$ F inclusive. In air, however, major decomposition occurs between $570^o$ and $1112^o$ F. Variation in heating rate from $9^o$ to $36^o$ F/min had no effect on the weight loss-at-temperature.

At the $1110^o$ F pyrolysis temperature, 63 mole percent of the volatile products found for silica-phenolic was water in contrast to 26 mole percent for the graphite-phenolic.

TGA studies give evidence that increasing the precharring temperature of the graphite-phenolic gives rise to greater resistance to oxidation of the material. This phenomenon is believed to be caused by either or both of two changes resulting from the charring procedure: first, an increase in carbon crystallinity (as evidenced by photomicrographic analysis); second, the removal of impurities in the graphite filler by volatilization and/or reaction.

## C. OPTICAL PROPERTIES OF OVEN CHARS

The major optical reflectance sensitivity of the silica-phenolic composites occurs between the material conditions-virgin to $1000^{\circ}$ F prechar, using standard reflectance measuring techniques. Only slight changes in total reflectance occur for the $2000^{\circ}$ F prechar. Reflectance of the MX4501 oven prechars was approximately 3 percent for all prechar temperatures. The apparent lack of resolution in the test series is attributed to the fact that a highly reflecting reference standard $(M_gO)$ was used to measure differences in the very low reflecting oven chars.

## D. X-RAY DIFFRACTION ANALYSIS OF OVEN CHARS

Silica-phenolic materials, oven-charred to $1000^{\circ}$ and $2000^{\circ}$ F, have similar crystalline structures, each consisting of slightly crystalline carbon, and amorphous material, such as $SiO_2$ and carbon, and no SiC. Increasing the charring temperature to $2400^{\circ}$ F yields small amounts of SiC, crystalline carbon, alpha crystobalite, and some amorphous material. At $2700^{\circ}$ and $2800^{\circ}$ prechar temperatures, MXS-89 contains heavy quantities of SiC, some alpha crystobalite, and amorphous material such as carbon.

Graphite-phenolic MX4501 prechars, on the other hand, show only small differences in crystal phases, particularly carbon, over the $1000^{\circ}$ to $4000^{\circ}$ F char temperature range. These changes reflect principally the behavior of the charring phenolic matrix.

## E. THERMAL PROPERTIES OF VIRGIN MATERIAL AND OVEN CHARS

The average thermal conductivity of silica-phenolic MXS-89 material in its unfired state is 0.322 Btu/hr-ft-$^{\circ}$F at an average temperature of $222^{\circ}$ F graphite-phenolic MX4501 is 1.57 Btu/hr-ft-$^{\circ}$ F at an average temperature of $134^{\circ}$ F when heat flows parallel to the fabric plane of the material laminates as in a fired nozzle. For MXS-89 precharred materials, the values of thermal conductivity are: $1000^{\circ}$ F prechar -- 0.330 Btu/hr-ft-$^{\circ}$ F; $2000^{\circ}$ F prechar -- 0.501 Btu/hr-ft-$^{\circ}$ F at $150^{\circ}$ F.

At $150^{\circ}$ F the thermal conductivities of MX4501 oven prechars are as follows:

$1000^{\circ}$ F prechar -- 2.40 Btu/hr-ft-$^{\circ}$ F

$2000^{\circ}$ F prechar -- 3.82 Btu/hr-ft-$^{\circ}$ F

$3000^{\circ}$ F prechar -- 4.64 Btu/hr-ft-$^{\circ}$ F

$3650^{\circ}$ F prechar -- 10.67 Btu/hr-ft-$^{\circ}$ F

$4000^{\circ}$ F prechar -- 15.54 Btu/hr-ft-$^{\circ}$ F

An abrupt increase in the thermal conductivity trend for MX4501 occurs around $3000^{\circ}$ F and is assumed to be attributable to increased graphitization of the charred phenolic matrix.

The specific heats of unfired MXS-89 and MX4501 billets are 0.249 Btu/lb-°F and 0.224 Btu/lb-°F respectively at 147°F.

The specific heat of MXS-89 silica-phenolic (at 200°F) increases uniformly from 0.249 Btu/lb-°F at near room temperature to 0.285 Btu/lb-°F when heated to 400°F, then gradually decreases to 0.189 Btu/lb-°F at a char temperature of 2800°F.

For MX4501 graphite-phenolic, the specific heat (at 200°F) increases from 0.215 Btu/lb-°F near room temperature to 0.255 Btu/lb-°F near 500°F, decreases significantly through the major decomposition temperature region to 0.12 Btu/lb-°F at 1000°F, and remains relatively unchanged to a char temperature of 4000°F where its value is 0.12 Btu/lb-°F.

F.  POST-FIRED ROCKET NOZZLE MATERIAL

1.  Microscopic Analyses

The in-depth charred throat section of the MXS-89 nozzle contains at the surface molten silica and heavy deposits of pyrolytic graphite onto fully charred phenolic matrices, molten fibers, and silicon carbide.  Further in-depth (approximately 0.027 inch from the final surface) the material consists of solid silica fibers, pyrolytic graphite, and charred phenolic.  At 0.238 inch from the final suface there exist silica fibers, charred phenolic, and no pyrolytic graphite.  The in-depth charred throat section of the MX4500 nozzle contains at the surface pyrolytic graphite, graphite fibers, and fully charred phenolic resin.  At 0.059 inch from the final surface there exist pyrolytic graphite deposits on fibers and along fissures.  A general gradation of pyrolytic graphite deposits diminishes in depth to the virgin region.

2.  Physical and Chemical Characterization of Nozzle Chars

A density inversion exists from the final char surface through a transition zone into the virgin material.  For the MXS-89 nozzle the density ranged from 81.6 lb/ft$^3$ at the surface, down to 59.5 lb/ft$^3$ in the transition zone (0.2 inch from the surface) and up to 101.0 lb/ft$^3$ in the virgin region. Similarly, but to a lesser extent, the MX4500 nozzle density ranged from 75.8 lb/ft$^3$ near the surface to 71.0 lb/ft$^3$ in the transition zone (0.33 inch from the surface) and up to 85.5 lb/ft$^3$ in the virgin region.

The density inversions are attributed to the removal of volatile products within the transition zone and subsequent cracking and redeposition of the products onto the charred material toward the nozzle surface.

The presence of SiC near the surface of the MXS-89 nozzle indicates that the reaction $SiO_2 + 3C \rightarrow SiC + 2CO$ took place.

From TGA tests a value of 1000°F is assigned to the following in-depth positions:  MXS-89--1.55 inches from the nozzle O.D.; MX4500--1.3 inches from the nozzle O.D.  The difference is attributed to the higher thermal conductivity of the MX4500 material allowing a deeper penetration of heat into the material.

### 3. Optical Property Determinations of Fired Nozzles

From a comparison between spectral reflectance measurements of oven chars and the zone bounded by the transition and degradation regions (at 0.275 inch from the final surface) of the MXS-89 nozzle char, the temperature reached at this location was 1000° F. No satisfactory results were obtained for postulating internal temperatures of the MX4500 nozzle based on optical reflectance measurements. The overall reflectance at all locations in depth agree with the oven char reflectances.

### 4. Thermal Characterization of the Nozzle Chars

A thermal conductivity inversion exists in depth for both silica- and graphite-phenolics. For the MXS-89 material the values ranged from 0.90 Btu/hr-ft-° F near the surface down to 0.24 Btu/hr-ft-° F within the transition and up to 0.32 Btu/hr-ft-° F in the virgin region (which agrees with the unfired materials measurements). For the MX4500 material the values ranged from 2.37 Btu/hr-ft-° F near the surface down to 1.87 Btu/hr-ft-° F in the transition region to 1.65 Btu/hr-ft-° F in the virgin region (which agrees with the unfired materials measurements).

The thermal conductivity inversions reflect the corresponding behavior of the density profiles.

The specific heat (at 200° F) profile in depth for the MXS-89 nozzle ranged from 0.165 Btu/lb-° F at the nozzle surface, down to 0.15 Btu/lb° F near the transition zone increasing to 0.245 Btu/lb-° F in the virgin zone (in agreement with unfired material measurements).

The specific heat (at 200° F) profile in depth for the MX4500 nozzle ranged from 0.15 Btu/lb-° F at the surface down to 0.11 Btu/lb-° F in the charred zone grading uniformly to 0.215 Btu/lb-° F near the virgin zone (agreeing with unfired nozzle data).

The general trends of the specific heat profiles reflect the gradation in chemical composition of the materials as indicated by the chemical and X-ray diffraction analyses.

# V. RECOMMENDATIONS

## A. ENHANCED EXPERIMENTAL CHARACTERIZATION OF FIRED NOZZLES

1. The experimental coverage of the study program pointed to the need for a more definitive and realistic characterization of the nozzle chars which can be obtained by analyses of the four regions (entrance, ramp, throat, and exit) of each nozzle instead of only one section, thereby describing the nozzle over its entire length.

2. Oven charring of the billet materials should be conducted at closer temperature intervals to avoid the sudden "step function" phenomena which occurred during this study, and thus make the evaluation of the degradation behavior more realistic.

3. Thermal conductivity profile tests on fired nozzles and on the various oven chars should be conducted at higher temperatures and ambient pressures to provide the ablation analysts with property data in the regions of high temperature and pressure of interest. This can be done on the existing Avco facilities with only minor modifications.

4. To obtain a more quantitative temperature profile of silica-phenolic chars, the amount of silicon carbide in char layers and in oven reference chars should be determined quantitively. This can be done by determining total carbon and "free" carbon on those samples known to contain silicon carbide. The difference in carbon values gives the amount of carbon considered as the carbide.

5. To obtain a more quantitative temperature profile of graphite-phenolic chars, a determination of total carbon should be combined with thermogravimetric analysis (TGA). TGA will indicate the amount of graphite filler. A knowledge of total carbon will then permit calculation of the amount of carbon due to degraded resin.

## B. IMPROVED ROCKET NOZZLE MATERIALS

Improved rocket nozzle materials should incorporate the following properties:

1. Lower weight: This can be achieved by using materials having:

    a. Lower recession rates,

    b. improved insulating properties, and

    c. higher resistance to those surface and internal chemical reactions leading to massive material loss by cracking, delamination, and spalling and with improved ability to withstand shearing forces.

2. Restart capability: The material must be able to withstand multiple, severe changes in the operational environment.

3. **Multiple propellant capacity:** Ideally, it would be desirable to develop material which would be capable of being used in many different propellant environments; e.g., not only $N_2O_4$-50 Aerozene systems under variations in oxidizer to fuel ratios but additionally with an aluminized solid propellant mixture.

4. **Lower cost:** This could be achieved by improved fabrication techniques and by using lower cost materials in addition to the development of a single material with multiple propellant capability.

All or many of these properties could be realized by judicious selections of 1) new and improved resins, 2) improved reinforcement materials, and 3) resin filler materials coupled with the application of unique processing techniques. To illustrate:

1) **Resins.**-- Among the resins to be considered are:

   a) Phenolic resins having higher thermal stability and higher char yield than those currently used.

   b) Chromium, or similar metallic modified phenolics, to impart oxidation resistance to the develop char.

   c) Phenolic resins modified to impart flexibility resulting in resistance to shock and vibration.

   d) Polyimides which have been shown to have higher thermal stability than phenolics and superior ablation performance.

   e) Silicones having high char yields and improved performance in oxidative propellant environments.

   f) Polyphenylenes which have exceptionally high char yields and erosion resistance.

   g) Polyorganophosphonitrilic resins having, potentially, improved oxidation resistance as well as high char yield.

2) **Reinforcement Materials.**-- Among the reinforcing fabrics from which selection may be made in designing new composites are:

   a) Silica having higher viscosity in the molten state which is attainable by high purity.

   b) Carbon and graphite having improved oxidation resistance which is attainable by high purity or the use of barrier coatings.

   c) Promising reinforcements in the experimental development stage such as silicon carbide, boron nitride, and aluminum oxide/aluminum nitride.

3) **Resin Fillers.**-- Preliminary work (Ref.9) indicates that favorable results are achievable by adding colloidal silica to resins reinforced with silica cloths. The oxidation resistance of carbon- and graphite-reinforced

composites, on the other hand, may be improved by the addition of fillers such as zirconium oxide or pyrophosphate, hafnium oxide, molybdenum silicide, or bo on phosphate.

4) Unique Processing Techniques.-- The application of specialized manufacturing techniques holds promise in minimizing massive material loss resulting from delamination, cracking, and spallation. These techniques include precharred, reimpregnated laminates, orthogonally (three-dimensionally) reinforced composites, and precharred, reimpregnated orthogonal constructions.

# VI. REFERENCES

1. Evaluation of the Thermophysical Properties of the Apollo Heat Shield, Avco Space Systems Division Final Report, AVSSD-0375-67RR for NASA MSC, Contract NAS 9-6940, 8 August 1967.

2. Zurbrick, J.R., NDT Survey of Silica Fabric/Phenolic and Graphite Fabric/ Phenolic Laminated Billets, Avco/SSD Interoffice Memorandum W270-10-67-96, October 4, 1967.

3. Jackson, W.M. and R.T. Conley, J. Appl. Polym. Sci., 8, pp. 2163-93, 1964.

4. DeSesa, M.A. and J.S. Perkins, Determination of Temperature Profile in Charred Phenolic Composites by Reconstruction of the Ablation Process, Thermophysics and Temperature Control of Spacecraft and Entry Vehicles, Progress in Astronautics and Aeronautics, Vol. 18, G.B. Heller, Ed., Academic Press, New York, New York, pp. 495-512, 1966.

5. (a) Beecher, N. and R.E. Rosensweig, ARS J., 31, pp. 532-539, 1961.
   (b) Beecher, N. and R.E. Rosensweig, AIAA J., 3, p. 1567, 1965.

6. Romie, R.E., Carbon-Silica Reaction in Silica-Phenolic Composites, AIAA J., 5(8), pp. 1511-13, 1967.

7. Ladacki, M., AIAA J., 4(8), pp. 1445-7, 1966.

8. Mellor, J.W., A Comprehensive Treatise on Inorganic and Theoretical Chemistry, Vol. VI, Longmans, Green and Co., London, New York, Toronto, 1957.

9. Broughton, R.F., Laminar Splash Ablation Results of Silica-Silica Loaded Phenolic, Interoffice Memorandum to L. McAllister R720-M-67-148, 18 December 1967.

APPENDIXES

# APPENDIX A

NONDESTRUCTIVE TEST OF THE AS-RECEIVED SILICA-PHENOLIC MXS-89
AND GRAPHITE-PHENOLIC MX4501 BILLETS

TO    M. A. DeSesa                                      DATE  October 4, 1967
                                                              W270-10-67-96

FROM    J. R. Zurbrick

SUBJECT    NDT Survey of Silica Fabric/Phenolic and Graphite Fabric/Phenolic
           Laminated Billets

COPY TO    See attached distribution list

## SUMMARY:

The results of the radiographic, radiometric and ultrasonic nondestructive test
survey on two 5-inch-diameter x 6-inch-length laminated billets, one silica
fabric/phenolic, and one graphite fabric/phenolic, are reported. The defect-
response information is pictorially presented, and the variability response data
is presented according to test location. All information was assembled for the
most complete and accurate interpretation of conditions in each billet. Guides
for interpreting individual sets of data are also included.

## CONCLUSIONS:

Silica Fabric/Phenolic: As this billet was fabricated, it cured from its ends and
circumference inward, resulting in a separation and distortion of about four
piles, located centrally between the ends. Between-ply macroporosity accumulated
in this region as an oblong area extending radially from the billet axis. The
overall density of this billet is remarkably uniform, both axially and radially.
The ultrasonic velocity data, however, showed the within-strand microporosity to
be least at the ends, and greatest halfway between them. The distributed porosity
throughout the billet is predominately a low percent by volume of within-strand
microporosity, which increases in volume percent from the circumference inward.
Some small volume percent of between-ply macroporosity was noted at the $0°$ and
$180°$ positions near the circumference in about the same plane as the central
distortion.

Graphite Fabric/Phenolic: As this billet was fabricated, it cured from
its axis outward, as caused by the high thermal conductivity of the
graphite fabric. The bottom half of this billet experienced a considerably
different heat history than did the top half. The bottom half exhibited a
fairly high volume percent of between-ply macroporosity, distributed as a "donut"
along the outer half of the billet radius. Between-ply macroporosity in the
upper half was relatively low. Within-strand microporosity was least at the
ends and increased toward the plane halfway between them. Again, the lower half
exhibited a generally higher level of within-strand microporosity than did the upper
half. The billet density viewed axially was greatest along the axis and decreased
radially to the circumference. Density viewed radially was greatest at the ends,

decreasing toward the center with the lower two-thirds showing a consistently low density and the upper one-third a significantly higher density.

DISCUSSION:

Nondestructive testing capabilities have been advanced, under AFML sponsorship, to the point where qualitative defect indications and quantitative response values may be used together to provide a detailed and exacting characterization of a reinforced plastic composite material. The conclusions in this memorandum for two different billets are typical examples of the characterization obtainable from a preliminary NDT survey conducted prior to specimen layout and machining. Correlations and predictive equations derived from quantitative specimen data then provide the basis for predicting component mixture concentrations and mechanical properties in materials subsequently produced under a continuing program.

The billets tested were supplied under Contract No. NAS 3-10300, "Post-Test Analysis of Ablative Materials', and designated by Fiberite Corporation thusly:

Silica Fabric/Phenolic:      SN 1429-1, MXS-89, LOT D-594, Roll 1-A

Graphite Fabric/Phenolic:    SN 1428-1, MX4501, LOT D-749, Roll 1

RESULTS:

Silica Fabric/Phenolic

Radiography: Figures A-1, A-2, and A-3 are positive contact prints from the original radiographs. Black is high density material, white is low density. The axial view, Figure A-1, is clear of any observable defects. The 0° radial view (Figure A-2) and the 90° radial view (Figure A-3) show the band pattern of the satin-weave ply layers. Note the "shrink-pull" at the billet center, and its extent as indicated in the two views. This was interpreted as a central distortion affecting four layers with an oblong area of between-ply macroporosity. Radiographic conditions were:

axial 150 kv, 10 ma, 2 minutes, 60-inch focus to film, "M" film
radial 150 kv, 5 ma, 2 minutes, 60-inch focus to film, "M" film

Ultrasonic Pulse-Echo: Sonoray pulse echo indications were observed at the locations shown in Figure A-4, at the relative amplitude levels indicated. Reflections result from significant impedance mismatches within the billet, and are greatest from a solid-gas interface.

Ultrasonic Longitudinal Wave Velocity: The ultrasonic velocity values ($V_L$) were determined at 1 MHz, which is known to be a frequency at which sound propagation is dramatically affected by distributed porosity. Velocity values taken in the axial direction are pictorially presented in Figure A-5. The velocities taken in the radial direction are given in Table A-I according to angle reference and position from the top surface. Generally speaking, a decrease in velocity indicated an increase in porosity volume percent. The axial velocities
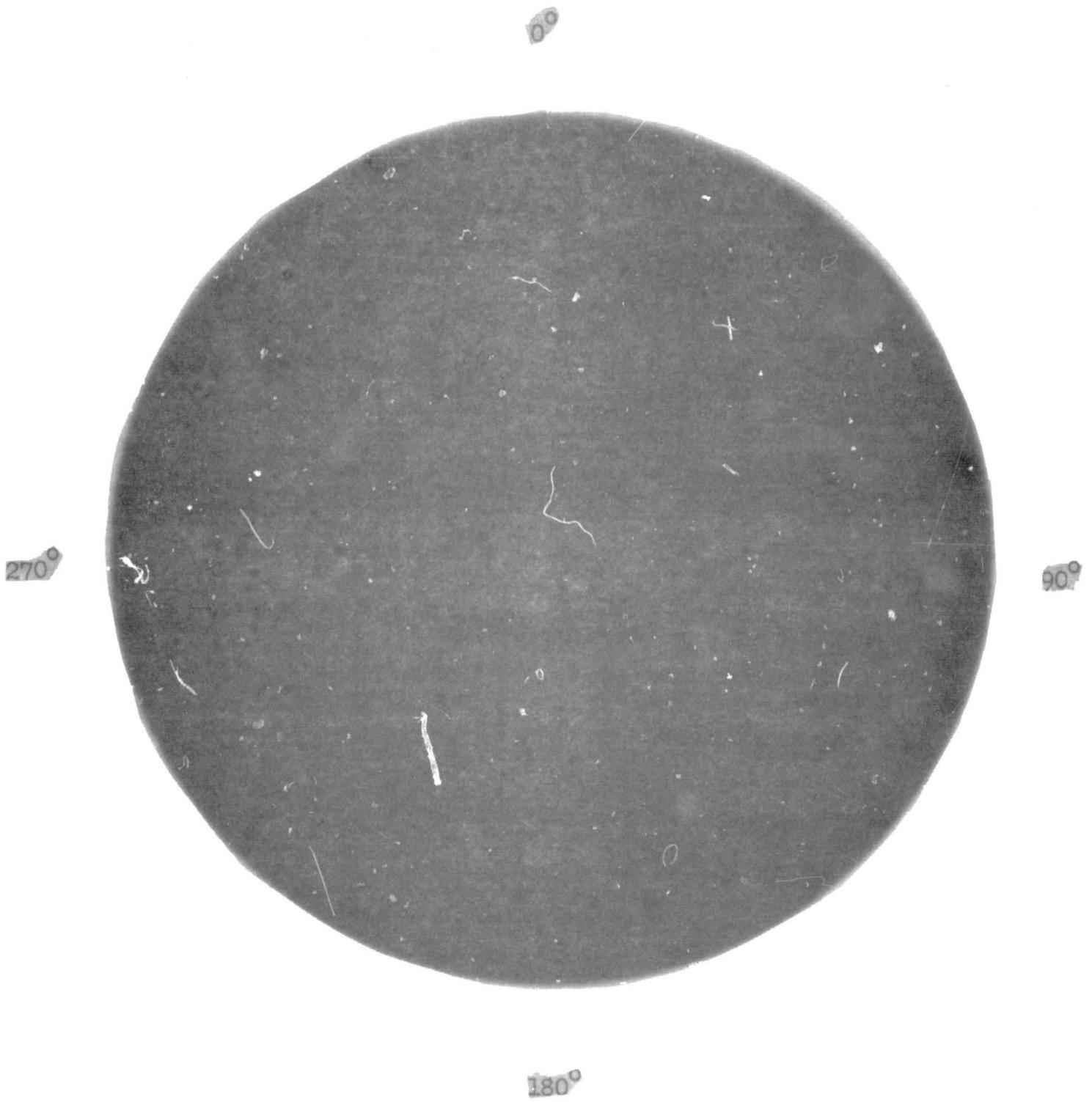
Figure A-1 AXIAL RADIOGRAPH OF SILICA FABRIC/PHENOLIC BILLET
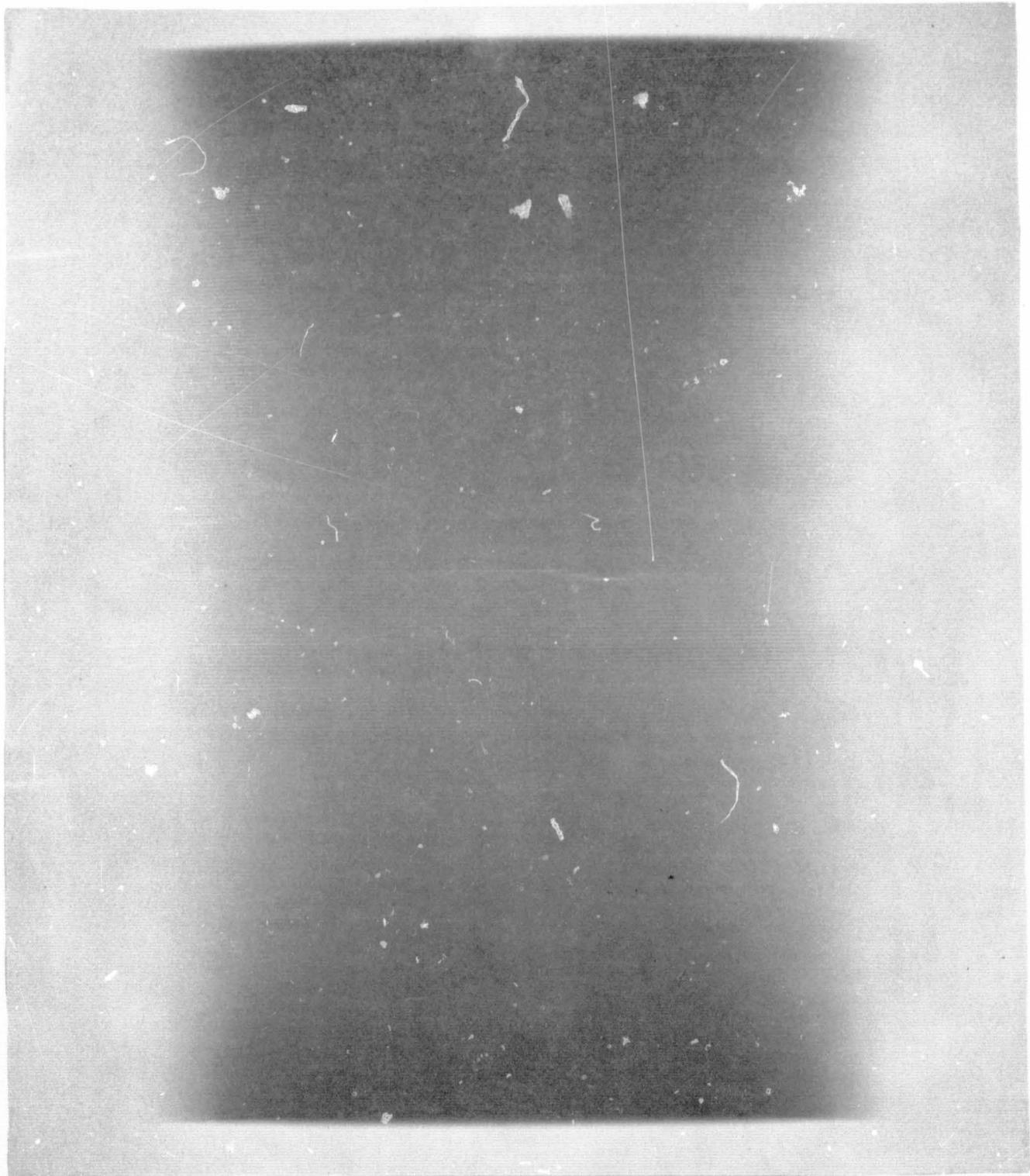
Figure A-2  RADIAL RADIOGRAPH (0° - 180° DIRECTION) OF SILICA FABRIC
PHENOLIC BILLET
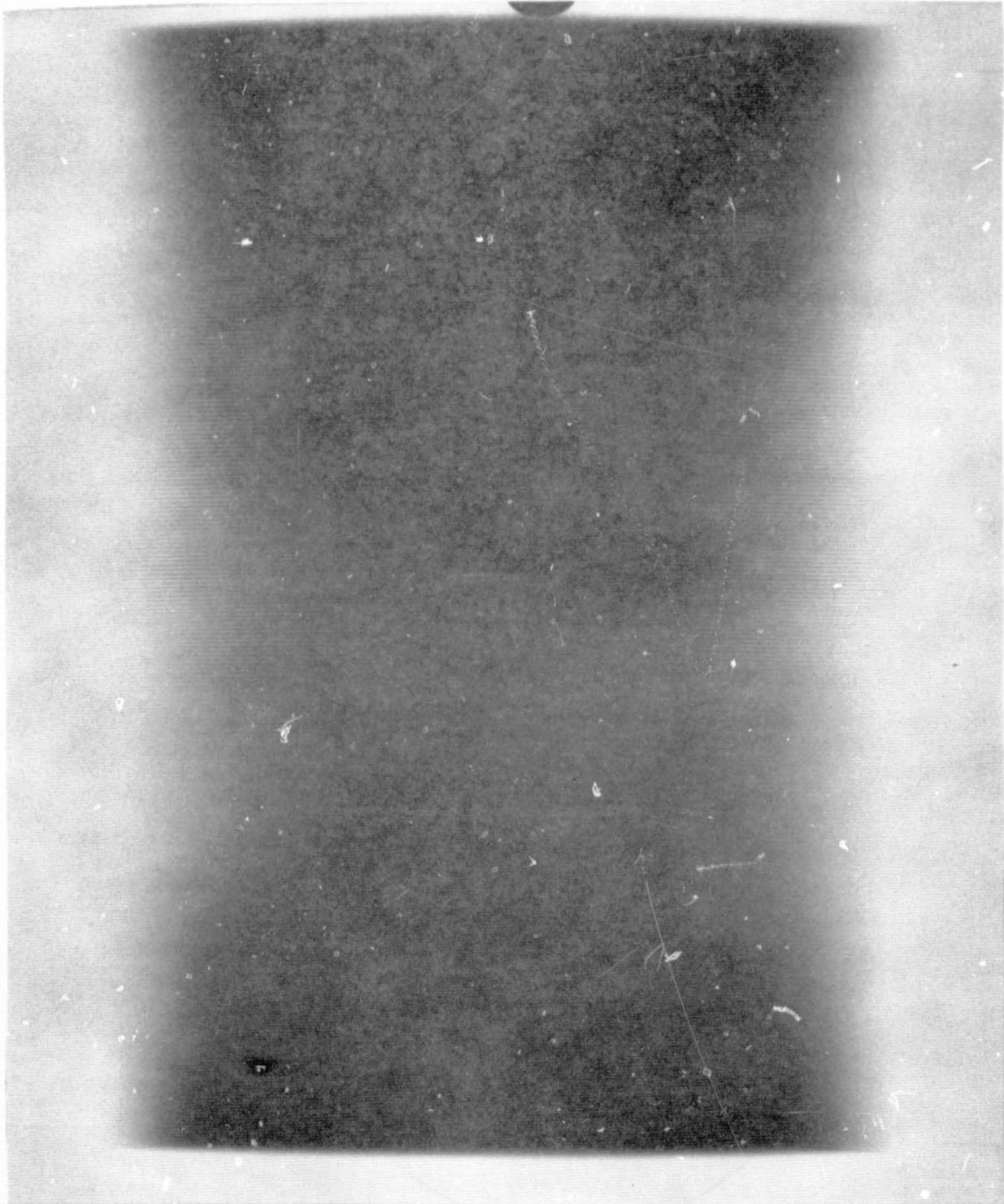
Figure A-3 RADIAL RADIOGRAPH (90° – 270° DIRECTION) OF SILICA FABRIC
PHENOLIC BILLET

TOP
0°

270°                    90°  270°                    90°

180°

BOTTOM
0°

180°

AMPLITUDE 70-100 percent
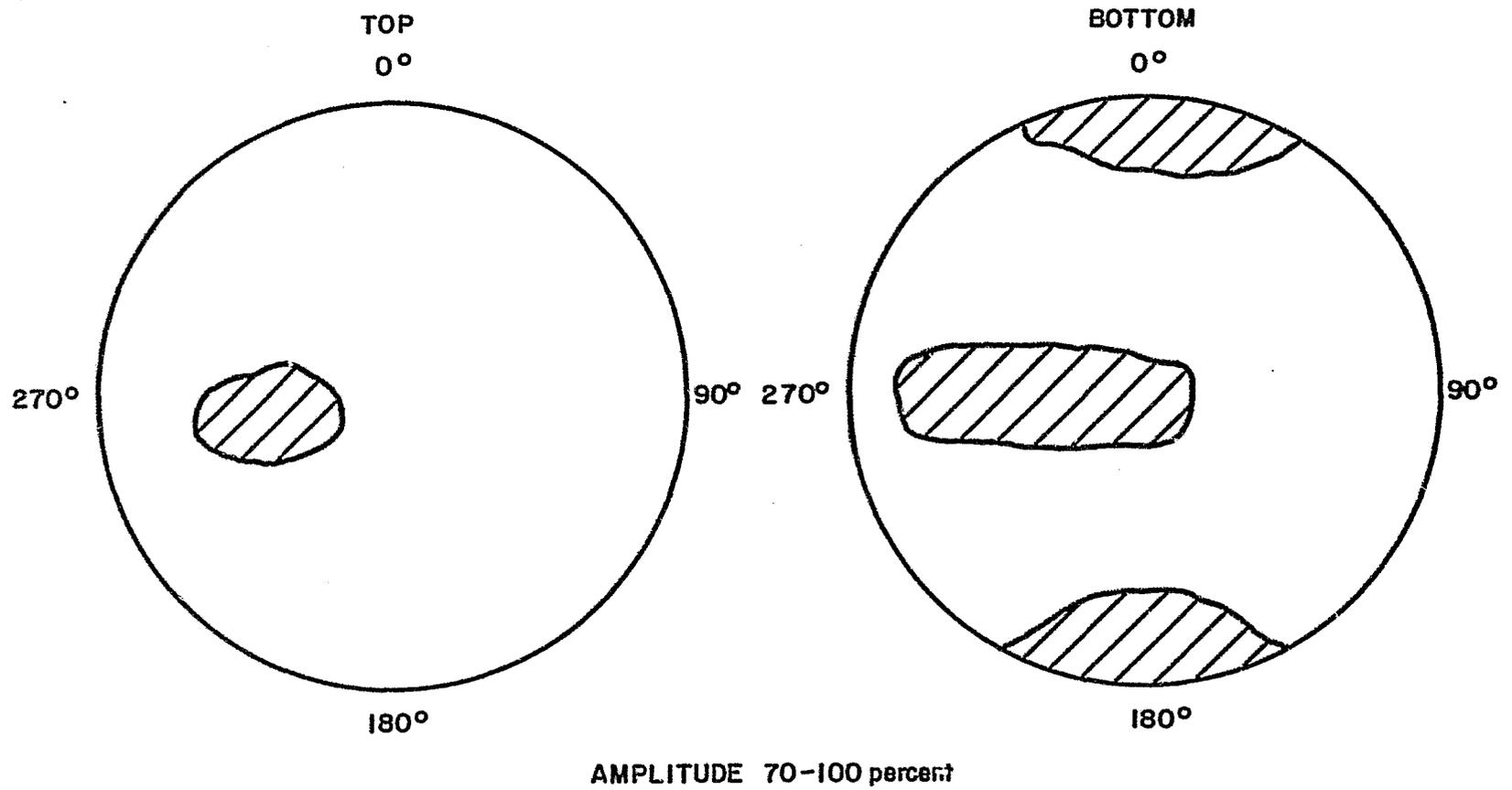
78-1567

Figure A-4  ULTRASONIC PULSE ECHO RESULTS FOR SILICA FABRIC/PHENOLIC
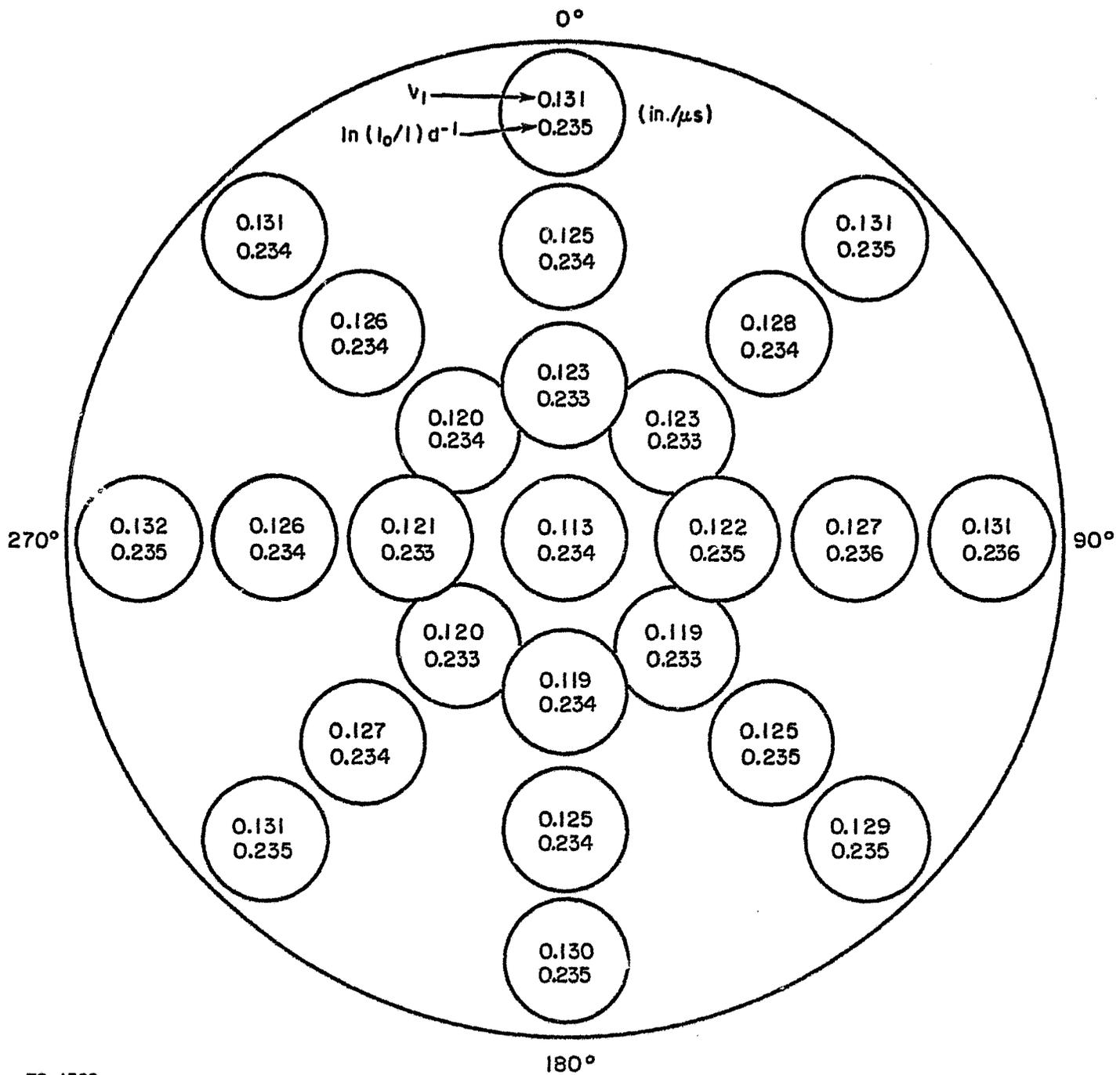
78-1568

Figure A-5   ULTRASONIC VELOCITY AND RADIOMETRIC GAUGING RESULTS FOR SILICA
FABRIC/PHENOLIC BILLET -- AXIAL DIRECTION

## TABLE A-I

| Nos. | 0–180° | | 45 – 225° | | 90 – 270° | | 135 – 315° | |
|---|---|---|---|---|---|---|---|---|
| | $V_L$ | $\ln(I_0/I)d^{-1}$ | $V_L$ | $\ln(I_0/I)d^{-1}$ | $V_L$ | $\ln(I_0/I)d^{-1}$ | $V_L$ | $\ln(I_0/I)d^{-1}$ |
| 1 | 0.150 | 0.234 | 0.150 | 0.236 | 0.153 | 0.236 | 0.144 | 0.233 |
| 2 | 0.146 | 0.235 | 0.148 | 0.235 | 0.149 | 0.234 | 0.144 | 0.234 |
| 3 | 0.138 | 0.234 | 0.144 | 0.234 | 0.145 | 0.234 | 0.141 | 0.234 |
| 4 | 0.136 | 0.234 | 0.142 | 0.234 | 0.145 | 0.233 | 0.137 | 0.233 |
| 5 | 0.137 | 0.232 | 0.140 | 0.232 | 0.145 | 0.233 | 0.132 | 0.235 |
| 6 | 0.139 | 0.233 | 0.135 | 0.233 | 0.138 | 0.229 | 0.129 | 0.231 |
| 7 | 0.139 | 0.234 | 0.132 | 0.233 | 0.138 | 0.233 | 0.139 | 0.233 |
| 8 | 0.135 | 0.233 | 0.135 | 0.233 | 0.139 | 0.233 | 0.140 | 0.233 |
| 9 | 0.140 | 0.234 | 0.138 | 0.234 | 0.134 | 0.235 | 0.140 | 0.234 |
| 10 | 0.146 | 0.233 | 0.148 | 0.235 | 0.142 | 0.235 | 0.141 | 0.233 |
| 11 | 0.147 | 0.235 | 0.150 | 0.235 | 0.144 | 0.235 | 0.138 | 0.235 |

$V_L$ = inches/ $\mu$sec.

Ultrasonic Velocity and Radiometric Gauging Results for Silica Fabric/Phenolic Billet –
   Radial Direction

(Data taken at 1/2-inch intervals from top to bottom)

accounted for both within-strand microporosity (fine needles between filaments) and between-ply macroporosity (rounded bubbles). The radial velocities were essentially only affected by within-strand microporosity.

Assuming that the predictive equation for elastic modulus (E) determined in our earlier work A-1, A-2 holds for this billet:

$$V_L{}^2 = 0.012 \, E \tag{A-1}$$

and using an average radial velocity of 0.141 in/ sec. and an average density ($\rho$) of 1.633 grams/cm$^3$, an average tensile or flexural modulus would be:

$$E = 2.7 \times 10^6 \, \text{psi}$$

This is offerred as an indication of size; the actual correlation and equation will be determined for destructive and nondestructive test data later.

Gamma Radiometry: The thickness-reduced gamma photon absorption values $d^{-1}$ $\ln(I_0/I)$ were determined using the cobalt-60 1.1-MeV peak and a 30-second counting interval. A 1/2-inch-diameter collimator provided an area of resolution similar to that in the ultrasonic velocity measurements. At the 1.1-MeV energy level, a direct proportionality exists between the absorption number and density of the interrogated volume. The $d^{-1} \ln(I_0/I)$ values are listed in Figure A-5 and Table A-I for the silica fabric/phenolic billet. Cadmium 109 (22-keV energy peak) was not used for lack of billet penetration.

## Graphite Fabric/Phenolic

Radiography: Figures A-6, A-7, and A-8 are positive contact prints from the original radiographs. Black is high-density material; white is low-density. The axial view, Figure A-6, is clear of any observable defects. The 0° radial view (Figure A-7) and the 90° radial view (Figure A-8) show the band pattern of the satin-weave ply layers. Note in the two views the between-ply low-density planes located along the outer half of the billet radius. Radiographic conditions were:

    axial 150 kv, 10 ma, 2 minutes, 60 inch focus to film, "M" film
    radial 150 kv, 5 ma, 2 minutes, 60 inch focus to film, "M" film

Ultrasonic Pulse Echo: Sonoray pulse echo indications were observed at the locations shown in Figure A-9, at the relative amplitude levels indicated. Note the continuous "donut" of reflection indications from measurement taken on the bottom surface.

Ultrasonic Longitudinal Wave Velocity: The ultrasonic velocity values ($V_L$) were determined at 1 MHz. Velocity values taken in the axial direction are pictorially presented in Figure A-10, and those taken in the radial direction are given in Table A-II. The "X" in Figure A-10 denotes the inability of the pulse to transverse the length of the billet due to reflection and scattering at the low-density planes. This corresponded with the pulse-echo indications. The "X" in Table A-II denotes a sufficiently distorted pulse waveform as to make the transit time determination impossible or unreliable. This situation has been observed in past

0°

270°                                              90°

180°
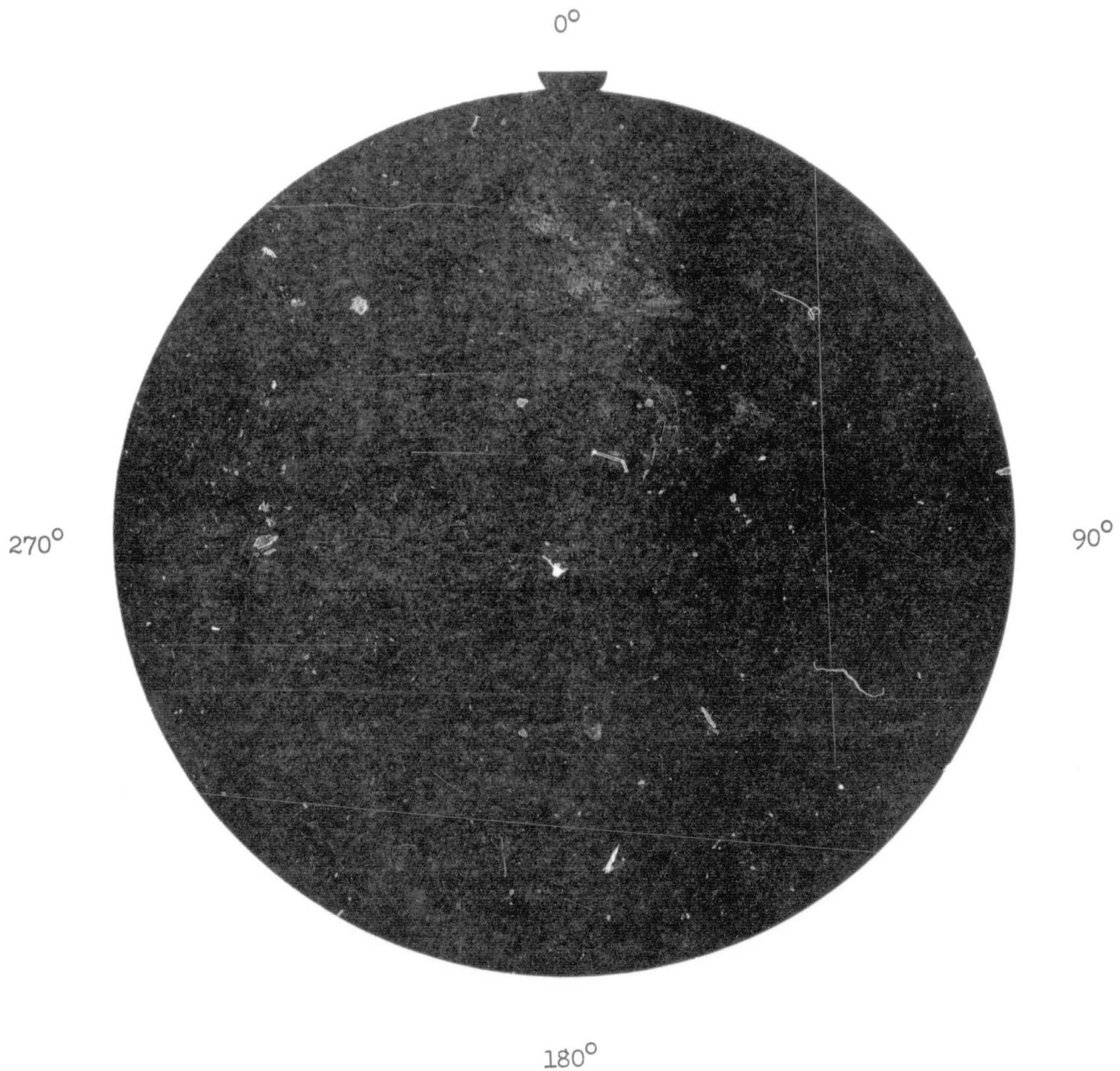
Figure A-6  AXIAL RADIOGRAPH OF GRAPHITE FABRIC/PHENOLIC BILLET
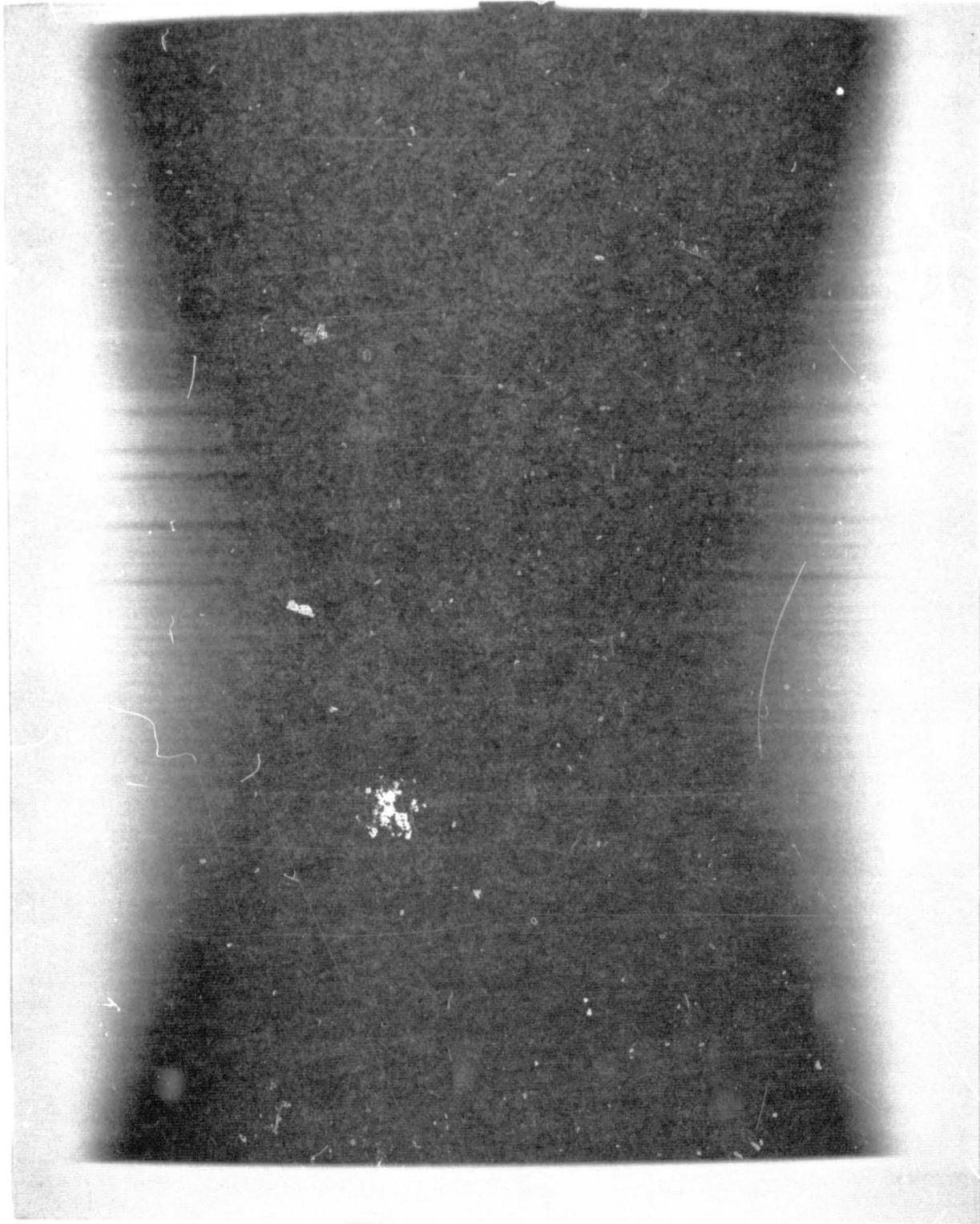
Figure A-7  RADIAL RADIOGRAPH (0° − 180° DIRECTION) OF GRAPHITE FABRIC
PHENOLIC BILLET
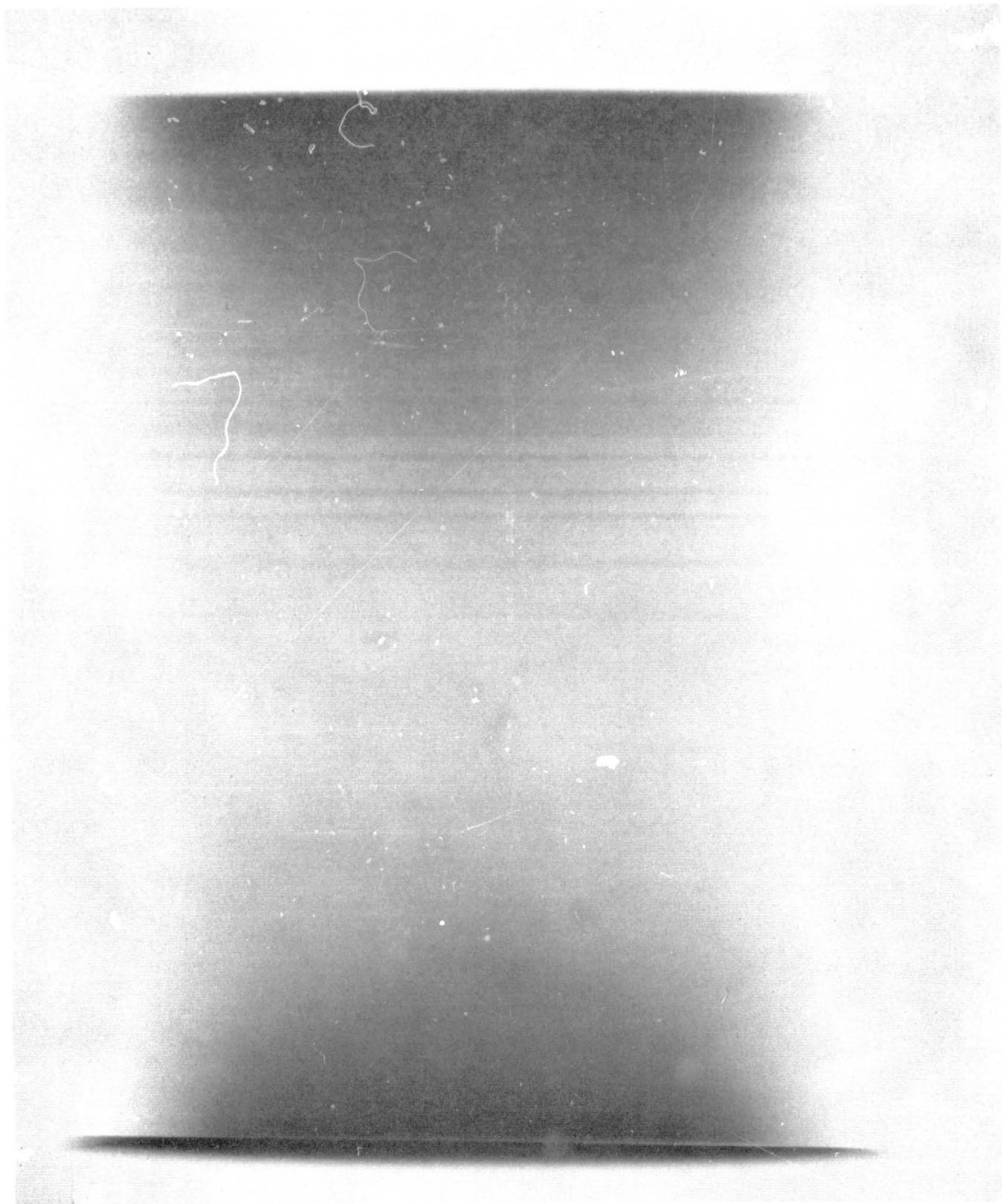
Figure A-8   RADIAL RADIOGRAPH (90° - 270° DIRECTION) OF GRAPHITE FABRIC
PHENOLIC BILLET

TOP
0°

BOTTOM
0°

270°          90°

270°          90°

180°

180°
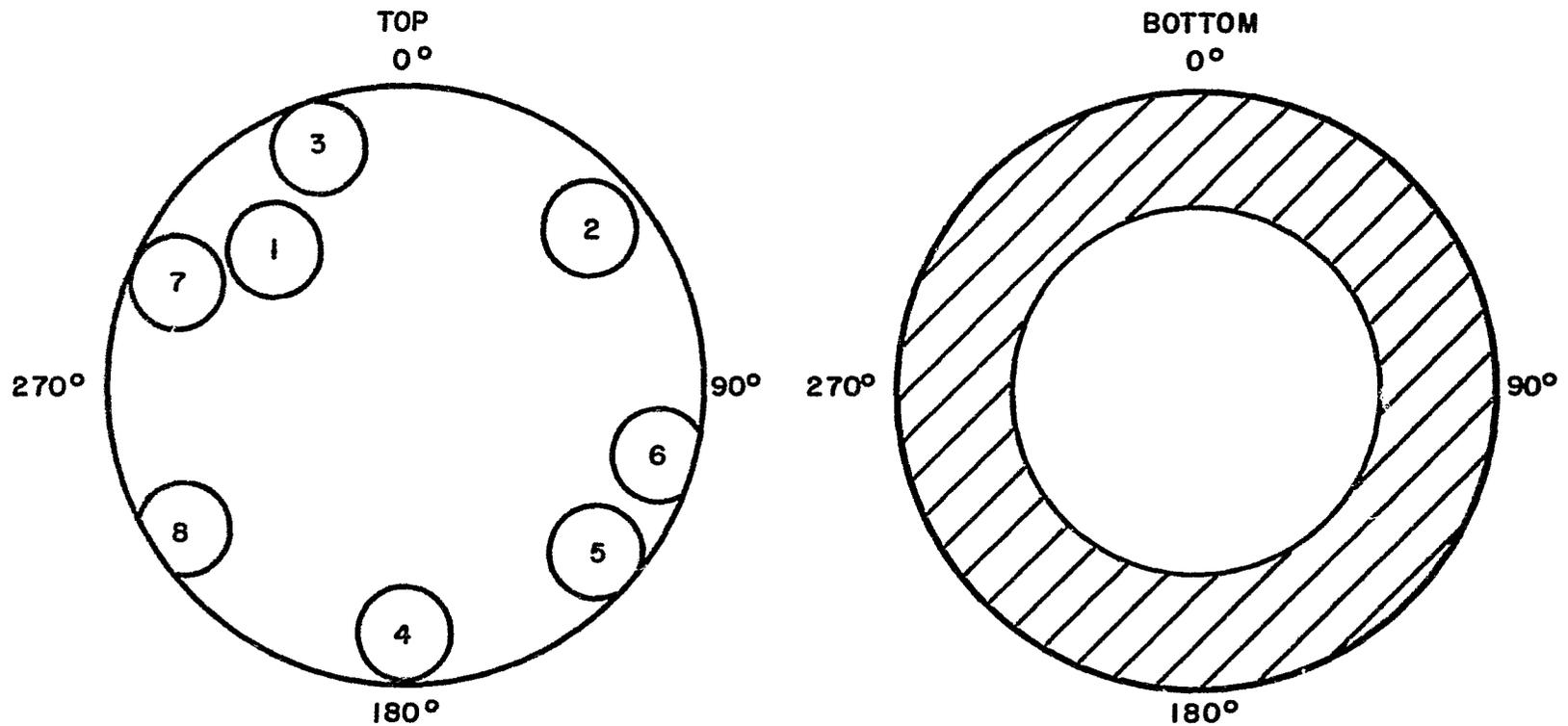
| LOCATION | RELATIVE AMPLITUDE, percent | RELATIVE FLAW DEPTH |
|----------|-----------------------------|---------------------|
| 1 | 50 | DEEPEST |
| 2 | 70 | |
| 3 | 100 | |
| 4 | 100 | |
| 5 | 80 | |
| 6 | 100 | |
| 7 | 100 | |
| 8 | 100 | SHALLOWEST |

APPROXIMATE DEPTH - 1 in. - 2 in.
AMPLITUDE 70 - 100 percent

78-1569

Figure A-9 ULTRASONIC PULSE ECHO RESULTS FOR GRAPHITE/PHENOLIC BILLET

Figure A-10 ULTRASONIC VELOCITY AND RADIOMETRIC GAUGING RESULTS FOR GRAPHITE/PHENOLIC BILLET -- AXIAL DIRECTION

X = INSUFFICIENT SIGNAL

78-1570

## TABLE A-II

| Nos. | 0-180° $V_L$ | 0-180° $\ln(I_0/I)d^{-1}$ | 45 - 225° $V_L$ | 45 - 225° $\ln(I_0/I)d^{-1}$ | 90 - 270° $V_L$ | 90 - 270° $\ln(I_0/I)d^{-1}$ | 135 - 315° $V_L$ | 135 - 315° $\ln(I_0/I)d^{-1}$ |
|---|---|---|---|---|---|---|---|---|
| 1 | 0.269 | 0.201 | 0.267 | 0.203 | 0.273 | 0.202 | 0.250 | 0.202 |
| 2 | 0.268 | 0.200 | 0.265 | 0.200 | 0.258 | 0.200 | 0.252 | 0.201 |
| 3 | 0.246 | 0.199 | 0.240 | 0.199 | 0.246 | 0.198 | 0.246 | 0.199 |
| 4 | 0.232 | 0.193 | 0.232 | 0.197 | 0.237 | 0.196 | 0.246 | 0.192 |
| 5 | 0.250 | 0.192 | 0.240 | 0.192 | 0.228 | 0.192 | 0.242 | 0.191 |
| 6 | 0.229 | 0.191 | 0.226 | 0.191 | X | 0.192 | 0.240 | 0.192 |
| 7 | 0.240 | 0.190 | X | 0.190 | 0.235 | 0.192 | 0.221 | 0.191 |
| 8 | 0.235 | 0.190 | X | 0.189 | X | 0.191 | 0.217 | 0.192 |
| 9 | 0.234 | 0.191 | X | 0.191 | X | 0.191 | 0.224 | 0.191 |
| 10 | 0.232 | 0.191 | X | 0.192 | 0.248 | 0.193 | 0.229 | 0.192 |
| 11 | 0.246 | 0.193 | 0.235 | 0.192 | 0.259 | 0.193 | 0.246 | 0.193 |

X -- Insufficient Signal

$V_L$ -- inches/$\mu$ sec.

Ultrasonic Velocity and Radiometric Gauging Results for Graphite Fabric/Phenolic Billet -
    Radial Direction

(Data taken at 1/2-inch intervals from top to bottom)

experience and is associated with significantly large volume percents of between-ply macroporosity which may or may not be interconnected in the manner of a de-lamination.

Using equation (A-1), a bulk density of 1.3⁻6 grams/cm$^3$, and an average $V_L$ of 0.243 in./$\mu$sec, an indication of average tensile or flexural modulus would be:

$$E = 6.7 \times 10^6 \text{ psi}$$

Gamma Radiometry: The $d^{-1} \ln(I_o/I)$ values were determined using the cobalt-60 1.1-MeV energy peak, a 30-second counting interval, and 1/2-inch-diameter collimation. These values are listed in Figure A-10 and Table A-II for the graphite fabric/phenolic billet.

J. R. ZURBRICK

Approved by: *E. A. Breuckert* /CHN.

REFERENCES FOR APPENDIX A

A-1. Zurbrick, J. R., Development of Nondestructive Methods for the Quantitative Evaluation of Glass-Reinforced Plastics, Technical Report AFML-TR-66-269 (June 1966).

A-2. Zurbrick, J. R., Development of Nondestructive Tests for Quantitatively Evaluating Glass Fabric Reinforced Laminates, Technical Report AFML-TR-67-170 (June 1967).

# APPENDIX B

## OPTICAL REFLECTANCE DETERMINATIONS USING A
## BECKMAN DK-2 SPECTROPHOTOMETER

## Optical Properties Measurements

The optical reflectance measurements made on both oven chars and fired nozzle chars were performed on a Beckman extended-range-ratio recording spectrophotometer, Model DK-2. To understand the experiments performed, a short discussion of the measurements is summarized below.

## Monochromator

The light path in a Monochromator can be described as follows (Refer to Figure B-1 for a schematic arrangement of the apparatus): An image of light source (A) is focused by the condensing mirror (B) and the 45-degree mirror (C) on the entrance slits (D) and (E), the lower of two slits placed vertically over each other. Light falling on the collimating mirror (F) is rendered parallel and reflected toward the quartz prism (G). The back surface of the prism is aluminized so that light refracted at the first surface is reflected back through the prism undergoing further refraction. The collimating mirror then focuses the spectrum in the plane of the slits. Light of the wavelength for which the prism is driven passes out of the monochromator through the exit slit, through the reference cell (J), then through the absorption cell (M). The two paths are then directed to the appropriate pickup tube (P or Q) by the semi-aluminized rotating mirror (N). The output of the phototube is amplified, and the ratio of the intensity of the two paths is directly recorded as percentage of light transmitted.

The unit chops the source beam at 480 cps to secure the optimum signal-to-noise ratio with the lead sulphide detector and automatically switches the beam 15 times a second from the reference to the sample.

## Reflectance

Figure B-2 illustrates the positions of the component units and the light paths for monochromatic illumination. The type of measurement made with the integrating sphere reflectance unit is described as follows.

To measure the reflectance of a sample, the sample and reference are placed at the exit ports of the integrating sphere. The sample and reference exit ports are equipped with shift plates. When the shift plates are used for diffuse reflectance, they position the sample-and-reference normal to the radiation beams so that the specular component is rejected and only the diffuse reflectance reaches the detector. When the plates are used for total reflectance, they position the sample-and-reference at a 5-degree angle to the incident beam; the specular component as well as the diffuse component reaches the detector. Total reflectance measurements only were performed during this contract.
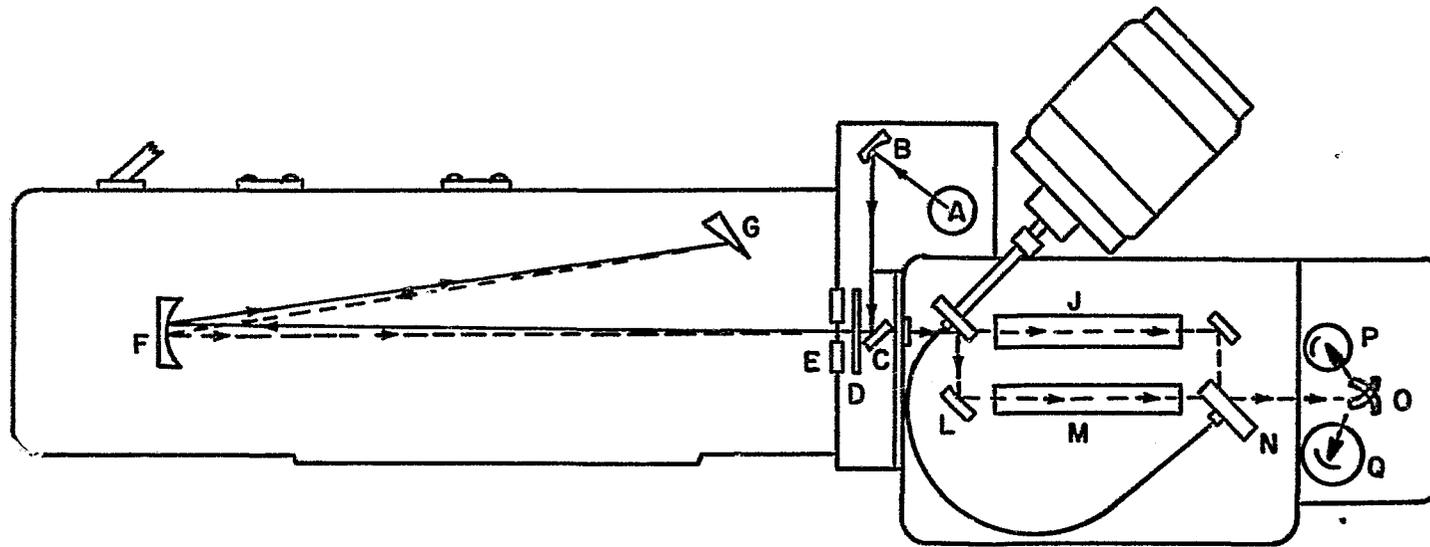
761157D

Figure B-1  MODEL DK, OPTICAL DIAGRAM, TRANSMISSIVITY

DETECTOR ADAPTER — — DETECTOR

LIGHT SOURCE

SOURCE ADAPTER

INTEGRATING SPHERE

DETECTOR ADAPTER — DETECTOR

LIGHT SOURCE

(REFERENCE)
EXIT PORTS
(SAMPLE)

MONOCHROMATOR          REFLECTANCE UNIT

INTEGRATING SPHERE

79-0299
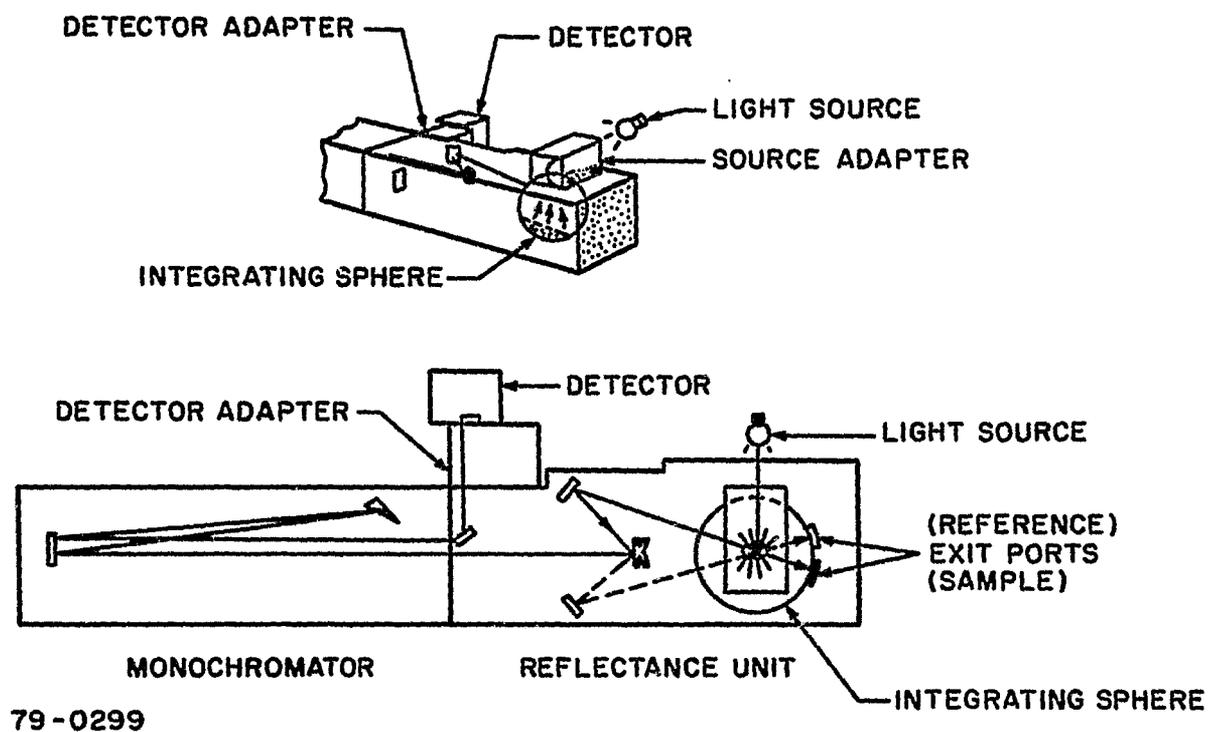
Figure B-2  MONOCHROMATIC DETECTION LIGHT PATH

# APPENDIX C

## DISCUSSION OF SPLIT (CUT) BAR TEST TECHNIQUE AND ITS APPLICATION FOR POST-FIRED NOZZLE CHAR CHARACTERIZATION

## Summary

The method used by Avco/SSD to obtain thermal conductivity profiles with respect
to the depth of the post-fired nozzle test cores is unique, and as such it was
deemed necessary to discuss its acceptability as a qualified measuring technique.
The discussion presented in this appendix considers qualifications and describes
the various testing methods which are recognized thermal property measuring tech-
niques, and then continues with a comparison between these methods and qualifies
Avco's post-test core measurement procedures. Recommendations have been included
in this discussion which will provide more significant support of the analysis
treatments of the post-test data.

## General Considerations

### Guarded Hot Plate Testing Technique

The guarded hot plate method of testing has long been recognized as a most suit-
able method for determining the apparent thermal conductivity of low-conductivity
materials such as thermal insulations, blankets, and ablative composites. It has
been assigned the specification C177-63 by the American Society For Testing
Materials. The wide acceptance of the method is attributed to several pertinent
factors. The system incorporates a symmetrical arrangement which facilitates the
control of heat flow and heat flux accountability. The measurements are based on
the fundamental parameters, length, area, temperature, and electrical energy
directly. Using relatively small specimen sizes, the method offers measurements
capabilities over a wide range (-320 to +2000°F) and can be utilized in a variety
of environments, e.g., vacuum, air, and inert gases. The test arrangement con-
sists of two disc-shaped specimens placed on opposite sides of a disc-shaped main
heater which is surrounded by a flat ring heater serving as a suppressor against
radial heat flow away from the main heater. Water-cooled end plates are used
against the opposite surfaces of the specimens. For better operation control and
higher test temperatures, the cooler plates are separated by an auxiliary heater
located between the specimen and the water cooled end plates. This arrangement
provides finer temperature adjustments through the regulation of both the water
flow rate and auxiliary heater power.

In operation, a regulated amount of heat is caused to flow from the main heater,
one-dimensionally, through each specimen to the auxiliary heaters and then to the
cooler assembly. The temperature drop across each test specimen is monitored and
used in conjunction with the main heater electrical power, specimen thickness and
cross section, to provide the necessary data for computation of the thermal
conductivity.

One critical requirement of ASTM specification C177-63 is that the ratio of the
specimen diameter to thickness should be large (i.e., 6:1) in order to keep edge
losses to a minimum. This restriction is one of the method's major disadvantages
when tests on post-fired nozzle cores are considered. To comply with this re-
quirement would mean that a specimen diameter of approximately 1 foot for a 2-
inch-thick post-fired nozzle sample would be required. It is obvious that
specimens of this size rule out the method for post-test core testing.

The nozzle geometry of the two materials tested limited the test specimen size to a maximum of 3/4-inch diameter in the ramp (C) section and 5/8-inch square in the exit (A) section. The available material limitation dictated that the split-bar method of evaluating conductivity be used.

## Split-Bar Testing Technique

The split-bar method of testing materials for thermal conductivity is a comparative technique, and its accuracy is limited by the accuracy with which the thermal properties of the reference material are known. The method has been recognized by ASTM and is given the specification C408-58. It must be pointed out that the method is specified as being for measurements on metals and ceramics. This ASTM specification unfortunately has not advanced with the state-of-art from a maximum temperature applicable and from the point of its applications to the general field of all materials. Avco/SSD has by extensive experience overcome the major problems presently confronting many experimenters and has made the split-bar scheme useful for determining properties of all materials, including insulating and ablating type composites. Figure C-1 shows a photograph of one of the split-bar test apparatuses used at Avco/SSD.

Basically the technique requires placing a specifically shaped specimen between two similar shapes of a reference material. The test arrangement is held together under a compressive force, and in this arrangement, similar to the guarded hot plate technique, heat is caused to flow axially through the test stack. Heat flow is accomplished by placing a heater at one end and a cooler at the other end of the test stack. Thermal guards in the form of ring heaters are placed coaxially along the stack and serve to eliminate radial heat losses. The selection of appropriate thermal insulation material around the test stack and the maintenance of relatively small thermal gradients radially outward is easily controlled. When the ratio of heat flow through the stack to that flowing radially is high, the precision of the measurement is enhanced. When the previous conditions are attained, one-dimensional heat flow is obtained and measurements can be performed. A temperature profile along the test column is obtained from differential thermocouples which are installed at specific locations in each of the three cylinders. This information is then used to calculate the specimen thermal conductivity using the relationship:

$$K_s = K_a \left(\frac{\Delta T}{\Delta x}\right)_a \left(\frac{\Delta x}{\Delta T}\right)_s$$

$K_s$ = Specimen thermal conductivity

$K_a$ = average reference thermal conductivity based on the average temperature between them

$\dfrac{\Delta T}{\Delta x}$ = average temperature gradient existing in the reference material

$\dfrac{\Delta x}{\Delta T}_s$ = reciprocal temperature gradient in the specimen

The relationship assumes a constant test column cross section.

It has been found that selection of an appropriate heat meter material as a reference, thermal insulation around the test stack, and the precision with which radial temperature gradients can be controlled are the predominate (sensitive)

16462 A
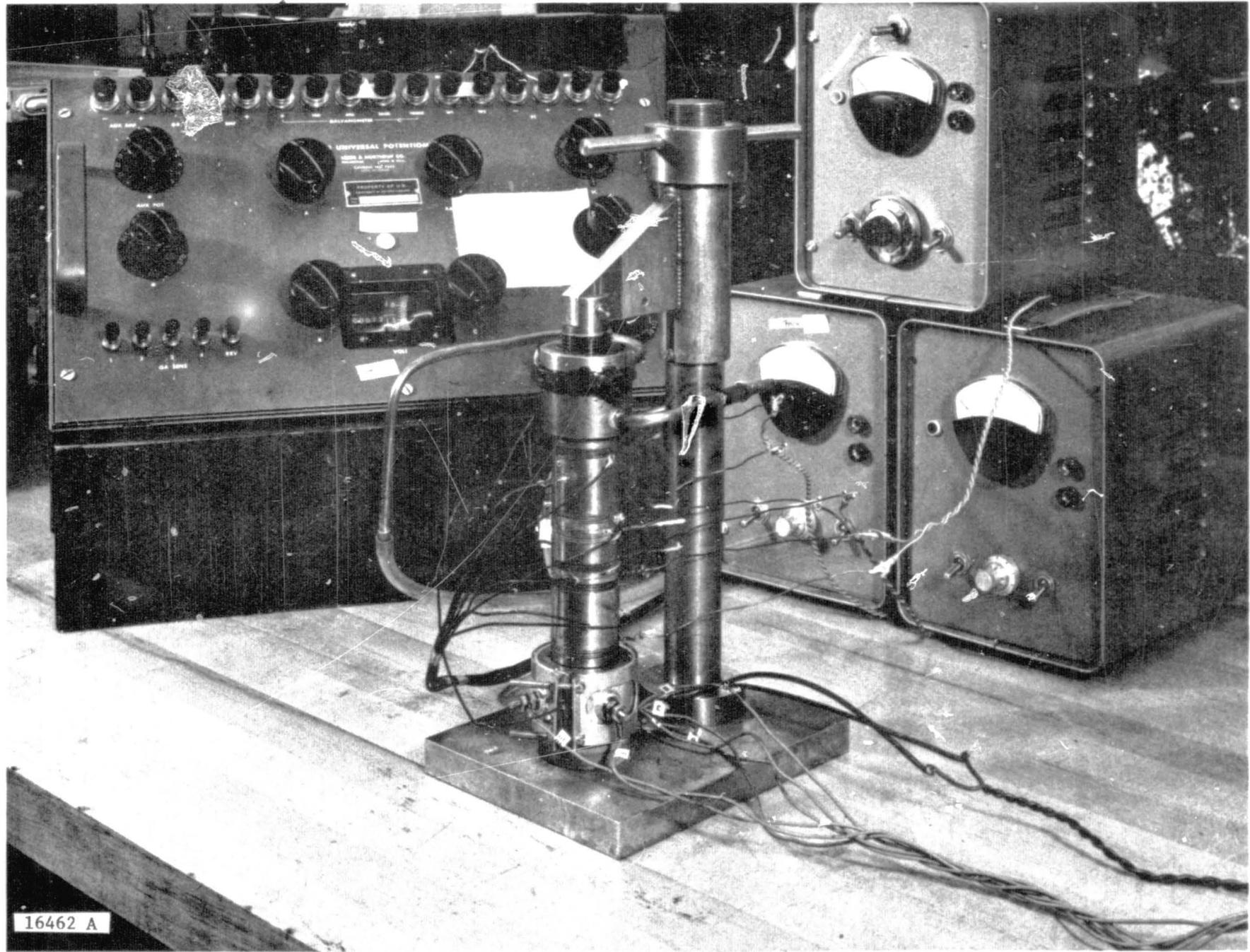
Figure C-1  STANDARD AVCO CUT-BAR APPARATUS

factors when using this technique. Materials which are N.B.S. recognized as heat meters for measurements in the low-conductivity ranges are very limited. The one material certified by the N.B.S which Avco uses as a cross check for guarded hot plate measurements is a fibrous blanket which is structurally suitable for use as a split-bar heat meter.

Avco/SSD has taken several compositions of its proprietary materials and others that have been extensively tested for their thermal properties and has qualified them as a secondary reference material. The material, charred OTWR (oblique tape wound refrasil), is one of these materials. This secondary standard was used for the tests conducted on the MXS-89 silica-phenolic nozzle material. Its thermal property characteristics are those shown in Figure C-2. The selection of a material for use as a reference candidate is based on mate 'al uniformity, machinability, opacity, and reproducibility. It is tested repeatedly in Avco's guarded hot plate apparatus in order to determine statistically its thermal conductivity and to verify its stability and reproducibility (hysteresis). During this time, the testing facility is constantly cross checked for stability using materials which were purchased from the N.B.S and certified for thermal conductivity calibration. When the Avco-developed references are used for programs, such as the one reported in this document, the specimens are remachined to a geometry consistent with test technique requirements. For tests of the fired MX4500 graphite-phenolic material, pyrolytic graphite ("C" direction) was used as reference standard material. It was cross checked against Pyroceram 9606, a well recognized reference material.

The thermal insulation which is used in the annular region between the test stack and the guard ring heaters must be selected with caution. The insulation material must have a thermal conductivity level significantly lower than that of the three stack elements, e.g., from 1 to 20 percent. Failure to observe this precaution as expected results in a significant heat exchange between the stack elements and their surrounding insulation and the loss of measurement precision. This requirement becomes increasingly difficult to satisfy as the conductivity of the elements becomes smaller and smaller (especially when in-vacuum environments are being used). Avco has tested a wide variety of thermal insulations and has selected a material known by the trade name TG 15000 (product of H. I. Thompson Corp.) which offers a suitable compromise between low thermal conductivity, handling ease, low degradation, stability and resiliency. Its thermal conductivity in air is in the order of 0.02 Btu/hr-ft-$^{\circ}$F (see Figure C-3). When it is used in conjunction with materials in the conductivity range 5.0 to 0.10 Btu/hr-ft-$^{\circ}$F such as encountered in the nozzle tests, it meets the criterion stated above and precise measurements are assured.

Guard ring temperature control is a critical requirement in maintaining split-bar measurement integrity. It is practically impossible to exactly match the temperature profiles of both the test column and guard column. A scheme which is felt to most closely approach a matched condition has been incorporated into the Avco apparatus in the form of multiple guard rings which are constructed of materials similar to those comprising the test column heat meters. Near the ends of each ring, a heating element is embedded into the cylinder so that for the three-element stack a guard ring assembly having six controllable heaters provides a means of duplicating the stack temperature profile as closely as is practical. Power to the various heaters are regulated by Avco-built automatic
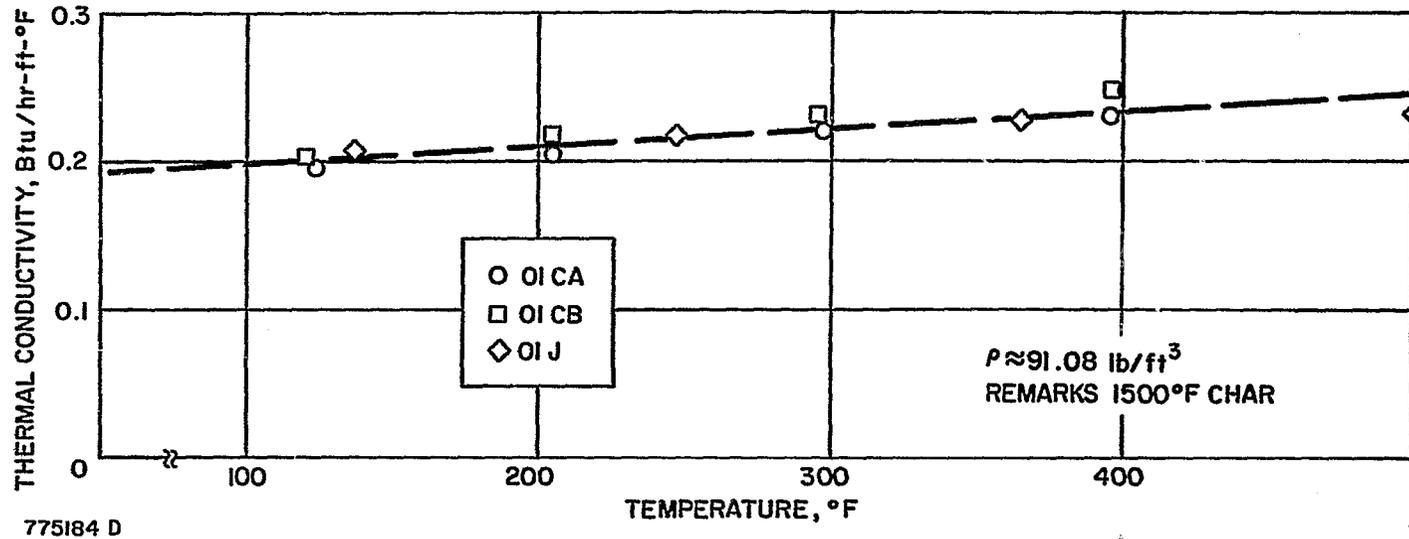
Figure C-2 THERMAL CONDUCTIVITY VERSUS TEMPERATURE FOR OTWR
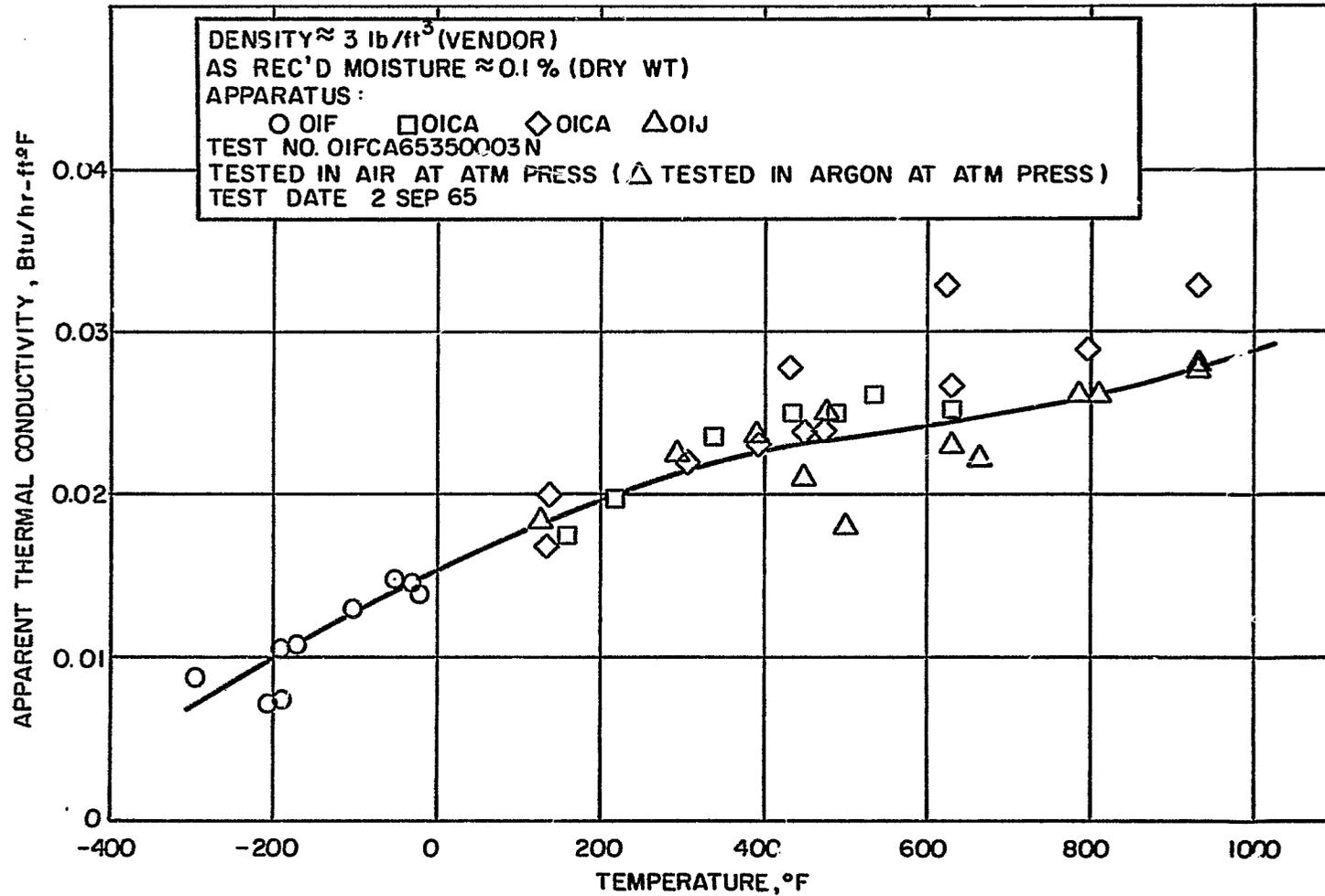
775184 D

Figure C-3 APPARENT THERMAL CONDUCTIVITY VERSUS TEMPERATURE, TG15000

760955D

differential controllers which operate on signals that represent the differential temperatures between the stack and guard assemblies. The error signal is generated by specially constructed differential miniature thermocouples. The ifferential thermocouples pass from the specimens to their guard ring counterpart in the same radial plane located in the region immediately adjacent to the corresponding heater plane. By this arrangement maximum temperature drift sensitivity and rapid controller response are achieved. The controller scheme is capable of ±0.1° F temperature regulation at any of the heater planes.

Routine calibrations of the various thermocouples which are used in all test facilities including the split-bar apparatus are conducted using N.B.S. certified freeze point materials which include tin, lead, zinc, and aluminum. The technique employed is the immersion of the couple (protected to avoid contamination of the reference metal) into a vessel of molten standard material. The thermocouple output is continually monitored on a recorder. The reference metal is allowed to cool, and when it reaches the isothermal liquid-solid phase (freeze point) precise temperature measurements are performed with the use of a high-precision Wenner potentiometer (high range $\pm 0.01$ percent $\pm 0.5$ $\mu v$; low range $\pm 0.1$ $\mu v$). Subsequent corrections are applied to all temperature measurements conducted during a test. In preliminary evaluations of new procedures, in-situ, calibrations are also performed to ascertain any installation errors which can occur.

In the performance of a split-bar test, the specific procedure is as follows: a regulated amount of power is applied to the main heater upon which the test stack rests, and a regulated flow low of coolant is passed through the cooler plate. The automatic differential controllers are actuated and the system is allowed to come to thermal equilibrium. When stability is achieved, usually after at least 2 hours, the entire complement of direct temperature and d ifferential temperature thermocouples are monitored and read. In general, no less than three direct readings and four differential thermocouples are required in each of the three-stack elements. The measured temperatures are used to calculate the desired property as described previously.

Technique Comparison

Many cross checks have been conducted between properties as measured on the guarded hot plate and the split-bar test apparatus. Recently, particular emphasis was placed on various material combinations appropriate to the nozzle work discussed in this report. Materials such as 5026/36/HC-G-P, 1500° F-charred OTWR, and N.B.S. certified silicon rubber were the comparison materials. Their properties are shown in Figure C-4.

These materials were first measured extensively on the guarded hot plate, and their properties were well established statistically. During the split-bar series of cross checks, different combinations were used, interchanging specimens and meter bars. For example, combinations of OTWR-silicon rubber-OTWR were arranged as meter-specimen-meter respectively. Then they were interchanged to a silicon rubber-OTWR-silicon rubber configuration and so on. The table below lists several such test comparisons.
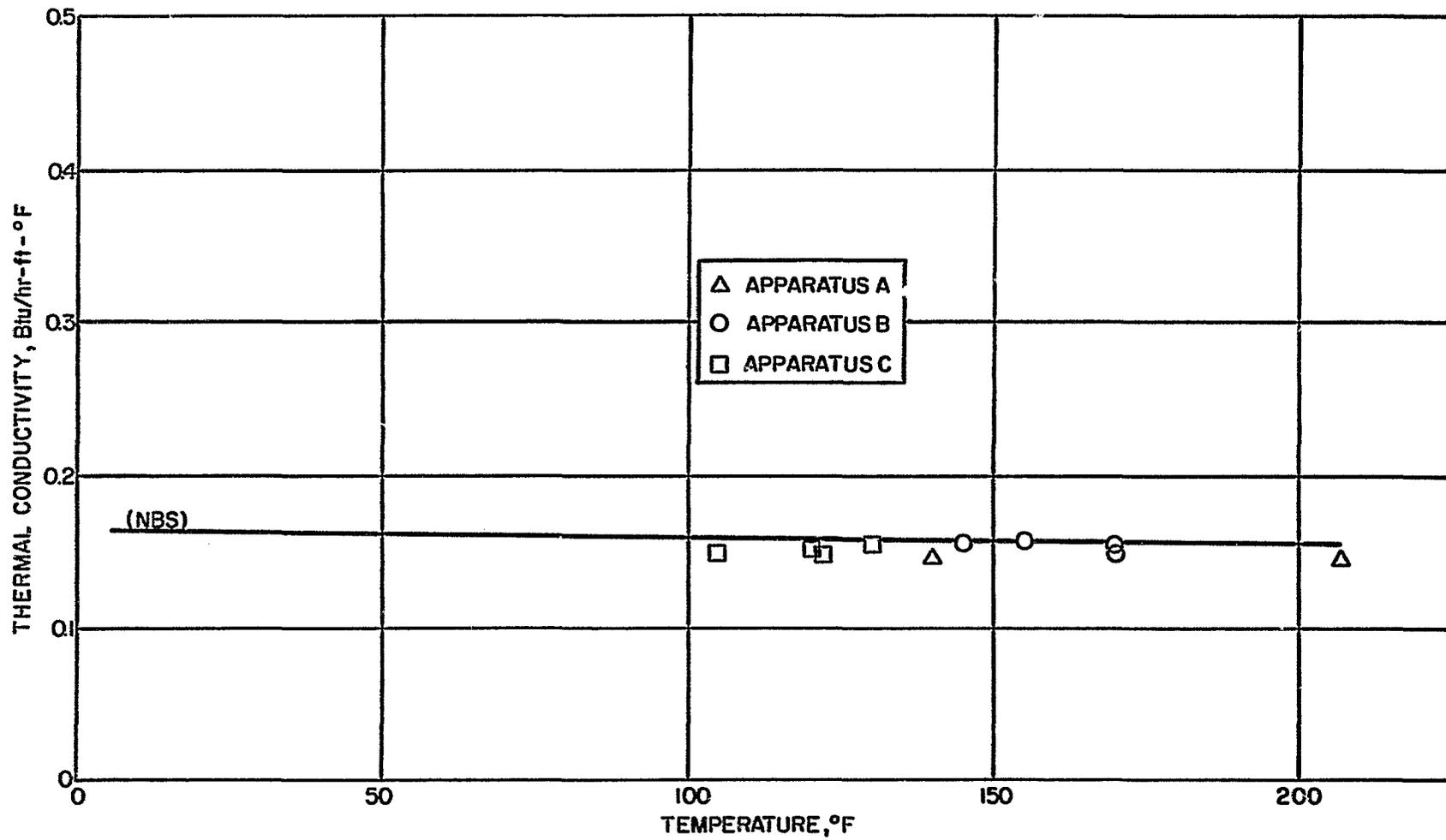
775185D

Figure C-4 APPARENT THERMAL CONDUCTIVITY VERIFICATION TEST DATA USING
NBS SILICONE RUBBER

| Combination | Split-Bar Conductivity (Btu/hr-ft-°F) | GHP Conductivity (Btu/hr-ft-°F) |
|---|---|---|
| Silicon Rubber-OTWR-Silicon Rubber | 0.206 | $0.22_3$ |
| Silicon Rubber-Silicon Rubber-Silicon Rubber | 0.158 | 0.158 |
| OTWR-OTWR-OTWR | $0.25_7$ | $0.24_0$ |

Figures 88 and 89 in the main body of this report show test results of two split-bar schemes utilizing circular and square test stack cross sections. These figures illustrate the good agreement between tests in the MXS-89 nozzle virgin zone and the virgin material tests on the raw billet.

These and prior verification efforts were considered to be adequate to assure that the apparent thermal conductivity data presented as a result of this program are precise to at least ±5 percent or better.

## Technique Critique

The unique character of the nozzle cores, the need to obtain a thermal conductivity nozzle char depth profile, and the relatively small specimen sizes were given prime consideration in the selection of a satisfactory test method. It was generally conceded that the split-bar technique was the only one suitable, although due recognition was given to the fact of the varying properties with depth, the brittleness of the char structure (and the fact that test thermocouples were located very close to one another, e.g., 0.10 inch). Figure C-5 shows a schematic of the split-bar modification for tests of the MXS-89 ramp section, and Figure C-6 illustrates the test method adaptation for rectangular specimen geometry (exit sections) used for both nozzle materials.

The variation in properties which were initially assumed on the basis of the graded nature of the specimen chars and later verified by measurements presented several problems which had to be resolved by assumptions and decisions. The question of where to locate thermocouples along the nozzle core depth to the greatest advantage was considered, and it was decided that in the charred region 1/10-inch spacing between couples and in the virgin zone 1/4-inch spacing would provide enough information for a suitable profile. In the event that a unique region such as a fissure or high-density area was evident from the density profiles, the distance between couples was varied in order to assess that region. In addition to the depth measurements, a thermocouple was located on the core surface (char) at the heat meter-specimen interface. To facilitate procedures, the surface char was necessarily the surface remaining after the specimen had been ground to a flat plane. In general, a minimum of material was removed to obtain flatness so that the final surface was assumed to be similar in composition to the original; however, the test does not exclude surface material evaluations which were considered important also.
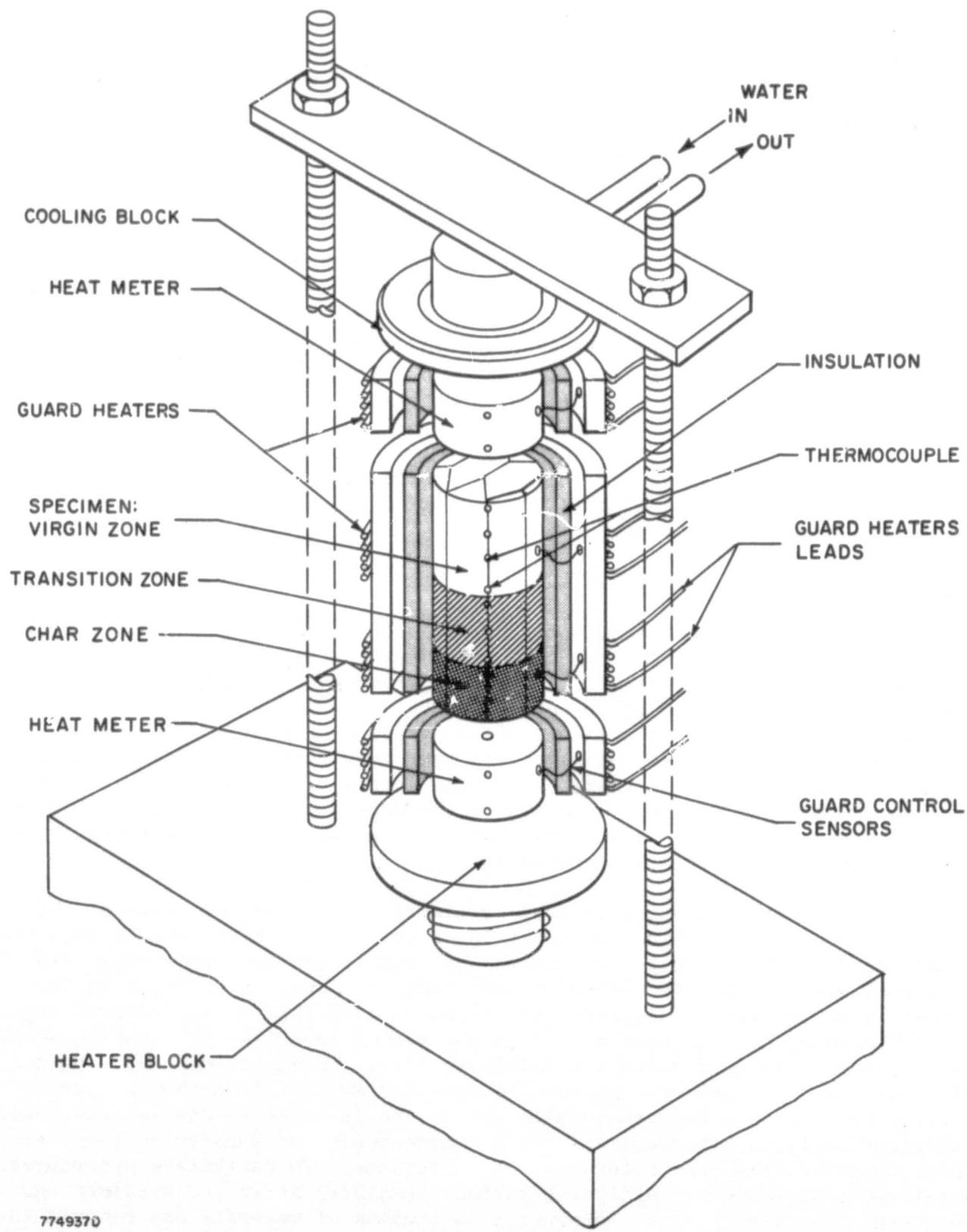
Figure C-5 MODIFIED CUT-BAR SCHEMATIC

COOLER

COPPER DISTRIBUTOR

HEAT METER

SST
ADHESIVE LAYER
VIRGIN ZONE

TG 15, 000 INSULATION (4)

TRANSITION ZONE

CHAR ZONE

THERMOCOUPLE
(TYPICAL)

HEAT METER

GUARD HEATERS WINDINGS

COPPER DISTRIBUTOR'

HEATER
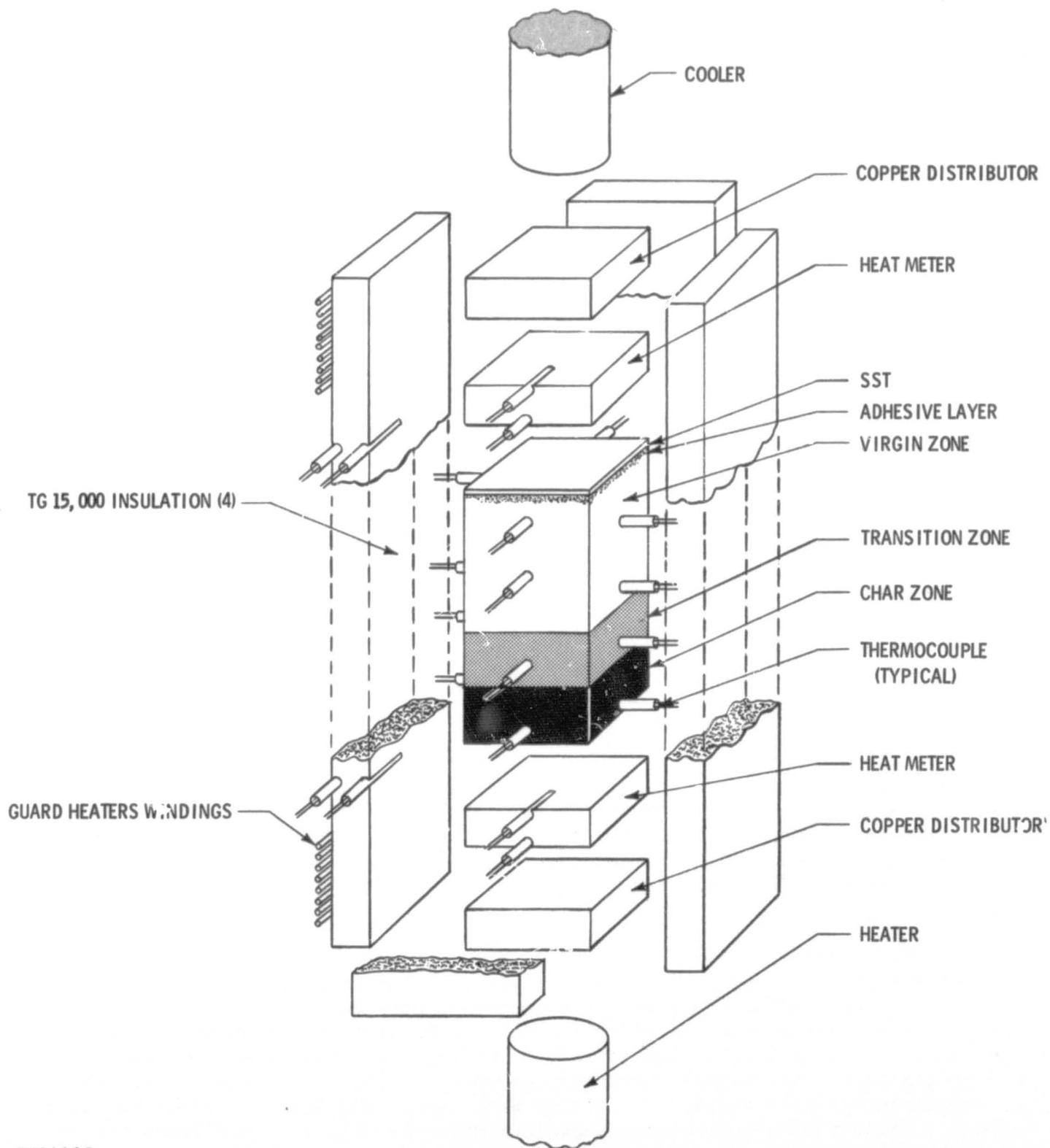
770444 D

Figure C-6  CUT-BAR THERMAL CONDUCTIVITY TEST APPARATUS ARRANGED FOR
RECTANGULAR FIRED NOZZLE CORE STUDIES

Heat flow by pure conduction was assumed and conductivity values were computed from Fourier's equation of heat flow by conduction at steady state:

$$q = KA \frac{\Delta T}{\Delta x} \qquad\qquad (C-1)$$

where

$q$  =  heat flow rate

$K$  =  thermal conductivity coefficient

$A$  =  specimen cross sectional area

$\Delta T$  =  temperature difference across the specimen thickness

$\Delta x$  =  specimen thickness

One of the fundamental assumptions in the above argument is that the temperature gradient $\Delta T$ is linear and the material is homogeneous, opaque, and stable. Assurance that this is the case for the nozzle cores cannot be made. The conductivity variation caused by the char gradation certainly results in certain non-linear distributions in the temperature profile as a function of nozzle core depth. It was finalized and accepted that a reasonable approximation of linearity existed between the thermocouples not randomly selected. The small distances required presented the problem that the location of each couple needed to be known with high confidence. Thermocouple installations were accomplished by using a precision drill press located in the property measurements area. The installation was made by drilling small holes (0.014 inch in diameter) carefully so as not to mechanically break the brittle char material simultaneously with the drilling of the holes in the guard ring. When the drilling operation was complete, the entire test column was instrumented and then completely assembled. The assembly was then X-rayed and thermocouple hot junction locations were determined with the use of a high-precision measuring microscope ($\pm$50 micro inches). As a check, several cores were cross sectioned after the tests were completed, and a comparison between direct hot junction locations and those measured prior to the test was made. Very good agreement was observed so that no significant error correction in the final apparent thermal conductivities was required on this account.

The holes that were drilled radially into the test specimens extended to the axis of the test cylinder. The thermocouple was then wrapped about one-half turn in the same radial plane as the hole before passing out of the test zone (outside the guard heater) in order to reduce heat flow away from the couple hot junction. Preselected hole locations included the charred surface zone and virgin zone. Additional thermocouples were located at critical points along the specimen cylinder surface to provide data confirming the test stack isothermal planes. These thermocouples were installed with the half turn configuration as were the differential thermocouples used to control the guard column temperatures.

The guard column was made up of several heater rings and spacer rings, the number of which depended upon the length of the test specimen. Each test was tailored to the characteristics of a particular core. A 1/16-inch annular gap was included between rings and specimens and was filled during assembly with TG 1500 insulation materials.

During a test, a very moderate force was exerted on the meter-specimen-meter column limited by the fact that no crushing of the material was desirable. It was found that even with this light pressure load, no significant temperature drop occurred across the various stack interfaces (interface error). This condition was attributed to the relatively low heat flow rate, the flatness of the mating surfaces, and the similarity compliance of the adjacent interface materials. To further ensure good contact over the cross sections of the various stacks with the heater and cooler plates, "Grafoil", a resilient pyrolytic graphite foil, was used as an interface material at those points where it was suspected that an error could occur. The thickness of the foil (0.005 inch) was used in the "c" plane of the graphite structure while the surface of the foil was in the "ab" plane. The fact that the material was used in the "ab" plane offers greater assurance that an isothermal condition existed at the interface in question.

Because perfect temperature profile matching between the test stack and guard rings was not possible, the criteria for determining when a satisfactory test condition was obtained (after temperature stability) was the predetermined criterion which required a) test column and guard column temperature profile agreement, and b) "hot" and "cold" test meter flux agreement. A $\pm 1/2^{\circ}$ F overall temperature profile tolerance and a $\pm 5$ percent tolerance between the heat flux through the two heat meters was used as a required test condition. In addition, the virgin zone immediately following the char zone in depth was chosen as the region which set the limit of the maximum test temperature of a particular core test. The temperature was limited at this location to $350^{\circ}$ F in order to minimize material decomposition during the test which causes percolating decomposition products to pass from the virgin regions through the char layers and a possibility of recondensation of the vapors further in depth. Unfortunately this requirement limited the maximum test temperatures in the char zones to about $400^{\circ}$ F which was acceptable insofar as obtaining conductivity profiles at three distinct temperature levels which was the requirement of this study; however, it was not a high enough temperature to allow characterization of the various core char zones except on a low-temperature comparative basis. Improvements of studies in this area are discussed further in the recommendations section of this document.

## Conclusions

A modification of the split-bar method of testing which utilizes low conductivity, Avco/SSD-formulated secondary reference material has been shown to be suitable for determining thermal conductivity profiles of nozzle test corings. Cross check tests against alternate techniques using standard materials proved the validity of the usefulness of the technique. The technique compares well with the method of the guarded hot plate technique but required additional operational precautions to ensure one-dimensional heat flow.

## Recommendations

In view of the several areas of interest which have arisen because of the nozzle core studies, some recommendations are presented because of their relevancy. The thermal conductivity tests which have been performed in this report should be extended to include measurements at higher temperatures. This need is particularly true of the char zones where data was obtained only to a maximum temperature of $400^{\circ}$ F. Correlation of these data with those which are postulated are

necessary in order to lend support to the predicted values at the higher temperatures. In order to perform these measurements, it is recommended that the char zone be physically separated from the virgin zone and each section tested independently after testing in the way described for this study. These tests can be performed using the techniques described previously without any modification of the available facilities.

It is also recommended that some tests be conducted in a pressurized atmosphere, the level of which corresponds to the test firing environmental pressures. Using the present testing scheme, pressure adaptations are simple and available. The purpose of this recommendation would be to assess the effects of pressure environments on the nozzle properties and to produce a conductivity-pressure-temperature characterization of both virgin and char regions which may be useful for prediction analysis.

APPENDIX D

DISCUSSION OF SPECIFIC HEAT DETERMINATIONS BY THE METHOD OF

MIXTURES AND DIFFERENTIAL SCAN CALORIMETRY.

## Mean Specific Heat of Thermal Insulations (ASTM C351-61) -- Method of Mixtures

The specification that deals with specific heat measurements is commonly referred to as the method of mixtures. The procedure consists of adding a known mass of test material at one temperature to a known mass of water (or other medium) at a different temperature and determining the resulting equilibrium temperature. The heat absorbed or liberated both by the water (or other medium) and the containing vessel can be calculated, and this value equated to the expression for the heat transferred by the test material.

From this equation, the unknown specific heat can be calculated:

$$C_s = \frac{\dfrac{(M_w + E)\, C_w (T_m - T_c)}{(T_h - T_M)} - M_c\, C_c}{M_s} \qquad (D-1)$$

where

$E$ = water equivalent of the calorimeter and its accessories

$M_w$ = mass of calorimeter water

$C_w$ = mean specific heat of calorimeter water

$M_s$ = mass of the specimen

$M_c\, C_c$ = thermal capacity of the capsule

$C_s$ = mean specific heat of the test specimen over the temperature range $T_h$ to $T_m$

$T_h$ = temperature of the capsule and specimen, capsule, or standard after heating

$T_m$ = temperature of the mixture extrapolated back to time = 10 minutes

$T_c$ = temperature extrapolated ahead to time = 10 minutes of the calorimeter water before capsule or standard is dropped.

A comparison of ASTM and Avco specifications for specific heat is presented in Tables D-I, D-II, and D-III. There was a notable difference between these specifications; therefore, Avco could not stipulate adherence to ASTM Procedures. Although the basic procedures were similar, Avco made the apparatus more versatile, eliminated the problems associated with water corrections, and avoided dropping the specimen directly into water.

## TABLE D-I

### MECHANICAL SPECIFICATIONS OF ASTM C351-61

| No. | Specification | ASTM | Avco |
|-----|---------------|------|------|
| 1. | Range of capacity of unlagged Dewar flask (ml) | 500 to 750 | 750 |
| 2. | Calorimetric medium | Water | OFHC Copper |
| 3. | Capsule assembly diameter (in.) | 1.0 | 0.37 I.D. |
| 4. | Calibration standard dimension (in.) | 2 x 1/4 x 1 in. | 0.32 dia x 1 length |
| 5. | Heater core dimensions (in.) | 1-1/2 dia x 10-in. length | 1/2 dia x 6 length |
| 6. | Insulation thickness-heater unit (in.) | 1 dia | 4 x 4 |
| 7. | Capsule assembly length (in.) | 2 | 1 |
| 8. | Thermocouple wire diameter (in.) | B & S 30 (0.010) | B & S 36 (0.005) |

## TABLE D-II

### PARAMETRIC SPECIFICATIONS OF ASTM C351-61

| No. | Specification | ASTM | Avco |
|-----|---------------|------|------|
| 1 | Mean temperature range | 68 to 212°F | -250 to 2000°F |
| 2 | Thermometry temperature range | 68 to 212°F | -250 to 2000°F |
| 3 | Readable thermometry increments | 0.02°F | 0.02°F |
| 4 | Maximum variation over heater length | ±2°F | ±0.5°F to ±3/4% |
| 5 | Voltage source stability | ±1% | ±1% |
| 6 | Maximum capsule capacity | $6 \times 10^{-3}$ Btu/°F | Variable or none |
| 7 | Measurement apparatus precision | 0.2°F | 0.2°F |
| 8 | Room temperature constant for 20-minute period | | Conform |
| 9 | Specific heat standard value | 0.093 Btu/lb°F | Variable based on NBS Data |

## TABLE D-III

### SPECIMEN SPECIFICATIONS OF ASTM C351-61

| No. | Specification | ASTM | Avco |
|-----|---------------|------|------|
| 1 | Homogeneous material in solid state | OK | OK |
| 2 | Calibration standard material | Electrolytic copper | Synthetic sapphire |
| 3 | Capsule assembly material | Brass | Aluminum foil |
| 4 | Test Sample dimensions (in.) | 2 x 1/4 x 1 | 0.32 dia x 1 or longer length |
| 5 | Number of test specimens per determination | 3 | 12 |

## Automatic Specific Heat Apparatus

With the exception of the sample loading requirement, the test facility used during this program was completely automatic. The facility consisted of five complete assemblies, automatic control, electrotyper, and a decimal converter, all shown in Figure D-1. The entire calorimeter assembly was enclosed in a plexiglass chamber, which prevented minor ambient variations from influencing a test. A schematic illustration of a single assembly is shown in Figure D-2. Each assembly was individually designed to provide a calorimeter block mass, matched to a corresponding furnace temperature. The matching process provided a uniform calorimeter temperature change over a large heater temperature range and permitted more accurate automatic recording of the test temperature changes.

The overall schematic arrangement of the specific-heat apparatus used is shown in Figure D-3. The programmer shown schematically in Figure D-4 shows the principal component in the automatic process. The unit contains two multiple cam timers and two multiple-throw-multiple-pole rotary switches. The long period timer sele ts the time interval over which a particular series of events occur and positions the master selection switch for information presentation (e.g., furnace emf, calorimeter emf, or reference-block emf). The short period timer positions a second rotary switch for sequential reading of the five furnace-calorimeter sets. Included in the programmer was a signal cam that delays digital readout until the analog resistance converter is balanced. The analog resistance converter consists of a high-gain amplifier operating at null balance, a direct-current reference supply, and a servo motor that drives two ganged precision potentiometers. The device provides a high-impedance signal for the decimal converter. The data obtained from this system was both in the form of typed reference copy and of IBM punch cards. The volume of data that was obtained using this apparatus was the basis for incorporating a small digital program (1663), written to provide an emf-to-temperature conversion, data calculation, and plots of enthalpy as a function of temperature.

The conversion of an enthalpy curve to specific heat must be performed with care, unless, of course, it is a straight-line curve. In general, the simplest curve of series of curves should be used to describe (fit) the enthalpy data. Over-fitting could result in erroneous inflections of "tailing off" at the data extremes. The simple fit minimizes errors in converting enthalpy to specific heat. It was found that in most cases enthalpy data are used directly; however, for this report the specific heat data were obtained using a derivimeter.

Instead of determining the water equivalent of copper, as described in the ASTM procedure summarized above, the apparatus used for this study was periodically calibrated using synthetic sapphire and data recommended by the NBS.

Several calibration series provided sufficient information to obtain an estimate of the system precision. This method obviates the need for an error analysis of the various system components.

The automation of this apparatus, as in the automating of thermal conductivity experiments, eliminated the human operator variable from the results.
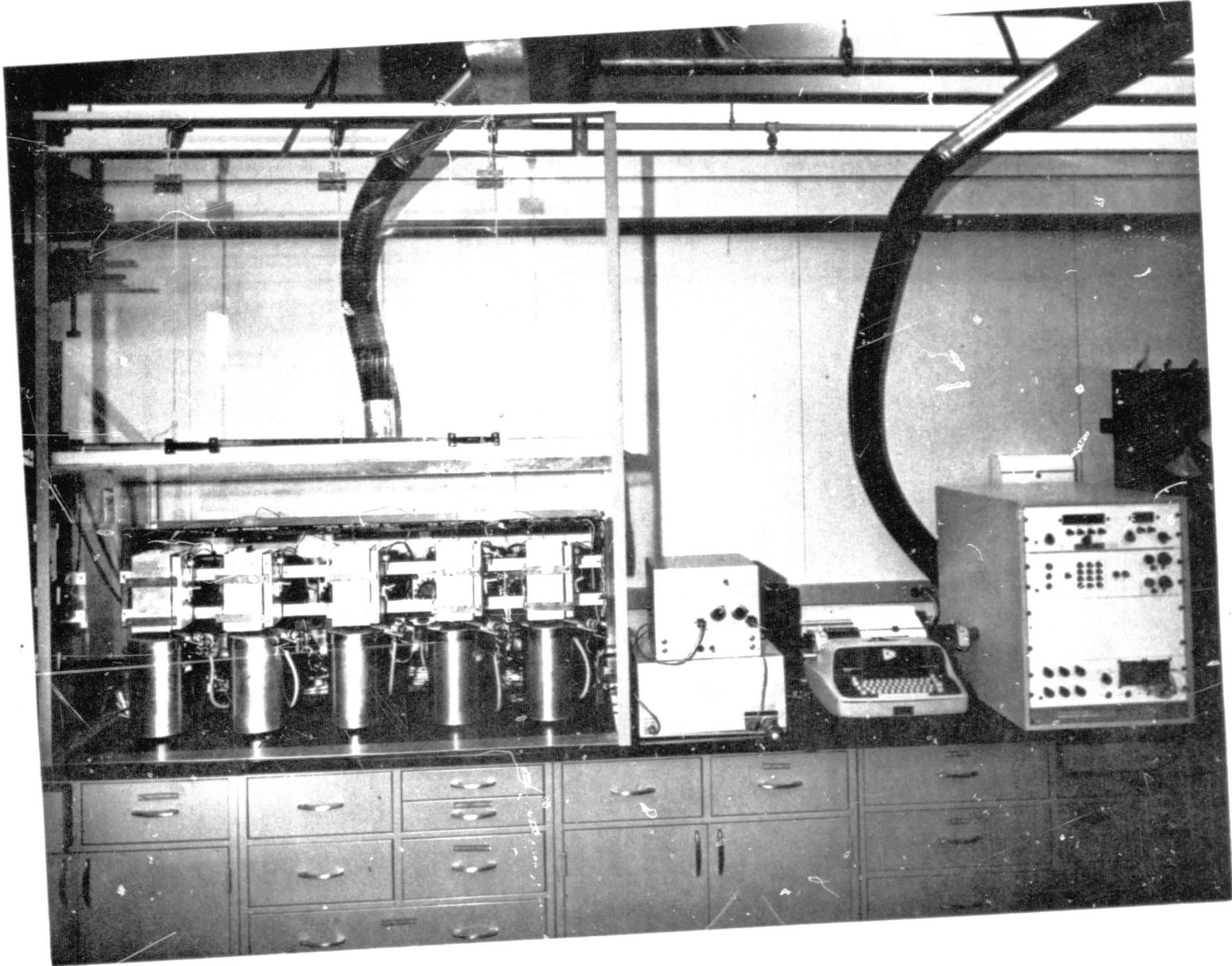
Figure D-1  AUTOMATIC SPECIFIC HEAT APPARATUS

THERMOCOUPLE LEAD

FURNACE CAP

FURNACE HEATER WIRE

SAMPLE DROP
SOLENOID

THERMOCOUPLE

FURNACE

SAMPLE

DOOR OPENING
SOLENOID

SWITCH

110 VOLTS AC

CALORIMETER DOOR

DEWAR

SUPPORT PIN

COPPER CALOROMETER

SAMPLE CAVITY
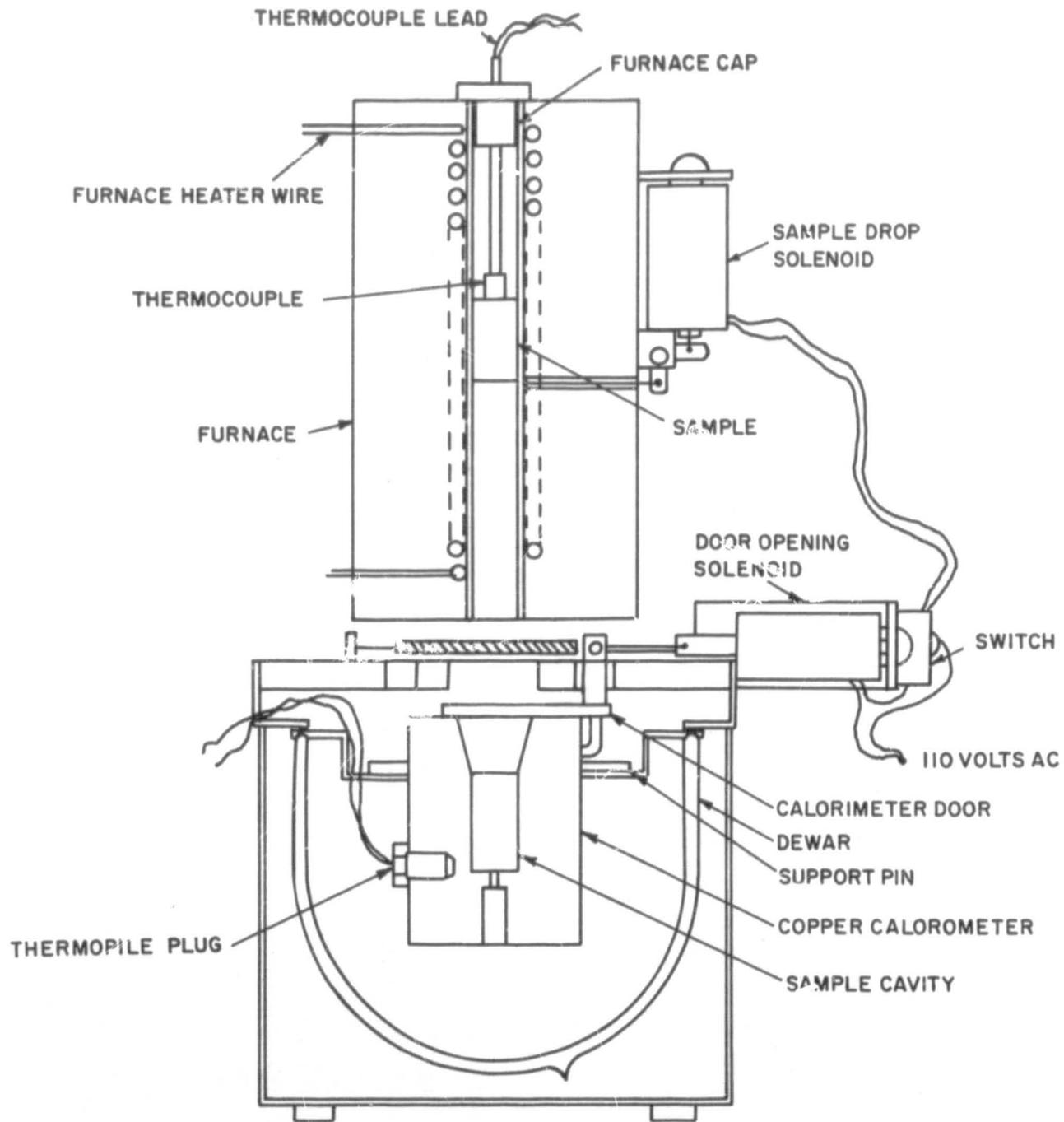
THERMOPILE PLUG

65-5427

Figure D-2 SCHEMATIC OF AUTOMATIC FURNACE CALORIMETER SPECIFIC HEAT SET

① FURNACE POWER

② FURNACE CALORIMETER SET

③ CALORIMETER THERMOPILE LEADS

④ DOOR OPEN & SAMPLE DROP LEADS

⑤ REFERENCE POWER

⑥ FURNACE THERMOCOUPLE LEADS
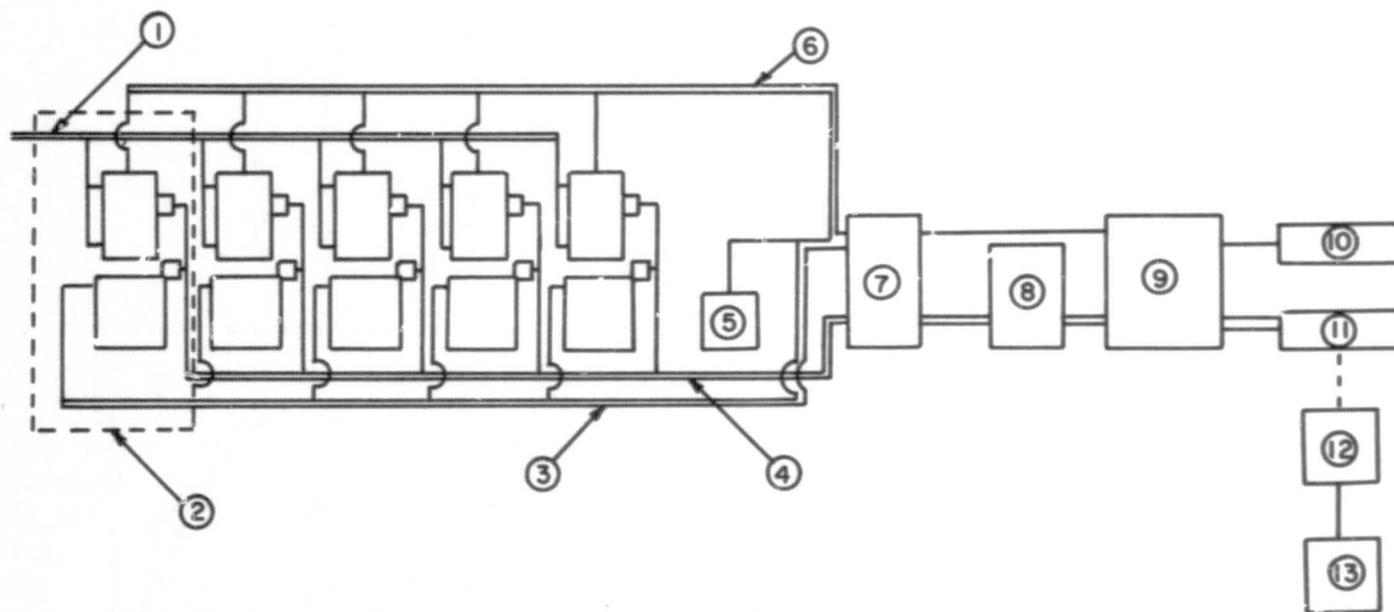
⑦ PROGRAMMER

⑧ EMF TO ANALOG RESISTANCE CONVERTER

⑨ ANALOG TO DIGITAL CONVERTER

⑩ TYPER

⑪ CARD PUNCH

⑫ DIGITAL COMPUTER

⑬ PLOTTER

65-5428

Figure D-3 SCHEMATIC ARRANGEMENT OF AUTOMATIC SPECIFIC HEAT COMPONENTS
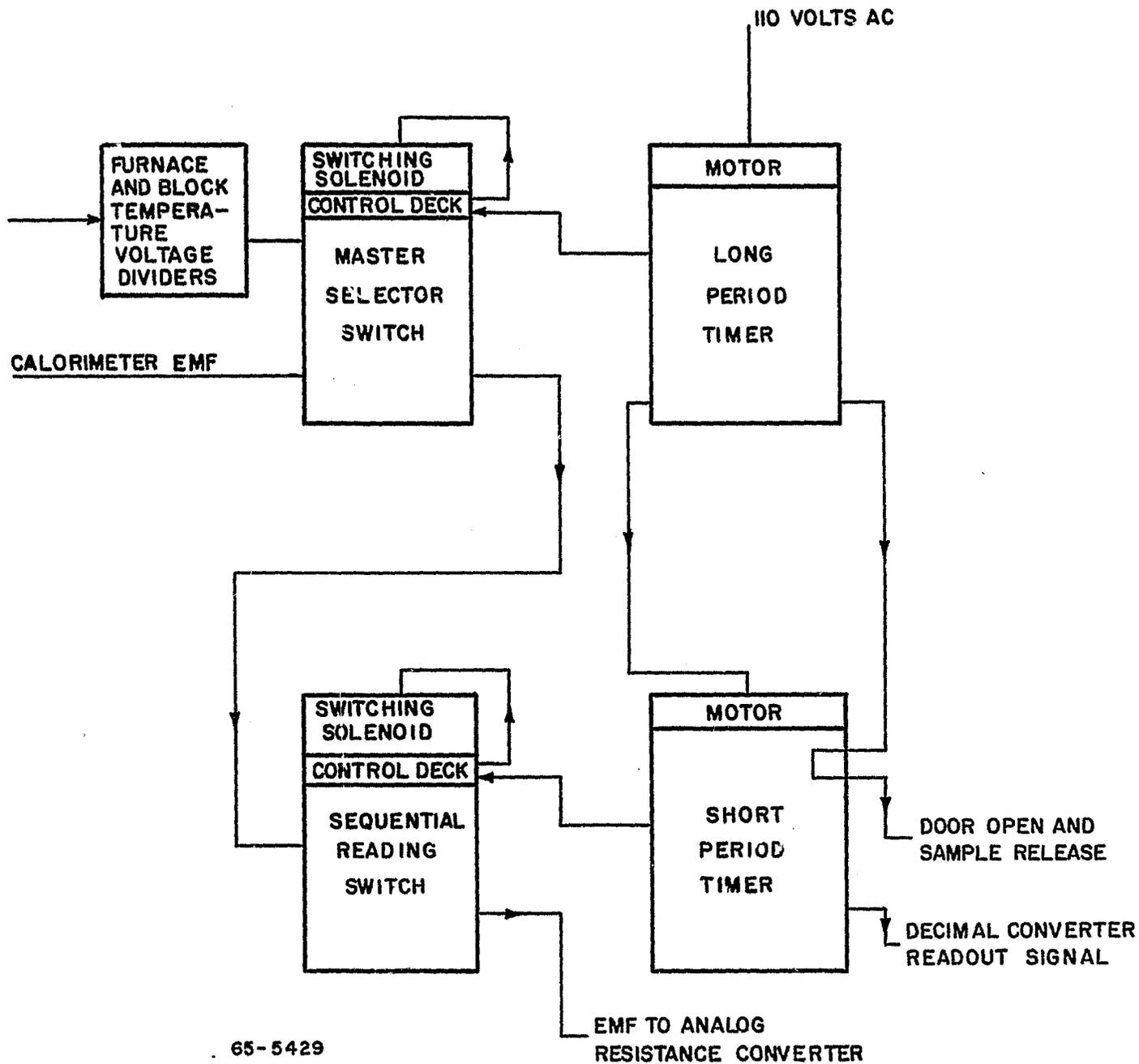
Figure D-4 SCHEMATIC ARRANGEMENT OF AUTOMATIC SPECIFIC HEAT PROGRAMMER

65-5429

## Specific Heat Profile Test Description

### Test Description

The specific heat (Cp) measurements which were performed during this study were performed using a Perkin-Elmer Differential Scan Calorimeter (DSC), (see Figure D-5). Basically, the operation of the instrument is one which maintains a state of temperature equilibriur between a specimen and a reference material while both undergo the same temperature transient simultaneous.y and at the same rate. The electrical power differential between the sample and reference heat sources required to accomplish teh above is used to measure the heat capacity and reaction energies. The DSC was employed for this study because of its small specimen size (30 milligrams) requirements which makes it uniquely appropriate for post-test nozzle specimen Cp profile characterizations.

The operation of the instrument was changed from its normal continuous scan to a pulsed scan for specific heat evaluations, thus the necessity of performing pre- and post-test baseline determinations was avoided. The continuous scan test data is presented in the form as shown in Figure D-6 which shows the baseline requirements, reference material test, and specimen test. The specific heat was determined by relating the deflections ds and dr by

$$Cp_s = Cp_r \times \frac{ds}{dr} \times \frac{mr}{ms}$$

where,

    cp = specific heat

    d  = recorder deflection

    m  = weight of the material

and the subscripts

    s  = sample

    r  = reference

Typical specific heat traces using the pulse technique are illustrated in Figure D-6. The pulse scheme provides the advantage of obtaining a continuous monitor of the baseline therby avoiding the problem of baseline variations during a run. As can be seen in the figure, the tests were performed at $18°$ intervals, at a temperature rise rate of $18°F/minute$. The baseline intervals represent a condition in which the instrument maintained an isothermal condition between specimen and reference while holding the temperature constant (rise rate = $0°F/min.$)

Figure D-5  PERKIN-ELMER DIFFERENTIAL SCANNING CALORIMETER, DSC-1
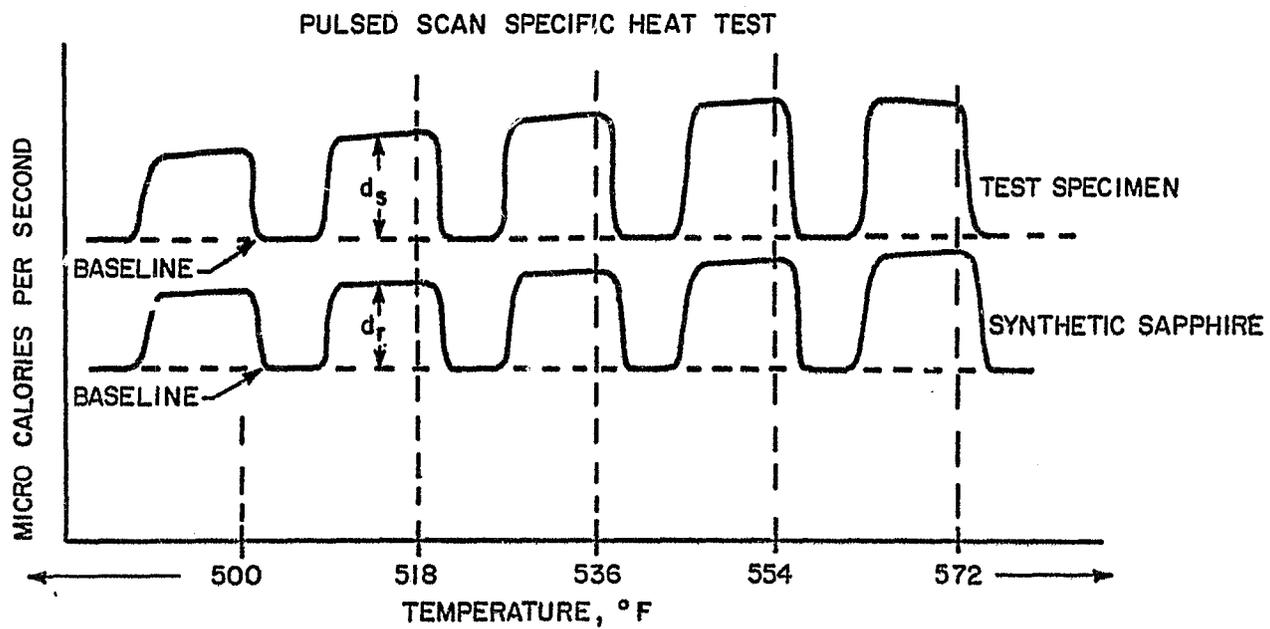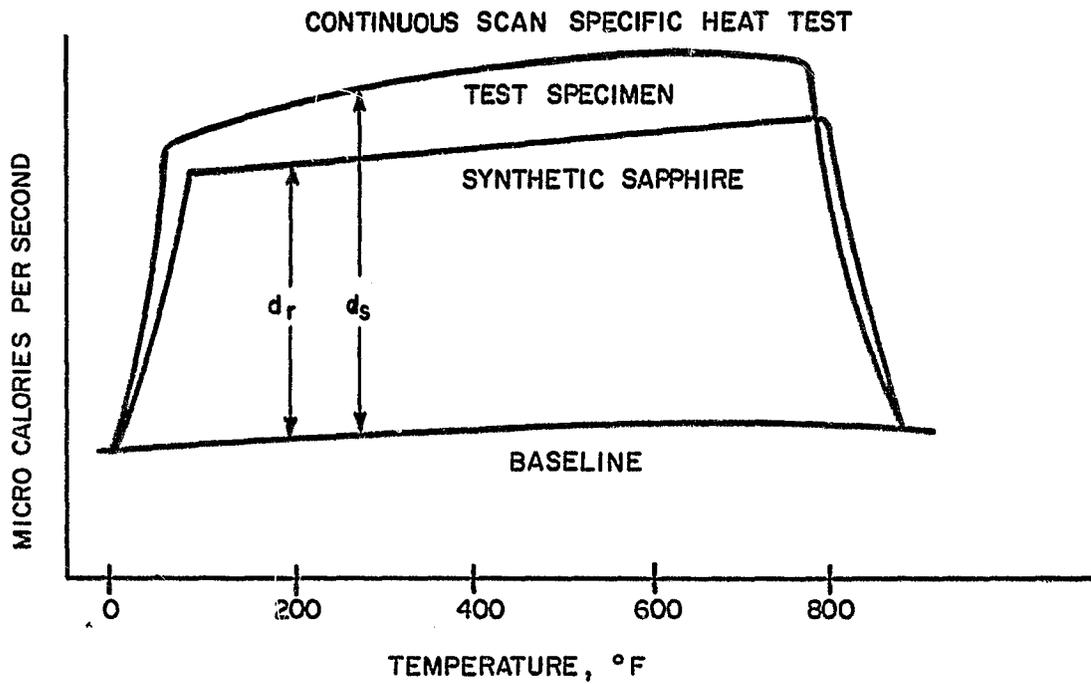
Figure D-6 TYPICAL DIFFERENTIAL SCAN CALORIMETER TRACES

774951D

The calibration material used throughout these tests was synthetic sapphire $(Al_2O_3)$ which has been thermally characterized by the National Bureau of Standards.

In operation, a specimen encapsulated in an aluminum container was placed into one of the two instrument heaters; the other heater contained an empty container to offset the effects of the specimen container. After the chamber cover has been placed over the heaters and the chamber allowed to purge with dry nitrogen, a pulse test was initiated and proceeded to 930°F. The test was then stopped and the heaters allowed to cool. This was then followed by an identical test except that synthetic sapphire was used in place of the specimen. This procedure produces the various parameters used in the above relationship to provide Cp measurements at 18°F intervals.

The study program for the nozzle char profile characterization was arranged so that maximum correlations between the various measured properties could be achieved. The latter was accomplished when the materials used for Cp measurements were obtained from layer grindings produced during the density profile test series. The layers were also used i1 'e chemical analysis and X-ray diffraction examinations and a common referen . between all tests was established so that data correlation was enhanced. The specific heat of each char and virgin layer was evaluated from room temperature to 930°F. The selection of the particular layers from each nozzle char specimen was governed by the density profile for that specimen. Greater emphasis was placed on characterizing the char and transition zones, intermediate measurements being made in the virgin zones to verify similarity with all nozzle specimens.

Of particular interest was the post-test weight loss percentages measured at the end of each specimen heat test run. These percentages were plotted as a function of the nozzle char depth to produce a weight loss profile. It was noted that some weight losses were observed not only in the virgin regions as was expected but also in the char zones which had been exposed to very high nozzle firing temperatures much in excess of the maximum 930°F specific heat test temperatures. The origins of these phenomena were considered including redeposition of decomposition products from the internal regions of the material during cool down, and water absorbed due to long time atmospheric exposure. Drying of powdered samples eliminated absorbed moisture, so that the conclusion was made that the weight losses are due to redeposited decomposition products.

No apparent reaction energies were observed in any of the specific heat tests. The general observation was that the Cp of each layer rose steadily showing no significant anomalies over the entire test temperature range. All Cp calculations were corrected for mass loss using thermogravimetric analysis (TGA) test data of the test material. The data were also corrected for the post-test weight loss for each layer.

The specific heat versus temperature results of each layer was replotted as specific heat as a function of heat shield depth to provide a profile curve which was consistent to the other properties evaluated.

# APPENDIX E

## PHYSICAL AND CHEMICAL PROPERTY MEASUREMENTS TECHNIQUES

## A. PHYSICAL PROPERTIES

### 1. Density

Two types of density values were calculated: bulk density (BD) and apparent density (AD). These were calculated from bulk volume (BV) and apparent volume (AV). Bulk volume, obtained by geometrical measurement, is the sum of the true volume of the material, the volume of the open pores or voids, and the volume of the closed pores. Apparent volume is the sum of the true volume and the volume of the closed pores. Apparent volume was measured by a Beckman Air Comparison Pycnometer, Model 930. This instrument uses the principle of immersing the sample in an appropriate medium (in this case a gas which may be air, argon, or helium) and measuring the increase in volume.

### 2. Porosity

The porosity is a measure of the ratio of the volume of all voids to the total volume of a material. For this program the percent apparent porosity, a measure of the interconnected (open) voids, was calculated from either the measured BV and AV or the measured BD and AD.

$$\text{Percent Apparent Porosity} = \frac{(BV - AV)}{BV} 100 = \frac{(AD - BD)}{AD} 100$$

### 3. Bulk Density and Apparent Porosity Profiles

For each specimen, a map was available from the Thermal Properties Group which indicated the location of various visible zones in the profile view of the material. The map was used as a guide for the precise machining required to layer each specimen so as to obtain samples representative of the layers of interest.

The sample was mounted on a table which can be moved laterally and vertically in precisely measured increments. The char layer was milled parallel to the surface of the char. The thickness of each slice taken from the char surface was usually 5 or 10 mils with the 5-mil cut being used when the char was especially fragile so as to avoid any chipping.

As part of the char layering operation, data were obtained from which the bulk density and apparent porosity of each layer were calculated. The weight of char removed in a layer was determined by weighing the total piece before and after the desired number of cuts. The depth of char removed in each layer was determined from the average of several depth gauge readings taken by a dial-indicating micrometer scribed to 0.001 inch. The bulk volume of each layer was calculated from the depth of each layer and the surface area of the specimen. The apparent volume of the removed layers was determined by difference. The apparent volume before and after cutting was measured by the air comparison pycnometer. The bulk density was calculated for each layer using the weight and bulk volume data. The porosity of each layer was calculated as described above by using both the values of bulk and apparent volume.

# B. CHEMICAL PROPERTIES

## 1. Degree of Cure

The extent to which virgin materials had been cured was determined by extracting the uncured resin from a powdered sample. This was done by refluxing with acetone in a Soxhlet apparatus.

## 2. Resin or Filler Content

### a. Silica-Phenolic

Duplicate samples were burned to constant weight in air in a muffle furnace at 1000°C to determine percent filler. The resin content was calculated by subtracting the percent ash from 100 percent.

### b. Graphite-Phenolic

1) Virgin -- Duplicate samples were decomposed in hot dimethylsulfoxide-nitric acid solutions. The unattacked graphite was filtered and weighed to give a value of observed percent filler. The actual percent filler content was read from a previously prepared curve of observed versus actual percent filler. The resin content was then calculated by subtracting the percent filler from 100 percent.

2) Oven Reference Chars -- Initial attempts to combust samples at a temperature low enough to prevent oxidation of the graphite filler gave inconsistent results. Therefore, the filler content was obtained by thermogravimetric analysis in air at a heating rate of 5°C per minute. The amount of filler was indicated by a plateau in the weight loss curve. This plateau reflected the loss in weight due to oxidation of resin and occurred just before the graphite filler began to oxidize. If no plateau was obtained in the weight loss curve, the sample was considered to be all graphite.

## 3. Trace Metals

### a. Silica-Phenolic

A sample was ashed as described above under part 2a, except that the temperature was 540°C so that no trace metal oxides would be lost by volatilization. The silica residue was treated with hydrofluoric and perchloric acids. After the silica had been removed as the volatile tetrafluoride, the crucible contents were dissolved in 1:3 hydrochloric acid, transferred to another container, and diluted to a volume of 50 ml with distilled, deionized water. The trace metals were determined by atomic absorption analysis using a Perkin-Elmer Model 303 Atomic Absorption Spectrophotometer.

### b. Graphite-Phenolic

These samples, too, were ashed at 540°C. The graphite residue was analyzed directly for trace metals by emission spectroscopy using the dc arc technique and a Jarrell-Ash 3.4 Meter Grating Emission Spectrograph.

4. Elemental Analysis

   a. Carbon, Hydrogen, and Nitrogen

   These elements were determined by the F&M Model 185 Carbon, Hydrogen, and Nitrogen Analyzer. A sample weighing between 0.6 and 0.8 milligram was mixed with an oxygen-containing catalyst and burned in a helium atmosphere at $1000^\circ$ C. The resultant mixture of gases was swept from the combustion chamber through heated tubes packed with copper oxide and copper to convert any carbon monoxide to carbon dioxide and any nitrogen oxides to nitrogen. These gases and water vapor ($CO_2$, $H_2O$, and $N_2$) then were separated and detected by a single-column gas chromatograph. The peak heights for $CO_2$, $H_2O$, and $N_2$ were compared with the peak heights obtained with standards; and the percentages of C, H, and N were calculated by direct proportion. The value of nitrogen in these determinations was essentially zero.

   b. Oxygen

   The percent oxygen in each sample was calculated by summing the percents of carbon, hydrogen, and ash and subtracting this value from 100 percent.

C. CHEMISTRY PROFILES

When the elemental composition had been obtained, the atomic ratios of C, H, and O were calculated by dividing the percent of each element by its atomic weight. The atomic ratios were normalized to the same inert ash content as the virgin material by multiplying each atomic ratio value by the ratio of the ash in the virgin material to the ash in the char slice analyzed. This method gave the change in atomic ratio of C, H, and O due to degradation and charring. These ratios were then plotted against depth from the outer surface.

D. CONSTITUENT ANALYSIS

The Debye-Scherrer technique of X-ray diffraction analysis was used to determine whether the following crystalline materials were present in selected char specimens: pyrolytic graphite, beta-quartz, cristobalite, silicon carbide, elemental silicon.

E. THERMOGRAVIMETRIC ANALYSIS

Thermogravimetric analysis (TGA) was carried out with a Harrop Precision Furnace Co. TGA-DTA (Differential Thermal Analysis) unit. Typically, 100 mg of powdered sample was heated from room temperature to about $900^\circ$ C. The change in weight of the sample was recorded as a function of temperature which changed at a fixed predetermined rate. Three heating rates were used: $5^\circ$, $10^\circ$, and $20^\circ$ C per minute. Runs were carried out in either air or helium flowing at the rate of 1 cubic foot per hour.

F. PYROLYSIS STUDIES

Pyrolysis was conducted so that volatile products were swept directly into the injection port of an F&M Model 720 Dual Column Programmed Temperature gas

chromatograph equipped with thermal conductivity detectors. Four different columns were used to obtain a complete distribution of all volatile products. These are listed in Table E-I together with the conditions for component resolution. Pyrolysis products were identified qualitatively and quantitatively by comparing retention times and peak areas or heights with those of known compounds. Duplicate determinations were made at each pyrolysis temperature.

Pyrolysis was carried out by a combustion tube assembly similar to and adopted from the assembly used in our F&M Model 185 carbon-hydrogen-nitrogen analyzer. One end of the Hastelloy metal combustion tube, 5/16 in. i.d. x 3/8 in. o.d. x 4 in. long, was connected to the injection port of the gas chromatograph. The other end of the tube was connected to an F&M sample port injection housing equipped with gas inlet fittings and designed to accommodate a push rod. The push rod is cavitated at one end to hold a small quartz boat in which up to 15 mg of powdered sample may be weighed.

Pyrolysis temperatures were attained by heating that part of the combustion tube nearest the injection port of the chromatograph with a Fisher Microcombustion Resistance Furnace. The heating zone of the furnace is 7 inches long. Midpoint in the furnace is a thermocouple for measuring the temperature. The furnace position along the tube was adjusted so that the thermocouple was opposite that location in the tube where the boat was placed by the push rod.

Pyrolysis was accomplished by pushing a preweighed sample into the hot zone which was preheated to the desired temperature. A fitting has to be loosened to accomplish this. Consequently there is a possiblity of air contamination. However, no air peaks were ever noted when empty boats were pushed into the combustion tube. The residence time in the hot zone for a given sample depended on the time necessary for the components of interest to elute from the chromatographic column. This time varied from 5 minutes for water determination to 30 minutes for cresylic derivatives. When a run was completed, the sample boat was removed from the system and reweighed to determine weight loss.

# TABLE E-I

## COLUMN AND COLUMN CONDITIONS USED IN ANALYSES OF VOLATILE PYROLYZATES

The columns listed below were all used under the following instrument conditions:

Helium Carrier Gas: 40 psig
Injection Port Temperature: 200° C
Detector Block Temperature: 300° C
Bridge Current: 150 ma

| Column | Column Temperature (°C) | Program Rate | Carrier Gas Flow Rate (ml/min) | Components Analyzed |
|---|---|---|---|---|
| Silica Gel; 30-60 m sh; 6-mm by 6-ft coiled stainless steel tubing | 35 | Isothermal | 60 | Carbon dioxide |
| Molecular Sieve 5A; 60-80 mesh; 6-mm by 6-ft coiled stainless steel tubing | 75 | Isothermal | 100 | Hydrogen Methane Carbon monoxide |

| Column | Column Temperature (°C) | Program Rate (°C/min) | Carrier Gas Flow Rate (ml/min) | Components Analyzed |
|---|---|---|---|---|
| Carbowax 1500, 10 weight percent on 30·60 mesh Haloport F; 6-mm x 12-ft stainless steel tubing | 100 | Isothermal | 100 | Water |
| Disodecylphthalate, 10 weight percent on 60-80 mesh Diatoport S; 6-mm x 6-ft stainless steel tubing | 35-170 | 5 | 75 | Cresylic materials Benzene Toluene Xylene Napthalene Benzaldehyde Ethanol Propanol |

## DOCUMENT CONTROL DATA - R & D

*(Security classification of title, body of abstract and indexing annotation must be entered when the overall report is classified)*

| 1. ORIGINATING ACTIVITY *(Corporate author)* | 2a. REPORT SECURITY CLASSIFICATION |
|---|---|
| Avco Government Products Group<br>Space Systems Division<br>201 Lowell Street, Wilmington, Massachusetts 01887 | None |
| | 2b. GROUP |

**3. REPORT TITLE**

The Post-Test Analysis of Ablative Materials

**4. DESCRIPTIVE NOTES** *(Type of report and inclusive dates)*

Final Report (11 July 1967 to 15 May 1968)

**5. AUTHOR(S)** *(First name, middle initial, last name)*

Burrell, B. W.   DeSesa, M. A.
Crowley, D. P.   Thuat, M. E.

| 6. REPORT DATE | 7a. TOTAL NO. OF PAGES | 7b. NO. OF REFS |
|---|---|---|
| 10 February 1969 | 266 | 9 |
| 8a. CONTRACT OR GRANT NO.<br>NAS3-10300<br>b. PROJECT NO.<br><br>c.<br><br>d. | 9a. ORIGINATOR'S REPORT NUMBER(S)<br>AVSSD-0090-69-RR<br><br>9b. OTHER REPORT NO(S) *(Any other numbers that may be assigned this report)*<br>NAS CR-72400 | |

**10. DISTRIBUTION STATEMENT**

| 11. SUPPLEMENTARY NOTES | 12. SPONSORING MILITARY ACTIVITY |
|---|---|
| | Technical Management, NASA Lewis<br>Research Center, Cleveland, Ohio<br>Liquid Rocket Technology Branch |

**13. ABSTRACT**

Silica and graphite-phenolic ablative materials were examined before and after test firing in a rocket engine nozzle. Chemical, thermal, and physical characterizations of the post-fired nozzle chars were performed in depth at selected nozzle locations. Similar characterizations were also performed on raw billets and laboratory oven-prepared chars.

The fired nozzle char property determinations were performed on various layers removed from the char zones and included carbon, hydrogen, oxygen, and ash analysis, trace metal analyses, density, porosity, X-ray diffraction analysis, optical reflectance, photomicrographic analysis, specific heat, and thermal conductivity. Data are presented in tabular and graphical property profile format.

**DD FORM 1473**
I NOV 65

| 14. KEY WORDS | LINK A | | LINK B | | LINK C | |
|---|---|---|---|---|---|---|
| | ROLE | WT | ROLE | WT | ROLE | WT |
| Post Test Analysis | | | | | | |
| Rocket Nozzle Performance | | | | | | |
| Ablation Materials | | | | | | |
| Ablative Rocket Nozzles | | | | | | |
| Silica Phenolic Laminates | | | | | | |
| Graphite Phenolic Laminates | | | | | | |
| Charring Ablators | | | | | | |
| Thermal Properties - Rocket Nozzles | | | | | | |
| Chemical Properties - Rocket Nozzles | | | | | | |
| Pyrolysis Studies | | | | | | |
| X-ray Diffraction - Charred Ablators | | | | | | |
| Thermal Properties Profiling Techniques | | | | | | |
| Chemical Properties Profiling Techniques | | | | | | |
| Fired Rocket Nozzle Analysis | | | | | | |
| Fired Rocket Nozzle Microscopic Studies | | | | | | |
| In-Depth Temperature Postulations - Ablators | | | | | | |
| Thermal Conductivity | | | | | | |
| Specific Heat | | | | | | |
| Density | | | | | | |
| Carbon | | | | | | |
| Hydrogen | | | | | | |
| Oxygen | | | | | | |
| Ash Analysis | | | | | | |
| Trace Metals Analysis | | | | | | |
| Photomicrographs | | | | | | |
| Crystal Structure - X-ray Diffraction | | | | | | |
| Oven Charring | | | | | | |